# Development of ovarian cancer-targeted adenoviral vectors

Hanni Katariina Uusi-Kerttula

Thesis submitted for the degree of Doctor of Philosophy

March 2017

Division of Cancer and Genetics
School of Medicine, Cardiff University
Cardiff, UK

# Declaration

This work has not been submitted in substance for any other degree or award at this or any other university or place of learning, nor is being submitted concurrently in candidature for any degree or other award.

Signed ……………………………………… (candidate)

Date ………………….…………….………

## STATEMENT 1

This thesis is being submitted in partial fulfilment of the requirements for the degree of PhD.

Signed ………………………………………….…………… (candidate)

Date ……………………………….……………

## STATEMENT 2

This thesis is the result of my own independent work/investigation, except where otherwise stated, and the thesis has not been edited by a third party beyond what is permitted by Cardiff University's Policy on the Use of Third Party Editors by Research Degree Students. Other sources are acknowledged by explicit references. The views expressed are my own.

Signed …………………………………………….…… (candidate)

Date ……………………….………………

## STATEMENT 3

I hereby give consent for my thesis, if accepted, to be available online in the University's Open Access repository and for inter-library loan, and for the title and summary to be made available to outside organisations.

Signed …………………………………………….…..….. (candidate)

Date …………………………………………

## STATEMENT 4: PREVIOUSLY APPROVED BAR ON ACCESS

I hereby give consent for my thesis, if accepted, to be available online in the University's Open Access repository and for inter-library loans after expiry of a bar on access previously approved by the Academic Standards & Quality Committee.

Signed ……………………………………….……… (candidate)

Date ……………………………….………

# Dedication

This thesis is dedicated to my beautiful, inspirational, and so much missed grandmother Ritva who died of pancreatic cancer in September 2005.

I wish you could have stayed longer.

♦

*Live fast, die happy.*

# Acknowledgements

# Abbreviations

| | |
|---|---|
| Δ | Deletion |
| Δ24 | A 24-base pair deletion in the viral *E1A* gene |
| 3D | A combination of three de-targeting mutations |

## A

| | |
|---|---|
| A20 | NAVPNLRGDLQVLAQKVART peptide from FMDV |
| aa | Amino acid |
| Ad | Adenovirus |
| AdZ | Homologous recombineering with zero cloning steps |
| Amp | Ampicillin |
| APC | Antigen-presenting cells |
| ATCC | American Type Culture Collection |
| αvβ3/5/6 | Alpha v beta 3/5/6 integrin |

## B

| | |
|---|---|
| β-Gal | Beta galactosidase |
| BAC | Bacterial artificial chromosome |
| BCA | Bicinchoninic acid protein assay |
| bp | Base pairs |
| *Brca1/2* | Breast cancer 1/2 gene |
| BSA | Bovine serum albumin |

## C

| | |
|---|---|
| CAF | Cancer-associated fibroblast |
| CAR | Coxsackie and adenovirus receptor |
| CD46 | Cluster of differentiation 46 |
| CDC | Centers of Disease Control |
| Chlor | Chloramphenicol |
| CHO | Chinese hamster ovary |
| CMV | Cytomegalovirus |
| CPE | Cytopathic effect |
| CR1 | Complement receptor 1 |
| CRAd | Conditionally-replicative adenovirus |
| CSC | Cancer stem cell |
| CsCl | Cesium chloride |
| CTLA-4 | Cytotoxic T-lymphocyte-associated protein 4 |

## D

| | |
|---|---|
| DAMP | Damage-associated molecular pattern |
| DAB | 3,3'-Diaminobenzidine |
| DMEM | Dulbecco's Modified Eagle's Medium |
| DMSO | Dimethyl sulfoxide |
| DNA | Deoxyribonucleic acid |
| DSG-2 | Desmoglein 2 |
| DTT | 1,4-Dithioreitol |

## E

| | |
|---|---|
| ECM | Extracellular matrix |
| EDTA | Ethylene diamino tetraacetic acid |
| EGFR | Epidermal growth factor receptor |
| ELISA | Enzyme-linked immunosorbent assay |
| EMA | European Medicines Agency |

| | |
|---|---|
| EMT | Epithelial-to-mesenchymal transition |
| EnAd | Enadenotucirev (previously ColoAd1) |
| EOC | Epithelial ovarian cancer |
| ER | Endoplasmic reticulum |
| ERK | Extracellular signal-regulated kinase |
| EtOH | Ethanol |

**F**

| | |
|---|---|
| F | Fiber |
| FACS | Fluorescence-activated cell sorting |
| FBS | Foetal bovine serum |
| FDA | U.S. Food and Drug Administration |
| FGFR1 | Fibroblast growth factor receptor 1 |
| FMDV | Foot-and-mouth disease virus |
| FX | Human coagulation factor 10 |

**G**

| | |
|---|---|
| GD1a | Ganglioside / glycan receptor |
| GFP | Green fluorescent protein |
| G-CSF | Granylocyte colony-stimulating factor |
| GM-CSF | Granulocyte macrophage colony-stimulating factor |

**H**

| | |
|---|---|
| HEK | Human embryonic kidney |
| HER2 | Human epidermal growth factor receptor 2 |
| HIS | Histidine |
| HRP | Horse radish peroxidase |
| HGS-OC | High-grade serous ovarian carcinoma |
| HSPG | Heparan sulphate proteoglycan |
| HSV | Herpes simplex virus |
| HTA | Human Tissue Act |
| HVR | Hypervariable region |
| HVR7 | Coagulation factor 10-binding mutation in the hexon protein |

**I**

| | |
|---|---|
| IgG | Immunoglobulin G |
| IL | Interleukin |
| IFN-γ | Interferon gamma |
| IHC-P | Immunohistochemical staining of paraffin-embedded sections |
| IPTG | Isopropyl β-D-1-thiogalactopyranoside |
| IP-10 | Interferon gamma-induced protein 10 |
| ITR | Internal terminal repeat |
| i.v. | Intravenous |
| IVIS | In Vivo Imaging System |
| i.p. | Intraperitoneal |

**K**

| | |
|---|---|
| Kan | Kanamycin |
| KC | Keratinocyte-derived cytokine |
| KC | Kupffer cell |
| kDa | kilodalton |
| kn | Knob |
| KO1 | CAR binding ablation mutation |

**L**

| | |
|---|---|
| L-Glut | L-glutamine |
| LAP | Latency-associated peptide |
| Luc | Luciferase |

## M

| | |
|---|---|
| MΦ | Macrophage |
| mAb | Monoclonal antibody |
| MCP-1 | Monocyte chemoattractant protein 1 |
| MHC | Major histocompatibility complex |
| MIP-1/2 | Macrophage inflammatory protein 1/2 |
| MMP | Matrix metalloproteinase |
| MTS | 3-(4,5-dimethylthiazol-2-yl)-5-(3-carboxymethoxyphenyl)-2-(4-sulfophenyl)-2H-tetrazolium |
| MZMΦ | Marginal zone macrophage |

## N

| | |
|---|---|
| nAb | Neutralising antibody |
| NCBI | National Center for Biotechnology Information |
| Ni-NTA | Nickel-nitrilotriacetic acid |
| NIH | U.S. National Institutes of Health |
| NOD/SCID | Non-obese diabetic severe combined immunodeficient |
| NPC | Nuclear pore complex |

## O

| | |
|---|---|
| OAd | Oncolytic adenovirus |
| OAS | Ovarian ascites |
| OD | Optical density |
| O/N | Overnight |

## P

| | |
|---|---|
| PAMP | Pathogen-associated molecular pattern |
| p.i. | Post-infection |
| p.i. | Post-injection |
| P/S | Penicillin/streptomycin |
| PBS | Phosphate buffered saline |
| PBS-T | Phosphate buffered saline / Tween-20 |
| PCR | Polymerase chain reaction |
| PD-1 | Programmed cell death protein 1 |
| PDB | Protein Data Bank |
| PDF | Patient-derived xenograft |
| PET | Positron emission tomography |
| PFA | Paraformaldehyde |
| PFU | Plaque forming unit |
| PMN | Polymorphonuclear leukocyte |
| pRB | Retinoblastoma protein |
| Puro | Puromycin |

## Q

| | |
|---|---|
| qPCR | Quantitative polymerase chain reaction |

## R

| | |
|---|---|
| RANTES | Chemokine ligand 5 (CCL5) |
| RGD | Integrin-binding Arg-Gly-Asp motif in the penton base |
| RGE | Integrin-binding ablation mutation in the penton base |
| RLU/mg | Relative light units per mg protein |
| rpm | Revolutions per minute |

| | |
|---|---|
| RPMI | Roswell Park Memorial Institute |
| RT | Room temperature |

## S

| | |
|---|---|
| SA | Sialic acid |
| scFv | Single-chain Fv antibody |
| SD | Standard deviation |
| SDS-PAGE | Sodium dodecyl sulfate polyacrylamide gel electrophoresis |
| SEM | Standard error of the mean |
| SPR | Surface plasmon resonance |
| SW102 | *E. coli* strain used for recombineering |

## T

| | |
|---|---|
| T* | Coagulation factor 10-binding mutation |
| T1 | Potency-enhancing mutation in the viral *E3-gp19K* gene |
| TAA | Tumour-associated antigen |
| TGF-β1 | Transforming growth factor beta 1 |
| Th | Helper T-cell |
| TIL | Tumour-infiltrating lymphocyte |
| TLR | Toll-like receptor |
| TME | Tumour microenvironment |
| TNF-α | Tumour necrosis factor alpha |

## U

| | |
|---|---|
| UV | Ultraviolet |

## V

| | |
|---|---|
| V | Volt |
| vp | Viral particle |
| vWF | von Willebrand factor |

## W

| | |
|---|---|
| WCRF | World Cancer Research Fund |

## Z

| | |
|---|---|
| ZO-1 | Zonula occludens-1 |

# Abstract

Ovarian cancer is the deadliest gynaecological cancer, with less than half of patients surviving five years from diagnosis. The asymptomatic nature of the early disease commonly results in diagnosis at an advanced stage where peritoneal metastases are prevalent, and the disease rapidly develops resistance to platinum-based agents. Innovative treatments are needed to combat this untreatable disease that has a poor prognosis.

Adenoviruses (Ad) are versatile gene therapy vehicles that have been studied for six decades. Their wider clinical use has been limited by poor tumour-specificity, pre-existing immunity, and toxicity-inducing off-target delivery. We have generated an Ad5.3D.A20 vector that is re-targeted to an epithelial cancer-specific marker, αvβ6 integrin, and fully de-targeted from native interactions – αvβ3/5 integrins, coxsackie and adenovirus receptor (CAR), and human coagulation factor 10 (FX). Ad5.3D.A20 selectively transduced αvβ6+ epithelial ovarian cancer (EOC) cells *in vitro* and clinical ovarian ascites-derived EOC cells *ex vivo*, including in the presence of neutralising anti-Ad antibodies. *In vivo*, Ad5.3D.A20 exhibited significantly reduced off-target accumulation and transduction of the liver, spleen and lungs, relative to Ad5. Efficacy studies are underway to investigate its oncolytic potential. Furthermore, we explored the potential use of alternative serotypes from the rare seroprevalence subgroup D. A novel Ad10 vector showed improved resistance from neutralisation and lack of FX binding. Chimaeric Ad5 vectors pseudotyped with Ad10, -15, -24, -29, -48 or -53 fiber had reduced interactions with CAR, but no binding to CD46.

Our strategy for translation initially is via intraperitoneal delivery of oncolytic vectors, bypassing many of the barriers presented by systemic delivery, but enabling transduction of disseminated metastases. These exquisitely tumour-targeted vectors may be further modulated to carry therapeutic moieties to complement their direct cell-killing activity via the stimulation of anti-cancer immunity. The generated tropism-modified vectors have significant therapeutic potential for a wide range of immuno-oncolytic applications.

# Table of Contents

# List of Tables

# List of Figures

# CHAPTER 1.     Introduction

# CHAPTER 1. Introduction

Ovarian cancer is the deadliest gynaecological cancer and fifth leading cause of cancer-related death in women, leading to 4500 annual mortalities in the UK alone (CRUK, 2012). According to the World Cancer Research Fund (WCRF), approximately 240 000 new cases are diagnosed every year worldwide (WCRF, 2012), with a 5-year survival rate of 46 % (NCI, 2012). Despite advantageous progress in the cancer therapy field and introduction of new chemotherapeutic agents, the survival rates have seen only minor improvements in the past decades. Current chemo- and radiotherapy regimens not only cause major adverse effects, but are also ineffective against metastatic tumours that often result in high mortality rates, particularly in patients with late diagnosis. One of the major hurdles is combating the aggressive, platinum-resistant forms of ovarian cancer that commonly develop in the advanced stage of the disease. Oncolytic virus therapy offers an innovative treatment strategy for the eradication of the resistant cell populations, and has potential for use as adjunct therapy in combination with conventional regimens. Ovarian cancer presents an excellent avenue for local therapies as viral vectors can be locally administered into the peritoneal cavity.

Adenoviruses (Ad) were originally isolated from a human adenoid tissue sample in 1953 (Rowe et al., 1953), and since then they have been extensively studied and utilised for clinical cancer applications. Ads are obligate intracellular parasites that can infect a wide variety of cell types and tissues in the human body, and generally cause mild common cold-like illnesses. Certain viruses such as Ads are inherently lytic, as host cell infection leads to cell destruction accompanied with a burst of progeny viruses. This further infects the neighbouring cells and amplifies the therapeutic effect. Vigorous research into viral gene therapy has provided compelling evidence of the oncolytic potential of Ad-based vectors, which infect both dividing and non-dividing cells and can be manipulated to incorporate large transgenes (up to 105 % of genomic size) (Bett et al., 1993) into their genome without the risk of integration into the host genome, and are therefore not considered to be intrinsically oncogenic. Due to the generally mild nature of the disease manifestation and long clinical history with 532 clinical trials conducted up to date (Abedia, 2016), Ads are widely considered to be safe delivery vectors for gene therapy applications. The Ad genome is well-characterised, compact and largely permissive for a plethora of genetic modifications.

Ad serotype 5 (Ad5) has been the most commonly used delivery vector for experimental and clinical purposes, and comprises the majority of gene therapy trials

worldwide (clinicaltrials.gov, 2016). The first Ad5-based, oncolytic vector ONYX-015 was approved for therapeutic use for head and neck cancers in China in 2005 (Ganly et al., 2000, Nemunaitis et al., 2001a) but has not been licensed elsewhere. The latest trends in oncolytic Ad gene therapy have included Ads with a variety of cancer-specificities, tumour vaccines, cancer immunotherapies and modulation of immune checkpoint control mechanisms [for reviews on oncolytic Ad-based therapies, see (Kanerva and Hemminki, 2005, Vähä-Koskela et al., 2007, Choi et al., 2012, Ribas, 2012, Russell et al., 2012, Uusi-Kerttula et al., 2015a)]. Significant existing limitations of viral cancer gene therapies include the low level of cancer cell -specificity due to lack of a cancer-specific cell receptor, toxic adverse effects due to off-target sequestration, and poor target delivery due to tumour heterogeneity and vector inactivation by innate immune responses. Vectors based on common human pathogens typically exhibit high seroprevalence rates in the population. Native viral infection elicits serotype-specific neutralising antibodies (nAbs) that, upon systemic administration of a therapeutic vector, rapidly opsonise and eliminate the virus based on highly specific humoral immune recognition. Below, we discuss the strategies for Ad vector development and suggests novel approaches for improving therapeutic targeting for ovarian cancer applications.

## 1.1 Ovarian cancer biology

Ovarian cancer is challenging to diagnose. Its symptoms are very non-specific, and may include pain in the abdomen or pelvis, bloating, changes in digestive functions, nausea, feeling of fullness, fluid or lump in the abdomen, fatigue, loss or appetite and weight loss (ACS, 2016). Unfortunately, ovarian cancer commonly remains asymptomatic – more than 75 % of ovarian cancers are diagnosed in the late advanced stages (Salani et al., 2011), which significantly contributes to its poor prognosis. The median age at the time of diagnosis is 63 years, and 70 years at the time of death (NCI, 2012). Ovarian cancer biology, classification, treatment and common features are discussed in the following sections.

### 1.1.1 *Classification, treatment and survival statistics*

Ovarian cancer progression is classified into four main stages according to the location and spread of the tumour, while grading is based on cell morphology (Figure 1–1). The majority (90 %) of ovarian cancers arise from transformation of the ovarian epithelium (Koonings et al., 1989, Holschneider and Berek, 2000) that covers the surface of ovaries. This leads to the development of epithelial ovarian cancer (EOC) – the most common and deadliest ovarian cancer type (Wefers et al., 2015). It can be classified into five types – serous, endometrioid, clear cell, mucinous and

undifferentiated / unclassifiable – based on the histology (CRUK, 2012). Germ cell ovarian cancer originates from the eggs residing in the ovaries and is extremely rare, comprising only 1–2 % of all ovarian cancers. Borderline ovarian tumours have low malignant potential and are responsible for 10 % of ovarian cancers. This type of cancer grows slowly and is typically diagnosed early, and therefore is commonly treatable with surgery alone.

**Classification**

- **I)** One or both ovaries
- **II)** One or both ovaries and spread to pelvis
- **III)** One or both ovaries, spread below pelvis & surrounding lymph nodes and/or i.p.
- **IV)** Spread beyond abdomen with distant metastases

**Grading**

- **GX)** Grade cannot be evaluated
- **GB)** Tissue borderline cancerous / low malignant potential
- **G1)** Well-differentiated
- **G2)** Moderately differentiated
- **G3–G4)** Poorly differentiated / undifferentiated

**Figure 1–1. Ovarian cancer classification and grading.** Classification scale (I–IV) is based on International Federation of Gynaecological Oncologists (FIGO) system (CRUK, 2012). Ovarian cancer grading (GX–G4) is based on cell morphology (CRUK, 2012, ASCO, 2015). i.p., intraperitoneal.

In healthy tissues, tumour antigen p53 is the guardian of DNA damage and stress, and activates DNA repair mechanisms, initiates apoptosis, prevents angiogenesis and controls excessive cell proliferation by cell division arrest at G1/S stage of the cell cycle [reviewed in (Vogelstein et al., 2000)]. Mutations in *p53* can lead to uncontrolled cell division and carcinogenesis due to aberrant apoptotic signalling pathways. Sequencing revealed an abnormal expression or a complete loss of p53 function, determined from six human ovarian carcinoma cell lines (PA-1, Caov-3 and -4, OVCAR3, SKOV3, and Kuramochi) (Yaginuma and Westphal, 1992). The analysis exposed variable mutations in p53, ranging from six-fold increased expression in PA-1 cell line, in contrast with complete loss of function in SKOV-3 cell line that had a rearrangement of the *p53* gene. Caov-3, OVCAR3 and Kuramochi cell lines all had point mutations in highly conserved domains, leading to single amino changes and undetectable p53 protein expression. High-throughput genomic analyses have shown

up to 96 % of high-grade serous ovarian carcinomas (HGS-OC) to have mutations in *TP53* (Bell et al., 2011, Patch et al., 2015).

The standard method of care for ovarian cancer is the combination of aggressive removal of the tumour by surgery and chemotherapy. Neo-adjuvant chemotherapy may be given to patients prior to surgery to reduce the size of the tumour and to facilitate its removal. The affected tissue is removed, which often means the removal of one or both ovaries, Fallopian tubes and the womb (including the cervix). This is followed by adjuvant chemotherapy, except for stage 1a cancers that do not require additional treatment. The first-line chemotherapy agents for ovarian cancer are commonly platinum-based, including cisplatin, carboplatin and oxaliplatin. These drugs are neutral platinum agents whose mechanism of action is based on the disruption of cell cycle regulation and the resulting apoptosis (Chen et al., 2013). They are often given in combination with taxanes, such as paclitaxel and docetaxel for a more pronounced response. Chemotherapy for EOC is given either intravenously (i.v.) or intraperitoneally (i.p.) through a catheter, every 3–4 weeks in a total of 3–6 cycles. There are reports of i.p. delivery of anti-cancer agents being more effective but also causing more intolerable adverse effects than i.v. delivery, which causes some patients to withdraw early from treatment (ACS, 2016). The reason for abdominal discomfort has been linked to the use of phosphate-buffered saline (PBS) as a carrier (Hosie et al., 2001), which led to the use of renal dialysis fluids, such as 4 % icodextrin, that have proven better tolerated with favourable pharmacokinetics (Hosie et al., 2003, McArdle et al., 1994).

Chemotherapy can be used in conjunction with targeted biological treatments that cause minimal harm to healthy cells. Commonly used agents include poly (ADP-ribose) polymerase (PARP-1) inhibitors and an angiogenesis inhibitor bevacizumab, a monoclonal antibody (mAb). Patients with advanced EOC who have breast cancer 1/2 (*Brca1/Brca2)* mutations may receive olaparib, which is a PARP-1 inhibitor designed to inhibit DNA repair mechanisms in cancer cells with defective BRCA-pathways. Other approaches include hormone treatments such as luteinizing-hormone-releasing hormone (LHRH) agonists, tamoxifen (anti-oestrogen) and aromatase inhibitors. Chemo- and biological therapies may also be combined with external beam radiation therapy that resembles diagnostic X-ray. More information on the treatment of ovarian cancer can be found on the American Cancer Society website (ACS, 2016). In 2010–2011 the 1-, 5- and 10-year overall survival (OS) from ovarian cancer was 73 %, 46 % and 3 %, respectively (CRUK, 2012). Holschneider and colleagues determined the stage-dependent survival from ovarian cancer as 93 % for

stage I, 70 % for stage II, 37 % for stage III and 25 % for stage IV disease (Holschneider and Berek, 2000). The authors also state that 80–90 % of ovarian cancers are diagnosed in women older than 40 years of age, and that 2/3 of the diagnosed cases have reached an advanced, metastasised stage. Up to 70 % of ovarian cancer-related deaths are caused by advanced stage HGS-OC (Koonings et al., 1989, Seidman et al., 2004). Improvement of treatment regimens and attempts for better ovarian cancer screening are vital for earlier diagnosis and improved survival of these patients.

### 1.1.2   Tumour microenvironment (TME), ascites and metastasis

One of the major hurdles in all cancer therapies is the poor accessibility of the tumour by therapeutic agents. This is not only due to physical barrier formed by the extremely complex architecture within the bulky tumour mass, but also due to acquired drug resistance and uneven angiogenesis within the tumour. Biologically, TME forms a highly complex structure consisting of numerous different immune cell types, vasculature, fibroblasts, stromal cells, immune infiltrates, cancer-associated fibroblasts (CAFs), lymphocytes and the extracellular matrix (ECM), in addition to the primary neoplastic cells (Figure 1–2). TME presents three main threats to anti-cancer treatment: fibroblast-, immune- and vasculature-mediated resistance [reviewed in (Junttila and de Sauvage, 2013)]. Angiogenesis is often unevenly distributed within the tumour mass, leaving poorly vascularised areas hypoxic and out of reach of systemically-delivered therapeutics.
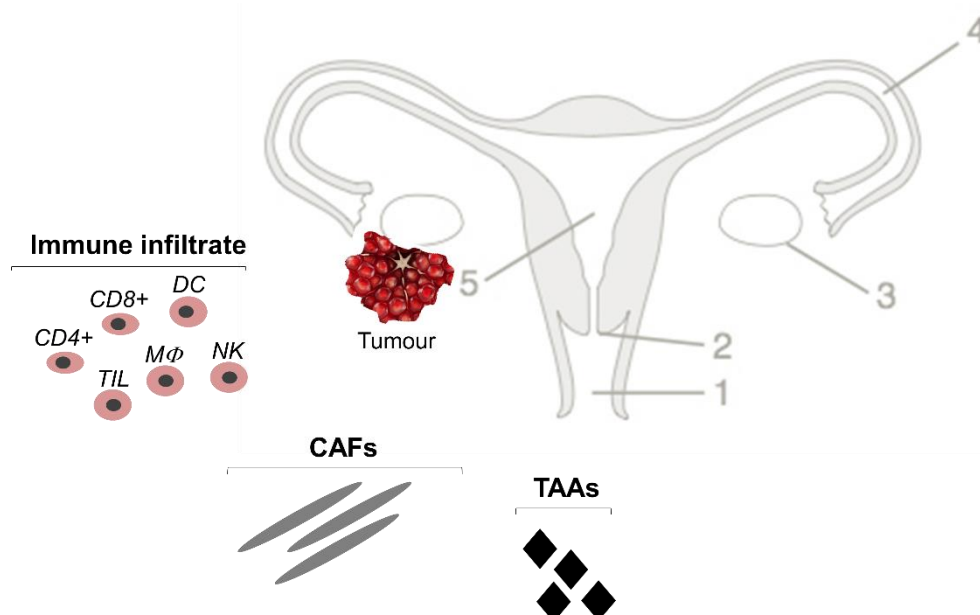


**Figure 1–2. Tumour microenvironment (TME) in ovarian cancer.** Female reproductive system: 1) vagina, 2) cervix, 3) ovary, 4) Fallopian tube, 5) womb. DC, dendritic cell; MΦ, macrophage; NK, natural killer cell; CAF, cancer-associated fibroblast; TIL, tumour-infiltrating lymphocyte; TAA, tumour-associated antigen. Figure based on reviews (Junttila and de Sauvage, 2013, Wefers et al., 2015).

Ovarian cancer TME is typically immunosuppressive and pro-tumourigenic [reviewed in (Zou, 2005, Wefers et al., 2015)], meaning that immune responses are effectively dampened down while the environment is tumour-promoting, both in favour of uncontrollable tumour growth. It is commonly rich in tumour-infiltrating lymphocytes (TILs), CD8+ T-cells, pro-angiogenic factors, such as vascular endothelial growth factor (VEGF), and immunosuppressive cytokines, such as IL-10 and TGF-β [reviewed in (Jakeman et al., 2015)]. HER/neu, MAGE-A1, folate-binding protein (FBP), p53, NY-ESO-1, EpCAM and CA-125 are examples of ovarian cancer-specific tumour-associated antigens (TAA) that are expressed during malignant transformation and could therefore be used as targets for immunotherapies [reviewed in (Wefers et al., 2015, Ren et al., 2016)]. CD44 and CD133 have been described as markers of cancer stem cell (CSC) phenotype (Chen et al., 2011b). The role of CSCs in chemoresistant ovarian cancer is discussed in a review by Ren and colleagues (Ren et al., 2016).

Ascites is the accumulation of serous or lymphatic fluid in the peritoneal cavity (Figure 1–3). Malignant ascites contains tumour cells and high concentrations of lactate dehydrogenase enzyme (Runyon et al., 1988), contrary to ascites that occurs due to other pathologies, most commonly found in liver diseases. A third of ovarian cancer patients have malignant ascites at the time of diagnosis, while the fluid is found in nearly all ovarian cancer patients with advanced disease. Ascites characterises the chemo-resistant and recurrent disease with a very poor prognosis. Large volumes of fluid cause problems with respiratory, gastrointestinal and urinary systems, abdominal pain, as well as general discomfort in the patients. Routine drainage (paracentesis) is required to temporarily ease the patients' symptoms (CRUK, 2012). For a comprehensive review on the characteristics and biology of malignant ovarian ascites, see excellent reviews (Ahmed and Stenvers, 2013, Kipps et al., 2013). Ascites contains diverse cell populations that have either originated from the surface epithelium of the ovaries by shedding or from the lymphatic system. EOC cells can either exist as free-floating single cells or spheroids that can form secondary lesions and distant metastases. Other cell types include CAFs, stromal cells, infiltrating MΦs/monocytes, myeloid cells, mesenchymal stem cells, T-cells and ECM fragments [reviewed in (Ahmed and Stenvers, 2013)].
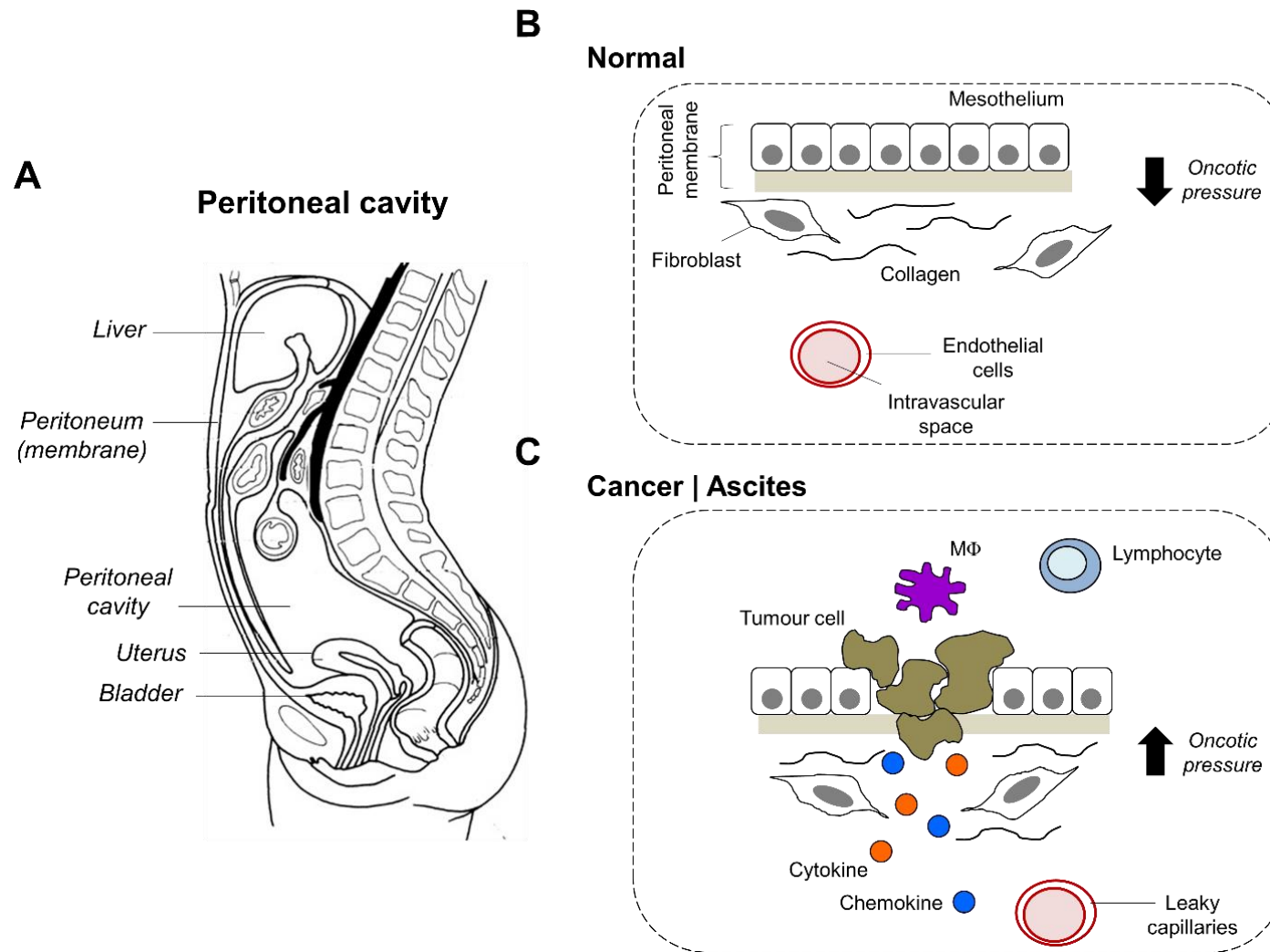
**Figure 1–3. Ascites in ovarian cancer.** A) Peritoneal membrane (peritoneum) consists of five layers and surrounds all major organs, including the ovaries, in the peritoneal cavity. B) Peritoneal membrane consists of mesothelial cells and basement membrane, supported by fibroblasts and collagen fibers residing below the membrane. C) Ascites formation and leakage into the peritoneal cavity occurs as a result of increase in oncotic pressure, leaky capillaries and disruptions in the endothelium. MΦ, macrophage. Modified from (Kipps et al., 2013).

Ascites has a tumour-promoting environment that contributes to the inhibition of chemotherapy agents, promotes tumour cell motility and growth, and facilitates cell spread across the peritoneum. The fluid contains a plethora of inflammatory cytokines and chemokines, including angiogenin, angiopoietin, GRO, ICAM-1, IL-6/-6R/-8, leptin, MCP-1, MIF, NAP-2, osteoprotegerin (OPG), RANTES, TIMP-2, and urokinase plasminogen activating receptor (uPAR). These and multiple other factors may have a critical role in facilitating the tumour to evade immunosurveillance and enabling unrestricted cancer cell growth. Cancer metastasis is a complex process that involves coordinated changes in cancer cell structure, adhesion and motility (Figure 1–4). Ovarian cancer presents an appealing target for virotherapies due to the potential for direct i.p. vector administration, thus having access to both primary and metastatic tumours, as well as other tumour-associated cell types residing in ascites. It is also desirable route to circumvent of many of the dose-limiting vector:host interactions that are encountered via the i.v. route. Unfortunately however, ascites has a protein content similar to serum, including frequently substantial levels of anti-Ad5 nAbs (Hemminki et al., 2002), which makes it a highly neutralising environment for Ad5-based vectors (Blackwell et al., 2000, Stallwood et al., 2000). In a study by Hemminki and colleagues, levels of nAbs in ovarian cancer patients were compared in both serum and ascites following i.p. delivery of Ad5. Induction of nAb production was rapid in both serum and ascites, and nAb titres were not affected by the administered dose. Surprisingly, Ad transgene expression was relatively unaffected by ascites, which may be due to 4-fold lower nAb titres in ascites as compared to serum nAb titres (Hemminki et al., 2002). Removal of the fluid prior to Ad virotherapy may help reduce vector neutralisation and improve bioavailability for active tumour targeting.

### *1.1.1 Chemo-resistance in ovarian cancer*

Ovarian cancers often show a good initial response to chemotherapies. Unfortunately, relapse is common, as aggressive, CSC-rich resistant cell populations develop over the course of prolonged drug regimens. Cisplatin-resistance has been linked to loss of *p53* function, even in the absence of a gene mutation (Eliopoulos et al., 1995, Righetti et al., 1996). Multidrug resistance (MDR) is a common reason for therapeutic failure in ovarian cancer, and involves both intrinsic and acquired factors. Clinical attempts to reverse MDR have included small molecule inhibitors and small interfering RNAs (siRNAs) that target *mdr1* gene encoded by P-glycoprotein (Pgp) (Penson et al., 2004, Wang et al., 2015), however without significant success due to low efficacy and high toxicity. Other factors contributing to chemo-resistance include CSCs, autophagy, de-regulated non-coding RNAs (ncRNAs) and tumour

heterogeneity that could be targeted therapeutically. CSCs have been shown to express distinct cell surface markers, including CD44, CD133, CD117 (c-kit) and aldehyde dehydrogenase isoform 1 (ALDH1), which could be targeted in attempt to eradicate chemo-resistant cell populations. Other markers flagged up in chemoresistant EOCs are EpCAM, as well as Wnt/β-catenin, Sonic Hedgehog (Shh), TGF-β, phosphatase and tensin homologue (PTEN)/Akt and Notch signalling pathways. Zhang and colleagues also suggested that high human epidermal growth factor receptor 2 (HER2) expression, high KRAS expression and low PTEN expression could be associated with higher platinum chemoresistance (Zhang et al., 2015).

Up-regulation of long non-coding (lnc) RNAs such as HOX transcript antisense intergenic RNA (HOTAIR), plasmacytoma variant translocation 1 (PVT1) and urothelial carcinoma associated 1 (UCA1), and down-regulation of BC200, are also associated with chemoresistant ovarian cancer. The contributing factors of chemoresistance in ovarian cancer are further discussed in a recent excellent review by Ren and colleagues (Ren et al., 2016). There is a severe lack of second-line options for patients with resistant tumours, which drives the vigorous research on novel strategies. Powerful approaches include modulation of anti-cancer immunity by therapeutic antibodies, antibody-drug conjugates, adoptive cell transfer therapies (ACT), DC-based vaccines [reviewed in (Wefers et al., 2015)] and viral oncolytic vectors.
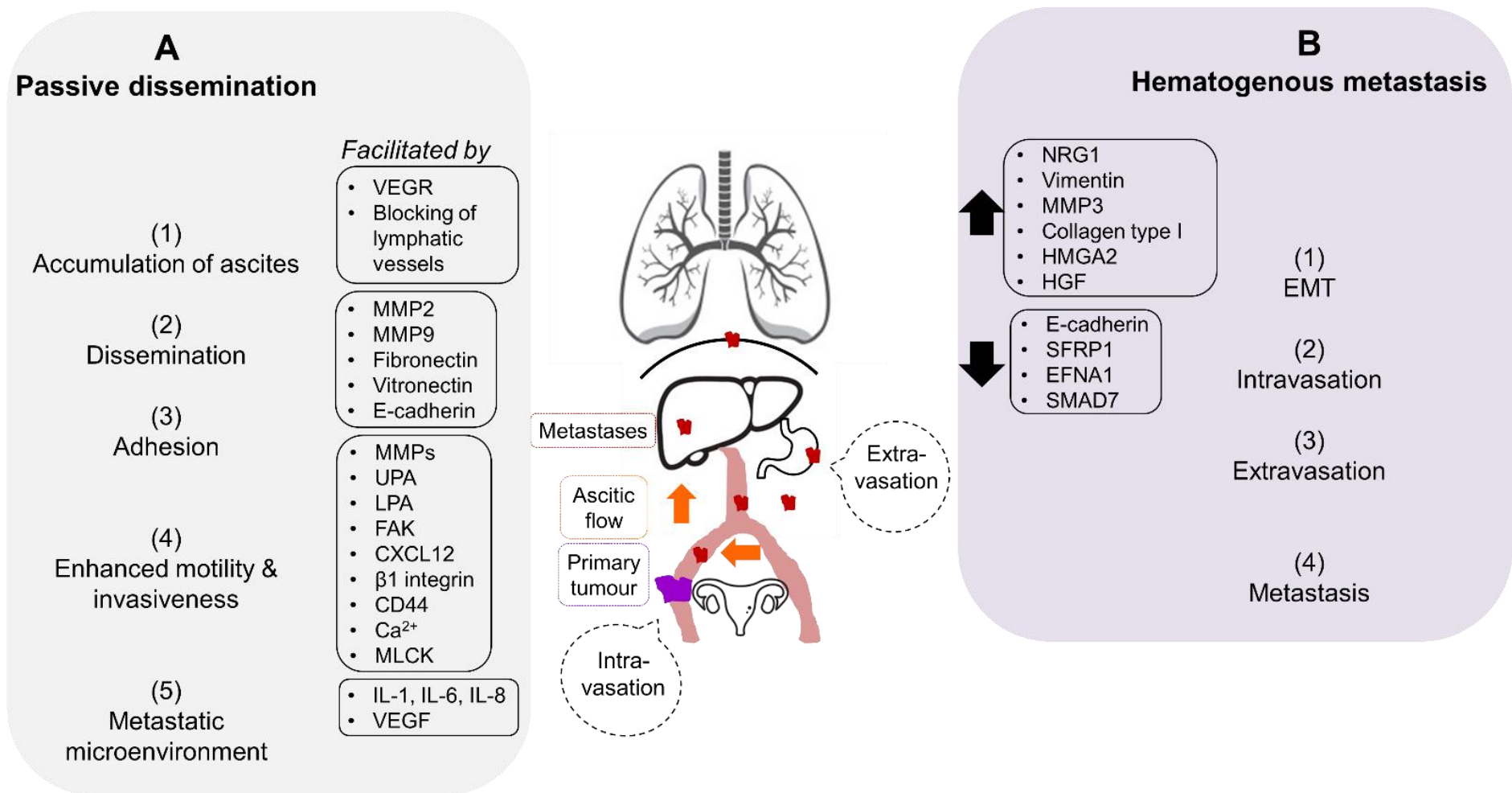
**Figure 1–4. Mechanisms of ovarian cancer metastasis.** (A) Passive dissemination: 1) Accumulation of ascites within the peritoneal cavity, 2) peritoneal dissemination of cancer cells from the primary tumour, 3) adhesion of cancer cells to the surface of metastatic cells, 4) enhanced cancer cell motility and invasiveness facilitate the establishment of tumour metastases, 5) metastases generate new supportive microenvironment. (B) Hematogenous metastasis: 1) Epithelial-to-mesenchymal transition (EMT) of cancer cells, 2) cancer cells enter circulation via intravasation at the primary tumour site, 3) cancer cells leave circulation via extravasation at metastatic site, 4) establishment of metastases. Primary tumour is shown in purple, metastases in dark red, and ascites circulation in orange arrows. Modified from (Yeung et al., 2015)

### *1.1.2   Tumour models of ovarian cancer*

The importance of representative tumour models is vital for the clinical translation. It is often impossible to mimic the physiological conditions of the human tissues in murine models that have variable cell phenotypes. Fortunately, there have been improvements in the human tumour models that aim at replicating the complex TME by utilising clinical specimens that can be adapted to laboratory conditions and tailored for each tumour type. A recent review by Jakeman and colleagues lists improvements in human tumour models developed for *in vitro* research applications (Jakeman et al., 2015). The current models include conventional cell culture monolayers, 3D cultures of spheroids and *ex vivo* tumour slice techniques of clinical tumour biopsies. These methods can be utilised to create a model that represents the tumour biology as accurately as possible, by preservation of the tumour architecture and TME.

Primary EOC cells can be readily cultured *ex vivo* from clinical patient-derived ascites (Shepherd et al., 2007, Thériault et al., 2013). These cultures can be obtained as a product of paracentesis, and represent a valuable model for functional analyses of EOC properties (O'Donnell et al., 2014). EOC cells have the characteristic 'cobblestone' monolayer phenotype (Dunfield et al., 2002) that distinguish EOC cells from other cell types residing in the fluid. Several groups have investigated the molecular phenotype of ascites-residing EOC cells. O'Donnell and colleagues report over-expression of EpCAM, pancytokeratin/cancer antigen 125 (CA125), epithelial-related antigen (MOC-31), D2-40 and vimentin, while HGS-OC was the most common histological phenotype (O'Donnell et al., 2014). EpCAM (O'Donnell et al., 2014) or tumor-associated glycoprotein 72 (TAG-72) (Barker et al., 2001) have also been used as selective markers for immunomagnetic separation methods of EOC cells, although these markers may not be exclusive for EOC separation (O'Donnell et al., 2014). Systematic EOC cell enrichment prior to subsequent *ex vivo* assessment is likely to improve assay integrity and reproducibility.

Spheroids are small (up to 500 µm) or large scale (> 500 µm) 3D cultures of tumour cells that can be grown to mimic the phenotype and TME of biological tumour masses. Small tissue biopsies can also be preserved on microscope slides, a technique that allows culture of primary tumour tissue for several days in oxygenated atmosphere. By examining multiple tissue sections throughout the primary mass, a comprehensive picture can be formed of the tumour stroma, including CAFs, tumour-associated immune cells and vasculature (Bremnes et al., 2011). Animal tumour models often lack the genetic variability that human tumours present. A potent gene editing

technology has recently been utilised to create improved murine models of the most widely used transplantable model of ovarian cancer, ID8 (Walton et al., 2016). In this study, the whole exome of ID8 was sequenced and shown to have functional *Trp53*, *RB*, *Brca1/2* or *Nf1* genes. This prompted the group to generate single *Trp53*$^{-/-}$ and double *Brca2*$^{-/-}$ knockout mice by CRISPR/Cas9 to mimic the genotype of HGS-OC. The authors also showed ID8 to have mutations in *Adamts3*, indicating its sensitivity to platinum-based agents and improved progress-free survival (Liu et al., 2015).

Potent *in vivo* and *ex vivo* models are desperately needed to better replicate different clinical scenarios. Study of the later stages of ovarian cancer that are characterised by the build-up of large amounts of ascites fluid will be very important for gaining knowledge of the progression of ovarian cancer and development of resistance. Fortunately, clinical EOC samples provide an excellent source of primary *ex vivo* cultures that can be utilised as a model for therapeutic assessment, both for viral and non-viral agents. Understandably, *ex vivo* cultures lack the complex TME, surrounding organs, vasculature and lymphatic system, and are therefore only one step closer to reliable pre-clinical systems. Future human tumour models are likely to be powered by novel innovations in tissue engineering and regenerative medicine to better resemble tumour biology.

## 1.2 Molecular virology of adenoviruses

Ads belong to the *Adenoviridae* virus family. Human Ads were historically classified into species A−G based on their DNA homology, haemagglutination, oncogenic and neutralisation properties, with species D containing the largest number of different Ad serotypes [for a comprehensive review, see (Russell, 2009)]. Systematic sequence analyses have yielded detailed information on the evolutionary relationships between different Ad serotypes and enabled the classification of the 57 human Ad serotypes (Figure 1–5) based on alignment of the main capsid proteins – fiber, hexon and penton base. Recent sequencing of 20 species D Ads revealed great diversity in the hypervariable regions (HVRs) of the capsid proteins hexon, fiber and penton (Robinson et al., 2013). The extensive variability within the species D is likely a result of natural homologous recombination, which is a common mechanism responsible for viral diversity and immune escape. Recombination occurs due to selective immune pressure in the human host, which results in novel variants with altered tropism and virulence (Robinson et al., 2013).
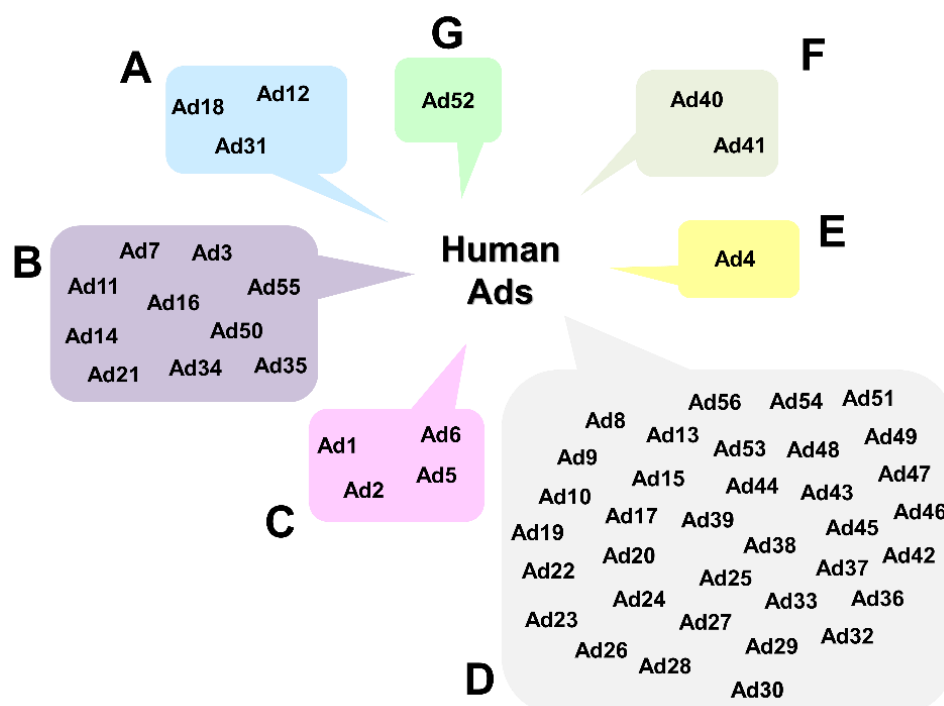
**Figure 1–5. All known 57 serotypes of human adenoviruses.** Species B viruses belong to haemagglutination group I (complete agglutination of monkey erythrocytes), species D viruses in group II (complete agglutination of rat erythrocytes), species C, E and F in group III (partial agglutination of rat erythrocytes) and species A viruses in group IV (little agglutination) [reviewed in (Young and McNeish, 2009)]. Figure modified from (Geisbert et al., 2011, Robinson et al., 2013).

Ads are circulating in the human population with small seasonal fluctuations. They infect individuals of all ages, although young children are most affected due to lack of adaptive immunity. Infections commonly result in mild upper and lower respiratory tract infections, gastroenteritis, cystitis or keratoconjunctivitis, but can in rare cases produce manifestations with high morbidity and mortality such as hepatitis, pneumonia, meningoencephalitis and myocarditis. Opportunistic infections are seen in severely immunosuppressed patients and allogeneic stem cell or organ transplant recipients, in whom the consequences can be fatal due to severe inflammatory host responses, cytokine 'storm', extensive immune attack and multi-organ failure due to viremia. Ad infections in immunocompetent and -compromised patients are discussed in detail in a recent review by Lion and colleagues (Lion, 2014). In 1999 a young gene therapy volunteer received intravascular delivery of a large dose ($3.8 \times 10^{13}$ viral particles) of Ad5 for ornithine transcarbamylase deficiency, and died as a result of cytokine storm (Lehrman, 1999). This case was a significant low point in the clinical development of Ad as a gene therapy, and highlighted the requirement to better understand and refine the interactions that limit efficacy and promote toxicity.

### 1.2.1 Adenovirus life cycle

Ads infect a wide variety of vertebrate hosts via aerosol droplets in the respiratory, urinary or gastrointestinal tract [reviewed in (Russell, 2009)]. ECM and the glycocalyx lining tissue surfaces form a physical barrier and the first line defence against intruding pathogens. They consist of various glycoproteins, proteoglycans, polysaccharides and tethered mucins that trap the Ad virions and limit infection (Pickles et al., 2000, Stonebraker et al., 2004). The viral replication cycle (Figure 1–6) is rapid, as the early phase takes 6–8 h and the late phase only another 4–6 h until mature virions are released. Ad5 recognises its primary entry receptor coxsackie and adenovirus receptor (CAR) (Kirby et al., 2000) via the fiber protein on the surface of the virion (Figure 1–7), while other serotypes use other primary attachment receptors (Table 1-1).

This initial attachment is accompanied by binding of the widely conserved Arg-Gly-Asp (RGD) motif (Ruoslahti, 1996) in the penton base protein to $\alpha v\beta3/5$ integrins on the cell surface. Integrins are structural proteins that are connected to ECM via laminin, collagen IV, leukocyte-specific ligands and fibronectin, but also mediate cell-to-cell interaction (Ganguly et al., 2013). They belong to a large family of heterodimers that consist of non-covalently linked $\alpha$ and $\beta$ subunits, a transmembrane helix and a short cytoplasmic tail (Arnaout et al., 2007). Integrin changes from an inactive (low-affinity) form into an active (high-affinity) stage when it binds to its ligand (Cantor et al., 2015). The role of integrins in signalling pathways, cell migration, growth, differentiation and apoptosis are further discussed in a number of excellent reviews (Ruoslahti, 1996, Giancotti and Ruoslahti, 1999, Arnaout et al., 2007).
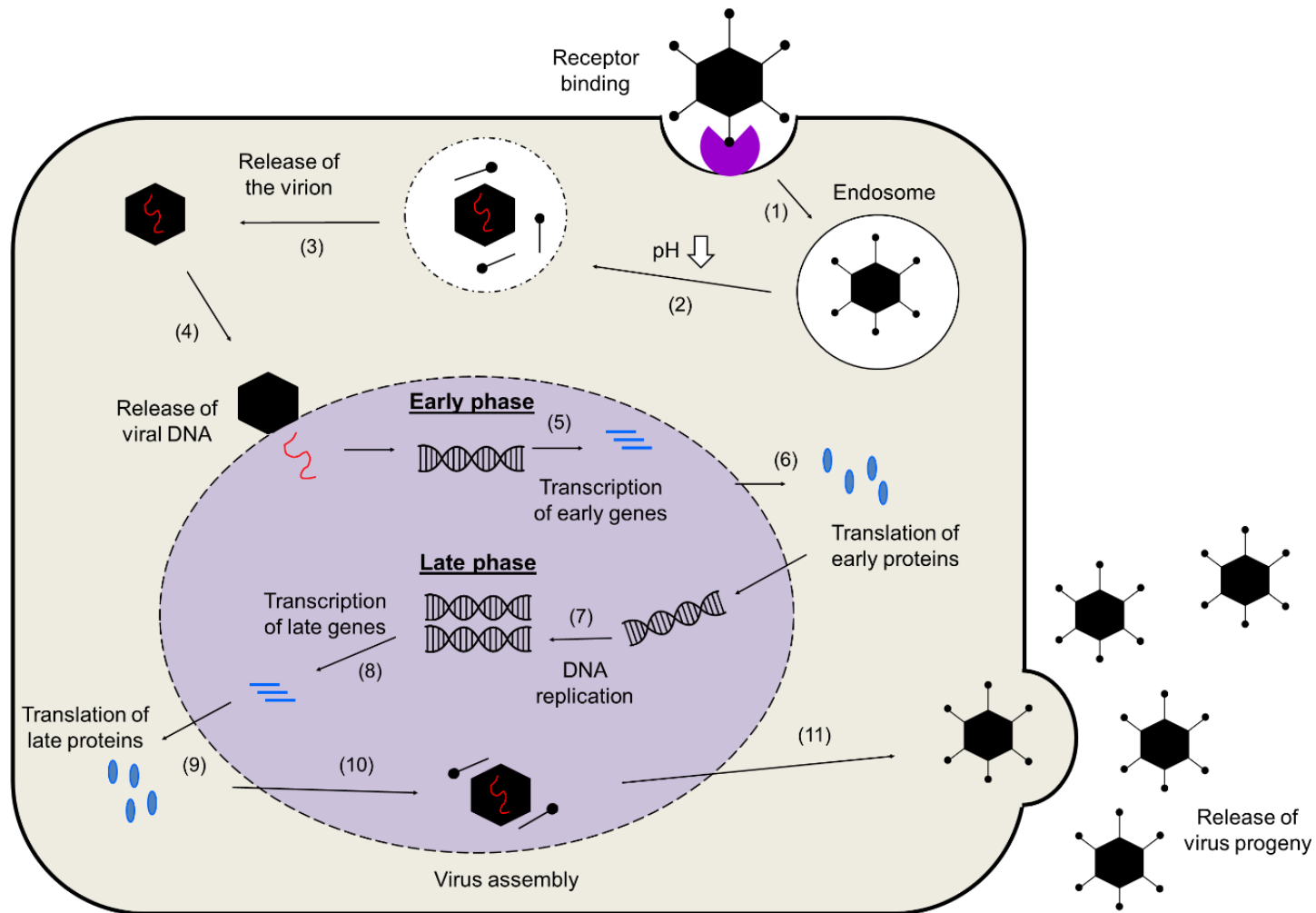
**Figure 1–6. Adenovirus life cycle.** (1) Virus binding to cellular receptors and endosomal entry, (2) endosomal acidification, (3) partial disassembly of the virion, (4) virus trafficking into the nuclear pore complex (NPC) via microtubules, and release of viral DNA, (5) transcription of early genes, (6) translation of early proteins, (7) DNA replication, (8) transcription of late genes, (9) transcription of late proteins, (10) virus assembly, (11) release of mature viruses by cell lysis. Figure adapted from (Russell, 2009, Russell, 2000, Coughlan et al., 2010).
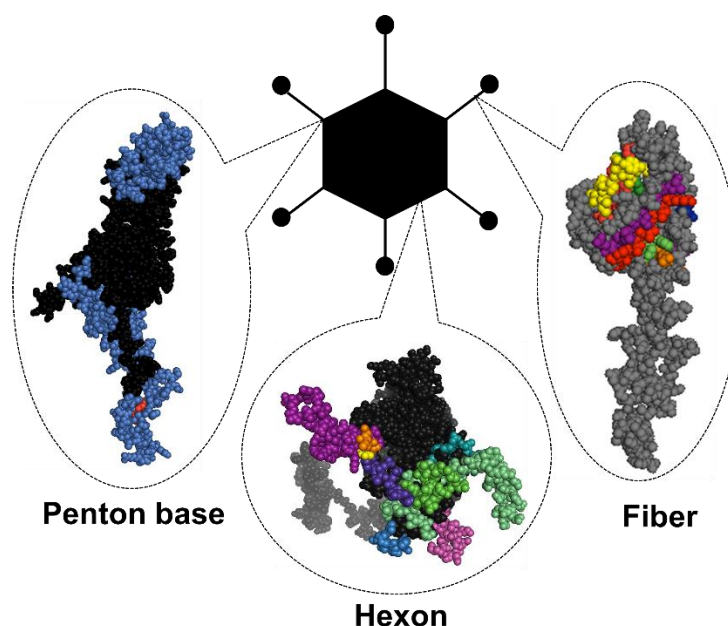
**Figure 1–7. Structural components of the adenovirus capsid.** Penton base, hexon and fiber (shown here as monomers) are the main building blocks of the eicosahedral capsid, but also contain the major immunogenic epitopes (highlighted in colours).

The coordinated interaction results in reorganisation of the actin cytoskeleton, which allows viral entry into the cell by phagocytosis via clathrin-coated pits (Figure 1–8). The acidification of the endosomes leads to disassembly of the virion as fiber proteins are cleaved by the activated virus-encoded protease and detached from the penton base (Nakano et al., 2000). Detached free fibers facilitate escape from the endosome and promote viral spread by opening up CAR-dependent, intracellular tight junctions (Walters et al., 2002). Excessive fiber production seems to be essential for epithelial permeability and viral spread. Fiber binding to CAR enables viral motility between cells, facilitating basolateral-to-apical trafficking and viral escape from the apical surface (Walters et al., 2002). The length of the fiber is dependent on the number of pseudorepeats (3–23) in the shaft domain, and varies between serotypes. Optimal fiber length (Roelvink et al., 1998, Shayakhmetov and Lieber, 2000) and flexibility (Wu et al., 2003) seems be crucial for entry of CAR-utilising Ads, for the geometrically challenging penton-integrin interaction to take place simultaneously with fiber-CAR interaction [reviewed in (Zhang and Bergelson, 2005)].

The partially disassembled virus is trafficked to the nucleus via microtubule network, either by direct binding to microtubule-associated motor proteins, such as dynamin, or by remaining in organelles that interact with microtubules and microtubule-associated motor proteins (Bremner et al., 2009) [reviewed in (Leopold and Crystal, 2007)]. The virion binds to the nuclear pore complex (NPC) and releases

its genome into the nucleus. Early viral regulatory proteins aid the late viral DNA replication, as well as transcription and translation of late structural proteins. Viral assembly takes place in the nucleus. Mature virions are released from the cell surface by lysis, leading to host cell death. The entry pathways and life cycle are discussed in great detail in the excellent reviews (Russell, 2000, Russell, 2009, Coughlan et al., 2010).
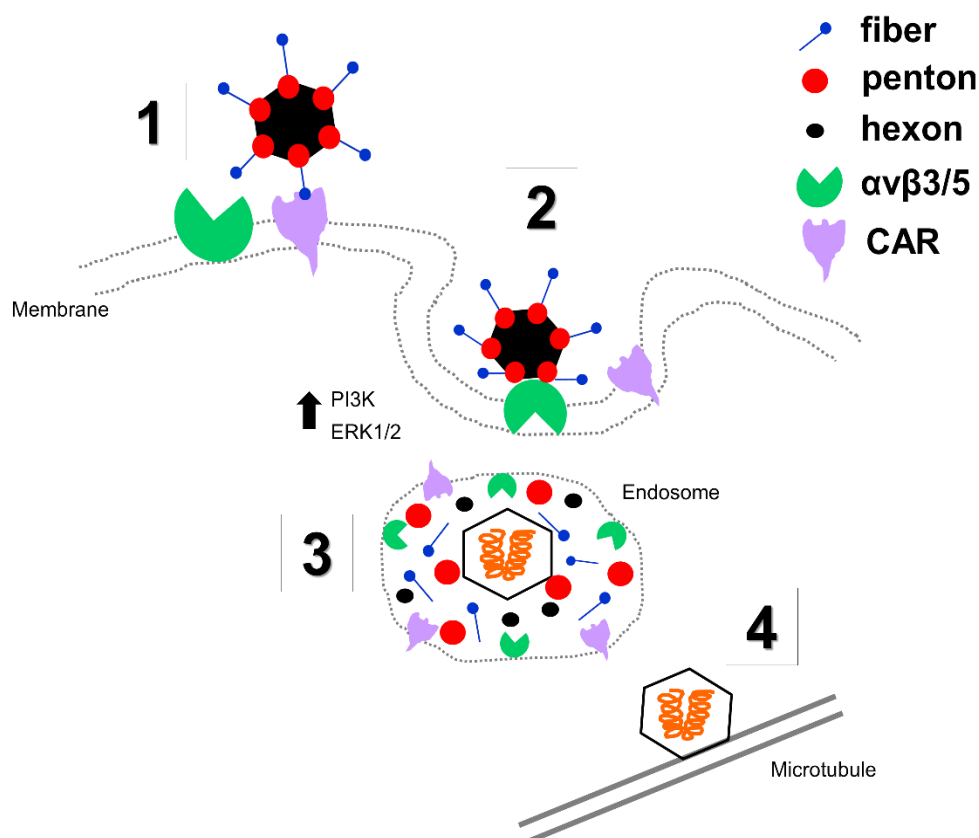


**Figure 1–8. Adenovirus attachment and internalisation.** (1) Primary attachment of adenovirus to the cell membrane occurs via coxsackie and adenovirus receptor (CAR) (Kirby et al., 2000). (2) Penton binding to αvβ3/5 integrins is required for viral internalisation (Wickham et al., 1993) via phagocytic clathrin-coated pits. Membrane permeabilisation is dependent on penton-mediated activation of phosphoinositide-3-OH kinase (PI3K) and ERK1/ERK2 mitogen pathways (Li et al., 1998) and excessive production of the fiber protein (Walters et al., 2002). (3) Viral components detach in the low pH endosome and are released to the cytosol. (4) The stripped virion is trafficked to the nucleus for DNA synthesis.

### 1.2.2 Viral structure

Ads are non-enveloped viruses that contain a linear, non-segmented, double-stranded 26−46 kb DNA genome that is transcribed in early and late phases of the viral life cycle (Figure 1–9A). Hexon (II), penton base (III), and fiber (IV) constitute the viral eicosahedral capsid (Figure 1–9B) and are responsible for viral tropism and immunogenicity. The minor proteins – IIIa, VI, VIII, IX and IVa2 – are associated with the capsid and have structural roles in the virion. The core proteins V, VII, μ peptide, terminal protein (TP) and are associated with the DNA, and the virus-coded protease

(Pr) is essential for viral assembly. The 5' terminus of the DNA is attached covalently to the TP and the molecule carries inverted terminal repeats (ITRs) at both termini. The early genes are organised in gene transcription cassettes, E1–E4, while L1–5 cassettes code for the late genes. Ad genome also codes for a set of VA RNAs that are not translated but are involved in cellular defence mechanisms. The genomic structure and roles of Ad proteins are discussed in detail in comprehensive reviews (Russell, 2000, Russell, 2009).

Main capsid proteins contain the major antigenic epitopes of the Ad particle (Figure 1–10). The Ad5 fiber is a homotrimeric ~ 62 kDa protein, each monomer containing 581 amino acids, and it is located on the 12 vertices of the eicosahedral capsid. It consists of a globular knob domain containing the receptor-binding domain that mediates binding to the native receptor CAR. Residues Ser408, Pro409, Tyr477 and Leu485 are known to be the key amino acid residues for CAR binding (Kirby et al., 2000). The fiber knob has a distinct electropotential in different Ad serotypes (Arnberg et al., 2002), which is likely to be crucial for their receptor binding properties. Distinct protruding loop structures with the 9 main antigenic epitopes (A–I) are involved in elicitation of serotype-specific nAbs (Xia et al., 1994). The C terminus of the fiber is a flexible shaft structure, mediating contact to the underlying penton protein that plays a central role in endosome-mediated entry into host cells via αvβ3/5 integrins [entry pathway reviewed in (Russell, 2009)].
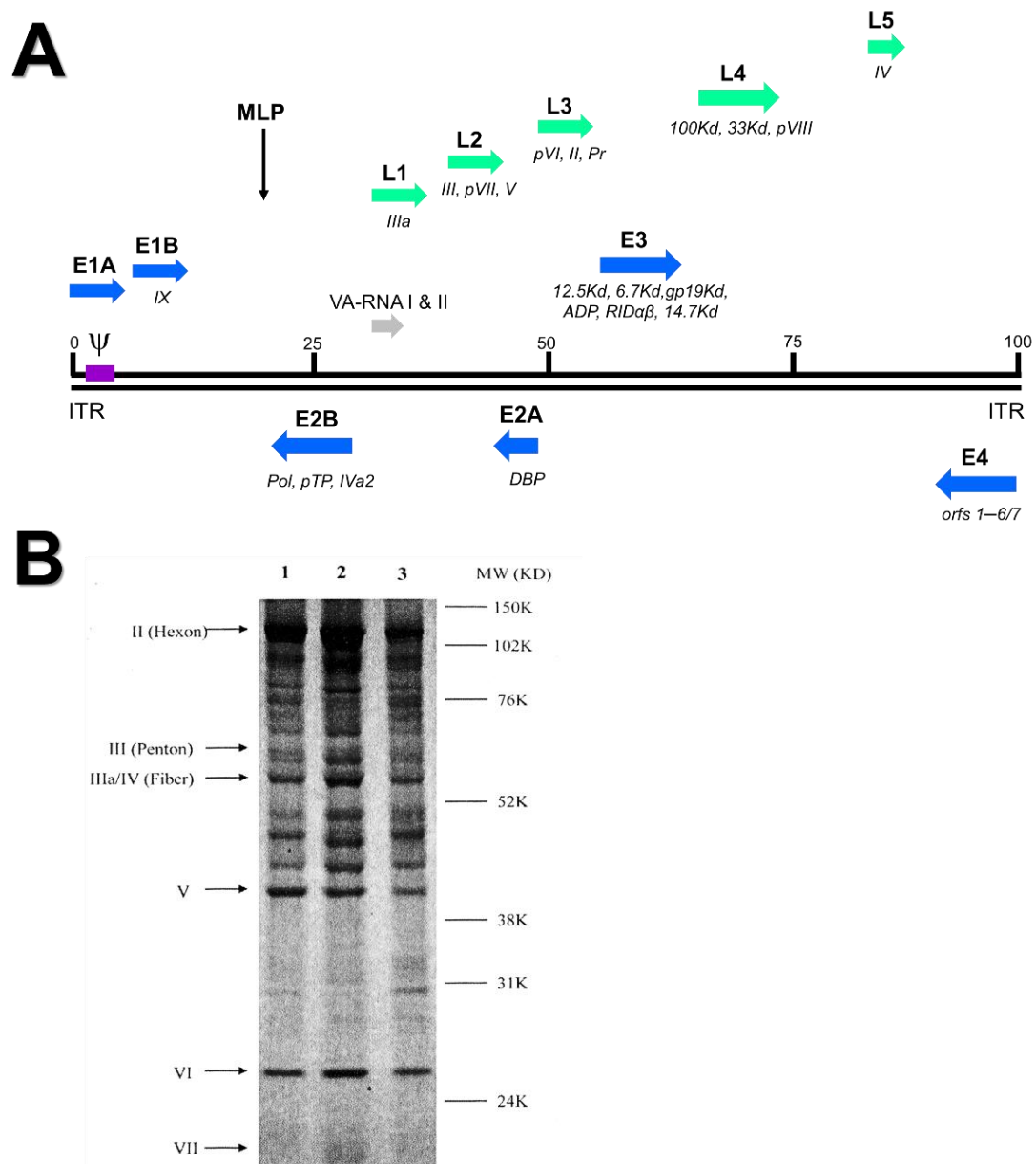
**Figure 1–9. Adenovirus structural components.** (A) Viral genomic structure. The early transcripts are in blue, late transcripts in green and protein products in italics. Pr, protease; MLP, major late promoter; ITR, internal terminal repeat. (B) Silver staining of adenoviral capsid proteins. $5 \times 10^{10}$ denatured virus particles/lane run on a 9 % SDS-PAGE gel and stained using Pierce silver staining kit (Thermo Scientific). Lane 1) Ad5-CMVLacZ, 2) Ad5-CMV-LacZ with hexon hypervariable region 5 (HVR5) mutations, 3) Ad5-CMV-LacZ with hexon hypervariable region (HVR7) mutations. Reproduced with permission from (Parker et al., 2014).

Fiber plays a key role in mediating viral endosome-cytoplasm transition through the detachment of the fiber protein and its membrane lytic activity in the low pH endosome. Ad serotypes have fiber shafts of variable lengths. Both the length and flexibility of the fiber protein are central in viral cellular uptake. This has been demonstrated by pseudotyping the long Ad5 shaft with short shafts from other serotypes, which resulted in reduced infectivity and attachment (Wu et al., 2003).

37

Introduction of point mutations into the KKTK motif within the fiber shaft showed impaired flexibility and drastically reduced cell transduction (Wu et al., 2003, Bayo-Puxan et al., 2006, Kritz et al., 2007). The KKTK motif was previously considered to be involved in Ad5-mediated hepatic delivery via heparan sulfate proteoglycan (HSPG) interactions (Smith et al., 2003, Bayo-Puxan et al., 2006). However, more recent studies demonstrate it to be non-essential for the interaction and rather to exist at an essential 'hinge region' within the shaft protein, where modification of this motif renders the fiber inflexible and unable to interact with cellular αvβ3/5 integrins (Bayo-Puxan et al., 2006, Di Paolo et al., 2007, Kritz et al., 2007, Corjon et al., 2011).

The homotrimeric hexon is the largest (~ 130 kDa) and most abundant capsid component, with 240 pseudo-hexagonal trimers lining the 20 facets of the virion surface. Hexons are classified into H1–H4 based on their interactions with neighbouring penton proteins. The hexon harbours the main neutralising epitope ε that can be utilised for serotyping by neutralisation tests, while the γ determinant in the fiber knob is responsible for hemagglutination properties. However, diagnostic typing is often non-exclusive due to cross-reactivity, resulting from extensive intra- and interspecies recombination (Madisch et al., 2005). They have up to nine HVRs (Khare et al., 2012) (dependent on the serotype) on the surface-exposed epitopes of the molecule (Figure 1–10B), which represent major antigenic targets for nAbs following virus challenge (Sumida et al., 2005, Roberts et al., 2006). Anti-hexon nAbs can act at both the extracellular level to sterically limit cellular association, or at the intracellular level to prevent virus uncoating and nuclear entry of viral DNA (Varghese et al., 2004). It has also been suggested that innate anti-Ad5 immune responses can be triggered by recognition of coagulation factor 10 (FX; Stuart-Prower factor) bound on the hexon protein (Doronin et al., 2012). On the contrary, a recent study reports the role of FX in shielding the Ad5 capsid from immune attack and subsequent neutralisation by natural IgM and complement proteins (Xu et al., 2013). Ad5 hexon HVRs have been suggested to be the specific sites determining sensitivity to the innate immune neutralisation (Ma et al., 2015), particularly following intramuscular (i.m.) vaccination or vector challenge (Bradley et al., 2012a, Bradley et al., 2012b). The exact target of anti-fiber nAbs remains a hot topic of debate, with compelling evidence that the antigenic loops within the fiber knob form the major immunodominant domains (Myhre et al., 2007, Bradley et al., 2012a), at least following a native Ad5 infection (Särkioja et al., 2008). Ad entry into the airway epithelia results in over-expression of the fiber protein (Walters et al., 2002) and thus directly exposes the fiber to the innate immune recognition mechanisms as it is the

most abundant viral component in the early stage of infection. There remains significant controversy surrounding the determination of primary antigenic determinants of the Ad5 virion, as earlier reports suggest that the fiber protein does not play a central role in nAb production (Gall et al., 1996), while more recent studies have demonstrated its involvement in eliciting the majority of anti-Ad5 nAbs following a natural inoculation (Särkioja et al., 2008). The role of anti-hexon and -fiber nAbs is discussed further in following sections.

The third major capsid building block is the penton base, a homopentameric ~82 kDa protein (Figure 1–10C) located on the base of each fiber trimer. The penton base protein is involved in viral internalisation, mediated by binding to αvβ3/5 integrins on the cell surface (Wickham et al., 1993) via the conserved integrin-binding RGD epitope (amino acid residues 485–488 (Neumann et al., 1988, Zubieta et al., 2005)). A number of integrin ligands involved in cell adhesion, such as fibronectin, vitronectin, fibrinogen, vWF, thrombospondin, laminin, entactin, tenascin, osteopontin and some collagens, have been shown to carry the RGD motif that mediates the attachment to a variety of integrin subtypes [reviewed in (Ruoslahti, 1996)]. The penton has three immunodominant neutralising epitopes – one of which overlaps with the RGD motif – that may contribute to virus neutralisation mainly at the internalisation step of the infectious cycle (Hong et al., 2003). Anti-RGD antibodies have been suggested to have a non-neutralising role in Ad infection (Hong et al., 2003). Ad5 binding to cellular αvβ3 integrins on marginal zone macrophages (MZMΦ) in the spleen (area between the red and white pulp) via the penton RGD motif has been shown to contribute to innate immune activation by triggering the IL-1α activation and subsequent IL-1RI-dependent induction of cytokine and chemokine C-X-C motif 1 (CXCL1) and CXCL2 production, as was demonstrated in a study utilising an Ad5 vector with RGD motif deletion (Ad5ΔRGD) (Di Paolo et al., 2009). Ad5ΔRGD vectors with an Ad35-pseudotyped short fiber (Chroboczek et al., 1995) were shown to have retained cellular attachment but an impaired internalisation, which may indicate role for this motif in endosomal escape and the importance of penton-integrin interactions for CD46-utilising species B Ads (Shayakhmetov et al., 2005a). Additionally, using Ad5 vectors with a point mutation that abolishes integrin-binding (RGD > RGE) resulted in reduced splenic uptake and attenuated inflammatory responses in mice (Bradshaw et al., 2012). These observations suggest a central role for RGD motif not only in the viral internalisation, but also in the activation of anti-Ad innate immune responses.
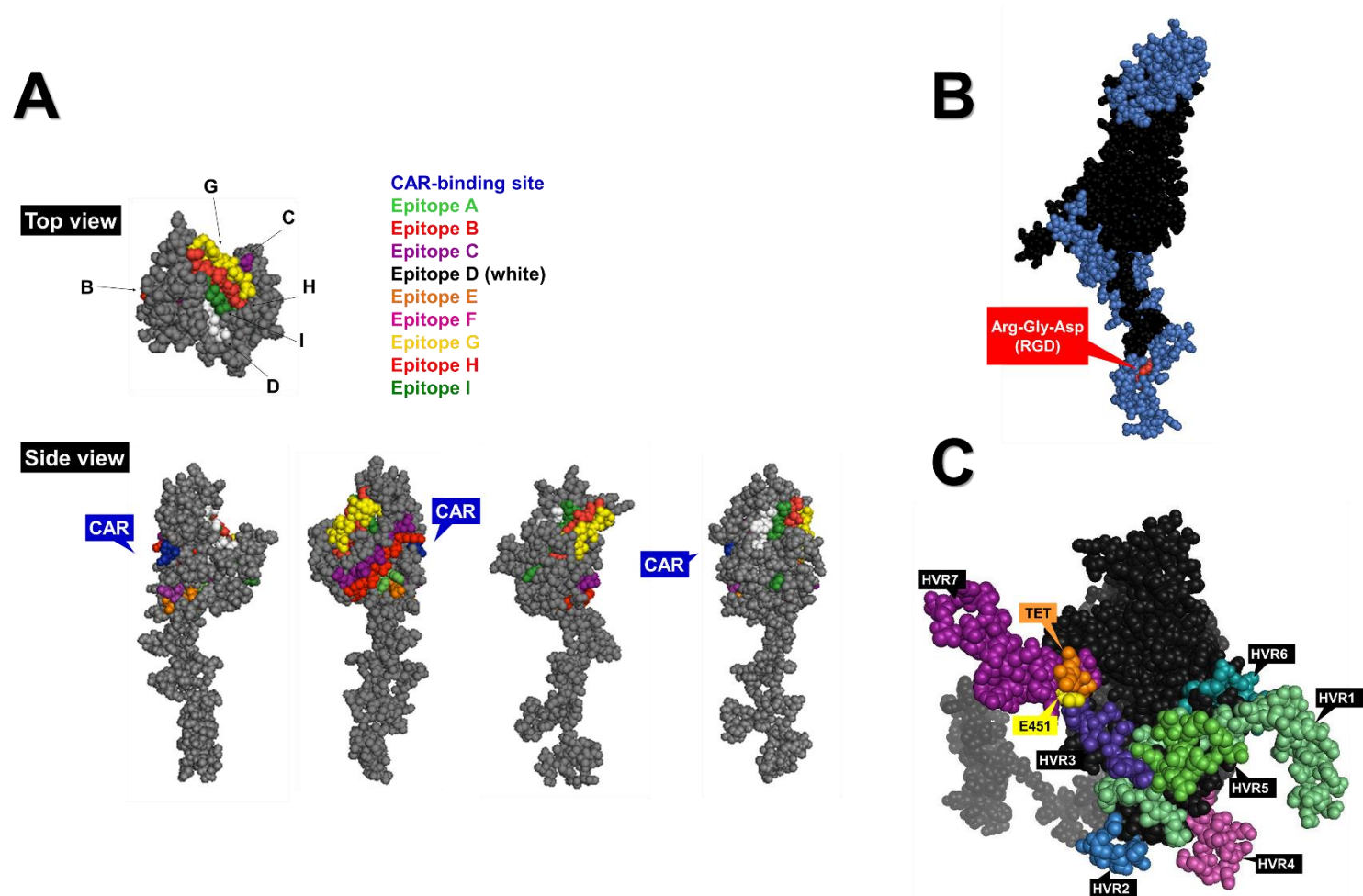
**Figure 1–10. The major antigenic proteins of adenovirus.** (A) Side and top view of the Ad5 fiber monomer. Main antigenic epitopes are highlighted in distinct colours (see legend) and CAR-binding site is indicated in blue (Xia et al., 1994), PDB ID: 1KNB. CAR, coxsackie and adenovirus receptor. (B) The Ad2 penton base monomer. The three main antigenic sites (Hong et al., 2003) are highlighted in blue, integrin-binding motif Arg-Gly-Asp (RGD) in red (Zubieta et al., 2005, Cao et al., 2012); PDB ID: 1X9P. (C) Top view of the Ad5 hexon monomer with the major antigenic epitopes. Hypervariable regions (HVRs) 1–7 shown in different colours; the site for point mutation (E451Q) central for ablation of human coagulation factor 10 (FX) binding is shown in yellow; TET motif central for the high affinity interaction with FX shown in orange (Irons et al., 2013). Modified from (Khare et al., 2012); PD ID: 3TG7. All models were constructed in PyMol version 1.1eval.

### *1.2.3 Cell and tissue tropism*

Ads utilise multiple cellular entry receptors (Figure 1–11) in a serotype-dependent manner (Table 1–1). The most widely used cell attachment receptor for all, except species B, Ads is CAR. It belongs to the family of immunoglobulin-like surface molecules and co-localises in the tight junctions with zonula occludens-1 (ZO-1) protein on polarised epithelial cells [reviewed in (Coyne and Bergelson, 2005)]. It is ubiquitously expressed in all human organs, including erythrocytes and platelets (Carlisle et al., 2009, Seiradake et al., 2009).
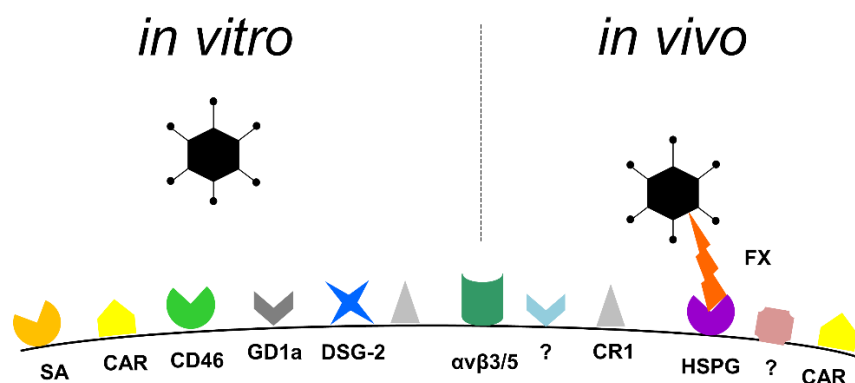


**Figure 1–11. Adenovirus receptor tropism *in vitro* and *in vivo*.** Adenoviruses utilise CAR as their main entry receptor *in vitro*, while *in vivo* entry is dictated by FX-mediated binding to HSPGs. CAR, coxsackie and adenovirus receptor; CD46, membrane co-factor protein; CR1, complement receptor 1; DSG-2, desmoglein 2; GD1a, disialoganglioside; HSPG, heparan sulphate proteoglycan.

**Table 1–1. Human adenovirus classification, receptor usage and tissue tropism.** CAR, coxsackie and adenovirus receptor; DSG-2, desmoglein-2; HSPG, heparan sulfate proteoglycan; VCAM-1, vascular cell adhesion molecule 1; SR, scavenge receptor; MHC1, major histocompatibility complex class 1; SA, sialic acid; nd, not determined. Table modified from (Uusi-Kerttula et al., 2015a).

| Species | Serotypes | Receptors | Tropism |
|---|---|---|---|
| A | 12, 18, 31 | CAR | Cryptic (enteric, respiratory) |
| B1 | 16, 21, 35, 50 | CD46 (Wang et al., 2007), CD80, CD86 | Respiratory, ocular |
| B2 | 3, 7, 14, 34, 35 | DSG-2 (Wang et al., 2011), CD80, CD86 | Renal, ocular, respiratory |
| B1/2 | 11 | CD46, DSG-2 (Wang et al., 2011) | Ocular, respiratory |
| C | 1, 2, 5, 6 | CAR (Kirby et al., 2000), HSPG, VCAM-1, SR, MHC1-α2 | Respiratory, ocular, lymphoid |
| D | 8–10, 13, 15, 17, 19, 20, 22–30, 32, 33, 36–39, 42–49, 51, 53 | SA (Burmeister et al., 2004), CD46 (Chen et al., 2010, Li et al., 2012), CAR (Chen et al., 2010), GD1a glycan (Nilsson et al., 2011) | Ocular, Enteric |
| E | 4 | CAR | Ocular, respiratory |
| F | 40, 41 | CAR | Enteric |
| G | 52 | nd | Enteric |

Following a natural respiratory tract infection with wild type Ad5, an early event involves the over-expression of the Ad fiber protein which disrupts tight junctions, thus facilitating viral translocation from the basolateral to apical surface of the epithelial cells and enabling onward virus spread (Walters et al., 2002). Ad3/7/11 binding to DSG-2 has been shown to stimulate epithelial-to-mesenchymal transition (EMT) that is a central event in carcinogenesis (Wang et al., 2011). This may hinder their use as anti-cancer vectors. Ads primarily utilise the fiber knob-CAR -mediated pathway for cell entry *in vitro*. Tropism *in vivo* however, appears to be dictated by a variety of other factors including the high affinity interaction between human coagulation factors (FX in particular) that largely determines their hepatic tropism following contact with the blood (Waddington et al., 2008, Alba et al., 2009) [reviewed in (Coughlan et al., 2010)]. These 'adapter molecules' – multiple vitamin K –dependent coagulation factors, play a central role in Ad5 hepatotropism (Parker et al., 2006, Waddington et al., 2007). FX is a serine endopeptidase that is part of the coagulation cascade (Figure 1–12A) and is activated upon vascular injury.
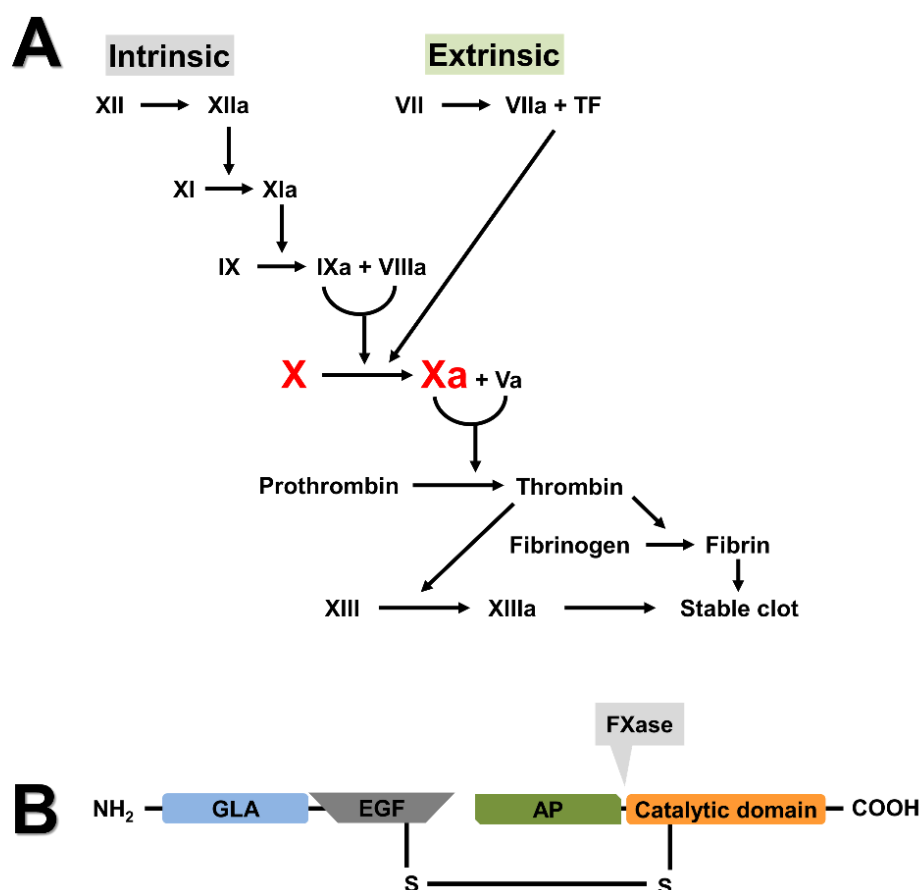


**Figure 1–12. Proteins of the coagulation pathway.** (A) The coagulation cascade. TF, tissue factor. Modified from (Davie et al., 1991). (B) The structure of human coagulation factor 10 (FX). The light N-terminal chain consists of 11 γ-carboxyglutamic acid (GLA) residues that are responsible for $Ca^{2+}$-mediated binding to cellular domains, and two epidermal growth factor (EGF) homology domains. The heavy C-terminal chain has a 52-amino acid activation peptide (AP) that is enzymatically cleaved by the FXase, and a latent serine protease domain (Davie et al., 1979, Jackson and Nemerson, 1980).

FX is a two-chain molecule that consists of several domains with specialised functions (Figure 1–12B) and circulates freely in the blood at a concentration of approximately 8 µg/ml. The high affinity, $Ca^{2+}$-dependent interaction between hexon and hepatocyte HSPGs is effectively 'bridged' by FX (Waddington et al., 2008, Parker et al., 2009). Ad5 HVR5, HVR7 (and possibly HVR3), located on the top of the hexon trimer (Kalyuzhniy et al., 2008, Waddington et al., 2008), bind to the γ-carboxylated glutamic acid (GLA) domain of FX, guiding the extensive liver sequestration of Ad5-based vectors (Waddington et al., 2008). A recent study has shed light on the role of HSPGs in the FX-mediated Ad hepatocyte transduction, suggesting the involvement of additional or auxiliary receptors (Zaiss et al., 2015). The FX:hexon interaction may have a potentially critical role that protects the Ad5 capsid from complement-mediated immune attack and destruction by natural antibodies. This recent finding casts further doubt over the role of FX as a hepatotropic adaptor or in protection of the Ad5 virion from immune attack (Xu et al., 2013). Notably, species D Ads have been shown to exhibit low or abolished affinity to FX (Figure 1–13) and subsequently reduced liver transduction relative to Ad5 (Waddington et al., 2008). This is likely to have important implications for design of novel vector candidates based on these rare serotypes.
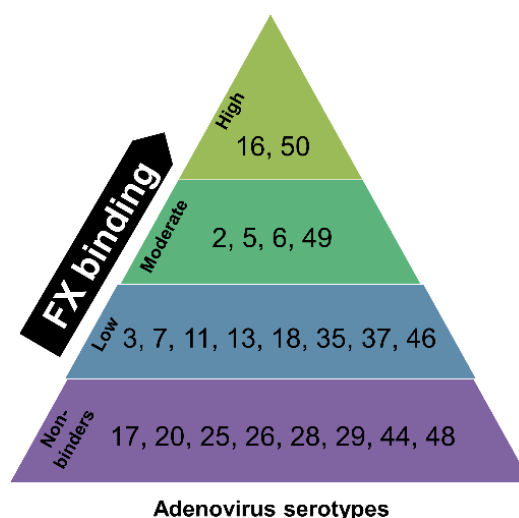


**Figure 1–13. Classification of adenovirus serotypes based on affinity to human coagulation factor 10 (FX).** Modified from (Waddington et al. 2008). Species D viruses are attractive vector candidates due to their low affinity to FX.

## 1.3 Adenovirus vectors for cancer therapy

The Ad5 genome has been extensively studied over the past six decades, following their initial discovery in the 1950's. Ads are popular gene therapy vectors because their genome can easily be altered by a number of well-described cloning and recombineering (Stanton et al., 2008) methods [first-generation vectors reviewed in (Danthinne and Imperiale, 2000)]. This involves deletions of genes essential for viral

replication and insertions of heterologous transgenes and targeting peptides into permissive regions in the capsid proteins. The fiber knob HI loop (Krasnykh et al., 1998, Krasnykh et al., 1996, Belousova et al., 2008, Belousova et al., 2002, Nicklin et al., 2001, Kritz et al., 2007, Coughlan et al., 2009a, Uusi-Kerttula et al., 2015b, Uusi-Kerttula et al., 2016), penton (Wickham et al., 1995) and hexon HVRs (Vigne et al., 1999) are frequently studied locations for peptide insertions. Ads are inherently lytic in their host cells, and release virus progeny to infect neighbouring cells. Their compact genome can be modified to incorporate large therapeutic transgenes up to 105 % of genomic size (Bett et al., 1993), which allows for the unique possibility of drug amplification in the TME, at the point of need. The therapeutic effect is amplified as the virus goes through repeated replication cycles and spreads through the tumour tissue. Another benefit is the good safety of Ad-based vectors as the pathogenicity of the wild type virus is low in immunocompetent individuals. Ads are able to infect both non-replicating and replicating cells (Barnes et al., 2002, Hawkins et al., 2002), which is an excellent feature for therapeutic purposes in a variety of tissue types. Delivery and expression of therapeutic transgenes into the nucleus makes Ads an attractive gene therapy vector. The advantages of Ads as gene therapy vectors are discussed further in comprehensive reviews (Russell, 2009, Russell, 2000, Coughlan et al., 2010).

### 1.3.1   *Oncolytic & conditionally-replicative adenoviruses*

Viruses often exploit the similar cell cycle aberrations as cancer cells for hijacking the host cell's replication machinery, and it is this overlap that makes viruses great cancer-attacking vectors. Ads are not inherently tumour-selective, unlike some other viruses such as reoviruses, some measles strains and vesicular stomatitis virus (VSV) (Hawkins et al., 2002). However, oncolytic Ads can be engineered by a number of genetic engineering strategies, including control mechanisms that target *transductional* (viral entry) and *transcriptional* (replication) processes and render the virus cancer-selective. Generally, this involves the combination of attenuation of genes essential for viral replication to achieve high selectivity and safety, and incorporation of genes that are expressed only in neoplastic cells. Substitution of the deleted gene regions in replication-deficient vectors with cancer-selective promoters can be utilised to generate conditionally-replicative Ad vectors (CRAds), which promotes restricted lysis of cancer cells with defective signalling pathways and/or characteristic TME.

Ad vectors have undergone three generations of development, involving the deletion of early genes E1–E4 that are central for viral replication, viral DNA

transcription/replication of late genes, modulation of immune responses and metabolism of virus mRNA/host protein synthesis, respectively. The first generation Ads had a *E1/E3* mutation, a basic attenuating mutation for generation of replication-deficient vectors, while second generation Ads had *E4* deletion in addition to *E1* and/or *E3* deletion [reviewed in (Bauerschmitz et al., 2002, Kanerva and Hemminki, 2005)]. So called 'gutless' helper-dependent Ad vectors that lack all viral genes can be produced efficiently in a co-infection with a helper plasmid that complements missing genes (Ehrke-Schulz et al., 2016). The main benefits of these vectors are their high packaging capacity (up to 35 kb), low toxicity and low immunogenicity. However, their production is relatively cumbersome compared to AdEasy (Zeng, 2001) and other homologous recombineering methods that involve zero cloning steps (Stanton et al., 2008).

### 1.3.2 *Clinical history*

U.S. National Institutes of Health (NIH) has records of 123 completed or ongoing clinical trials (clinicaltrials.gov, 2016) for adenovirus therapies for cancer between 2006–2016 worldwide (Figure 1–14). Ad vectors have been modified to selectively replicate in cancer cells, mainly via introduction of selected deletions in viral genes *E1A* and *E1B* that are responsible for viral replication, to target cells with defective p53 and retinoblastoma protein (pRB) pathways (Table 1–2).



Colors indicate the number of studies with locations in that region

Least ▬▬▬▬▬▬▬▬▬ Most

Labels give the exact number of studies

Source:https://ClinicalTrials.gov
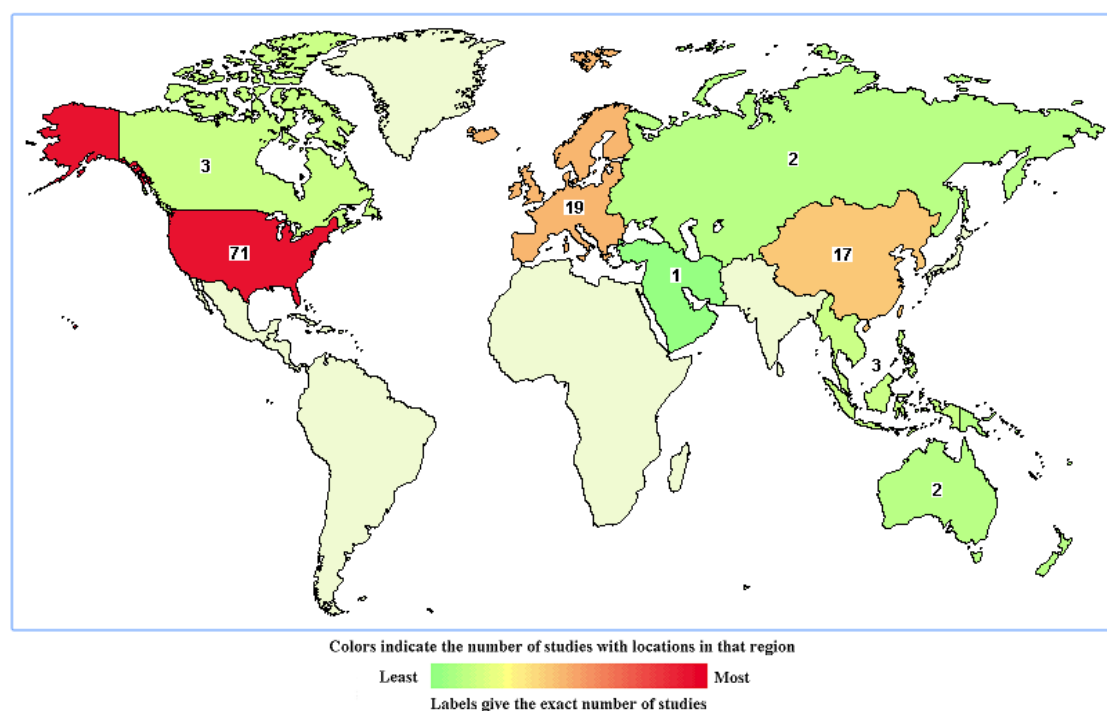
**Figure 1–14. Clinical trials involving adenovirus vectors for cancer treatment during the past decade.** Trials were searched using terms "adenovirus AND cancer" between 01 Jan 2006 and 24 Oct 2016. The search returned 123 completed or ongoing trials worldwide (clinicaltrials.gov, 2016).

The pRB tumor-suppressor pathway may be defective in all human cancer types (Sherr, 1996), which indicates its feasibility for cancer targeting (Fueyo et al., 2000). Wild type Ad E1A protein inactivates cellular pRB, which reverses transcriptional repression and enables transition from G1 to S phase (Sherr, 1996), allowing viral replication. One of the earliest attempts of an Ad therapy for ovarian cancer was a replication-deficient Ad (SCH 585000) expressing a wild type *p53* under a cytomegalovirus (CMV) immediate early promoter (Buller et al., 2002). I.p. delivery of the vector in phase I and II trials resulted in elevated levels of p53 targets, such as Bax and p21, but with a very high inter-patient variance, and a multitude of adverse events. Phase III trial combining surgery and conventional chemotherapy with or without Ad gene therapy was commenced but soon halted due to unexpectedly low efficacy in the treatment arm – the results from this study were never reported (Zeimet and Marth, 2003). Oncolytic Ad vectors tailored for ovarian cancer treatment are discussed in an excellent review (Young and McNeish, 2009).

**Table 1–2. Selected oncolytic Ads involved in pre-clinical and clinical studies.** Ad, adenovirus; EnAd, enadenotucirev; ER, endoplasmic reticulum; GM-CSF, granulocyte-macrophage colony stimulating factor; HIF, hypoxia-inducible factor; pRB, retinoblastoma protein; Δ, deletion. For a list of vectors from early 2000, see (Chu et al., 2004).

| Name (serotype) | Gene controlled | Target | Mutations | References |
|---|---|---|---|---|
| ONYX-015 (Ad5) | *E1B 55kD* | p53 | *dl1520* | (Ganly et al., 2000) |
| ICOVIR-5 (Ad5) | *E1A* | pRB | Δ24; *dl922–947* (Fueyo et al., 2000) | (Cascallo et al., 2007, Nokisalmi et al., 2010) |
| HYPR-Ad5 (Ad5) | *E1A* | hypoxic cells | HIF | (Post and Van Meir, 2003) |
| ORCA-010 (Ad5) | *E3/19K* | ER retention domain | T1 | (Dong et al., 2014a) |
| ONCOS-102 (Ad5/3) | *E1A* | pRB | Δ24 + GM-CSF + chimaera | (Koski et al., 2010, Vassilev et al., 2015, Kuryk et al., 2016, Targovax, 2016) |
| EnAd (Ad3/11p) | *ΔE1A/E1B (E4orf4)* | not known | chimaera | (Kuhn et al., 2008, Tedcastle et al., 2015, PsiOxus, 2016) |

The first oncolytic Ad5-based vector ONYX-015 was approved more than a decade ago by the Chinese authorities for treatment of head and neck cancers (Ganly et al., 2000). The product of the Ad *E1B* 55 kD gene binds to and 'neutralises' p53, preventing p53-induced cell death and apoptosis, and allowing viral replication (Wiman, 2007). ONYX-015 vector has a complete deletion of *E1B* (*dl1520*) that renders it capable of selectively infecting p53-defective cells (Bergh et al., 1995).

However, since the treatment is only effective on p53-deficient tumours – an estimated 50 % of all cancer patients (Vogelstein et al., 2000) – complementing strategies are needed. However, ~ 97 % of ovarian cancer patients with HGS-OC have been tested positive for defective p53 pathways in large scale genomic analyses (Ahmed et al., 2010, Bell et al., 2011), highlighting the potential of targeting this pathway in ovarian cancer. Contradicting data indicates that ONYX-015 may not be as p53-specific as was previously thought. The vector has been shown to replicate in some cancer cells with an intact p53-pathway, which may come down to the involvement of Mdm2 and p14ARF pathways [reviewed in (McCormick, 2000)]. Clinical Ad applications based on the p53-pathway are reviewed in (Chen et al., 2014).

The C-X-C chemokine receptor 4 (CXCR4) is over-expressed in EOC cells and primary cultures, but not detected in healthy ovarian epithelium (Scotton et al., 2001). Double-targeting approach combining the insertion of CXCR4 promoter and Ad5 fiber pseudotyping from Ad3 (Ad5-CXCR4-F5/3) showed increased replication in ovarian cancer cell lines but decreased replication in normal tissues, indicating beneficial selectivity and oncolytic efficacy for this virus (Rocconi et al., 2007). A 24-base pair deletion (Δ24; *dl922–947*) in the pRB-binding domain of *E1A* efficiently restricts viral replication into proliferating, pRB-defective cells (Fueyo et al., 2000). A triple-targeted Ad5 with an epithelial cancer-induced cyclo-oxygenase (Cox2) promoter (Kanerva et al., 2004) driving the *E1A* mutation Δ24 and pseudotyped fiber knob from Ad3 (Cox2-Δ24-Ad5/3), showed up to 100 000-fold increased transduction compared to Ad5 wild type (Bauerschmitz et al., 2006). Unfortunately, neither of these EOC-specific vectors have been tested in clinical studies. An Ad5-based ICOVIR-5 vector combines *E1A* transcriptional control by EF2 promoter mutation with Δ24 mutation and an RGD-4C modification in the fiber HI loop (Cascallo et al., 2007, Nokisalmi et al., 2010), and has shown promising safety and anti-tumour efficacy in phase I trials for advanced melanoma (Nokisalmi et al., 2010). A HYPR-Ad5 vector developed by Post and colleagues utilises hypoxia-dependent *E1A* expression and selective lysis of hypoxic cells that dominate in chemo- and radiotherapy-resistant in solid tumours (Post and Van Meir, 2003).

ORCA-010 vector carrying a novel 'T1' mutation has shown enhanced oncolytic efficacy and safety in pre-clinical *in vivo* studies, and seems to be significantly more potent than the licensed ONYX-015 (Dong et al., 2014a). T1 mutation is an insertion of a single adenine base at position 445 within the endoplasmic reticulum (ER) retention domain of the *E3/19K* gene that has been shown to greatly enhance oncolytic potency of Ad5, presumably due to increased release of the virus progeny

from the ER and efficient spread within the tumour mass (Gros et al., 2008). Ad5/3-Δ24-GMCSF (ONCOS-102) – a chimaeric Ad5/kn3 vector armed with a potent immunostimulatory granulocyte-MΦ colony stimulating factor (GM-CSF) – has completed phase I clinical studies with increased cancer-specific CD8+ T-cell responses and good safety profile in heavily pre-treated patients with injectable solid advanced tumours (Vassilev et al., 2015), and is ready to enter four new phase I/II trials (Targovax, 2016). Phase I studies demonstrated enhanced immunologic response, good safety and a significant correlation between anti-viral and anti-tumour T-cells, while safety nor efficacy were affected by the Ad5/kn3 fiber pseudotyping (Kanerva et al., 2013). Recently, immunogenic cell death and a synergistic anti-cancer effect was observed using ONCOS-102 in combination with chemotherapy (pemetrexed and cisplatin or carboplatin) for the treatment of malignant mesothelioma in a mouse xenograft model (Kuryk et al., 2016).

A novel 'directed evolution' approach was used to create the first wholly non-Ad5-based oncolytic species B vector, enadenotucirev (EnAd; previously ColoAd1). EnAd is a complex and highly potent chimaeric Ad3/Ad11p virus that was generated on several tumour cell lines through forced recombination between a pool of Ads from different subgroups. EnAd has a small 24-bp deletion in the region encoding E4orf4 that, in the context of Ad5, induces protein phosphatase 2A (PP2A)-mediated, p53-independent apoptosis (Branton and Roopchand, 2001). However, the oncolytic mechanism of EnAd is entirely apoptosis-independent and its enhanced potency may be related to the chimeric E4 region that may alter the expression of additional, yet unknown genes (Kuhn et al., 2008). EnAd has shown significantly improved selectivity and cancer-killing as compared to ONYX-015 (Kuhn et al., 2008), as well as superior blood persistence and oncolysis in the highly neutralising environment of the whole human blood (Di et al., 2014). EnAd is being developed by PsiOxus Therapeutics (Oxfordshire, UK) and is currently (autumn 2016) undergoing a number of phase I and II trials (PsiOxus, 2016). SPICE, a phase I clinical trial evaluates its use in combination with pembrolizumab for metastatic or advanced epithelial tumours. EVOLVE is a phase I/II trial assessing the safety, tolerability and efficacy of intravenously (i.v.) administered EnAd in patients with epithelial, colorectal or bladder solid tumours. OCTAVE is a phase I/II clinical trial in patients with platinum-resistant EOC, and assesses i.p. or i.v. delivery of EnAd, either alone or in combination with paclitaxel.

**Table 1–3. Adenovirus vectors in clinical trials for ovarian cancer.** Search was limited to years 2006–2016 and performed using Boolean operators "adenovirus AND ovarian cancer" and "oncolytic virus AND ovarian cancer". CR, complete resolution; EnAd, enadenotucirev; EOC, epithelial ovarian cancer; i.p., intraperitoneal; MTD, maximum tolerated dose; NA, not available; NCI, National Cancer Institute; PFS, progress-free survival; RR, response rate; SD, stable disease.

| Trial | Vector (+ chemotherapy) | Indications | Route | Primary endpoint | Stage | Best outcome |
|---|---|---|---|---|---|---|
| NCT00562003 | Ad5Δ24RGD | recurrent ovarian | i.p. | MTD | completed | 14/21 patients with stable disease (Kimball et al., 2010) |
| NCT00964756 | Ad5.SSTR/TK.RGD (ganciclovir) | recurrent ovarian / other gynaecologic | i.p. | toxicity | completed | 5/12 patients with SD, 1 patient with CR (Kim et al., 2012) |
| NCT02435186 | rec. Ad human p53 (cisplatin/paclitaxel) | recurrent EOC, Fallopian tube, primary peritoneal | i.p. | RR, PFS | not open yet | NA |
| NCT02028117 (OCTAVE) | Ad3/11p, EnAd (paclitaxel) | recurrent, platinum-resistant EOC | i.p. | MTD | recruiting | NA |

A recent review further discusses the administration schedule and compares single-shot regimens with triple-hit courses for oncolytic Ad and other anti-cancer vectors (Ruf and Lauer, 2015). The efficacy of Ad vectors as monotherapies remains frustratingly low (Ganly et al., 2000, Nemunaitis et al., 2001b), which is why combination therapies are now gaining ground in Ad therapies for ovarian (Table 1–3) and other cancers. Khuri and colleagues showed that intratumoural ONYX-015 injection in combination with cisplatin and 5-fluorouracil (5-FU) in patients with recurrent squamous cell carcinoma of the head and neck (SCCHN) showed objective response (63 %), with 27 % complete and 36 % partial responses (Khuri et al., 2000), which is significantly higher that phase I monotherapy trial outcomes with ONYX-015, where no objective responses were observed by conventional criteria (Ganly et al., 2000). Modest anti-tumoural activity was observed in a phase II study in SCCHN patients receiving i.t. ONYX-015 delivery, with reported 10 % complete response, 62 % stable disease, and 29 % progressive disease rates (Nemunaitis et al., 2001b). Combination of potent Ad vectors with existing gene-, chemo- and radiotherapies is likely to result in better therapeutic responses due to multiple mechanisms of cancer cell killing, viral sensitisation and long-lasting anti-tumour immune responses [reviewed in (Chu et al., 2004, Jiang et al., 2011, Russell et al., 2012)].

### 1.3.3 *Immuno-oncolytic applications & cancer vaccines*

The persistent dilemma in Ad cancer therapies is tackling evasion of immune recognition whilst simultaneously stimulating long-term immunity against TAAs. Cancer immunotherapy is a currently a hot research topic in the cancer therapy field, and Ad-based vectors have great promise within this arena. Novel viral vectors commonly utilise two main mechanisms for host immune activation: (A) immune priming or cancer vaccination – lysis of infected tumour cells that leads to innate and adaptive immune responses against TAAs, and (B) localised expression of immunoregulatory agents that modulate signalling pathways defective in different cancer types (Figure 1–15) [reviewed in (Lichty et al., 2014)]. TAAs are derived from proteins synthesised by the tumour cell, and may be either membrane-bound, secreted, cytoplasmic or nuclear-localized (Zarour et al., 2003). For an excellent review on the use of Ad vector for immuno-oncolytic applications, see (Jiang et al., 2015). Recent years have seen the development and approval of multiple therapeutic mAbs called immune checkpoint inhibitors, that aim to break the cancer-driven immune tolerance. Suppressors of immune signalling pathways – cytotoxic T-lymphocyte-associated protein 4 (CTLA-4; CD152) and programmed cell death protein 1 / programmed cell death protein ligand 1 (PD-1/PD-L1) – are currently the

most commonly targeted molecules for mAbs. Ipilimumab and tremelimumab are anti-CTLA-4 antibodies, while an anti-PD1 mAbs nivolumab and pembrolizumab dampen down the PD-1 pathway, and atezolizumab targets PD-L1. They have already been approved for several indications by U.S. Food and Drug Administration (FDA) and European Medicines Agency (EMA), and are undergoing extensive clinical evaluation in various cancer types. Immune checkpoint blockade strategies for cancer immunotherapies are further discussed in an excellent review (Postow et al., 2015).

Immuno-oncolytic Ad vectors can potentially be used in combination with conventional chemo- and radiotherapies in order to target both primary and metastatic tumours, and to achieve an enhanced and long-lasting therapeutic effect. Combining the oncolytic activity of the virus with an immunostimulatory agent is likely to result in improved tumour eradication. Oncolytic Ads can be modified to carry 'cargo' molecules – to express mAbs directed towards TAAs, T-cell receptors, immune checkpoint inhibitors, cytokines, and programmed to target DCs and TILs. Ads infect cells in a receptor-dependent manner, and elicit subtle innate and adaptive immune responses, which makes them feasible cancer vaccine vectors for priming and stimulation of the host's immune system [reviewed in (Majhen et al., 2014)]. Ads can be rendered tumour-selective, *in situ* cancer vaccines, providing higher cancer-specificity and better safety margin. Additionally, they are able to kill cancer cells through a range of mechanisms from direct virus-mediated cytotoxicity, cell death due to anti-angiogenesis and vasculature targeting, to cytotoxic immune effector-induced cytotoxicity by apoptosis, necrosis, and autophagy (Woller et al., 2014). In an ideal situation, the strong elicited immune memory will be able to recognise and attack the tumour cells in the event of a relapse or development metastatic tumours at any anatomical location later in the patient's life. Immuno-oncolytic applications are discussed in greater depth in the recent review by our group (Uusi-Kerttula et al., 2015a).
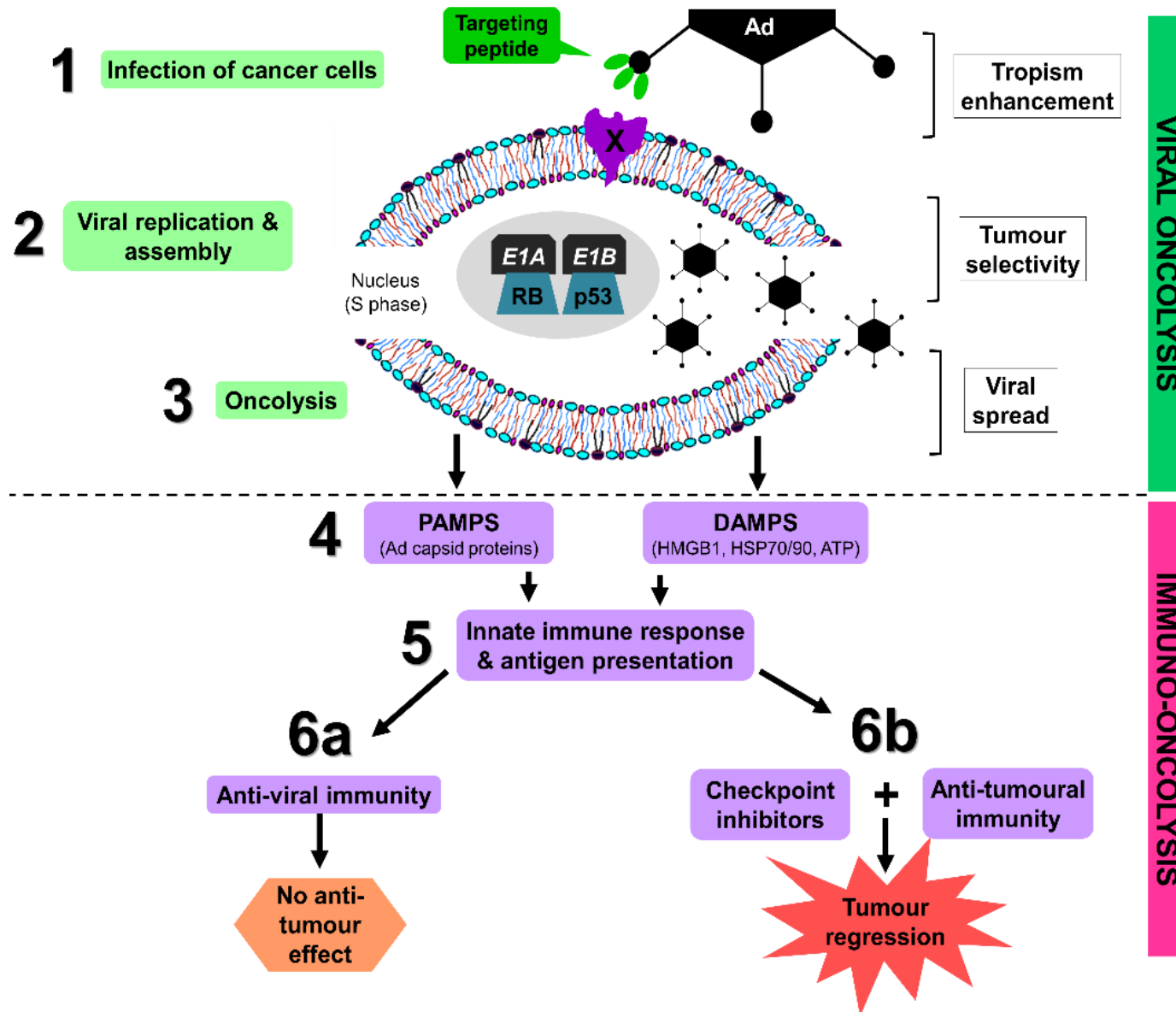
**Figure 1–15. The dual mechanism of oncolytic virotherapy.** (1) Tropism-modified adenoviruses (Ad) infect cells via cancer-specific cell receptors (X). (2) Viral replication occurs in the nucleus of cancer cells with aberrant retinoblastoma protein (RB) or p53 signalling pathways. (3) Viruses are released via autophagy, leading to bursting of the cell membrane. (4) Cytolysis activates pathogen-associated molecular patterns (PAMPs) and damage-associated molecular patterns (DAMPs) that (5) activate immune responses and antigen presentation. Viral oncolysis may cause (6a) anti-viral immunity without tumour regression. Ideally, oncolysis leads to (6b) anti-tumoural immunity and tumour progression, enhanced by the viral-encoded checkpoint inhibitors such as anti-programmed cell death protein 1 (PD1) monoclonal antibodies. ATP, adenosine triphosphate; HMGB1, high mobility group box protein 1; HSP, heat shock protein. Modified from (Jiang et al., 2015).

### *1.3.4 Future directions*

Promising clinical outcomes (Kaufman and Bines, 2010, Andtbacka et al., 2014) from the OPTiM phase III clinical trial of a herpes simplex type 1-based immuno-oncolytic vector talimogene laherparepvec (T-VEC; trade name Imlygic) helped to re-energise the field of oncolytics. T-VEC was licenced for the treatment of advanced, unresectable melanoma by FDA in October 2015 (FDA, 2015) and by EMA in December 2015 as the first oncolytic immunotherapy in Europe. There is now clear evidence that virotherapies are finally coming of age in the clinical field. Technologies based on Ad are likely to be heavily represented among clinical virotherapies due to their ease of scale up, amenable genomes, long clinical history and potential to achieve tumour-selectivity. It is clear that a wide variety of safety and efficacy considerations must be addressed with regards to Ad-based delivery systems. Thorough molecular knowledge of the basic underpinning biology to delineate the virus: host interactions that determine off-target tropism and toxicity, is needed. Firstly, Ads must be re-engineered and optimised to evade pre-existing immunity and other dose-limiting interactions that promote uptake into a wide variety of non-tumour sites. Secondly, to ensure selectivity of transduction, tumour-selective targeting ligands are to be inserted into the viral capsid. Thirdly, "safety nets" must be integrated into the viral genome to ensure replication/transgene expression is unique to cancerous cells, for example, through the inclusion of tumour-specific promoter elements or miRNA silencing elements. Finally, the delivery of a suitable payload must be incorporated into the viral genome, whether a gene that directly or indirectly induces cell suicide in the tumour cells, or one that helps to stimulate a suitable host anti-tumour immune response. The relationships between cancer biomarkers and oncolytic viral vectors is likely to become increasingly important and warrants thorough investigation. Tookman and colleagues recently showed increased cytotoxicity using a oncolytic Ad5 in *Brca2*-positive HGS-OC cells that have an intact homologous recombination (HR) function (Tookman et al., 2016). This is a remarkable finding as cancers with intact HR commonly have a low response rate to platinum chemotherapy and PARP-inhibitors, accompanied with a poor prognosis. Evidently, innovative strategies for Ad vector design, coupled with cancer biomarker evaluation and selective immune stimulation within the TME, hold significant promise for effective cancer eradication.

### 1.4    Limitations of adenoviral cancer therapies

Despite decades-long investigations of Ad utilisation for therapeutic purposes, severe limitations to its potent and safe clinical use remain (Figure 1–16). Improvement strategies for therapeutic Ad vector design are discussed in section 1.6.
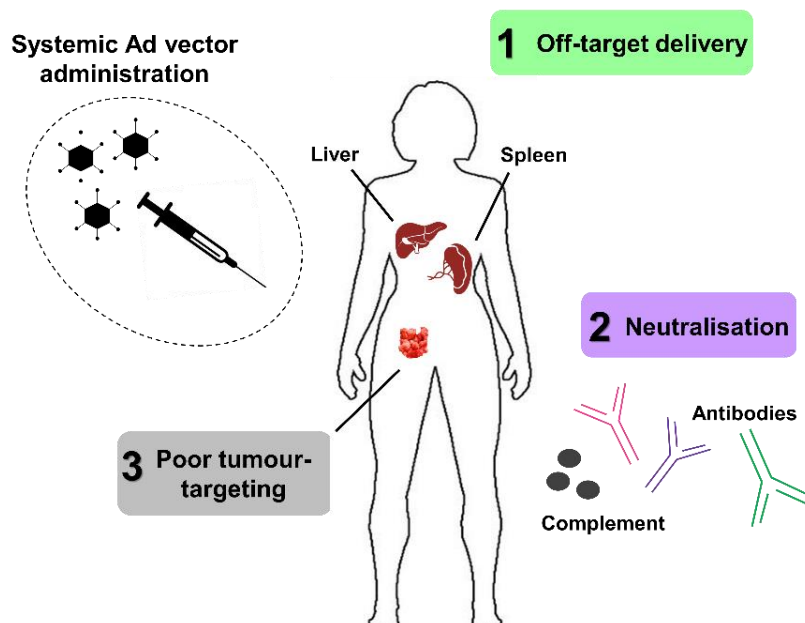


**Figure 1–16. Limitations of adenoviral (Ad) cancer therapies.** (1) Ad vectors are sequestered by multiple circulating proteins and cells in the blood, and end up taken up by the liver and spleen. (2) Pre-existing anti-Ad neutralising antibodies and complement proteins opsonise and inactivate the virus. (3) Anti-tumour efficacy is low due to down-regulation of the native coxsackie and adenovirus receptor (CAR) in progressive cancers and poor accessibility of the tumour mass.

#### 1.4.1    Native CAR down-regulation & inaccessibility in cancer

The native receptor of Ad5, CAR, is ubiquitously expressed on the apical surface of healthy polarised epithelial cells [reviewed in (Coyne and Bergelson, 2005)]. Early reports documented decreased CAR expression among various cancer types, such as bladder (Li et al., 1999b), lung (Pearson et al., 1999), pancreatic (Pearson et al., 1999) and ovarian cancer (You et al., 2001, Kim et al., 2002b, Kim et al., 2002a), as well as SCCHN (Li et al., 1999a) and malignant gliomas (Asaoka et al., 2000). In a recent large study (Reeh et al., 2013) involving 3714 specimens from 100 malignancies and from 273 normal control tissues the frequency of CAR expression was widely varied, based on immunohistochemical staining from tissue microarrays (Table 1–4). The observations of this study largely agree with previous findings, with the exception of bladder cancer that has shown CAR down-regulation in previous studies (Li et al., 1999b, Sachs et al., 2002, Matsumoto et al., 2005, Buscarini et al., 2007). The absence of CAR in the target tissue has a great impact on Ad transduction, and hampers therapeutic efficacy.

**Table 1–4. Coxsackie and adenovirus receptor (CAR) expression level in human tissues. * =** CAR tissue distribution based on a large study involving 3714 samples (Reeh et al., 2013), unless indicated otherwise. Expression in neoplastic tissues in grey; expression in normal tissues *in italics*. Range indicates the variation between different cancer types in the specified organ.

| Organ | % of positives | Organ | % of positives |
|---|---|---|---|
| adrenal cortex | *0* | ovary | *0* |
| | 25–60.5 | | 31.6–100 |
| anal skin | *20* | pancreas | *80* |
| | 46.7 | | 72.2–82.1 |
| bone tumours | *nd* | parotis | *50* |
| | 50 | | 11.7–85.2 |
| brain | *0* | penis | *40* |
| | 10–54.2 | | 45.7 |
| breast | *18.2* | platelets | *positive* (Carlisle et al., 2009, Seiradake et al., 2009) |
| | 4.3–24.1 | | nd |
| cervix | *25* | prostate | *69.2* |
| | 50–82.5 | | 7.9 |
| colon | *92.3* | renal cell cancer | *73.7* |
| | 50–80 | | 5.9–78.6 |
| endometrium | *21.1* | skin | *41.2* |
| | 75.5–91.7 | | 0–91.3 |
| erythrocytes | *positive* (Carlisle et al., 2009, Seiradake et al., 2009) | small intestine | *42.9* |
| | nd | | 50 |
| gall bladder | *88.9* | stomach | *80* |
| | 45.7–60 | | 37–87.1 |
| heart | *low in adults* (Noutsias et al., 2001) | tendon sheat | *50* |
| | nd | | 12.5–72.7 |
| larynx | *0* | testis | *40* |
| | 63.6 | | 26.1–29.5 |
| liver | *100* | thymus | *0* |
| | 84.9 | | 36.4 |
| lung | *45.8* | thyroid | *25* |
| | 20–84.2 | | 0–90.3 |
| lymph node | *25* | urinary bladder | *0* |
| | 12.5–13.2 | | 30–88.3 |
| muscle | *35.7* | vagina | *40* |
| | 0–28.6 | | 70 |
| naevus | *60* | vulva | *75* |
| | 41.2–48.9 | | 90 |
| oesophagus | *80* | | |
| | 67.8–85.7 | | |

In earlier reports, CAR and αvβ3/5 integrin expression were highly variable between five analysed ovarian cancer cell lines, resulting in variation in the Ad vector transduction efficiency (You et al., 2001). Similarly, Kim and colleagues demonstrated that the efficacy of Ad cancer therapies was severely hampered by the absence of CAR receptors in tumours (Kim et al., 2002b), while transient expression of CAR in ovarian cancer cells enhanced Ad transduction (Kim et al., 2002a). Highlighting the importance of cell sensitivity to oncolytic Ads, a recent study by Ingemarsdotter and colleagues showed that paclitaxel-induced CAR up-regulation enhanced oncolytic Ad5 vector efficacy in paclitaxel-resistant ovarian cancer cells via aberrant cell cycle control mechanisms (Ingemarsdotter et al., 2015).

Another obstacle is the localisation of the cellular target receptors within cancer tissue (Figure 1–17). CAR is localised in tight junctions between the epithelial cells within the epithelium and is therefore not directly accessible on the surface of the tumour.  In order to infect the cancerous tissue, the virus has to be able to break its way through the ECM into the tumour mass. The process of breaking through the first-line barriers of infection may be facilitated by using tight junction openers and ECM-degrading proteases that help the virus to penetrate deep into the tissues [reviewed in (Vähä-Koskela et al., 2007). Once inside the tissues the virus can process into oncolysis and release more helper proteases that boost virus spread. The loss of CAR expression in advanced cancers necessitates the development of alternative cellular receptors for cancer targeting. In an ideal situation, an optimal cancer marker would be over-expressed on the surface of cancer cells but virtually absent in healthy adult tissues. This feature is crucial for enabling the high level of cancer-selectivity and to avoid undesired adverse effects.
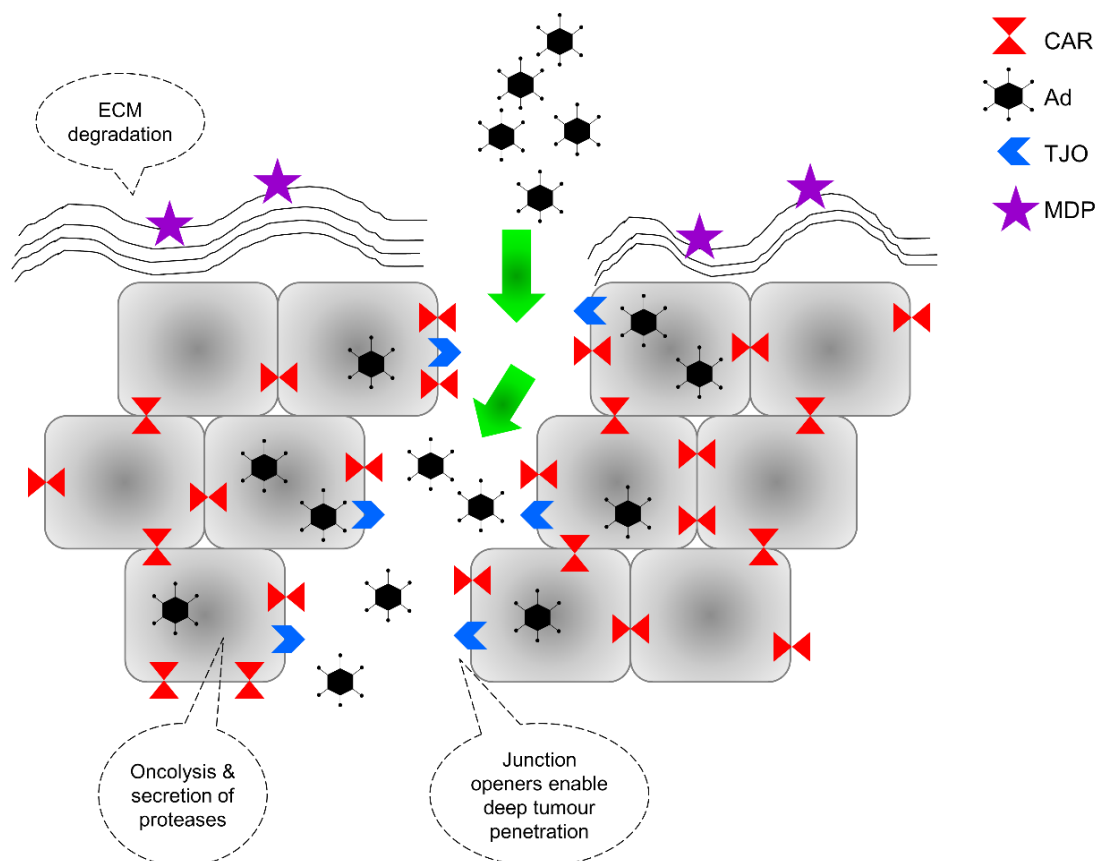


**Figure 1–17. Strategies for improving receptor accessibility for therapeutic viruses.** ECM restricts Ad entry into the epithelium, which can be facilitated by matrix-degrading proteases (MDP) that degrade the extracellular matrix (ECM). TJOs can be utilised to open tight junctions and facilitate Ad access to CAR. Ad, adenovirus; TJO, tight junction opener. Modified from (Vähä-Koskela et al. 2007).

### 1.4.2   Sequestration by blood factors and off-target delivery

Intravascular delivery of Ad5 vectors results in rapid recognition and opsonisation by various blood cells such as MΦs, platelets (Othman et al., 2007, Gupalo et al., 2011) and erythrocytes (Carlisle et al., 2009) [reviewed in (Coughlan et al., 2010)]. Vitamin K–dependent coagulation factors FVII, FIX, FX and protein C have been shown to enhance vector transduction *in vitro* (Parker et al., 2006). FX has been shown to be able to rescue liver transduction in mice that had been treated with warfarin to deplete vitamin K–dependent zymogens (Waddington et al., 2007, Waddington et al., 2008). Ad5 is trapped from the bloodstream and trafficked into the liver (Smith et al., 2002) within the first hour of systemic administration (Green et al., 2004). Ad vectors (via HVR1, 2, 5 and 7) are rapidly sequestered by Kupffer cells (KCs) that hijack Ad via scavenger receptors (Khare et al., 2012), leading to viral saturation and destruction of the KCs. The FX-decorated virus is then taken up by hepatocytes – the major cell type of the liver parenchyma – and tissue-resident MΦs (Wolff et al., 1997) via HSPGs. The high affinity interaction between Ad5 hexon HVRs and FX is well-characterised and further discussed in sections 1.2.2 and 1.2.3. Up to 98 % of systemically administered Ad5 seems to end up in the liver (Green et al., 2004), which triggers the production of chemokines/interferons (INF) and leads to recruitment of neutrophils. In severe cases, the extensive innate inflammatory attack may also result in hepatic necrosis and apoptosis [reviewed in (Russell, 2000, Russell, 2009), which together contribute to the development of acute transaminitis, vascular damage and severe toxicities (Shayakhmetov et al., 2005b). Extended blood availability and decreased hepatotoxicity have been described for Ad5 vectors whose surface was masked with poly(N-(2-hydroxypropyl)methacrylamide) (HPMA) polymer (Green et al., 2004).

Spleen is the secondary off-target site for systemically-administered Ad5 vectors (Di Paolo et al., 2009). It is a central part of the lymphatic system and the main factory for cytokine and antibody production. Scavenging marginal zone MΦ (MARCO+) and marginal metallophilic MΦ (CD169+) within the marginal zone are the primary target cells of systemically-delivered Ad5 vectors in the spleen (Di Paolo et al., 2009). In this study, Di Paolo and colleagues showed that Ad5 binding via RGD motif to αvβ3 integrins on the surface of marginal zone MΦ triggers IL-1α production, thus contributing to innate anti-viral immune responses. Substitution of Ad5 HVRs 1–7 with the corresponding regions from non-FX binding Ad48 serotype (AdHVR48(1–7)) did not result in significantly increased vector uptake in the spleen but did increase production of inflammatory chemokines (interferon γ-induced protein 10 (IP-10),

MCP-1, and MIP-1α) and cytokines (IL-5, IL-6, MCP-1, and IP-10) (Coughlan et al., 2012). In the same study, Ad5 and Ad5HVR48 were also associated with ER-TR7+ reticular fibroblasts and MAdCAM-1+ cells in the spleens of MΦ-depleted animals. Based on these observations the splenotropism of pseudotyped Ads appears unpredictable, involving penton-independent mechanisms and may be dictated by various interactions between multiple cell types. Further investigating the splenotropism of different Ad serotypes will be crucial in future vector development strategies.

### 1.4.3  Innate & adaptive immune responses

The three major capsid proteins, early proteins E1A, E1B, E2 and E4, and virus-associated non-coding RNAs VA-I and VA-II, are central in the synergistic activation of innate immune responses that lead to inflammation and vector clearance [reviewed in (Hartman et al., 2008, Hendrickx et al., 2014)]. Following systemic Ad5 vector administration, the virus is rapidly recognised and coated by proteins of the complement cascade (Figure 1–12) (Cichon et al., 2001, Appledorn et al., 2008) and IgM antibodies that readily recognise repetitive pathogen structures such as virus capsids (Ochsenbein et al., 1999) [*in vivo* blood interactions reviewed in (Coughlan et al., 2010)]. Human (but not murine) erythrocytes express CAR and complement receptor 1 (CR1) and are can rapidly coat and inactivate the Ad5 particles following systemic delivery (Carlisle et al., 2009). Ad5-based vectors are efficiently opsonised by complement factors – even in the absence of nAbs – which indicates central involvement of this pathway in both innate and adaptive arms of anti-Ad immunity (Cichon et al., 2001). Rapid chemokine and cytokine production, as well as Ad5-induced thrombocytopenia mediated by p-selectin and von Willebrand factor (vWF) (Othman et al., 2007), are all elicited in a C3-dependent manner, with the help of other complement factors (Appledorn et al., 2008) such as C2 and C1q [reviewed in (Coughlan et al., 2010)]. Innate activation of IFN production by viral infection boosts production of chemokines, attracting neutrophils, mononuclear and natural killer (NK) cells.

Systemic Ad delivery results in vector binding to β3 integrins via penton RGD motif on marginal zone macrophages (MZMΦ) leading to accumulation in the spleen, which initiates IL-1α-mediated activation of chemokine- and complement cascade, promoting polymorphonuclear leukocyte (PMN) activation and local inflammation (Di Paolo et al., 2009). Recent publications have also reported novel roles for the non-inflammatory factor of the coagulation pathway, namely FX, indicating its involvement in Ad5 virus shielding from neutralisation by natural IgM antibodies and subsequent

activation of the complement cascade (Xu et al., 2013). Conversely, decoration of the virus particle with host FX has also been suggested to function as a pathogen-associated molecular pattern (PAMP), triggering innate immune responses via Toll-like receptor / nuclear factor κB (TLR/NF-κB) pathway (Doronin et al., 2012).

Therapeutic Ad vector delivery results in long-lasting humoral and cellular immune responses in the human host (Juillard et al., 1995). Antigen-presenting cells (APCs) – DCs and immature MΦs – recognise PAMPs and direct DC maturation and T-cell activation, leading to subsequent adaptive immune responses [reviewed in (Jooss and Chirmule, 2003, Thaci et al., 2011)]. Ad infection elicits NK cell (Tomasec et al., 2007), cytotoxic CD8+ T-cell (Sumida et al., 2004) and memory CD4+ T-cell activation (Olive et al., 2002). In addition to containing major nAb epitopes as described earlier (Sumida et al., 2005, Sumida et al., 2004, Roberts et al., 2006), the highly conserved regions of the hexon protein contain at least three major CD4+ T-cell epitopes (Olive et al., 2002, Onion et al., 2007). Systemic production of serotype-specific IgM, IgA and IgG (Ariyawansa and Tobin, 1976) and nAb seroconversion has been reported to occur within 2–4 weeks of the primary virus exposure (Crawford-Miksza and Schnurr, 1996). There is evidence that the intensity of humoral immune responses may be determined by vector administration site and pre-existing nAb titres rather than the therapeutic dose (Harvey et al., 1999). Different human and animal serotypes have been shown to have minimal levels of cross-reactivity, as nAbs seem to be specific to the homologous virus (Sharma et al., 2010).

Anti-Ad nAbs comprise primarily fiber-, penton- and hexon-specific IgG1, IgG4 and IgA antibodies [reviewed in (Jooss and Chirmule, 2003)] that can inactivate the virion at different points of its infectious cycle (Gall et al., 1996, Sumida et al., 2005). Anti-fiber nAbs seem to contribute to blocking the initial virus attachment to the cell surface by extracellular virion aggregation (Wohlfart et al., 1985), while anti-penton nAbs may be responsible for inhibiting the internalisation step (Hong et al., 2003) and a proportion of anti-hexon nAbs potentially account for intracellular, post-entry neutralisation (Varghese et al., 2004), although this remains controversial. It has been demonstrated that 1.4 individual serotype-specific anti-hexon nAbs are needed for full neutralisation of Ad2 (Wohlfart, 1988). Intriguingly, this study also describes how the neutralisation efficiency of anti-penton nAbs can be increased from 50 % to 100 % efficiency by lowering the pH from 7 to 5, which is presumably due to the exposure of the penton antigenic epitopes and subsequent interaction with anti-penton nAbs.

### *1.4.4   Pre-existing humoral immunity*

Ad5 is a common respiratory virus, and the majority of human populations have anti-Ad5 nAbs that are highly capable of neutralising the virus upon a secondary infection or re-exposure to a therapeutic vector. The highest seroprevalence rates are reported in the developing world, sub-Saharan Africa in particular (Nwanegbo et al., 2004), while pre-existing nAbs levels against rare human serotypes from subgroups B and D are substantially lower in the studied populations (Nwanegbo et al., 2004, Abbink et al., 2007, Mast et al., 2010). The prevalence of nAbs against subgroup C viruses Ad5 and Ad6, and subgroup D viruses Ad26 and Ad36 was evaluated in an international study (Mast et al., 2010) that revealed overall high prevalence of pre-existing anti-Ad5 immunity (85.2 %), Thailand having close to 100 % prevalence (Mast et al., 2010). Both subgroup D viruses had remarkably lower seroprevalence, overall values being 58 % for Ad26 and 46.4 % for Ad36. In paediatric populations in sub-Saharan Africa, maternally-derived anti-Ad5 Ab titres were high until 6 months of age, then remained low until the age of two years the increasing rapidly until seroprevalence rates reached adult levels by seven years of age (Thorner et al., 2006). It is thus crucial to take into account the variable seroprevalence rates between different Ad serogroups when selecting new Ad vector candidates for patients from different age groups, particularly when intended for i.v. delivery.

Anti-fiber nAbs emerge first after the delivery of therapeutic Ad vector, followed by generation of anti-penton nAbs and anti-hexon nAbs, suggesting that all three are needed for a full synergistic neutralising effect (Gahéry-Ségard et al., 1998). However, there has been considerable controversy surrounding the specificity and immunogenicity of the capsid protein-induced nAbs that seem to vary based on the inoculation route. Reports have suggested a primary role for anti-hexon nAbs in vaccine-induced immunity (Sumida et al., 2005) and anti-fiber nAbs in natural infection (Särkioja et al., 2008, Parker et al., 2009, Cheng et al., 2010). According to Parker and colleagues, nAbs elicited by replication-deficient Ad5 vaccine vectors in seronegative individuals were directed against capsid components other than the fiber, while nAbs elicited by natural infection mainly were directed against the fiber (Parker et al., 2009). Previously seropositive individuals had nAbs against both fiber and other capsid components after vaccine challenge (Cheng et al., 2010). On the contrary, a recent study reports only subtle differences between the specificity of nAbs relative to the infection type (vaccination vs. natural), suggesting the immunodominance of hexon and subdominant assisting role for anti-fiber nAbs in neutralising immunity (Bradley et al., 2012a).

## 1.5 αvβ6 integrin – an epithelial cancer marker

Cancer cells often express a variety of cell surface markers that can give cues to the origin, metastatic spread, stage and prognosis of the primary tumour they originate from. EOC cells have been shown to express various markers including CD326 (EpCAM), HER2 (Zhang et al., 2015), BRCA1/2 (Zhang et al., 2015), murine sarcoma viral oncogene homolog B (BRAF) (Zhang et al., 2015), Kirsten rat sarcoma viral oncogene homolog (KRAS) (Zhang et al., 2015), epidermal growth factor receptor (EGFR) (Zhang et al., 2015) and tumor protein 53 (TP53) (Zhang et al., 2015). CSC markers CD44 and CD133 have been suggested to be prevalent in tumour-initiating cells (TICs) (Garson and Vanderhyden, 2015), while endometrioid and HGS-OC has been shown to exhibit high EGFR expression (Zhang et al., 2015). Importantly, for any biomarker to be specific enough for successful cancer therapeutic applications, it has to be virtually absent in healthy adult tissues but significantly up-regulated throughout the process of carcinogenesis. Many of the markers mentioned above are expressed across various different cell types, and are thus not strictly EOC-specific. αvβ6 integrin however, is a highly cancer-specific marker and therefore has significant potential to be utilised for highly selective therapeutic cancer targeting.

### 1.5.1 Structure and function of αvβ6 integrin

Integrins play a central role in cell adhesion, cell motility and signalling processes, as discussed in section 1.2.3 of this thesis. Interestingly, RGD-binding integrins – including αvβ1, αvβ3, αvβ5, αvβ6, αvβ8 and α5v1 – also play central roles in cancer metastasis (Ganguly et al., 2013, Cantor et al., 2015). The integrin β6 subunit was originally identified from human pancreatic carcinoma epithelial cells in the early 1990s, and shown to share 43, 38, and 47 % sequence homology with other β subunits 1, 3 and 5, respectively (Sheppard et al., 1990). αvβ6 is heterodimer that consists of an αv subunit (681 aa; GenPept GI: 720063178) and a β6 subunit (788 aa; GenPept GI: 720063179) that contains an EGF-like motif (Dong et al., 2014b). The receptor has an open conformation on the membrane, and assumes a closed conformation when bound to its native ligands. Sheppard and colleagues identified an 11-amino acid extension in its C-terminus, absent in other β subunits, that has unique cytoplasmic interaction with extracellular signal-regulated kinase (ERK2) and activates ERK/MAPK pathway [mentioned in (Sowmya et al., 2014)]. αvβ6 integrin binds to fibronectin but not to vitronectin or collagen I, unlike other αvβx integrins (Busk et al., 1992). The β6 subunit pairs exclusively with αv and no other alpha subunits (Hynes, 2002). Alpha v integrins are the main up-stream regulators of transforming growth factor β1 (TGF-β1) – a pleiotropic tumour suppressor cytokine

involved in control of epithelial cell division, whose activation is tightly controlled. In addition to TGF-β1, αvβ6 binds to TGF-β3 with high affinity (Dong et al., 2014b). In cancer cells, resistance to TGF-β1 suppression is orchestrated by an αv integrin-mediated activation of the latent form of TGF-β1, which directly contributes to cancer metastasis (Figure 1–18). The role of TGF-β1 in tumour development is further discussed in an excellent recent review (Khan and Marshall, 2016). Compared to other integrins, αvβ6 has an extraordinarily high affinity to its ligands, which may be indicative of its specialised role in TGF-β activation rather than cell migration (Dong et al., 2014b).

In addition to its cellular ligands, functional binding studies have shown αvβ6 integrin to have natively high affinity to a structural VP1 protein from a single-stranded positive-strand RNA virus, type O1 foot-and-mouth virus (FMDV) (Dicara et al., 2008, Slack et al., 2016). This interaction is mediated via the integrin-binding RGD motif within a 20-amino acid peptide (A20, NAVPNL*RGD*LQVLAQKVART) in the VP1 protein (DiCara et al., 2007) (Figure 1–19) that contains the viral major antigenic epitopes and is responsible for attachment of FMDV to host epithelial cells (Acharya et al., 1989). The A20-αvβ6 interaction has recently been characterised into great pharmacological and kinetic detail (Slack et al., 2016). According to the detailed evaluation by this group, αvβ6 binding to A20 peptide is equally strong as it is to its cellular ligand, TGF-β1. Interestingly, the RGD motif and its surrounding amino acid residues in TGF-β1 seem to form a similarly protruding hairpin loop structure (Dong et al., 2014b) as does the A20 peptide in FMDV in context of αvβ6 receptor binding (DiCara et al., 2007). The A20 peptide interaction is highly stable and EDTA-resistant, similar to the complex that an infectious FMDV forms with αvβ6 (Dicara et al., 2008). DiCara and colleagues also demonstrated that the αvβ6-mediated interaction is dependent on the presence of a conserved DLXXL motif in a post-RGD α-helical loop. In line with the observation, Dong and colleagues showed that αvβ6 recognises an LXXL/I motif in TGF-β3 that folds into an amphipathic α-helix, fitting snugly to the hydrophobic pocket in β6 subunit (Dong et al., 2014b).
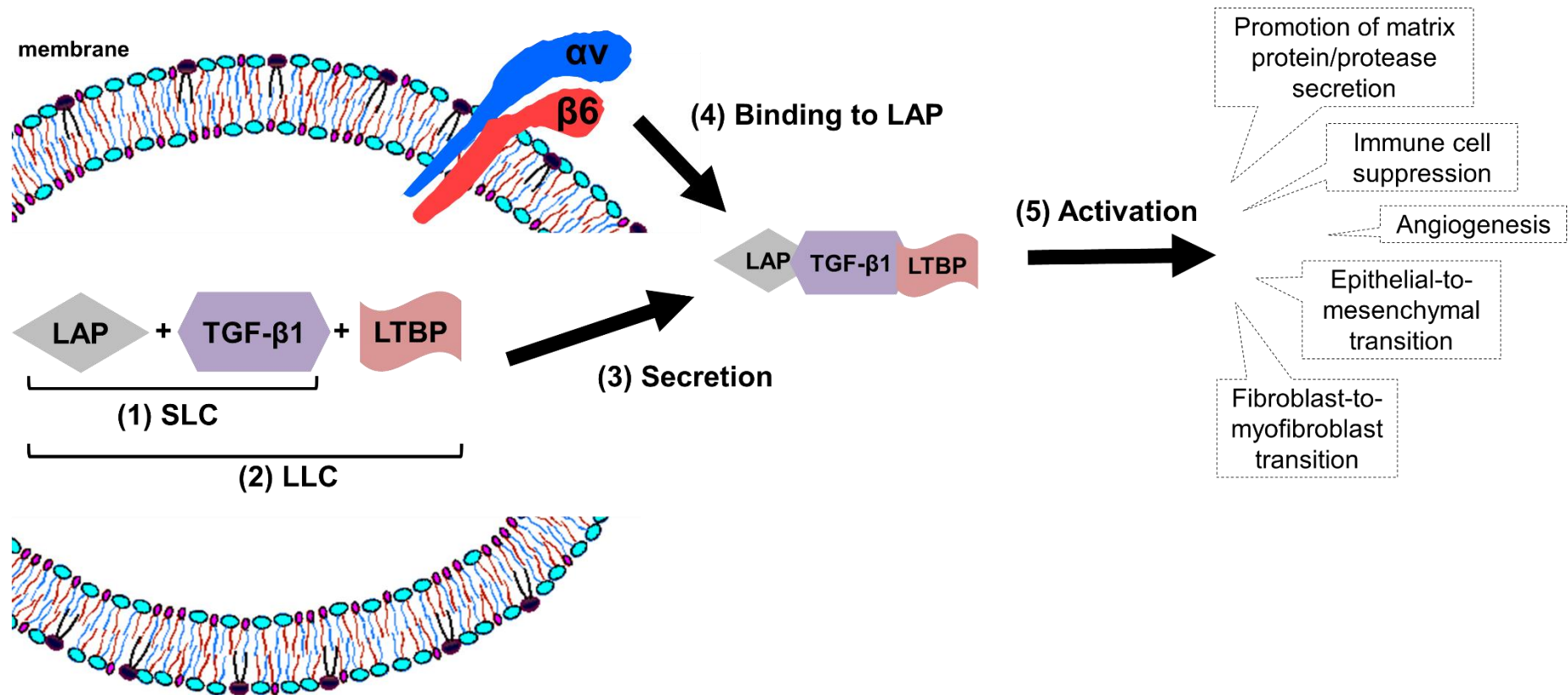
**Figure 1–18. Activation of transforming growth factor β1 (TGF-β1) by αvβ6 integrin and its role in carcinogenesis.** Mutations in the TGF-β1 signalling pathway promote carcinogenesis. (1) Latency associated peptide (LAP) together with latent TGF-β1 forms the small latent complex (SLC). (2) Binding of SLC to latent TGF-β-binding protein (LTBP) forms the large latent complex (LLC). (3) The LLC is secreted to the extracellular matrix (ECM), where αvβ6 binds LAP via its Arg-Gly-Asp (RGD) motif, thereby triggering activation of TGF-β1 either by a conformational change pathway or proteolytic cleavage pathway. Figure based on the comprehensive review by Khan and Marshall (Khan and Marshall, 2016).
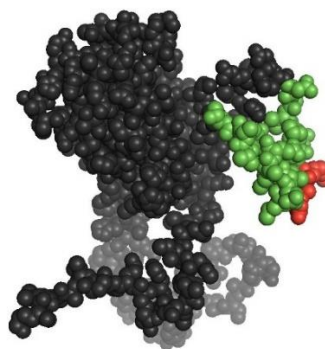
**Figure 1–19. Foot-and-mouth disease virus (FMDV) capsid protein VP1.** A20 peptide (NAVPNLRGDLQVLAQKVART) highlighted in green, integrin-binding motif (RGD, Arg-Gly-Asp) highlighted in red. GenPept GI: CAA00045.1, PDB ID: 1FOD1. Generated in PyMol version eval 1.1.

αvβ6 is strictly epithelial-restricted and undetectable in healthy adult tissues (Weinacker et al., 1994, Ahmed et al., 2002b). αvβ6 is an intriguing member of the integrin family, as it has been linked to various tissue re-modelling, developmental and neoplastic events. In addition to carcinogenesis, these include foetal tissue development, wound healing (Haapasalmi et al., 1996), acute lung injury and idiopathic pulmonary fibrosis in the lung (Breuss et al., 1995, Horan et al., 2008), and fibrosis in the kidney and liver (Peng et al., 2016). Its over-expression correlates with cancer progression (Allen et al., 2014) and extremely poor survival. αvβ6 upregulation has also been linked to respiratory pathogen-induced pathogenesis (Meliopoulos et al., 2016). β6 knockout (KO) mice with normal lung morphology exhibited increased survival upon influenza infection, with high levels of CD11b+ alveolar MΦ and type I IFN, due to loss of TGF-β. β6 KO mice have also been shown to present with juvenile baldness, immune cell infiltration to the skin and airway epithelia, and hyperresponsiveness to acetylcholine, indicative of asthma (Huang et al., 1996). Female endometrium during menstrual cycle (Busk et al., 1992), and subclinical inflammation in the lung and skin (Huang et al., 1996) are the only known exceptions of its exclusive role in pathological tissue remodelling events. Low level of αvβ6 expression has been observed in healthy basal keratinocytes, and in few cells in the kidney and trophoblastic cells in placenta (Professor John F Marshall, Barts Cancer Institute, London; personal communication).

### 1.5.2  *αvβ6 integrin expression in different cancers*

The initiation process for αvβ6 over-expression is not well established, although it is likely to be connected to changes in TGF-β1 signalling pathways. αvβ6 expression seems to be activated following an interaction between stromal border close to basal membrane, starting from just a couple of cells and then spreading around the tissue.

A patchy and non-uniform coverage is often observed within the tumour mass (Professor John F Marshall, Barts Cancer Institute, London; personal communication). αvβ6 integrin expression has been documented in a plethora of different cancer types (Table 1–5), including breast (Allen et al., 2014, Koopman Van Aarsen et al., 2008), cervical (Koopman Van Aarsen et al., 2008), skin (Koopman Van Aarsen et al., 2008), ovarian (Ahmed et al., 2002b, Koopman Van Aarsen et al., 2008), colorectal (Yang et al., 2008, Koopman Van Aarsen et al., 2008), prostate (Dutta et al., 2014), head and neck (Nothelfer et al., 2009), and cancer of the oral cavity (Thomas et al., 2006).

**Table 1–5. αvβ6 integrin expression in different cancer types.** Modified from (Koopman Van Aarsen et al., 2008). N, number of analysed samples.

| Tumour site | Positive expression % | N |
|---|---|---|
| Cervix | 92 | 46 |
| Skin | 84 | 49 |
| Oesophagus | 68 | 56 |
| Head & neck | 64 | 100 |
| Breast | 43 | 145 |
| Lung | 35 | 54 |
| Ovarian | 33 | 52 |
| Kidney | 21 | 103 |
| Colorectal | 12 | 60 |
| Hepatocellular | < 2 | 59 |

Evaluation of 66 ovarian epithelial tissues revealed that αvβ6 was absent in all healthy ovarian tissues but expressed on all 45 carcinomas, of which 14 were borderline (low malignant potential) and 31 malignant tumours (Ahmed et al., 2002b). Additionally, the expression of αvβ6 correlated with cancer progression, observed as increased staining intensity on histological ovarian tissue samples, while no significant difference was observed between serous, endometrioid and mucinous tumour subtypes. Ahmed and colleagues also showed grade III tumours to have strong αvβ6 expression throughout the tissue, while benign tumours expressed αvβ6 expression only at the epithelial edge of the tumour. The reports suggest an important role for αvβ6 in EOC progression, which implies it could be a promising target for ovarian cancer therapies. However, another study showed αvβ6 to be expressed in only a third of ovarian cancers (Koopman Van Aarsen et al., 2008), and therefore patient stratification may be required. Dutta and colleagues identified αvβ6 integrin up-regulated in human prostate cancer bone metastases (Dutta et al., 2014). The authors also suggest its involvement in regulation of osteolysis by promoting matrix metalloproteinase 2 (MMP2) in an androgen receptor-independent manner, and co-

localisation with parathyroid hormone-related protein (PTHrP) that is an inducer of osteoclastogenesis. It has also been shown to be involved in thyroid carcinoma colorectal cancer metastasis via activation of transcription factors and cell migration (Cantor et al., 2015). This excellent review highlights the role of the β6 subunit in activation of ERK2 and SDF-1/CXCR4, TGF-β1 and uPAR, which in turn is thought to contribute to metastasis. In prostate cancer cells, αvβ6 integrin is localised in focal contacts and binds to fibronectin and latency-associated peptide (LAP)-TGF-β1, thus mediating  attachment and migration (Dutta et al., 2014). Binding to LAP-TGF-β1 promotes the activation of TGF-β1, leading to pro-metastatic and pro-invasive signalling pathways (Sheppard, 2000). Additionally, the role of αvβ6 in cancer progression has been demonstrated by using a function-blocking anti-αvβ6 antibody on head and neck cancer xenografts, which led to TGF-β-mediated inhibition of tumour growth (Koopman Van Aarsen et al., 2008). Taken together, αvβ6 may be a promising therapeutic target in cancers with a disrupted TGF-β activation.

### 1.5.3   αvβ6 in cancer diagnostics, imaging and therapeutic targeting

αvβ6 integrin presents a good molecular target for cancer therapies. Direct binding of ERK to β6 subunit is responsible for increase in cytosolic MAP kinase activation upon EGF stimulation (Ahmed et al., 2002a). In this study the deletion of ERK-binding domain from β6 inhibited tumour growth *in vivo*. A U.S. patent 7150871 claims that treatment with a function-blocking mAb anti-αvβ6 antibody 10D5 reduced the number of cancer cells in lung metastasis (USPTO, 2004). Furthermore, by blocking αvβ6 using this antibody, apoptosis was induced in αvβ6-positive colon cancer cells (Zhao-Yang et al., 2008), which is an interesting finding with therapeutic potential. A humanised single-chain Fv (scFv) antibody B6-2 was constructed by inserting a 17-mer specificity-determining domain of FMDV A20 peptide (*N*AVPNLRGDLQVLAQKVA*RT*) into a murine scFv that is reactive with carcinoembryonic antigen (Kogelberg et al., 2008). The B6-2 antibody was shown to inhibit αvβ6-mediated cell migration and adhesion, and could potentially be used as a delivery vehicle of tumour-toxic agents. An αvβ6-blocking antibody 264RAD has shown great efficacy in HER2^{+}/αvβ6[+] breast cancers in combination with a mAb trastuzumab (Herceptin) *in vivo* (Moore et al., 2014). It is currently being developed for phase I clinical trials (BCI, 2015) and has great promise for the treatment of aggressive and resistant forms of breast cancer. The potential use of αvβ6 as a target for chimaeric antigen receptor (CAR) T-cell immunotherapies is reviewed in (Whilding et al., 2016).

The A20 peptide has also been evaluated for use in diagnostic applications for αvβ6 integrin-positive cancers. These cancers are known to present with an extremely poor prognosis and highly invasive and metastatic disease [reviewed in (Bandyopadhyay and Raghavan, 2009)], which underlines the necessity for their accurate and timely diagnosis. Hausner and colleagues have described conjugation of A20 peptide to a radiotracer for positron emission tomography (PET) imaging of αvβ6$^{high}$ pancreatic tumour model (Hausner et al., 2009). The authors demonstrate this to be a highly specific method with potential implications for non-invasive detection of pancreatic metastases. The A20 peptide can be used as an informative functional accessory for pre-clinical assessment of cancer and other disease models. By using a radiolabelled form of A20 ([$^3$H]A20FMDV2), Slack and colleagues showed its affinity and selectivity for αvβ6 to be at least 85-fold higher than for other members of the integrin family (Slack et al., 2016). The authors also showed that the concentration-dependent and fast ligand-induced internalisation of αvβ6 receptor was followed by a relatively slow recycling of αvβ6 back to the cell surface, which may be due to the unique interaction between the RGD-motif with its binding site. Additionally, the ligand-receptor interaction was shown to be dependent on bivalent cations, $Mn^{2+}$, $Mg^{2+}$ and $Ca^{2+}$. This study is the first one reporting comparable ability for the radioconjugated A20 peptide and LAP$_1$ – the endogenous ligand of αvβ6 – to internalise the αvβ6 receptor (Slack et al., 2016). In a study by Liu and colleagues, a 21-mer αvβ6-targeting peptide RGDLATLRQLAQEDGVVGVRK conjugated with 6-hydrazinonicotinyl and radiolabelled with technetium-99m ($^{99m}$Tc) showed promising usability for non-invasive single-photon emission computed tomography (SPECT) imaging of αvβ6+ cancers (Liu et al., 2014).

Due to its cancer-specificity, αvβ6 presents a highly cancer-specific cell surface marker and a potential cellular target for cancer gene therapies. Pameijer and colleagues successfully generated primary human T cells that carried a 12-mer αvβ6-specific peptide (screened by phage display) as a CAR-targeting domain (Pameijer et al., 2007). In this study, cytotoxic T cells were successfully shown to kill αvβ6-expressing ovarian cancer cells. Coughlan and colleagues reported the first attempt of targeting Ad5 vectors to αvβ6-positive cancer cells by an insertion of the A20 peptide in the viral fiber knob (Coughlan et al., 2009a). In the current doctoral thesis, the approach validated by Dr Coughlan was taken further by incorporating additional de-targeting mutations in the αvβ6-targeted vector background in order to improve its off-target delivery profile.

## 1.6 Adenovirus vector design: de-targeting and re-targeting

Systemic vector delivery remains the 'Holy Grail' for Ad therapies for cancer applications. To this end, the vectors require extensive genetic modifications to allow effective and safe therapies (Figure 1–20). Successful vector targeting to the liver, however, demands effective alteration of the viral tropism. These strategies all aim at avoidance of vector delivery into the liver, spleen and other organs, improving its availability for therapeutic function. Genetic modification strategies, including point mutations in the tropism-dictating viral proteins and swapping of capsid proteins from rare Ad serotypes, are discussed in the following sections. For an extensive review on chemical and physical de-targeting strategies, see our recent review (Uusi-Kerttula et al., 2015a).
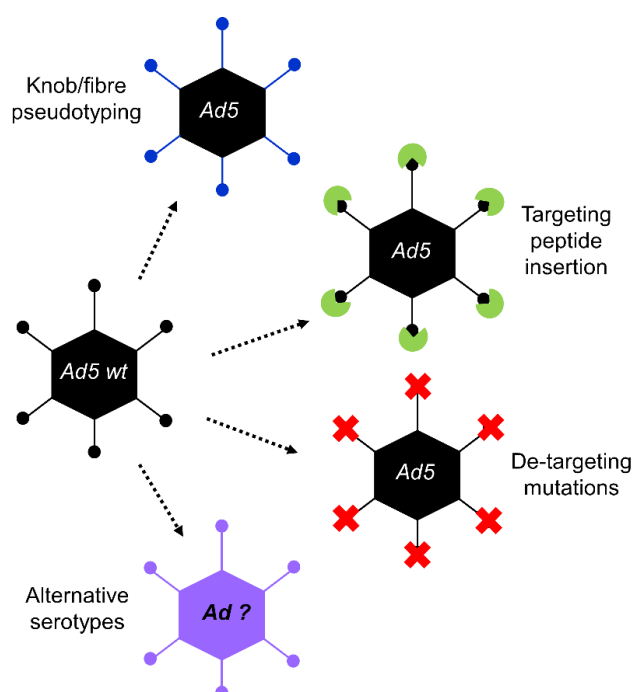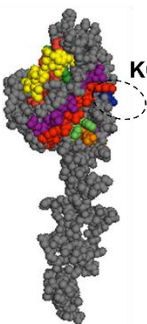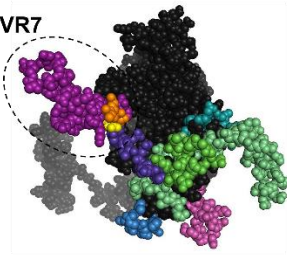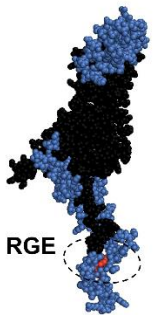


**Figure 1–20. Transductional strategies for improved adenoviral vectors.** Adenoviruses (Ad) can be modified by swapping the fiber knob domain or the whole fiber protein from other serotypes. Heterologous targeting peptide moieties can be genetically inserted in the viral capsid proteins. The vectors can also be directed away from the native receptors by introduction of de-targeting mutations in fiber, penton and hexon. The fourth option is utilisation of alternative serotypes that have novel receptor tropisms and low levels of pre-existing immunity.

### 1.6.1 Ablation of native tissue tropisms

The first, and the most important, step for improvement of vector blood-availability for the tumour tissue is the ablation of the three major tropism-determining interactions (Figure 1–21). Several CAR-binding mutations have been described for Ad vectors, including residues in AB (S408E, P409A) and CD (ΔV441, ΔK442) loops. CAR-interaction is commonly knocked out by the introduction of two amino acid substitutions in fiber knob AB loop, Ser408Glu and Pro409Ala. This double

substitution was named 'KO1' by Smith and colleagues (Smith et al., 2002) – the name is used for all CAR-binding-ablated Ad vectors throughout the thesis. In a pioneering study by Smith and colleagues, KO1 mutation abrogated fiber-mediated Ad transduction into CAR-expressing A549 (lung adenocarcinoma) cells (Smith et al., 2002). No negative impact was observed from the mutation for fiber protein production or viability of the virions. To the authors' surprise, the KO1-modified vectors were still capable of transducing hepatocytes at equal or even increased levels compared to the parental Ad5. This was a very important observation that prompted scientists in the Ad field to study the involvement of alternative receptors in *in vivo* Ad entry. Rigorously implemented studies on Ad tissue tropism subsequently revealed that Ad5 hexon protein binds to hepatocytes via FX, leading to vector uptake and liver infection *in vivo* (Waddington et al., 2008). A point mutation E451Q in HVR7 has been dominated as the central for ablating the interaction, and has been introduced as a common method for de-targeting Ad5 from FX. Alba and colleagues performed an extensive comparison of a panel of hexon HVR mutations, assessing their impact on binding affinity to FX (Alba et al., 2009). A combination of five mutations – I421G, T423N, E424S, L426Y and E451Q – in hexon HVR7 showed superior ability to completely block binding to FX. Based on this comprehensive assessment, this combination of HVR7 mutations was chosen to be incorporated into our Ad vectors, and is called 'HVR7' mutation for simplicity throughout this thesis.



| Protein | **Fibre** | **Hexon** | **Penton** |
|---|---|---|---|
| Name of mutation | | | |
| Substitutions | S408E, P409A | I421G, T423N, E424S, L426Y | D342E |

**Figure 1–21. Tropism-ablating amino acid substitutions in adenovirus capsid proteins.** KO1 mutation in fiber knob ablates binding to coxsackie and adenovirus receptor (CAR) (Smith et al., 2002), HVR7 mutation in hexon ablates binding to coagulation factor X (FX) (Alba et al., 2009), and RGE mutation in penton ablates binding to αvβ3/5 integrins (Wickham et al., 1993). HVR7, hypervariable region 7; RGD, integrin-binding motif.

Ad penton base mediates viral internalisation into the host cells, and plays a role in induction of innate immune responses against the Ad virion. A single amino acid point mutation D342E within the RGD motif (RGD > RGE) has been characterised to

ablate vector internalisation into αvβ3/5 integrin-expressing cells (Wickham et al., 1993). Additionally, this motif has a secondary role in the induction of innate immune and anti-Ad5 inflammatory responses (Di Paolo et al., 2009), which emphasises the importance of mutating this site for an ablated vector backbone. In a previous study by Bradshaw and colleagues, the combination of FX-binding ablation and RGD > RGE mutation led to decreased splenic uptake and attenuated antiviral responses as compared to the wild type Ad5 (Bradshaw et al., 2012). This mutation has been incorporated into the vectors generated in this thesis study, and is referred to as 'RGE' mutation. It is likely that a combination of the described tropism-ablating mutations is needed for successful deterioration of therapeutic Ad vector entry into the main off-target sites, namely the liver, spleen and lungs. As the Ad field is geared towards designing systemically-delivered therapeutic anti-cancer agents, it is important that these mutations and their clinical significance is comprehensively assessed. The experimental part of this thesis discusses the evaluation of these de-targeted mutations *in vitro* and *in vivo* settings.

### 1.6.2 *Serotypes with alternative tropisms*

The utilisation of alternative Ad serotypes for cancer therapies is intriguing for two reasons: (A) anti-Ad5 humoral immunity may be circumvented by using less common serotypes that have low natural seroprevalence in the general human population, and (B) tumour-targeting may be improved due to their variable (non-CAR) receptor and tissue tropisms. Ad vectors have been extensively modified by exchanging specific capsid components with those from less seroprevalent or immunogenic serotypes [virus chimaeras reviewed in (Kaufmann and Nettelbeck, 2012)]. Chimaeric or pseudotyped vectors with altered cell selectivity, antigenicity and tissue tropism have been successfully tested in both pre-clinical (Gall et al., 1996, Ophorst et al., 2004, Roberts et al., 2006, Abbink et al., 2007, Särkioja et al., 2008, Penaloza-MacMaster et al., 2013) and clinical trials (Kuhn et al., 2008, Nokisalmi et al., 2010, Vassilev et al., 2015) over the past decades.

Ad subgroup D has the largest diversity of viruses, coupled with other advantages such as low seroprevalence rates (Abbink et al., 2007) and low affinity to FX (Waddington et al., 2008). The members can infect their host cells via multiple surface receptors, such as CD46 (Chen et al., 2010, Li et al., 2012), CAR (Chen et al., 2010), SA (Burmeister et al., 2004) and GD1a glycan (Nilsson et al., 2011), whilst the involvement of additional receptors has not yet been ruled out. In a recent study Ad9 was the most efficient at infecting both CAR⁺ and CAR⁻ cells out of 16 different species D Ads (Uchino et al., 2014). Ad35, -26 and -48 vaccine vectors have been

demonstrated to be more immunogenic in rhesus monkeys than Ad5 (Teigler et al., 2012). An interesting study compared the replication efficacy and oncolytic potency of 15 different species B, C, D and F viruses on B-cell cancer cell lines and primary cancers (Chen et al., 2011a). Species D viruses were overall most oncolytic *in vitro*, while serotypes Ad26, -45 and -48 showed markedly improved oncolysis compared to all other viruses, including Ad5. Mastrangeli and colleagues demonstrated no cross-reactivity between Ad4 (species E) and Ad30 (species D) with Ad5 (species C) (Mastrangeli et al., 1996), showing that Ad4 and Ad30 were capable of efficiently transducing the airway the epithelium, regardless of a prior exposure to Ad5. Another subgroup C vector, Ad2, indicated circumvention of pre-existing immunity but compromised transgene expression (Mack et al., 1997).

One of the selection criteria for a good anti-cancer virus is its potent replication and oncolysis. Accelerated evolution is a novel technique that has been introduced into the field of Ad vector design. It may be utilised for generation of potent recombinant viruses with altered virulence, tropism and immunogenic properties that are deviant from the properties of their parent serotypes. This strategy mimics the inherent random recombination occurring between different Ad serotypes in human populations. In a study by Kuhn and colleagues, multiple Ad serotypes from various subgroups were passaged on a panel of cancer cell lines, directing the emergence of a chimaeric Ad3/11p serotype vector (Kuhn et al., 2008). EnAd (discussed in section 1.3.2) has shown superior oncolytic properties on colon cancer cell lines as compared to the previously developed oncolytic Ads (Kuhn et al., 2008). The vector carries a large deletion in E3 region, a small 24 bp deletion in E4 region and a chimaeric Ad3/Ad11p E2B region such that the pTP and DNA pol regions have been swapped to those from a species B1 virus Ad3. Its major capsid proteins appear to originate from a species B2 virus Ad11p. EnAd has a superior blood persistence as compared to Ad5 (Di et al., 2014) – a highly advantageous feature for an oncolytic vector intended for i.v. treatment of disseminated solid tumours. The use of non-human or 'xeno' Ads as cancer vectors is discussed in a recent review by our group (Uusi-Kerttula et al., 2015a).

### 1.6.3 Immune-naïve vectors: rare species D and non-human Ads

Commonly utilised Ad5 vectors can be 'pseudotyped' by switching the major immunodominant regions into domains from less seroprevalent or immunogenic serotypes [for a review, see (Kaufmann and Nettelbeck, 2012)]. Exchange of Ad5 hexon HVRs with low seroprevalence, species D Ad48 HVRs (Ad5HVR48) resulted in altered vector immunogenicity. In one study Ad5HVR48 efficiently escaped anti-

Ad5 nAb responses and showed comparative immunogenicity to the parental Ad5 (Roberts et al., 2006), while *in vivo* studies by Coughlan and colleagues showed significantly increased splenotoxicity and immunogenicity for Ad5HVR48 in mice following i.v. delivery, despite favourably decreased hepatotropism (Coughlan et al., 2012). More recently, Teigler and colleagues showed that Ad5HVR48 could evade pre-existing anti-Ad5 nAbs with reduced hepatotoxicity and comparable T-cell responses with Ad5 (Teigler et al., 2014). These conflicting observations highlight the unpredictable nature of chimeric Ad vectors and reinforce the importance of rigorous preclinical evaluation of recombinant vectors.

Another widely exploited genetic modification approach is the swapping of either the Ad5 fiber knob domain or complete fiber protein with rare Ad serotypes. Fiber pseudotyping results in altered innate (Schoggins et al., 2005) and adaptive immune activation (Rogee et al., 2010, Parker et al., 2009), which implicates an important role for this genetic modification strategy. However, Ad5 fiber replacement with Ad7 (species B) fiber did not change vector immunogenicity, despite successfully altered tropism (Gall et al., 1996). Similarly, Ophorst and colleagues have reported increased DC transduction and T-cell activation *in vivo* using an Ad35 fiber-substituted Ad5 vector, but no protection from anti-Ad5 immunity (Ophorst et al., 2004). In contrast, Särkioja and colleagues showed increased gene delivery in mice treated with an Ad5 vector with fiber knob domain pseudotyped with Ad3 fiber knob (Ad5/3) in presence of low and high nAb titres, in comparison to Ad5 (Särkioja et al., 2008). However, higher nAb titres induced by triple immunisation with Ad5/3 were capable of cross-neutralisation of Ad5, which indicates the involvement of other neutralising epitopes either within fiber shaft or other capsomers.

Denby and colleagues pseudotyped Ad5 with fibers from a species B virus Ad16 and two species D viruses Ad19p and Ad37, showing equal or improved cell transduction, as compared to Ad5 (Denby et al., 2004). Parker and colleagues evaluated a panel of pseudotyped Ad5 vectors with fiber derived from subgroup D Ads Ad17, -24, -30, -33, -45 and -47 and showed these vectors to directly interact with FX and to efficiently transduce the liver, demonstrating that hepatotropism is not fiber-mediated (Parker et al., 2007). Pre-existing immunity was partially bypassed by pseudotyping Ad5 with fiber from a species D virus Ad45 (Ad5/F45) (Parker et al., 2009) that had previously shown high levels of FX-mediated cell binding and transduction (Parker et al., 2007). The study demonstrated greatly improved protection for Ad5/F45 from highly neutralising anti-Ad5 nAbs, indicating that nAbs

are at least partially directed against the fiber protein and may contribute to extracellular neutralisation (Wohlfart, 1988).

An Ad5-based Ad35 (species B) fiber-chimaeric virus (Ad5T*F35++) showed improved cell transduction and protection from anti-Ad5 nAbs in human sera (White et al., 2013). In addition to having the fiber protein from Ad35, Ad5T*F35++ has a mutation (T*) that ablates FX interactions (Alba et al., 2010), for combining potential immune evasion with efficient liver de-targeting. Coupled with penton pseudotyping, Ad5/F35/P35 vector transduced *in vitro* cultures, mouse CD46-transgenic *ex vivo* cultures, and human *ex vivo* cultures at significantly higher levels than either Ad5 or Ad/F35 (Parker et al., 2013). The observations suggest potential utility of this vector for targeting CD46^high cancers. The comparative immunogenicity of different Ad serotypes is further discussed in our extensive review (Uusi-Kerttula et al., 2015a).

### 1.6.4  *Enhancement of tumour-tropism by targeting peptide insertion*

Ad vectors do not preferentially infect cancer cells, and therefore various strategies have been implemented to enhance their tumour-tropism. Modification of the main capsid proteins by genetic engineering to incorporate short heterologous targeting peptide sequences has been widely investigated within the field [reviewed in (Reetz et al., 2014, Coughlan et al., 2010)]. Peptide ligands could potentially serve for dual purposes, as the insertion of peptides may favourably shift antigenic recognition away from the major antigenic epitopes, in addition to efficient targeting to cancer markers. The fiber protein has been the most frequently modified for these purposes (Särkioja et al., 2008, Uusi-Kerttula et al., 2015b), due to the location of major antigenic epitopes within the knob domain (Xia et al., 1994), its native role in primary cell tethering, and its tolerance of genetic manipulation.

Pre-existing anti-Ad nAbs present in the blood and bodily fluids rapidly recognise and eliminate systemically- or locally administered Ad vectors. For ovarian cancer applications, vector neutralisation by ascites may be circumvented by genetic masking of the fiber. Blackwell and colleagues reported successful evasion of nAbs in ascites using a tropism-modified Ad5 vector with an integrin-binding RGD motif insertion in the fiber knob (Blackwell et al., 2000). Our research has utilised a similar masking approach by genetically inserting short high affinity peptides targeted to receptors over-expressed on various tumours into the Ad5 fiber knob (Uusi-Kerttula et al., 2015b, Uusi-Kerttula et al., 2016). We genetically incorporated a short GE11 peptide (YHWYGYTPQNVI) targeting cellular EGFR, or two peptides M* (MQLPLAT) (Maruta et al., 2002) and LS (LSPPRYP) (Wu et al., 2013) targeting FGFR1, into a

replication-deficient Ad5 vector (Uusi-Kerttula et al., 2015b). Although cancer targeting was not markedly improved, these vectors exhibited improved protection from anti-Ad5 nAb-mediated neutralisation.

αvβ6 integrin is a particularly interesting cellular target receptor due to its over-expression in progressive cancers (discussed in section 1.5.2). Several reports have described genetic incorporation of the A20 peptide from FMDV into viral vectors for targeting into αvβ6 integrin-expressing cancer cells (Coughlan et al., 2009b, Coughlan et al., 2014, Uusi-Kerttula et al., 2016). In a study by Coughlan and colleagues, A20 was genetically incorporated into the fiber knob HI loop within a recombinant enhanced green fluorescent protein (EGFP)-expressing Ad5 vector background (Ad5EGFP$_{A20}$) (Coughlan et al., 2009a). This vector exhibited ~50-fold increased CAR-independent transduction and greatly enhanced cytotoxicity in αvβ6$^{high}$ cancer cells as compared to the parent vector Ad5EGFP$_{WT}$, confirming successful A20-mediated cancer-targeting. Importantly, the safety of this vector was greatly improved relative to the natively hepatotropic Ad5EGFP$_{WT}$, with significantly reduced liver uptake following systemic delivery. In this thesis we aim to utilise a similar approach for Ad vector targeting to αvβ6-expressing EOC.

## 1.7    Hypotheses of this thesis

The three experimental aims are: (1) Generation of de-targeted Ad5-based vectors with mutations in fiber knob, hexon and penton proteins to ablate native interactions with CAR, FX and αvβ3/5 integrins, respectively; (2) Generation of novel pseudotyped Ad5-based vectors with fiber or fiber knob from species D serotypes to study alternative receptor tropisms *in vitro*; (3) Generation of de-targeted, tropism-modified vectors by a genetic incorporation of the A20 peptide ligand from FMDV, targeting an epithelial-specific cancer marker αvβ6 integrin.

We hypothesise that the combination of de-targeting mutations ('3D') will lead to strictly selective vectors that fail to transduce normal, healthy cells in the liver, spleen and other off-target sites, thus improving their toxicity profile. The A20 peptide-modified vectors are expected to selectively transduce αvβ6+ cancer cells *in vitro*, primary clinical ascites-derived EOC cultures *ex vivo* and tumour xenograft models *in vivo*. The combination of A20 peptide insertion and fiber-pseudotyping is expected to facilitate vector protection from neutralisation by anti-Ad5 nAbs present in malignant ovarian ascites. Local i.p. delivery for the treatment of ovarian cancer is our proposed route to clinical translation.

# CHAPTER 2. Materials and methods

## 2.1 Phenotyping of cell lines, primary cells and ovarian ascites

This section describes the phenotyping and validation of suitable ovarian cancer model cell lines and primary EOC cell *ex vivo* cultures from clinical ovarian ascites. Ovarian ascites cell-free supernatants were also characterised for their anti-Ad vector neutralising properties and for the concentration of free FX.

### *2.1.1 Basic cell culture techniques*

All cells were grown in a Human Tissue Act (HTA) certified cell culture incubator (HERA Cell, Thermo Scientific) at 37°C in a humidified atmosphere with 5 % $CO_2$. All reagents and materials used for cell culture were sterile, disposable and individually packed. Cell lines were sourced either from American Type Culture Collection (ATCC) or collaborators, and cultured in a cell line-specific media and supplements (Table 2–1).

**Table 2–1. Cell culture media.** Basic cell culture media was used for culture of cell lines and primary cells. All media were supplemented with P/S, L-Glut and FBS.

| Abbreviation | Full name | Supplier | Cat. # |
|---|---|---|---|
| α-MEM | Minimum Essential Medium Eagle alpha modification with | Sigma, Gillingham, UK | M8042 |
| DMEM | Dulbecco's Modified Eagle's Medium | Sigma, Gillingham, UK | D5796 |
| DMEM/F12 | DMEM with F12 modification | Sigma, Gillingham, UK | D6421 |
| FBS | Foetal Bovine Serum, heat inactivated | Gibco, Paisley, UK | 10500-064 |
| L-Glutamine | L-Glutamine, stock 200 mM | Gibco, Paisley, UK | 25030-024 |
| DPBS | Dulbecco's Phosphate Buffered Saline | Sigma, Gillingham, UK | D8537 |
| P/S | Penicillin 100 U/mL, streptomycin 100 µg/mL | Gibco, Paisley, UK | 15070-063 |
| RBC lysis | Red blood cell lysis buffer | Sigma, Gillingham, UK | R7757 |
| RPMI 1640 | Roswell Park Memorial Institute 1640 | Gibco, Paisley, UK | 21875-034 |
| Trypsin | 0.05 % Trypsin-EDTA, phenol red | Gibco, Paisley, UK | 25300-054 |

Mammalian cell lines (Table 2–2) were regularly sub-cultured once or twice weekly by passaging into new sterile flasks when they reached 80–100 % confluency. Slowly growing cells were generally cultured in T75 flasks (Corning, UK) and not split with higher ratio than 1:3, while very rapidly growing cells were split even 1:10 twice weekly into T150 flasks (Corning, UK). Sub-culture of cells growing in T150 flasks involved aspirating the cell culture medium and washing the cells with 10 mL (T75) or 20 mL (T150) of PBS. 2.5 % (T75) or 5 mL (T150) of 0.05 % trypsin was then added to the cells, swirled around to cover the entire monolayer, and incubated for ~ 5 min at 37°C. The side of the flask was then gently tapped until the cells were completely detached, as observed under the light microscope. BT-20 and SKOV3 cells attached to the flask more firmly than other cell types, and therefore detachment required two washes with PBS and scraping the bottom of the flask with a sterile single-use cell scraper (Greiner Bio-One, #82050-468, VWR) to collect all the cells. The cell suspension was then

divided into new flasks with an appropriate ratio (1:2–1:10), depending on their subsequent usage. 10 mL (T75) or 20 mL (T150) of fresh cell culture medium was added into each flask and the cells incubated until appropriate level of confluency was reached. The cells were then sub-cultured once or twice a week for maintenance or used for *in vitro* assays.

**Table 2–2. Mammalian cell lines and growth conditions.** collab., collaborators at Cardiff University; DMEM, Dulbecco's Modified Eagle's Medium; FBS, foetal bovine serum; LC, Dr Lynda Coughlan (Oxford University, UK); puro, puromycin; RPMI, Roswell Park Memorial Institute.

| Cell line | Cell origin | Medium | % FBS | Suppl. | Source |
|---|---|---|---|---|---|
| A549 | Human lung carcinoma | RPMI1640 | 10 | – | collab. |
| BT-20 | Human breast cancer | α-MEM | 20 | – | LC |
| CHO-K1 | Chinese hamster ovarian epithelial | DMEM/F12 | 10 | – | collab. |
| CHO-CAR | CHO transfected to express hCAR | DMEM/F12 | 10 | – | collab. |
| HEK293 | Human embryonic kidney | DMEM | 10 | – | LC |
| IGROV-1 | Human ovarian adenocarcinoma | RPMI1640 | 10 | – | collab. |
| HEK293-β6 | HEK293 expressing β6 integrin | DMEM | 10 | 5 µg/mL puro | LC |
| OVCAR3 | Ovarian cancer | RPMI1640 | 20 | – | collab. |
| SKOV3 | Human ovarian adenocarcinoma | DMEM | 10 | – | LC |
| SKOV3-β6 | SKOV3 expressing αvβ6 integrin | DMEM | | 5 µg/mL puro | in-house |
| T24 | Human urinary bladder transitional cell carcinoma | DMEM | 10 | – | collab. |
| T-REx 293 | Human embryonic kidney | DMEM | 10 | – | Invitrogen |

### 2.1.2 Generation of SKOV3-β6 ovarian cancer cell line

A pBABE puro plasmid with human *itgb6* gene (2400 bp; GenBank ID: NM_000888) from (pBABE-β6 puro; #13596, Addgene) (Figure 2–1) was received as a bacterial stab in DH5-α *E. coli* cells. This plasmid expresses the human integrin β6 subunit that pairs in cells with αv subunit only, forming the αvβ6 heterodimer (Hynes, 2002). The bacteria were amplified in an O/N culture of 250 mL low-salt powder (LB; #L1703, Melford Laboratories, Suffolk, UK) supplemented with 100 µg/mL Amp and plasmid was purified using NucleoBond BAC 100 purification kit (#740579, Macherey-Nagel, Duren, Germany). DNA concentration was determined using NanoDrop ND-1000 (Thermo Scientific, UK) and transfected into a packaging cell line 293Phoenix in a confluent T25 flask using Effectene transfection reagent (#301425; Qiagen, Manchester, UK) according to manufacturer's instructions. After 48 h, the retrovirus-containing supernatant was harvested and filtered through a 0.4 µm syringe filter to ensure complete removal of the 293Phoenix cells. The virus was snap-frozen in dry ice and stored at –80°C for subsequent use.
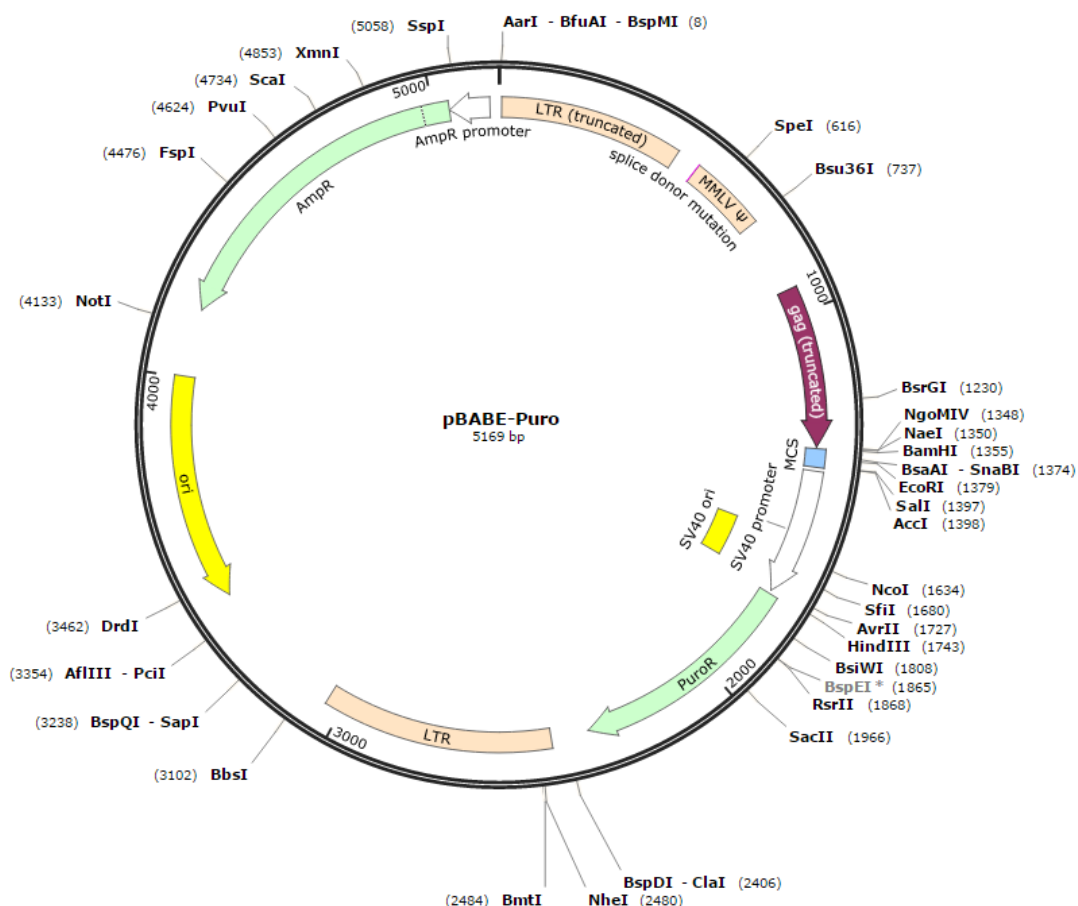
**Figure 2–1. pBABE-puro plasmid backbone.** The plasmid was purchased from Addgene with *itgb6* gene coding for the β6 integrin subunit cloned in (Snapgene, 2016). The plasmid carries ampicillin and puromycin resistance genes.

In the following step the retrovirus was transfected into the target cell line, SKOV3. A 6-well plate was coated with RetroNectin reagent (#T100B, Takara Bio Europe SAS, France) O/N at 4ºC, washed with PBS. 1.5 mL of virus (supernatant from step above) was added in the coated well, the plate sealed in a bag and centrifuged at 2800 rpm at 30°C for 2 h to bind the virus to the bottom of the dish. The virus was removed, the bottom of the well was washed once with PBS and SKOV3 cells seeded at ~ 70 % density ($1 \times 10^5$ cells/mL). After 48 h, the cells were detached from the plate using trypsin and seeded into a T25 tissue culture flask in DMEM medium supplemented with 5 µg/mL puromycin (#P8833, Sigma Aldrich, Gillingham, UK). After 3–4 days the only surviving cells were cells expressing αvβ6 integrin.

### 2.1.3   *Ex vivo primary epithelial ovarian cancer (EOC) cell culture*

Permission for the collection and cultivation of EOC cells from ovarian ascites was granted through a Wales Cancer Bank application for biomaterials, reference WCB 14/004. All patients gave written informed consent for the use of their samples prior

to collection. A 400–600 mL total volume of clinical ovarian ascites (OAS) was drained from ovarian cancer patients using an intraperitoneal (i.p.) catheter (paracentesis) as part of routine cancer care by trained nurses at Velindre Cancer Centre, Cardiff. OAS samples were received in sterile 500 mL containers generally within 3 hours from paracentesis. Samples were assigned into treatment groups according to the stage of chemotherapy (1, pre-treatment/chemo naïve; 2, 1st line chemo; 3, relapsed disease/platinum sensitive; 4, relapsed disease/platinum resistant). Samples were given 'OAS' codes to retain anonymity.

Fluids were stored at 4°C following paracentesis and processed fresh within 24 h. *Ex vivo* cultures were established essentially according to a protocol by Dr Sandra Bell (Leeds Institute of Biomedical & Clinical Sciences, St James's University Hospital Leeds) and previously described methods (Shepherd et al., 2007, Thériault et al., 2013). Initially, 100 mL of the original sample was aliquoted into five T75 tissue culture flasks (20 mL each) and 20 mL RPMI 1640 medium supplemented with 1 % Glutamax/L-Glutamin, 10 % FBS, 100 U/mL penicillin and 100 µg/mL streptomycin was added into each flask. The cells were allowed to attach for 3 days undisturbed. Media was then removed, cells washed with PBS and grown in complete EOC medium additionally supplemented with 10 % of cell-free autologous fluid supernatant. Medium was then changed twice a week and cells sub-cultured when they reached confluency (2–4 weeks from culture initiation). Cell morphology of the established *ex vivo* cultures was monitored several times a week by visual examination under light microscope throughout cell passages. The cultures that were heavily contaminated with fibroblasts, were partially trypsinised for 1 min to remove fibroblasts that were more loosely attached to the plastic than EOC cells. Primary EOC cells in the remaining OAS sample (~ 400 mL) were pelleted by centrifugation at 1000 rpm for 5 min. Ascites supernatant was decanted into 50 mL falcon tubes and stored at −70°C. Cell pellets were pooled and treated twice with 2 mL of RBC lysis buffer according to the manufacturer's protocol, in case of a heavy erythrocyte contamination. The cell pellet was washed with PBS and re-suspended in freezing medium (10 % dimethyl sulfoxide (DMSO) in 90 % FBS) and stored in liquid nitrogen tanks at −130°C (passage 0) for long term stocks.

### 2.1.4 Long-term storage and recovery of cell lines

Mammalian cell lines and primary EOC cell cultures were grown until confluent, washed with PBS and detached with trypsin. They were neutralised with complete medium and pelleted at 1200 rpm for 3 min, supernatant discarded and the pellet re-suspended into 3 mL of 10 % DMSO in FBS. Cell suspensions were aliquoted into 1

mL and stored long-term in 1.5 mL cryovials (Corning, UK) in −130°C liquid nitrogen tanks. Primary EOC cell stocks were always established at passage 0 and 1. Passage numbers were not recorded for other cell lines. When cell culture was initiated, a vial of each cell type was removed from the tank, placed immediately on dry ice and rapidly thawed in a pre-warmed 37°C water bath for ~ 2–3 min until no ice was visible. The contents of the vial were then removed with a 1 mL pipette into a T25 flask with 10 mL of pre-warmed complete cell line-specific medium and left undisturbed for 24 h. On the following day medium was aspirated and replaced with 5 mL of fresh complete medium, and cultured until a confluent cell monolayer was reached. Cells were sub-cultured as described in section 2.1.1.

### 2.1.5 Direct ELISA for detection of anti-adenovirus antibodies in ascites

Anti-Ad antibodies were detected from ascites according to a previously published protocol (Stallwood et al., 2000) (Figure 2–2). Viruses were diluted at 200 ng protein/ml in coating buffer ($NaHCO_3/Na_2HCO_3$, pH 9.6) and heat-inactivated at 56ºC for 30 min. 96-well flat-bottom ELISA plates (#44-2404-21, MaxiSorp, Nunc; Affymetrix eBioscience) were coated with 100 µL of virus / well and incubated O/N at 4ºC. Each well was washed six times with 200 µL of PBS-T (0.01 % Tween-20 in PBS). 2-fold dilutions (1:50–1:51 200) of ascites samples and serum control were prepared in 1 % BSA/PBS-T and 100 µl of added into each well in duplicate for 2 h at room temperature (RT). The wash was repeated and wells incubated with 100 µL of anti-human IgG-HRP (1:10 000; goat α-human IgG-HRP, sc-2907, #J0914, Santa Cruz) in 1 % BSA/PBS-T for 1 h at RT. After a wash, 100 µL of substrate (1:1 mix of BD OptEIA TMB substrate reagents; #555214, Benkton Dickinson, Oxford, UK) was added into each well and incubated for 20 min at RT. The reaction was then stopped with 100 µL of 0.2 M $H_2SO_4$ and absorbance measured immediately at λ450 nm.
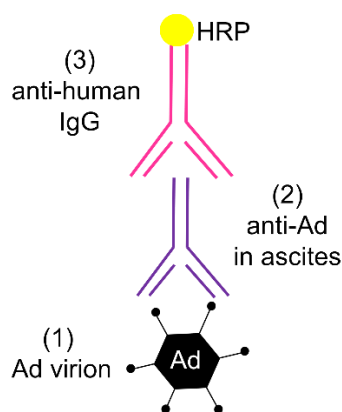


**Figure 2–2. Direct enzyme-linked immunosorbent assay (ELISA) for the quantification of anti-adenovirus (Ad) antibodies in ovarian ascites.** The order of reagents is depicted in numbers (1–3). After adding the TMB substrate, absorbance was measured at λ490 nm. HRP, horse radish peroxidase.

### 2.1.6  Sandwich ELISA for detection of coagulation factor X in ascites

An ELISA protocol was developed in-house for the detection of FX from ascites (Figure 2–3). Each well on a 96-well flat-bottom ELISA plates (MaxiSorp, Nunc; #44-2404-21, Affymetrix eBioscience) was coated with 100 µL of a sheep anti-human coagulation factor X (FX) capture antibody (#ab110138, Abcam) at 2 µg/mL and incubated O/N at 4ºC. The wells were washed four times with 200 µL of PBS-T (0.01 % Tween-20 in PBS) and plate dried on an absorbent tissue between each wash. 2-fold dilutions (neat, 1:2 and 1:4) of ascites samples and serum control were prepared in 1 % milk/PBS-T and 100 µL added into each well in duplicate for 2 h at 37ºC on a rocker. Purified human FX (#HCX0050, Haematologic Technologies, Cambridge Bioscience, Cambridge, UK) was diluted (0–10 µg/ml) in sample buffer and assayed on the same plate to generate a standard curve. After washing the wells four times with wash buffer as before, they were incubated with 100 µL of rabbit anti-human FX detection antibody (#ab80345, Abcam, Cambridge, UK) for 2 h at RT. The wash was repeated, and wells incubated with 100 µL of goat anti-rabbit IgG (H + L)-HRP conjugate (1:3000; #1706515, BioRad, Hertfordshire, UK) in 1 % milk/PBS-T for 1 h at RT. After serial washes, 100 µL of substrate (1:1 mix of BD OptEIA TMB substrate reagents; #555214, Benkton Dickinson, Oxford, UK) was added into each well and incubated for 20 min at RT. The reaction was then stopped with 100 µL of 0.2 M $H_2SO_4$ and absorbance measured immediately at λ450 nm.
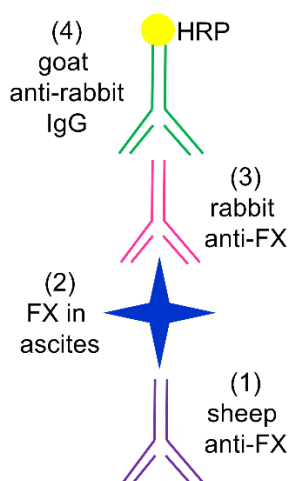


**Figure 2–3. Sandwich enzyme-linked immunosorbent assay (ELISA) for the quantification of human coagulation factor 10 (FX) in ovarian ascites.** The order of reagents is depicted in numbers (1–3). After adding the TMB substrate, absorbance was measured at λ490 nm. HRP, horse radish peroxidase.

### 2.1.7  Western blot for qualification of anti-Ad antibodies in ascites

Viruses were run in a pre-cast NuPAGE Novex® 10 % Bis-Tris SDS-PAGE gels (#WG1201BOX; Life Technologies, Loughborough, UK) at 0.625, 1.25, 2.5 and 5 µg

of protein/well (1 µg of protein corresponding to $4 \times 10^9$ viral particles (Von Seggern et al., 1998)) in a total volume of 40 µl (including 2 µl of DTT and 10 µl of 4 x NuPAGE LDS sample buffer) for 1 h 20 min at 150 V. The proteins were transferred onto an Amersham Protran 0.45 µm nitrocellulose blotting membrane (#10600002; GE Healthcare Life Science, Little Chalfont, UK) by semi-dry blotting in a Trans-blot SD Semi-dry Transfer Cell (Bio-Rad, Hertfordshire, UK) for 1 h at 20 V. The membrane was blocked in 5 % milk/TBS-T for 90 min at RT or O/N at 4ºC on a rocker and incubated in ascites or serum at 1:500 in 5 %/TBS-T for 90 min at RT on a rocker. It was then washed three times for 10 min in TBS-T on a rocker at RT and incubated in secondary anti-human IgG-HRP (goat α-human IgG-HRP sc-2907 #J0914, Santa Cruz) at 1:2000 in 5 %/TBS-T for 1 h at RT on a rocker, and washed again three times for 10 min in TBS-T at RT on a rocker. The proteins were then visualised by incubating the membrane in 1:1 mixture of West Pico SuperSignal (#34078; Thermo Scientific, Paisley, UK) reagents for 10 min, and membrane imaged in G:BOX Chemi XX6 imager (Syngene, Cambridge, UK).

### 2.1.8   Flow cytometry for cell line receptor profiling

Receptor expression profiles were determined for each cell line and EOC *ex vivo* culture by flow cytometry. A sufficient number of sub-cultured cells were detached from the flasks using 0.05 % trypsin, washed with complete DMEM at 1200 rpm for 3 min and then re-suspended into 10 mL of ice-cold wash buffer (0.5 % FBS in PBS). Cells were counted on a haemocytometer and $1 \times 10^5$ cells added into each well in duplicate on a U-bottom 96-well plate (#268200, Nunc, Thermo Scientific, UK). Cells were then washed in 200 µL of ice-cold wash buffer, pelleted at 1500 rpm for 3 min at 4°C and kept on ice for the remainder of the protocol. Cells were incubated in 100 µL of diluted primary antibodies (Table 2–3) on ice for 1 h and mixed well. The cells were re-pelleted, washed three times in 200 µL of ice-cold wash buffer, re-pelleted and incubated with 100 µL of diluted secondary antibody F(ab')2-goat α-mouse IgG (H+L) IgG AlexaFluor 647 (#A21237, Life Technologies, Paisley, UK) for 30 min on ice in the dark. After three washing steps the cells were re-pelleted and fixed in 200 µL of ice-cold 4 % paraformaldehyde (PFA) for a minimum of 10 min (or O/N). Cells were analysed on a BD Accuri C6 version 1.0.264.21 (BD Biosciences, Oxford, UK) flow cytometer with pre-run washing steps according to the manufacturer's instructions. Initially, the measurement was gated with unstained cells, and $2 \times 10^4$ gated events were recorded per sample. The results were analysed using the BD Accuri software.

**Table 2–3. Mouse anti-human primary antibodies used in flow cytometry.** CAR, coxsackie and adenovirus receptor; EGFR, epidermal growth factor receptor.

| Target | Clone | Dilution | Cat # | Supplier |
|--------|-------|----------|-------|----------|
| αvβ6 | 10D5 | 1:100 | MAB2077Z | Millipore, Watford, UK |
| CAR | RmcB | 1:500 | 05-644 | Millipore, Watford, UK |
| EGFR | H11 | 1:200 | MA5-13070 | Thermo Scientific, Paisley, UK |
| CD44 | F10442 | 1:100 | ABIN135705 | antibodies-online |
| CD46 | MEM258 | 1:100 | MA1-82140 | Thermo Scientific, Paisley, UK |
| normal IgG | − | 1:200 | sc-2025 | Santa Cruz Biotechnologies, Heidelberg, Germany |

### 2.1.9  Fluorescence activated cell sorting (FACS)

SKOV3-β6 cells were sorted into high αvβ6 expressing populations prior to *in vitro* assays. Cells were stained with primary anti-αvβ6 antibody 10D5 (1:100) and secondary AlexaFluor 647 according to the flow cytometry protocol (section 2.1.8), except that the cells were left non-fixed. Cell sorting was performed on BD FACSAria II multicolour cell sorter (BD Biosciences) by Dr Kristin Ladell, Institute of Infection and Immunity, Cardiff University. Data were analysed in BD FACSDiva 8.0.1 software (BD Biosciences). Cells with the highest 10 % fluorescence intensity were selected, propagated and used for assays. SKOV3-β6 cell sorting prior to implantation of *in vivo* ovarian cancer xenografts was performed at the Microscopy and Cytometry Core at Mayo Clinic, Rochester, MN, USA. $2 \times 10^7$ cells were stained with a primary anti-αvβ6 antibody 10D5 (1:100) and a secondary anti-mouse IgG/IgA/IgM-FITC conjugate (1:100; #0855499; MP Biomedicals, USA). The population with 10 % highest αvβ6 expression was sorted and propagated in the presence of 5 μg/mL of puromycin selection antibiotic prior to implantation into mice.

## 2.2  Recombinant fiber knob protein engineering

Recombinant, soluble Ad fiber knob proteins were produced for competition inhibition assays for the assessment of pseudotyped vector tropism. The production and purification method has been previously validated and optimised elsewhere by Dr Lynda Coughlan [Oxford University, UK, (Coughlan et al., 2014)]. The pQE30 expression plasmids contain a 6 x His tag at the C terminus of the knob sequence to enable efficient and rapid protein purification by nickel ion nitrilotriacetic acid ($Ni^{2+}$-NTA) affinity chromatography. The method is based on high affinity binding to the $Ni^{2+}$-NTA agarose matrix between the polyhistidine tag (Figure 2–4) in the recombinant protein and increasing concentrations of imidazole present in the elution buffer. Histidine and imidazole have very similar ring structures that forms the basis for competitive binding into the agarose matrix.
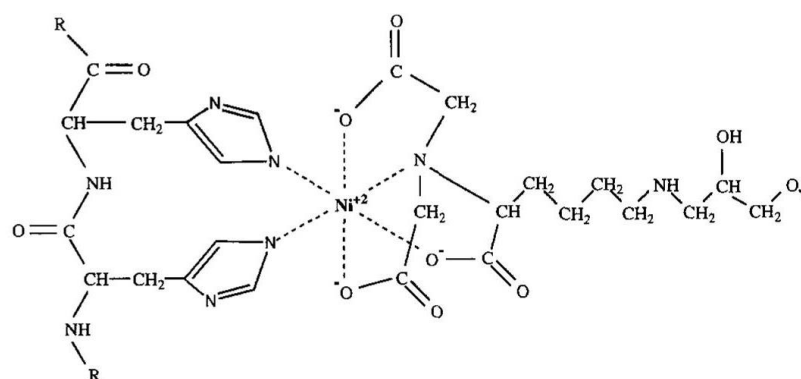
**Figure 2–4. Interactions between polyhistidine tag (left) and nickel–nitrilotriacetic acid (Ni2+-NTA) matrix.** The Ni2+ ion lies in octahedral coordination relative to two histidine side chains and four matrix ligands (Bornhorst and Falke, 2000).

### 2.2.1 Predictive structural modelling of knob domains

The potential knob protein structures with targeting peptide insertions were created to assess the spatial conformation of the inserted peptides in the context of the homotrimeric knob structure to predict their feasibility as complete virus particles. Ad5 (GenPept: AAP31231.1), Ad48 (GenPept: ABO61306.1) and Ad35 (GenPept: AP_000601.1) fiber amino acid sequences were downloaded from the National Center for Biotechnology Information (NCBI) database and aligned in BioEdit (Hall, 1999) version 7.2.5 using the ClustalW Multiple Alignment command. Knob domains were edited to contain the A20 peptide amino acid sequence and the sequences were submitted to the predictive online 3D modelling software SWISS-MODEL (Arnold et al., 2006, Bordoli et al., 2009, Biasini et al., 2014) (Biozentrum, Basel, Switzerland) in an automated mode. Previously crystallised Ad knob structures with the highest homology (%) were chosen to be used as templates, and the models were saved as Protein Data Bank (PDB) files for further manipulation. Ad5 knob models were based on PDB structure 1KNB, species D knob models were based on either Ad19p knob (PDB ID: 1UXB) or Ad37 knob (PDB ID: 2WGU). Crystallisation data is currently not available for other species D Ad knobs. Molecular graphics and analyses were performed using the UCSF Chimera package (Pettersen et al., 2004) version 1.10.2 (Resource for Biocomputing, Visualization, and Informatics; University of California, San Francisco, USA).

### 2.2.2 Generation of pQE30 expression plasmids

Recombinant fiber knob proteins were produced in *E. coli* essentially as described previously (Coughlan et al., 2009b, Coughlan et al., 2014). The pQE30knob48 expression plasmids were a kind gift from Dr Lynda Coughlan (Oxford University, UK), and readily contained the knob48 sequence and the A20 peptide sequence in the four different locations (loops CD, DG, HI, IJ). These plasmids carry an ampicillin (Amp)

resistance gene. Plasmid sequences were received as Whatman paper preparations, and were first dissolved into 50 μL of TE buffer. The DNA were then transformed into commercially available chemically competent, high copy number *E. coli* strain JM109 (#L1001, Promega, Southampton, UK) for plasmid amplification. In brief, 50 μL cells were mixed with 10 ng of plasmid DNA on ice, incubated for 30 min on ice and transferred into 42°C water bath for exactly 45 seconds. Cells were then recovered on ice for 2 min and incubated at 37°C for 1 h, after which they were plated on LB (+ 100 μg/mL Amp / 50 μg/mL Kan) plates and incubated at 37°C for 24–48 h. Individual colonies were then picked and inoculated into 5 mL of LB + Amp for O/N incubation at 37°C. On the following day the DNA was purified by using a miniprep kit and DNA concentration verified by Nanodrop. The Kan-resistant *E. coli* strain SG13009 was utilised for knob protein production from the pQE30 plasmids (Figure 2–5). Initially, the SG13009 bacteria were made chemically competent by a rubidium chloride method (QIAexpressionist 06/2003 protocol).
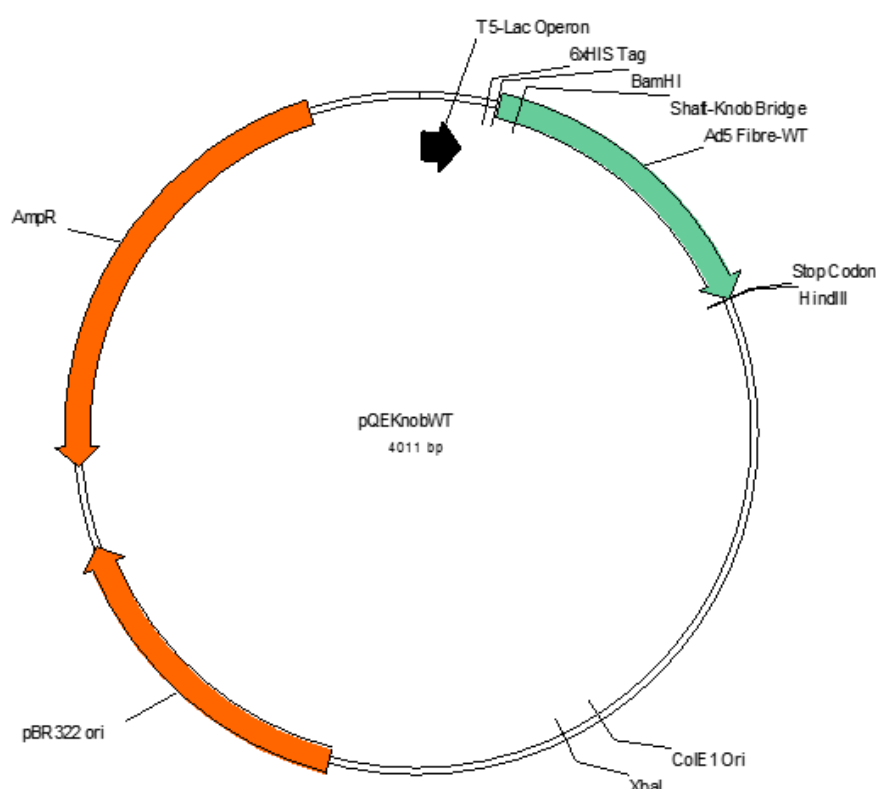


**Figure 2–5. Schematic presentation of the pQE30 plasmid.** The plasmids were based on pQE30 plasmids (Qiagen) and were kindly gifted by Dr Lynda Coughlan, Oxford University.

A single colony of SG13009 was first inoculated into 10 mL of LB (+ Kan) and grown O/N. On the following day 1 mL of the culture was incubated in 100 mL of LB (+ Kan) until optical density (OD) reached 0.5 (λ600 nm). The culture was then pelleted at 4000 x g at 4°C for 5 min in a sterile round-bottomed tube and re-

suspended into 30 mL of sterile-filtered (0.22 µm) ice-cold TFB1 buffer (100 mM RbCl, 50 mM MnCl2, 30 mM KAc, 10 mM CaCl2, 15 % glycerol, pH 5.8), incubated on ice for 90 min and pelleted as previously. The pellet was then re-suspended into 4 mL of sterile-filtered, ice-cold TFB2 buffer (10 mM MOPS, 10 mM RbCl, 75 mM CaCl2, 15 % glycerol, pH 6.8), divided into 200 µL aliquots in 1.5 ml cryovials and stored at –80°C. For protein production, 10 µg of each pQE30 plasmid DNA was transformed into 50 µL of the competent SG13009 bacteria by heat shock method as described earlier, and grown on selective LB (+Amp/Kan) plates for 48 h.

### 2.2.3 Isopropyl β-D-1-thiogalactopyranoside (IPTG)-induced protein production

Protein production was initiated by culturing a pre-culture that served as a seed culture for protein induction. For preparation of a pre-culture, multiple colonies of each pQE30 plasmid-containing SG13009 cells were picked from the LB (+Amp/Kan) plates and grown in 100 mL of LB (+Amp/Kan) O/N at 37°C with aeration (250 rpm). On the following day the cells were pelleted at 4000 x g for 10 min, re-suspended into 20 mL of LB, divided into five 4 mL aliquots, pelleted again and frozen down at –20 °C for subsequent protein induction. For induction of protein production, a "4 mL" aliquot was thawed in a 37°C water bath and inoculated into 1 L of Terrific Broth (#T0918, Sigma Aldrich, Gillingham, UK) supplemented with 0.8% glycerol, 100 µg/mL Amp and 50 µg/mL Kan in a 2 L flask. The culture was incubated at 37 °C (250 rpm) until OD reached 0.6 (λ600 nm). Protein expression was then induced by adding isopropyl β-D-1-thiogalactopyranoside (IPTG) to a final concentration of 0.5 mM at 20°C for 16 h. The optimisation of knob protein induction conditions has previously shown that these conditions are preferable to a shorter (4 h) induction at 37°C (Coughlan et al., 2009a). The culture was then harvested at 4000 × g for 15 min and the pellet was washed with 50 mL of PBS, re-pelleted at 4000 × g for 10 min and frozen at –80°C if not used immediately.

### 2.2.4 Protein purification by nickel-nitrilotriacetic acid (Ni-NTA) affinity chromatography

A 1 mL aliquot was taken from each pre-purification and purification step for analysis by SDS-PAGE. The pellet from a 1 L culture was re-suspended in 50 mL of lysis buffer (50 mM Tris, 300 mM NaCl, 10 mM imidazole, 1 % NP40 substitute, 1 mg/mL lysozyme, 1 mM β-merkaptoethanol, pH 8.0 in $H_2O$) and agitated on roller for 1 h at 4°C in the cold room. The suspension was transferred into 2 x 25 ml high speed centrifuge tubes, balanced with equal volumes and spun at 30 000 x g for 20 min at 4 °C in a high speed centrifuge (rotor JA 25.50). The cleared lysate was divided into 2

x 50 mL clean tubes and agitated on a roller with 0.5 mL of high binding capacity Ni-NTA Agarose (#30210, Qiagen, Manchester, UK) for 1 h at 4°C. The matrix was then collected by spinning at 1000 x g for 10 min and the supernatant was carefully removed (but kept in case protein had not bound to matrix) and loaded into a disposable plastic chromatography column (#7321010, Biorad, Hertfordshire, UK). The column was washed with 50 mL of wash buffer (50 mM Tris, 300 mM NaCl, 1 mM β-merkaptoethanol, 10 mM imidazole, pH 8.0 in $H_2O$). 5 x 1.0 mL fractions were then eluted for each concentration for a gradient of 50–300 mM imidazole (50 mM Tris, 300 mM NaCl, 1 mM β-merkaptoethanol, 50/100/200/300 mM imidazole, pH 8.0 in dd$H_2O$) by allowing it to flow through, collecting each 1 mL fraction manually in a 1.5 mL tube. The aliquots were stored short term at 4°C prior to analysis by SDS-PAGE.

### 2.2.5   Coomassie brilliant blue staining for protein

All SDS-PAGE analyses were performed using the NuPAGE Novex® (Life Technologies, Loughborough, UK) systems and buffers. 14 µL of eluted protein fractions were mixed with 1 µL of DTT and 5 µL of NuPAGE LDS sample buffer (4 x concentrated, Thermo Scientific), boiled at 95 °C for 10 min and loaded into pre-cast midi NuPAGE Novex® 10 % Bis-Tris SDS-PAGE gels (#WG1201BOX, Life Technologies, UK). The samples were run along with 10 µL Novex® Sharp Pre-stained protein standard (#LC5800, Thermo Fisher Scientific, UK) for 1 h 15 min at 150 V and stained in Coomassie stain (0.25% Coomassie brilliant blue, 50 % methanol, 10 % acetic acid in $H_2O$) for 30 min, after which they were de-stained (30 % methanol, 10 % acetic acid in $H_2O$) with multiple changes of buffer O/N or until no background staining was visible. The gels were then visualised in gel imager (GelDocIt, Ultra-Violet Products Ltd, Cambridge, UK or G:BOX Chemi XX6 imager, Syngene, Cambridge, UK).

## 2.3   Virus engineering by homologous recombination (AdZ recombineering)

All viral vectors produced in this thesis were generated by rapid AdZ recombineering techniques (Figure 2–6).

### 2.3.1   Generation of bacterial artificial chromosomes (BACs)

The wild type Ad5 virus was originally gifted by Vivien Mautner at University of Birmingham, UK. The viral genome was captured within a bacterial artificial chromosome (BAC) and has since been vectorised and heavily genetically modified in our laboratory (Stanton et al., 2008). Generated recombinant Ad5 genomes are based on luciferase (Luc) or green fluorescent protein (GFP) -expressing Ad5 vector

genome (Figure 2–7). This vectors have been made replication-deficient by deleting the *E1* and *E3* gene regions (*ΔE1/ΔE3*) that are responsible for viral replication. Oncolytic viruses contain the E1 and E3 gene regions, making them replication-competent. These vectors were made cancer-selective by an insertion of a 24-base pair deletion (*dl*922–947, Δ24) in the retinoblastoma protein (pRB) binding domain of E1A gene (Fueyo et al., 2000), which restricts viral replication into cancer cells with aberrant pRB signalling pathways. Additionally, T1 mutation – a single adenine insertion at position 445 within the endoplasmic reticulum (ER) retention domain of the *E3/19K* gene (Gros et al., 2008) – was inserted to enhance viral release from the ER.
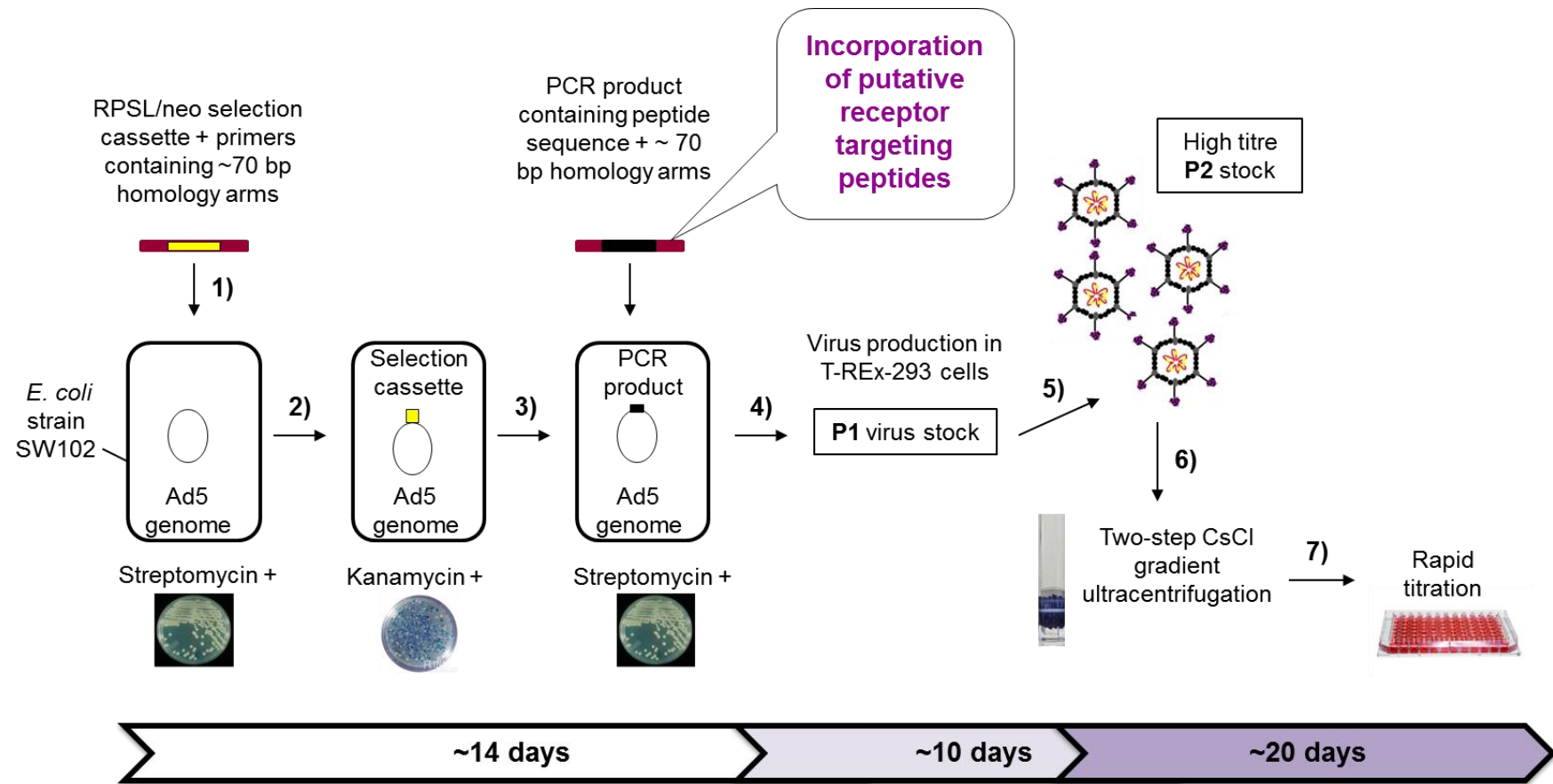
**Figure 2–6. Complete production cycle of Ad5 vectors from AdZ recombineering to purified virus particles.** (1) Transformation by electroporation, (2) & (3) temperature-induced recombineering (42˚C), (4) purification of BAC DNA and transfection into T-Rex-293 cells, (5) propagation of high titre stocks in T-Rex-293 cells, (6) purification of viral particles by CsCl gradient ultracentrifugation, (7) titration by microBCA and/or rapid plaque assay.
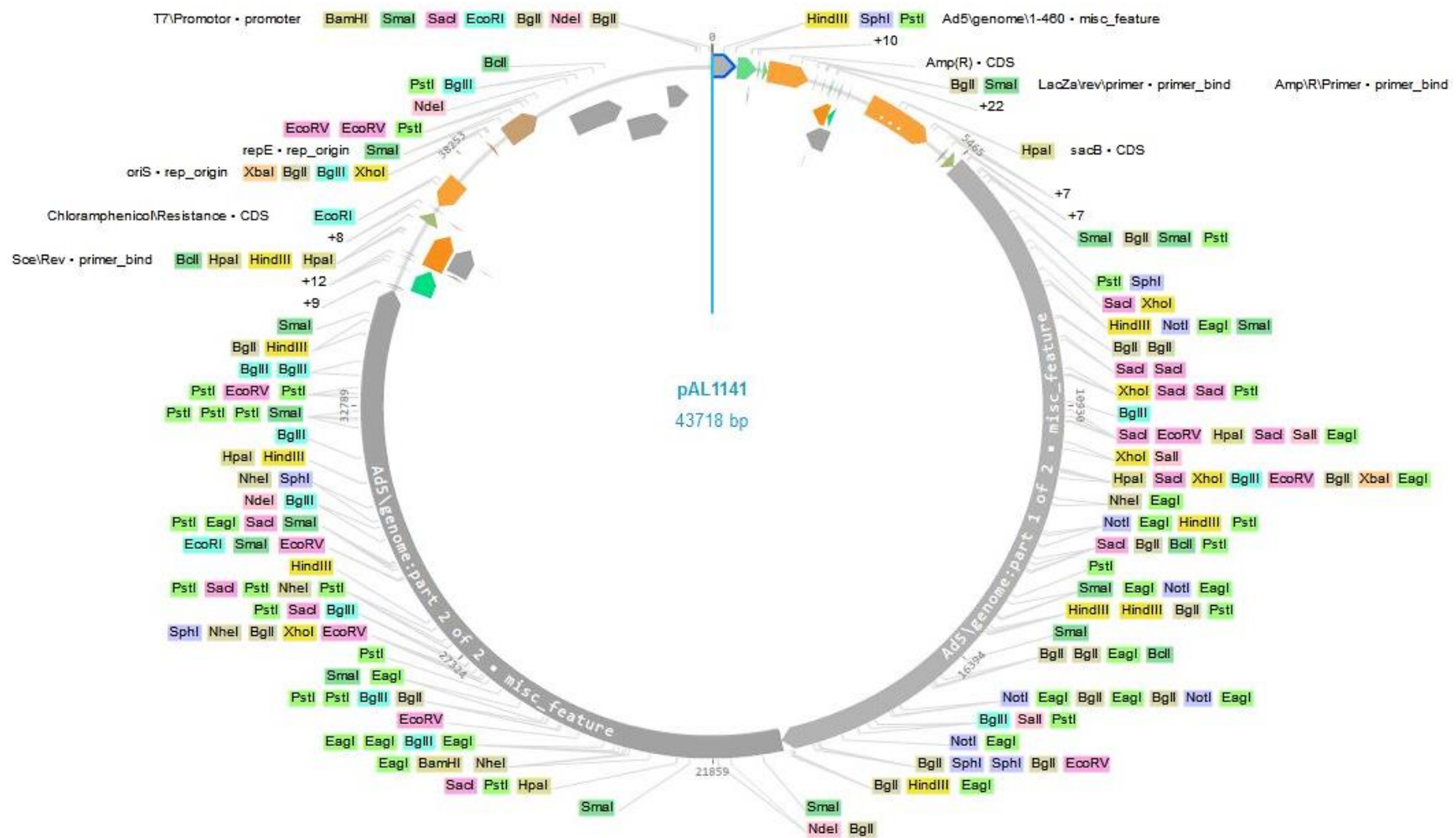
**Figure 2–7. Plasmid map of the bacterial artificial chromosome (BAC) containing green fluorescent protein-expressing adenovirus serotype 5 (Ad5.GFP) sequence.**
This BAC contains the sacB selection cassette, chloramphenicol and ampicillin resistance genes (image created in Genome Compiler).

Selection cassettes and de-targeting mutation (Table 2–4) encoding DNA fragments with ~70 bp homology arms were generated by PCR using Expand High Fidelity PCR system (#11732650001, Roche Applied Science, East Sussex, UK). Gene synthesis of the complete species D whole fiber and fiber knob sequences for pseudotyping Ad5 was ordered from GeneArt (Invitrogen; Regensburg, Germany). To allow a straightforward insertion into the Ad5 BAC, these sequences were designed to contain homologous overlapping sequences at either end to match the Ad5 sequence. The Ad5 genome was modified by temperature-induced AdZ homologous recombination ('recombineering') in *E. coli* strain SW102 in a two-step process by using autoclaved-sterilised reagents and disposable plastic ware. First an RPSL/neo selection cassette ('cassette in') was inserted into the region of interest, and then replaced with a DNA oligo containing the appropriate sequence ('cassette out'). The first step involved growing the bacteria containing the correct target BAC O/N in 5 mL of LB in a 30-mL universal tube (#128B/FS, Sterilin, Thermo Scientific, UK) in a shaker at 32°C. This was done by streaking the –70 °C glycerol stock of the target strain with a pipette tip and inoculating into the medium containing selective antibiotics.

**Table 2–4. Primer sequences for insertion of de-targeting mutations.** CAR-binding ablating KO1 mutation (S408E, P409A) (Smith et al., 2002) was inserted into the AB loop of Ad5 fiber knob. A combination of five FX-binding mutations (HVR7; I421G, T423N, E424S, L426Y and E451Q) (Alba et al., 2009) was inserted into the HVR7 region, and integrin-binding ablation (RGE; D342E) in penton base (Wickham et al., 1993). ***Homology arms***.

| Primer | Sequence |
|---|---|
| RGD>RGE cass in *F* | GGCGCGGAAGAGAACTCCAACGCGGCAGCCGCGGCAATGCAGCCGGTGGAGG ACATGAACGATCATGCCATTCGCGGC***CCTGTGACGGAAGATCACTTCG*** |
| RGD>RGE cass in *R* | CGGGTTGCGCAGCGGGGGCGGCAGCTTCGGCCGCTGCTTCGGCCTCAGCGCG CTTCTCCTCAGCCCGTGTGGCAAAGGTCTGAGGTTCTTATGGCTCTTG |
| RGD>RGE cass out | CGCGGCAATGCAGCCGGTGGAGGACATGAACGATCATGCCATTCGCGGCGAAA CCTTTGCCACACGGGCTGAGGAGAAGCGCGCTGAGGCCGAAGCAGCG |
| KO1 fiber cass in *F* | AGTTTTGACAGCACAGGTGCCATTACAGTAGGAAACAAAAATAATGATAAGCTAA CTTTGTGGACCACACCAGCTCCA***CCTGTGACGGAAGATCACTTCG*** |
| KO1 fiber cass in *R* | CTGTAGCAAGTATTTGACTGCCACATTTTGTTAAGACCAAAGTGAGTTTAGCATCT TTCTCTGCATTTAGTCTACAGTTCTGAGGTTCTTATGGCTCTTG |
| KO1 fiber cass out | GAAACAAAAATAATGATAAGCTAACTTTGTGGACCACACCAGCTCCAGAGGCCAA CTGTAGACTAAATGCAGAGAAAGATGCTAAACTCACTTTGGTCTT |
| HVR7 cass in *F* | GATCCAGATGTTAGAATTATTGAAAATCATGGAACTGAAGATGAACTTCCAAATTA CTGCTTTCCACTGGGAGGTGTG***CCTGTGACGGAAGATCACTTCG*** |
| HVR7 cass in *R* | TTATTTCATTTTTATCTGAAAATTCTGTAGCATCTTTTTCCCATCCATTTTCCTGACC TGTTTTAGGTTTTACCTTGGTCTGAGGTTCTTATGGCTCTTG |
| HVR7 cass out | AAGATGAACTTCCAAATTACTGCTTTCCACTGGGAGGTGTGGGCAATAACTCCAC TTACACCAAGGTAAAACCTAAAACAGGTCAGGAAAATGGATGGGA |

On the following morning 2 mL of the O/N culture was inoculated into 50 mL of LB and grown until log phase was reached (OD ~ 0.6 at λ600 nm). Lambda genes were induced by incubating 25 mL of the culture in a 42°C water bath for exactly 15 min, after which the cultures were cooled down on a shaker on ice for 15–20 min. The cells were then pelleted at 4000 rpm in a pre-cooled centrifuge for 5 min at 0°C and washed with 25 ml of ice-cold $H_2O$. The pellet was re-suspended first into 1 mL of ice-cold $H_2O$ by gently swirling and tapping the tube, and adding further 25 mL of $H_2O$. Cells were then re-pelleted and wash repeated once. Supernatant was decanted and cells re-suspended into the remaining $H_2O$ (~ 400 µL). 25 µL of the suspension was added into pre-cooled 0.5 mL Eppendorf tubes with 3 µL of the RPSL/neo or sacB cassette and mixed gently by flicking the tube. The mix was added into pre-cooled disposable 2 mm electroporation cuvettes (#71-2020, HiMaX, Isogen Life Science, The Netherlands) and incubated on ice for 5 min. The cuvette was briefly dried with tissue and cells electropermeabilised (MicroPulser Electroporator, Bio-Rad, Hertfordshire, UK) using a pre-set program "Ec2" for bacterial electroporation. The cells were then recovered in 1 mL of LB for 1 h in a shaker at 32°C. The recombineering technology relies on blue/white selection based on IPTG-inducible expression of the *lacZ* gene. The selection for the cassette was performed using Kan (15 µg/mL) while the selection against the cassette was performed using Strep (400 µg/mL). After the recovery step following the first round of recombineering, 150 µL of cells were plated on LB-agar (1.5 %) plates containing IPTG, Kan/Strep, X-Gal and Chlor and incubated for 48–72 h until blue colonies appeared. Three blue colonies per construct were then picked and re-suspended into 10 µL of $H_2O$ and each divided into two cultures: 5 µL was inoculated into 5 mL of LB (+ Kan, Chlor) and 5 µL into 5 mL of LB (+ Strep, Chlor). This was done to verify the Kan-resistance and Strep-sensitivity of the selected colonies in order to proceed into the second round of recombineering.

**Table 2–5. A20 peptide insertion sites within the Ad5, Ad10 and Ad48 knob.** Insertion sites in Ad5 (Krasnykh et al., 1998, Coughlan et al., 2009a) and Ad48 had been previously determined (Coughlan et al., 2014). The flanking sequences and amino acid (aa) numbers indicate the insertion site within the knob domain. A20, NAVPNLRGDLQVLAQKVART. aa, amino acid; F, whole fiber pseudotyped; kn, knob domain pseudotyped.

| Vector | Flanking | preceding | following | Flanking |
|---|---|---|---|---|
| Ad5.HI.A20 | QETG | 546 | 547 | DTTP |
| Ad10.DG | SKKY | 304 | 305 | ARDI |
| Ad10.Δ5aaDG.A20 | KPSN | 300 | 306 | RDIV |
| Ad10.HI.A20 | QETG | 334 | 335 | CEYS |
| Ad5/kn48.CD.A20 | MINN | 232 | 233 | KVNG |
| Ad5/kn48.Δ13aaDG.A20 | KPPT | 297 | 311 | AKNK |
| Ad5/kn48.HI.A20 | KETG | 340 | 341 | CTYS |
| Ad5/kn48.IJ.A20 | FAWN | 352 | 353 | KTYE |

On the following morning, 2 mL of one Kan-resistant colony of each construct was inoculated into 50 mL of LB and the following recombineering steps performed as described for the first round of recombineering. In the second round, oligonucleotides containing DNA sequences coding for the modified target sequence (de-targeting mutations and/or targeting peptide insertions) were generated by PCR and inserted into the respective gene location. The generated vector backbones were further modified by insertion an αvβ6-targeting A20 peptide within the fiber knob domain – in HI loop in Ad5 (Krasnykh et al., 1998, Coughlan et al., 2009a), in CD, Δ13aa.DG (a 13-aa deletion), HI and IJ loops in Ad48 (Coughlan et al., 2014) and in DG, Δ5aa.DG (a 5-aa deletion) and HI loops in Ad10 knob (Table 2–5). Primers that were used for the insertion are in Table 2–6.

**Table 2–6. Primers used for the A20 peptide insertion.** Overlapping sequence for the A20 is in green, and overlapping sequence for the RPSL cassette is shown in blue.

| Primer | Sequence |
|---|---|
| A20 peptide | **AATGCTGTGCCCAACTTGAG**AGGTGACCTTCAAGTGTTGGCTCAAAAGGTGGCACGGACG |
| RPSL neo_kn5 *F* | **CCTGTGACGGAAGATCACTTCG** |
| RPSL neo_kn5 *R* | **CTGAGGTTCTTATGGCTCTTG** |
| Ad5.HI.A20 *F* | TCAGTCAAGTTTACTTAAACGGAGACAAAACTAAACCTGTAACACTAACCATTACACTAAACGGTACACAGGAAACA**AATGCTGTGCCCAACTTGAGAG** |
| Ad5.HI.A20 *R* | CAAATATTTCATTAATGTAGTTGTGGCCAGACCAGTCCCATGAAAATGACATAGAGTATGCACTTGGAGTTGTGTCTCCCGTCCGTGCCACCTTTTGAG |
| RPSL_kn48.CD *F* | ATGTGGGAGTCAGATTTTGGCTAATATGTCTTTGCTGGTAGTTAAAGGAAAATTTTCCATGATAAATAA C**CCTGTGACGGAAGATCACTTCG** |
| RPSL_kn48.CD *R* | ATAAAACACCCTTTTCATCAAATAATAACTTTATTGTAAATTTTTTATAATCATCAGTTCCATTTACTTT**CTGAGGTTCTTATGGCTCTTG** |
| RPSL_kn48.DGΔ13aa *F* | TGTTGGAAGTGCATATGAAGAAGCTGTTGGTTTTATGCCAAGTACAACAGCTTATCCTAAACCACCTACT**CCTGTGACGGAAGATCACTTCG** |
| RPSL_kn48.DGΔ13aa *R* | TAACAGTTGTGGCAACTGGGTTGCCTGCTTGTCCGCCAAGGTAGACGTTACTTACGTATTTATTTTTTG C**CTGAGGTTCTTATGGCTCTTG** |
| RPSL_kn48.HI *F* | TAACGTCTACCTTGGCGGACAAGCAGGCAACCCAGTTGCCACAACTGTTAGTTTTAATAAGGAAACGGGG**CCTGTGACGGAAGATCACTTCG** |
| RPSL_kn48.HI *R* | AGGAGGAATCAAACTGCACATTTTCATAAGTTTTGTTCCAAGCAAAGTCAATGTAATCGAATAAGTACA**CTGAGGTTCTTATGGCTCTTG** |
| RPSL_kn48.IJ *F* | TGCCACAACTGTTAGTTTTAATAAGGAAACGGGGTGTACTTATTCGATTACATTTGACTTTGCTTGGAA C**CCTGTGACGGAAGATCACTTCG** |
| RPSL_kn48.IJ *R* | AAGCTTATTCTTGGGCAATATAGGAGAAAGTTAAAAAGGAGGAATCAAACTGCACATTTTCATAAGTTTT**CTGAGGTTCTTATGGCTCTTG** |
| kn48.CD_A20 *F* | ATGTGGGAGTCAGATTTTGGCTAATATGTCTTTGCTGGTAGTTAAAGGAAAATTTTCCATGATAAATAAC**AATGCTGTGCCCAACTTGAGAGGTGAC** |
| kn48.CD_A20 *R* | ATAAAACACCCTTTTCATCAAATAATAACTTTATTGTAAATTTTTTATAATCATCAGTTCCATTTACTTT**CGTCCGTGCCACCTTTTGAGCCAAC** |
| kn48.DGΔ13aa_A20 *F* | TGT TGG AAG TGC ATA TGA AGA AGC TGT TGG TTT TAT GCC AAG TAC AACAGCTTATCCTAAACCACCTACT**AATGCTGTGCCCAACTTGAGAGGTGAC** |
| kn48.DGΔ13aa_A20 *R* | TAACAGTTGTGGCAACTGGGTTGCCTGCTTGTCCGCCAAGGTAGACGTTACTTACGTATTTATTTTTTGC**CGTCCGTGCCACCTTTTGAGCCAAC** |
| kn48.HI_A20 *F* | TAACGTCTACCTTGGCGGACAAGCAGGCAACCCAGTTGCCACAACTGTTAGTTTTAATAAGGAAACGGGG**AATGCTGTGCCCAACTTGAGAGGTGAC** |
| kn48.HI_A20 *R* | AGGAGGAATCAAACTGCACATTTTCATAAGTTTTGTTCCAAGCAAAGTCAAATGTAATCGAATAAGTACA**CGTCCGTGCCACCTTTTGAGCCAAC** |
| kn48.IJ_A20 *F* | TGC CAC AAC TGT TAG TTT TAA TAA GGA AAC GGG GTG TAC TTA TTC GATTACATTTGACTTTGCTTGGAAC**AATGCTGTGCCCAACTTGAGAGGTGAC** |
| kn48.IJ_A20 *R* | AAGCTTATTCTTGGGCAATATAGGAGAAAGTTAAAAAGGAGGAATCAAACTGCACATTTTCATAAGTTTT**CGTCCGTGCCAC CTTTTGAGCCAAC** |
| RPSL_kn10.DG *F* | TTATGAAAAAGCAATTGGTTTTATGCCTAATTTGGTAGCGTATCCGAAACCCAGTAATTCTAAAAAATAT**CCTGTGACGGAAGATCACTTCG** |
| RPSL_kn10.DG *R* | TAGTTTTAATGACTGCTGGCTGATCAGGTTTTCCACCAAGATATATAGTTCCATAAACTATGTCTCTTGC **CTGAGGTTCTTATGGCTCTTG** |
| RPSL_kn10.DGΔ5aa *F* | TGTTTCGACAGCTTATGAAAAAGCAATTGGTTTTATGCCTAATTTGGTAGCGTATCCGAAACCCAGTAAT **CCTGTGACGGAAGATCACTTCG** |
| RPSL_kn10.DGΔ5aa *R* | AGGTAGTTTTAATGACTGCTGGCTGATCAGGTTTTCCACCAAGATATATAGTTCCATAAACTATGTCTCT **CTGAGGTTCTTATGGCTCTTG** |
| RPSL_kn10.HI *F* | AACTATATATCTTGGTGGAAAACCTGATCAGCCAGCAGTCATTAAAACTACCTTTAACCAAGAAACTGGA **CCTGTGACGGAAGATCACTTCG** |
| RPSL_kn10.HI *R* | AGGTGGTTTCAAATTCAACATTTTCATAGGTTTTGGACCAACTAAAGTCAAATGTTATAGAGTATTCACA **CTGAGGTTCTTATGGCTCTTG** |
| kn10.DG.A20 *F* | TTATGAAAAAGCAATTGGTTTTATGCCTAATTTGGTAGCGTATCCGAAACCCAGTAATTCTAAAAAATAT **AATGCTGTGCCCAACTTGAGAGGTGAC** |
| kn10.DG.A20 *R* | TAGTTTTAATGACTGCTGGCTGATCAGGTTTTCCACCAAGATATATAGTTCCATAAACTATGTCTCTTGC **CGTCCGTGCCACCTTTTGAGCCAAC** |
| kn10.DGΔ5aa.A20 *F* | TGTTTCGACAGCTTATGAAAAAGCAATTGGTTTTATGCCTAATTTGGTAGCGTATCCGAAACCCAGTAAT **AATGCTGTGCCCAACTTGAGAGGTGAC** |
| kn10.DGΔ5aa.A20 *R* | AGGTAGTTTTAATGACTGCTGGCTGATCAGGTTTTCCACCAAGATATATAGTTCCATAAACTATGTCTCT **CGTCCGTGCCACCTTTTGAGCCAAC** |
| kn10.HI.A20 *F* | AACTATATATCTTGGTGGAAAACCTGATCAGCCAGCAGTCATTAAAACTACCTTTAACCAAGAAACTGGA **AATGCTGTGCCCAACTTGAGAGGTGAC** |
| kn10.HI.A20 *R* | AGGTGGTTTCAAATTCAACATTTTCATAGGTTTTGGACCAACTAAAGTCAAATGTTATAGAGTATTCACA **CGTCCGTGCCACCTTTTGAGCCAAC** |

### *2.3.2 Verification of genome modifications by sequencing*

The correct construction of Ad5 BAC genomes was confirmed by sequencing across the modified region by using either internal or external sequencing services. BigDye® Terminator v3.1. Cycle Sequencing Kit (Life Technologies) was used to prepare the samples for sequencing [95°C – 5 min, 100 x (95°C – 30 s, 55°C – 10 s, 60°C – 4 min), 4°C − ∞] and PCR products were purified using Performa DTR columns (Edge Biosystems, Gaithersburg, MD, USA). Sequencing based on this method was performed at Central Biotechnology Services (School of Medicine, Cardiff University). Alternatively, sequences were prepared by PCR using primers (Table 2–7), PCR products purified using columns and 150 ng of DNA samples sent to sequencing in pre-coded sequencing tubes with 2 µL sequencing primers in a total volume of 17 µL (Eurofins, Ebersberg, Germany). Forward (*F)* and reverse (R) primers were used in separate reactions to sequence both strands of the generated DNA. The correct sequence modifications were verified using CLC Main Workbench 6 software (Qiagen) or Genome Compiler (Los Altos, CA, USA) software. Permanent glycerol stocks were prepared of the verified correct clones by mixing 700 µL of the bacterial culture with 300 µL of glycerol (30 %) and stored at –70°C.

**Table 2–7. Primers for verification of correct mutation by sequencing.** *F*, forward primer; HVR7, coagulation factor 10-binding mutation; KO1, coxsackie and adenovirus-binding mutation; *R*, reverse primer; RGE, αvβ3/5 integrin-binding mutation.

| Primer | Sequence |
|---|---|
| Sequencing RGE | GCACTGTTGGATGTGGACGC |
| Sequencing KO1 | GTTCACCTAATGCACCAAACAC |
| Sequencing HVR7 | TCCATTGGTGATAGAACCAGG |
| | |
| PCR for seq around Ad5 fiber *F* | GCAAATTTCTGTCCAGTTTATTCAGCAGCA |
| PCR for seq around Ad5 fiber *R* | GCCAGCCGGGGAGAAAGGACT |
| PCR for seq knob swap *F* | CTACAGCCATAGCCATTAATGCAGGAGAT |
| | |
| Seq Ad5 fiber swap *F* | CTCCTTGCCCTCCTCCCAGCT |
| Seq Ad5 fiber swap *R* | GTACTCTGTGTGTTGGGAGGGAGGT |
| Seq knob swap *F* | GGCTTGAATTTGGTTCACCTAATGCACCA |
| | |
| PCR for seq within Ad10 knob *F* | AACACCAGACACTTCTCCAAACTGCAC |
| PCR for seq within Ad10 knob *R* | TACACTGTGAAATGGGCTGGTGGTGG |
| | |
| Seq of Ad10 knob *F* | ATTGCTCAGGATAAGGACTCTAAACTAACTC |
| Seq of Ad10 knob *R* | AGACTGACTACCCGTGCTGGTGTAAAAATC |
| | |
| Seq Ad48 fiber | CACTGCCAAGGGGTTGATG |
| Seq Ad48 fiber | CCAGCCGGGGAGAAAGG |

### 2.3.3 *Amplification and purification of virus genomes*

Viral genomic BACs were purified using the commercial NucleoBond BAC 100 kit (#740579, Macherey-Nagel, Duren, Germany). All materials and reagents were sterilised by autoclaving prior to DNA purification. The BACs containing correct insertions (as verified by sequencing) were amplified in 5 mL of LB (+ Strep, Chlor) in a shaker for 8 h at 32°C. In the evening, the 5 mL pre-culture was inoculated into 250 mL of LB (+ Strep, Chlor) in a 1 L conical flask and incubated in a shaker O/N at 32°C. The culture was pelleted at 6000 rpm for 15 min at 4°C in a high-speed centrifuge (Avanti J-20 XP, Beckman Coulter, USA) and pellet re-suspended into 24 mL of S1 buffer (+ RNAse) by using a 5 mL stripette. 24 mL of S2 lysis buffer was added, mixed by inverting the tube 6–8 times and incubated for exactly 5 min at RT. To neutralise the suspension, 24 mL pre-cooled S3 buffer was added, suspension mixed by inverting and incubated for 5 min on ice. The lysed suspension was then pelleted at 6000 rpm for 15 min at 4°C. Meanwhile, the purification column was equilibrated by adding 6 mL of N2 buffer and the flow-through discarded. The separated lysate was then bound to the column through a funnel covered with a filter, and the column washed twice with 18 mL of wash buffer N3. The flow-through was discarded and the column was taped onto a 15-mL centrifuge tube. The DNA was eluted by adding 15 mL of pre-heated (50°C) N5 elution buffer, and the eluate mixed with 11 mL of RT isopropanol. The DNA was pelleted at 15 000 rpm for 30 min at 4°C and supernatant discarded. The pellet was washed with 70 % ethanol, mixed briefly on a vortex, and re-pelleted at 15 000 rpm for 10 min at RT. Ethanol was decanted and pellet dried in a 37°C incubator for ~1 h. DNA was re-suspended into 100 µL of $H_2O$ by allowing it to stand for ~15 min, scraping the pellet and collecting the liquid by a brief spin. DNA concentration was consistently verified to be ~ 100–600 ng/µL as estimated in Nanodrop ND-1000 (Thermo Scientific, UK). Maxiprep DNAs were stored at –20°C for subsequent cell transfection.

### 2.3.4 *Virus rescue and propagation for high titre stocks*

T-REx-293 cells were generally used for virus propagation and titration, while A20 peptide-containing viruses were rescued in HEK293-β6 cells that express αvβ6 integrin. On the previous day prior to DNA transfection, cells were seeded on T25 tissue culture flasks (Corning CellBIND, Amsterdam, The Netherlands) at $5.0 \times 10^5$ cells/flask and allowed to adhere O/N. Cell monolayers were washed in 5 mL of PBS and 1 µg of purified DNA was transfected into in a total volume of 5 mL complete medium using Effectene transfection reagent (#301425; Qiagen, Manchester, UK) according to the manufacturer's instructions. A control plasmid pmaxGFP (SiRNA test

kit, #VSC-1001; Lonza, Slough, UK; Figure 2–8) was used for evaluating the transfection efficiency of the Effectene reagent by transfecting cells with 1 µL of the reagent and quantifying the proportion of GFP-positive cells in flow cytometer after a 48 h incubation. Rescue of de-targeted Ad5 vectors containing native receptor-binding KO1 and RGD > RGE mutations was facilitated by addition of 8 µL/mg of FX (#HCX0050, Haematologic Technologies, Cambridge Bioscience, Cambridge, UK) into the growth medium. Cells were left untouched for 24 h, after which they were washed in 5 mL of PBS and 5 mL of fresh complete DMEM was changed. Media were replaced every 1−2 days until cytopathic effect (CPE) was visible and the whole monolayer was rounded up in grape-like structures. The cells were observed daily under inverted microscope (Nikon TMS; Surrey, UK) until CPE was complete, ~10–14 days post-transfection. Cell pellets were then collected at 1500 rpm for 5 min and re-suspended into 1 mL of medium. The viruses were crude-extracted from the infected host cells by addition of an equal amount (1 mL) of tetrachloroethylene (TCE; Fisher Scientific, Loughborough, UK) by vigorous shaking for 30 s and centrifugation at 2000 rpm for 10 min. The upper layer containing the virus particles was then carefully extracted by decanting with a 1-mL pipette into a fresh 1.5 mL cryo vial. This was marked as the passage 1 virus stock (P1 stock) that was either stored at –80ºC long-term or immediately proceeded into propagation of P2 high titre stocks.
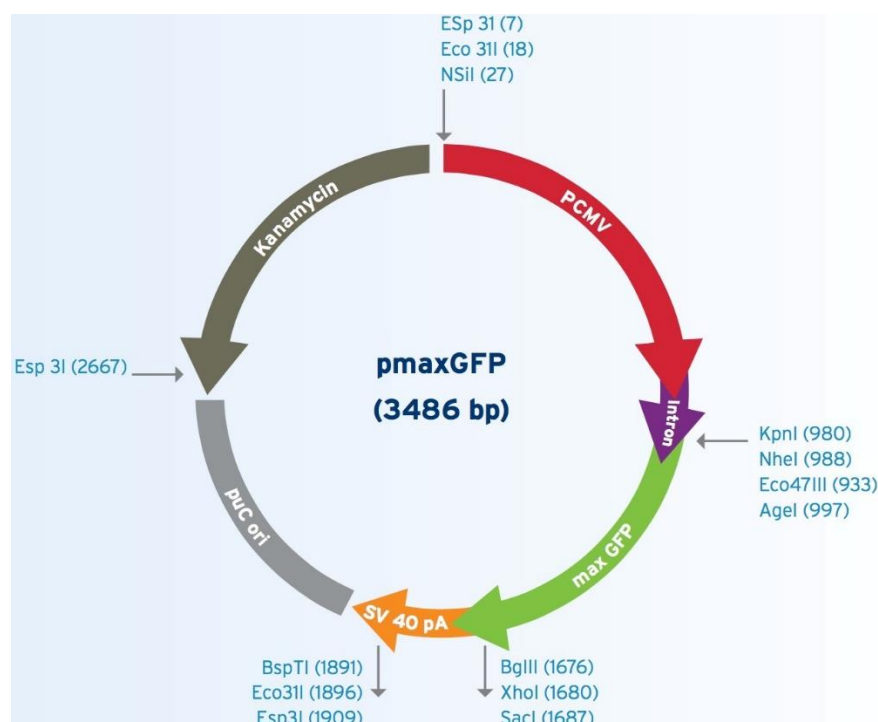


**Figure 2–8. Plasmid map of the transfection control pmaxGFP.** Green fluorescent protein (GFP)-expressing plasmid pmaxGFP was used as a negative control to assess transfection efficiency of Effectene transfection reagent in T-REx-293 cells (Amaxa, 2017).

For generation of high titre P2 stocks, cells were seeded in five T150 tissue culture flasks (Corning CellBIND, Amsterdam, The Netherlands) per virus, and allowed to attach O/N to obtain 60–70 % confluent monolayer. Medium was replaced with 20 mL of fresh complete DMEM into each flask prior to infection. The cells were infected with TCE crude-extracted P1 stocks by mixing 100 µL of virus with 900 µL of complete DMEM in a 1.5 mL Eppendorf and by adding 200 µL into each confluent T150 flask. Cells were observed daily and medium changed approximately every two days, when it turned acidic (yellow). When the cells were getting close to full CPE, ~ 200 µL of sterile 7.5 % sodium bicarbonate (#S8761; Sigma Aldrich, Gillingham, UK) was added into each flask to turn the medium back to red in order to disturb the monolayer as little as possible and to keep the infection progressing. Cell pellets were collected at 1200 rpm for 5 min when CPE was complete (3−8 days post-infection), after which they were re-suspended in 5 mL of PBS. Pellets could be frozen –70ºC at this point if virus purification didn't immediately follow. The P2 virus stocks were thawed in 37ºC water bath and crude-extracted by adding 5 mL of TCE, followed by centrifugation at 2000 rpm for 20 min. Upper layer containing the virus particles was decanted into a clean 15 mL tube by using a 1 mL pipette and proceeded into ultracentrifugation.

### 2.3.5   Virus purification by CsCl gradient ultracentrifugation

Virus particles were purified by two-step ultracentrifugation. Cesium chloride (CsCl) gradients were prepared into UltraClear 14 × 89 mm tubes (#344059, Beckman Coulter) tubes holding a total volume of 13.2 mL. Initially, 2.5 mL of 1.40 g/mL density CsCl was pipetted to the tube, followed by 2.5 mL addition of 1.25 g/mL density CsCl on the top and addition of 5 mL of P2 virus stock as the uppermost layer. The gradients were prepared with extreme care, by expelling the liquid very slowly and by using a 5 mL disposable stripette. The tubes were then balanced with sterile PBS on a scale in the hood in order to achieve equally balanced counter tubes. The viruses were subjected to 35 600 rpm for 1.5 h at RT in swinging bucket Sw41Ti rotor in Optima XPN-80 Ultracentrifuge (Beckman Coulter). As a result, the mature virus particles could be seen as a distinct grey band on the lower quarter of the tube, with a faint band on the top consisting of empty virus capsids (Figure 2–9). The virus band was extracted by using a 19-gauge needle and 1 mL syringe into a sterile 15 mL tube. The second gradient was prepared by adding 5 mL of 1.34 g/mL density CsCl on the bottom of an ultracentrifuge tube and 1 mL of the purified virus stock from the first step was carefully added on the top by using a 1 mL pipette.
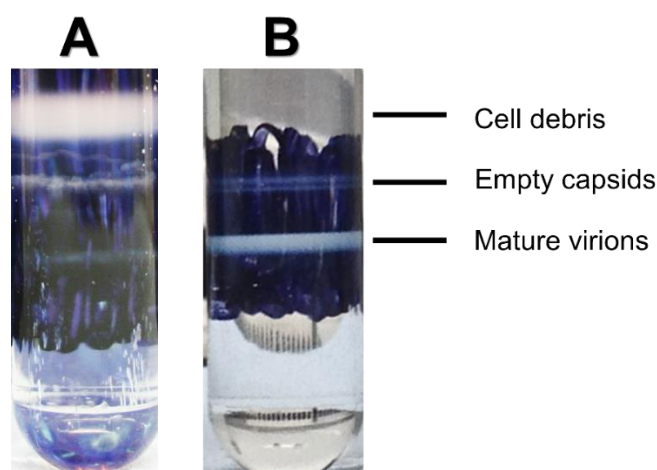
**Figure 2–9. Adenovirus purification by caesium chloride (CsCl) ultracentrifugation.** (A) Poorly purified preparation with a very small proportion of mature virions. (B) Well purified virus preparation with a very strong band of mature virions.

The viruses were then subjected to 35 600 rpm centrifugation for 18 h (O/N) in the same rotor as in the first centrifugation step. The visible virus band was then extracted as before and transferred into a sterile 15 mL tube. One ~ 20 cm piece of dialysis tubing (#DTV12000.01.15, Visking 6.3 mm, MWCO 12–14 000 Daltons; MediCell Membranes Ltd, London, UK) was cut for each virus with EtOH-sterilised scissors and sterilised in 500 mL of dialysis buffer (10 % glycerol, 10 mM Tris-HCl (pH 7.8), 135 mM NaCl and 1 mM $MgCl_2 \times 6H_2O$) by heating in the microwave until boiling. One end of the tubing was tied with a single knot and the purified virus was carefully added into the tube by using a 1 mL pipette. The tubing was carefully depleted of air and closed with a single knot; both ends were also tied with Mediclips (MediCell Membranes Ltd, London, UK) to prevent accidental leakage. Each virus was dialysed in a separate 1 L conical flask in dialysis buffer for 24 h with a single change of buffer on the following day.

### 2.3.6 Viral titration

Viral titres were determined using a micro-BCA assay kit (#23235; Pierce, Thermo Fisher Scientific, Loughborough, UK) according to the manufacturer's protocol. Briefly, 1, 3 and 5 μL of purified virus stocks was added on a sterile flat-bottom 96-well plate (#163320; Nunc Microwell, Thermo Fisher Scientific, Loughborough, UK) in triplicate and the volume adjusted to 150 μL with PBS. On the same plate, 150 μL of bovine serum albumin (BSA) standards (0, 0.5, 1, 2.5, 5, 10, 20, 40, 200 μg/ml in PBS) were assayed in duplicate. Working solution was prepared by mixing reagents A, B and C in the ratio of 25:24:1 and 150 μL of the solution added into each well and mixed briefly on a shaker. The plate was incubated at 37°C for 2 h and absorbance measured at λ570 nm on an iMark™ Microplate Absorbance Reader (BioRad,

Hertfordshire, UK). The values of the blank (PBS only) were subtracted from all values and standard curve was prepared of the OD values of the BSA standards. Protein concentration in each sample well was deducted from the equation of the standard curve and normalised to the corresponding sample volume. The viral particle titres per ml (vp/mL) were determined by assuming that 1 µg protein equals $4 \times 10^9$ vp (Von Seggern et al., 1998).

Rapid plaque assay (Bewig and Schmidt, 2000) was used for titering the CsCl-purified viruses based on expression of the Ad hexon protein. T-REx-293 cells were seeded at $1 \times 10^6$/well in 12-well plates and allowed to adhere O/N. Cells were infected with 100 µL of $10^{-3}$, $10^{-4}$ and $10^{-5}$ dilutions of virus stocks for 1 h at 37°C, complete medium changed and cells incubated for further 48 h. Medium was aspirated and cells allowed to air dry. 1 mL of ice-cold 50/50 acetone/methanol was added for 10 min at –20°C, aspirated and cells washed three times in wash buffer (1% BSA in PBS). Polyclonal goat anti-Ad2 antibody (1:5000; #AB1056, Millipore, Watford, UK) was added for 1 h at 37°C on a rocker and cells washed then three times with the wash buffer. Cells were incubated with 500 µL of secondary antibody anti-goat (#sc-2056, Biotechnologies, Heidelberg, Germany) for 1 h at 37°C on a rocker. Cells were then stained with 500 µL of 3, 3'-diaminobenzidine (DAB) substrate (#SK-4100; Vector Laboratories Ltd, Peterborough, UK) for 10 min at RT, after which the substrate was removed and 1 mL PBS added into each well. The number of positive cells was counted in three separate fields of view using an objective that gave 5–50 positive cells/field. The average number of positive cells/well was then calculated and plaque forming units (pfu)/mL determined (Figure 2–10).

$$\frac{\text{(infected cells / field)} \times \text{(fields / well)}}{\text{volume of virus (mL)} \times \text{dilution factor}}$$

**Figure 2–10 Calculation of viral plaque-forming units per mL (pfu/mL).**

## 2.4   *In Vitro* characterisation of recombinant vectors

The generated vectors were assessed in multiple well-documented *in vitro* assays to validate their structural and functional integrity.

### 2.4.1   *Sequencing of the fiber protein from viral DNAs*

Viral DNA of Ad5-based pseudotyped viruses was sequenced to exclude the possibility of incorporated accidental mutations post-virus production. Viral DNA was first precipitated from CsCl-purified high titre virus stocks by ethanol precipitation. 50

µL of purified virus was mixed with 5 µL of 3 M sodium acetate (pH 5.2) and 150 µL of 100 % molecular grade ethanol (Fisher Scientific, UK). The mixtures were incubated on dry ice for 15 min and DNA pelleted by centrifugation for 30 min at 4°C. The pellets were washed with 70 % ethanol, air-dried and re-suspended in 30 µL of $H_2O$. This DNA was then used as a template for PCR to amplify the fiber protein. Primers specific for Ad5 sequence immediately outside of the exchanged fiber region were used for the PCR reactions (Table 2–7). Sequencing was performed by Eurofins Genomics (Ebersberg, Germany).

### 2.4.2  Fiber integrity assessment by Western blot

The structural integrity of the Ad fiber proteins was assessed by Western blotting. $5 \times 10^9$ vp/virus stock were run on pre-cast NuPAGE Novex® 10 % Bis-Tris SDS-PAGE gels (#WG1201BOX; Life Technologies, Loughborough, UK) with 1 µL of DTT and 5 µL of 4 x NuPAGE LDS sample buffer (#NP0008; Life Technologies, Loughborough, UK) in a total volume of 20 µL. Proteins were transferred to Amersham Protran 0.45 µm nitrocellulose blotting membrane (#10600002; GE Healthcare Life Science, Little Chalfont, UK) by semi-dry blotting in a Trans-blot SD Semi-dry Transfer Cell (Bio-Rad, Hertfordshire, UK). Nitrocellulose membranes were prepared by treating with 5 mL of Pierce Miser antibody extender (#32110; Thermo Scientific, Paisley, UK) for 10 min and washing seven times with $H_2O$. Membranes were blocked in 5 % milk in Tris-buffered saline containing 0.05 % TWEEN-20 and 0.05 % Triton X-100 (TBS-T) O/N at 4°C. The membrane was then incubated in primary anti-Ad antibody 4D2 (1:2000) at 37°C for 1 h, then washed 5 times for 5 min in TBS-T, and incubated in anti-mouse IgG-HRP conjugate (1:2000; Insight Biotechnology Ltd, Wembley, UK) for 1 h at RT. After washing a further 5 times for 5 min in TBS-T, the membrane was incubated for 5 min in SuperSignal West Pico Chemiluminescent substrate (#34078; Thermo Scientific, Paisley, UK), and analysed on GelDoc autoChem camera (Ultra-Violet Products Ltd, Cambridge, UK) or G:BOX Chemi XX6 imager (Syngene, Cambridge, UK).

### 2.4.3  Silver staining of viral proteins

The presence of viral proteins in the recombinant pseudotyped vectors was verified by silver staining. $1 \times 10^{10}$ vp of each purified virus stock was diluted in PBS in a total volume of 14 µL and loaded into each well with 5 µL of loading buffer and 1 µL of DTT. The samples were first run for 1 h 20 min at 150 V. The viral proteins were stained by using the Pierce Silver Stain kit (#24612; Thermo Scientific).
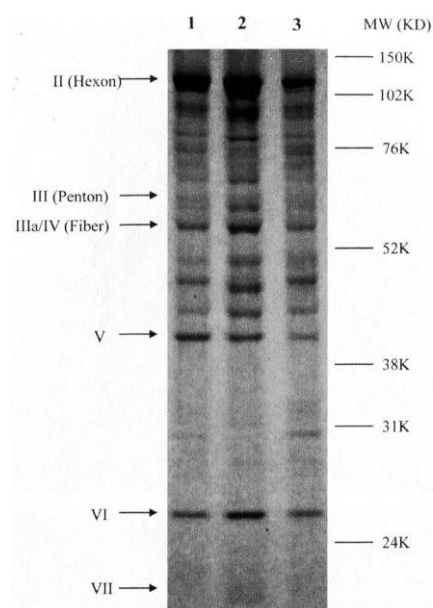
**Figure 2–11. Silver staining of adenovirus particles.** Figure reproduced from (Parker et al., 2014).

The gel was washed twice in ultrapure $H_2O$ for 5 min and fixed in 30 % ethanol:10% acetic acid for 30 min. It was then washed twice in 10 % ethanol and twice in ultrapure $H_2O$ for 5 min, and incubated in sensitiser working solution for 1 min at RT. After washing in ultrapure $H_2O$ twice for 1 min, the gel was stained in stain working solution for 30 min at RT and then washed twice for 20 s in ultrapure $H_2O$. The gel was then developed for 5 min at RT, reaction stopped with 5 % acetic acid and bands documented in G:BOX Chemi XX6 imager (Syngene, Cambridge, UK).

### 2.4.4 Transduction assay for quantification of luciferase expression

The assay was performed using the Luciferase Assay System kit, essentially according to the manufacturer's protocol (#E1501; Promega UK Ltd, Southampton, UK). Cells were seeded on a sterile 96-microwell Nunc delta surface plate (#163320; Thermo Scientific, Paisley, UK) in 200 µL of complete growth medium at a density of $2 \times 10^4$ cells / well in triplicate 24 h prior to the experiment and allowed to adhere at 37°C in order to reach ~ 60−70% confluency. Medium was then removed, cells washed with 200 µL of PBS and viruses were added at doses of $1 \times 10^3$, $5 \times 10^3$ and $1 \times 10^4$ vp/cell in serum-free RPMI1640 for 3 h. After this, media were replaced with cell line-specific complete growth media. 48 h post-infection the cells were lysed with $1 \times$ Cell Culture Lysis Buffer diluted in $H_2O$ (#E1531, Promega UK Ltd, Southampton, UK) and plates frozen at −70°C. The cells were then thawed and prepared for the analysis by Luciferase Assay System (#1501, Promega UK Ltd, Southampton, UK) according to manufacturers' protocol.

10 or 20 µL of cell suspensions were mixed with 100 µL of luciferase assay reagent on a white 96-well Nunc microwell plate (#236105; Thermo Fisher Scientific, Loughborough, UK) and the luciferase activity in relative light units (RLU) was then immediately measured on a multimode plate reader (FLUOstar Omega, BMG Labtech, Aylesbury, UK). Protein concentration (mg/mL) in each well of the sample plate was determined using a bicinchoninic acid (BCA) protein assay according to manufacturer's protocol (#23227; Pierce™ BCA Protein Assay Kit, Thermo Scientific, Loughborough, UK). Bovine serum albumin (BSA) was used as a protein standard at concentrations 2.0, 1.5, 1.0, 0.75, 0.5, 0.25, 0.125, 0.025 and 0 mg/mL in PBS in duplicate. Samples and standards were incubated with the working reagent (A:B = 50:1) for 30 min, after which absorbance was measured at λ570 nm on an iMark™ Microplate Absorbance Reader (BioRad, Hertfordshire, UK). Blank OD (PBS only) was subtracted from all values and standard curve was prepared of the OD values of the BSA standards. Protein concentration in each sample well was deducted from the equation of the standard curve and normalised to the corresponding sample volume. RLU values in each sample well were normalised for total cellular protein (RLU/mg).

### 2.4.5  The effect of FX on transduction efficiency

For assessment of the impact of physiological concentrations of human coagulation FX on transduction efficiency, the assays were performed essentially as described for the luciferase assay above. Virus dilutions were prepared in serum-free medium that was supplemented with 10 µg/mL of FX (#HCX0050, Haematologic Technologies, Cambridge Bioscience, Cambridge, UK) for 3 h. Volumes were scaled down to a total volume of 100 µL / well to save valuable reagents. FX can be depleted from blood or transduction medium by the addition of a two-chain heterogeneous anticoagulant X-bp that binds to GLA-domain and depletes FX (Waddington et al., 2008). The venom was originally extracted from the hundred pace snake *(Deinagkistrodon acutus)* (Atoda, 1998). X-bp was used for depletion of FX from serum or ascites at a ratio of 3:1 (X-bp:FX).

### 2.4.6  Transduction assays on β-galactosidase-expressing vectors

Transduction assay for β-galactosidase (β-Gal)-expressing viruses was performed using Galacto-Light Plus System according to manufacturer's instructions (Applied Biosystems, Bedford, Massachusetts, USA). Cells were seeded on 96-well Nunc delta surface plates (#236105; Thermo Scientific, Loughborough, UK) and infected as described in section 2.4.4. Infected cells were lysed 48 h post-infection in 100 µL of home-made lysis buffer (0.2 % Triton X-100 in PBS) and plate frozen at –70°C for a minimum of 1 h. Cells were thawed and 10 µL of suspension was mixed with 70 µL of

Galacton Plus Tropix reagent (1:100 in 100 mM $NaH_2PO_4$ / 1 mM $MgCl_2$ diluent, pH 8.0) on a black 96-well microwell plate (#237105 Thermo Scientific, Loughborough, UK), covered with foil and incubated for 1 h at RT. 100 μL of Tropix II accelerator was added into each well and β-Gal activity in RLU) was then immediately measured on luminescence mode on a multimode plate reader (FLUOstar Omega, BMG Labtech, Aylesbury, UK). Protein concentration (mg/mL) in each well of the sample plate was determined using microBCA assay kit and BSA as a protein standard. RLU values in each sample well were then normalised for total cellular protein (RLU/mg).

### 2.4.7 Neutralisation assays in the presence of ovarian ascites

Cell-free ascites samples were used for neutralisation assays to assess the effect of pre-existing anti-Ad nAbs on viral transduction efficiency. Working stocks of freshly isolated fluids were stored as 1 mL aliquots at –20°C for further use (section 2.1.2). Prior to *in vitro* assays, a vial of each fluid was rapidly thawed in a 37°C and kept on ice. Neutralisation assays were performed essentially as described in section 2.4.4, with the exception that cells were pre-incubated with 2-fold serial dilutions (1:40–1:2.5, corresponding to final concentration of 2.5–40 %) of ascites. The dilutions were prepared in serum-free medium (RPMI 1640) by mixing equal amounts of the previous dilution with medium in 1.5 mL Eppendorf tubes. The cells in each well were washed with 200 μL of sterile PBS and 100 μL of ascites dilutions added on the cells for 1 h at 37°C, prior to virus addition for 2 h at 37°C. After this the cells were washed with 200 μL of PBS, 100 μL cell lysis reagent added and the plate frozen at –70°C for a minimum of 1 h. The plate was thawed in RT for a minimum of 1 h and 10–20 μL of cell suspension analysed for luciferase activity, as described in section 2.4.4. Ascites supernatant that exhibited > 90 % inhibition of transduction was considered to be neutralising, as described and validated previously for serum neutralisation assays (Parker et al., 2009).

### 2.4.8 Competition inhibition assays

Vector tropism for cellular receptors CAR, CD46 and αvβ6 integrin was assessed in competition inhibition assays, which is a variation of a standard luciferase transduction assay described above. 20 000 cells were seeded in each well on a 96-well tissue culture plate and pre-incubated with Ni-NTA purified recombinant His-tagged knob proteins (section 2.2) – kn5.wt, kn5.hCAR–, kn5.HI.A20, kn48.wt and kn48.DG.A20 at a final concentration of 10 μg/$10^5$ cells in triplicate. For binding inhibition with function-blocking antibodies, cells were pre-incubated anti-αvβ6 antibody clone 10D5 (Abcam, Cambridge, UK), anti-CD46 clone MEM-258 (Abcam, Cambridge, UK) or normal anti-mouse control IgG (Santa Cruz Biotechnologies,

Heidelberg, Germany) for 30 min on ice (all 10 µg/mL). Total sample volume was 100 µL/well. The viruses were then added on the top at 5000 vp/cell and the mixture incubated for further 1 h on ice. Viruses were then removed, and cells incubated in complete medium for further 47 h at 37ºC. Cells were then washed with 200 µL of PBS, lysed with 100 µL of cell culture lysis buffer and plates frozen at –70ºC. RLU values were measured from 20 µL of cell lysate at 48 h post-infection and normalised to total cellular protein (mg/mL) as described above.

### 2.4.9  Cytotoxicity assays

The cytotoxicity of the oncolytic vectors was assessed using a semi-quantitative, colorimetric CellTiter 96 Aqueous One Solution Cell Proliferation Assay (#G3580; Promega, Madison, WI, USA) according to the manufacturer's instructions. A tetrazolium compound [3-(4,5-dimethylthiazol-2-yl)-5-(3-carboxymethoxyphenyl)-2-(4-sulfophenyl)-2H-tetrazolium, inner salt; MTS] together with an electron coupling reagent phenazine ethosulfate (PES) is reduced into a coloured formazan product by NADPH/NADH produced by dehydrogenase enzymes in metabolically active cells (Figure 2–12). Cells were infected at 1000, 5000 and 25 000 vp/cell in triplicate in a total volume of 100 µL for 3 h, as described in section 2.4.4. Medium was then replaced with 100 µL of complete medium, and cells incubated at 37ºC in a closed humidified container. Cell viability was assessed by addition of 20 µL of assay reagent in each well (5 % final concentration) at pre-determined 24 h time-points. Absorbance was measured at λ490 nm in an iMark™ Microplate Absorbance Reader (BioRad, Hertfordshire, UK) following a 2 h incubation at 37ºC covered in the dark. The number of live cells is directly proportional to the intensity of the produced dark brown colour. The absorbance from uninfected cells was used as a reference of 100 % cell viability.
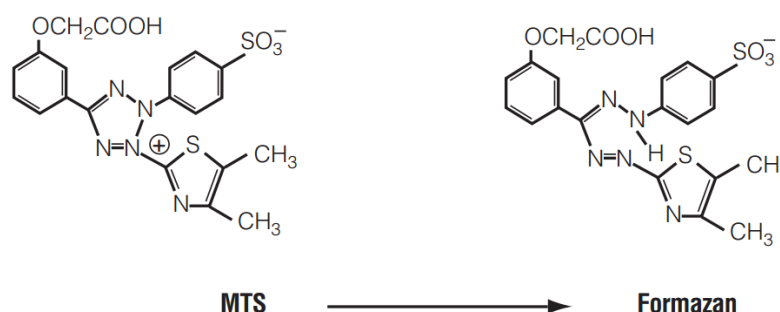


**Figure 2–12. The cell viability assay is based on a colorimetric reaction.** 3-(4,5-dimethylthiazol-2-yl)-5-(3-carboxymethoxyphenyl)-2-(4-sulfophenyl)-2H-tetrazolium (MTS) is reduced to a coloured product formazan by dehydrogenase enzymes in live cells (Promega, 2017).

## 2.4.10 Haemagglutination assays

Ethics permission was obtained for collection of blood from healthy volunteers (Cardiff University School of Medicine Research Ethics committee (SMREC) reference number: 16/45). Recombinant Ad vector tropism was assessed in standard haemagglutination assays (Dooley et al., 1982, Cichon et al., 2003, Nicol et al., 2004). The assay is based on erythrocyte agglutination and the formation of a characteristic erythrocyte network on the surface of the well, due to Ad binding to CAR on erythrocytes (Nicol et al., 2004). Non-CAR-binding Ads fail to agglutinate blood and therefore characteristic erythrocyte pellet forms at the bottom of the well. Leftover erythrocytes were received from other researchers who had separated the blood by serial centrifugation and removed plasma to be used for other assays. The erythrocyte cell pellet was transferred to a fresh 15-mL tube and washed two times with 5 mL of PBS by centrifugation for 8 min at 1000 rpm. The erythrocytes were then diluted to 1 % (v/v) in PBS, and virus dilutions were prepared at $1 \times 10^9$, $7.5 \times 10^8$ and $5 \times 10^8$ vp in PBS. 50 µL of erythrocyte suspension was added in each well of V-bottom 96-well plate, 50 µL of virus dilutions added on the top and mixed gently. After a 2 h incubation at 37ºC haemagglutination was graded as –, no haemagglutination, +, partial, ++, midrange, +++, complete haemagglutination (Cichon et al., 2003).

## 2.5  *In vivo* characterisation of recombinant vectors

All *in vivo* experiments were performed at Professor Richard Vile's laboratory at the Department of Immunology/Molecular Medicine (Mayo Clinic, Minnesota, USA). All procedures were approved by the local Mayo Foundation Institutional Animal Care and Use Committee (IACUC). Permissions for the international export and use of replication-deficient and oncolytic Ad vectors were requested from Centers for Disease Control (CDC, USA). Animal experiments were funded from Mayo Clinic PAU funding #91939 and International Collaboration Seedcorn grant awarded to Dr Alan Parker by School of Medicine, Cardiff University, UK (#AH1170A001; £10 000). Cancer Research Wales (CRW) charity funded part of the research done in this thesis but did not allow funding of animal experiments. The Seedcorn grant was therefore obtained for the purposes of funding the *in vivo* experiments that were considered pivotal for the successful completion of this thesis. The completion of *in vivo* studies involved a 2-month collaborative visit to Prof Richard Vile's laboratory. In order to achieve consistency of results, all animals were sex-matched; female mice were chosen due to the ease of housing. Mice were allowed to acclimatise for a minimum of 48 h prior to experiments. All injections and animal handling were performed by a

highly qualified veterinary technologist Jill M. Thompson (Mayo Clinic, Rochester, MN, USA).

### 2.5.1 Biodistribution profile following systemic vector delivery
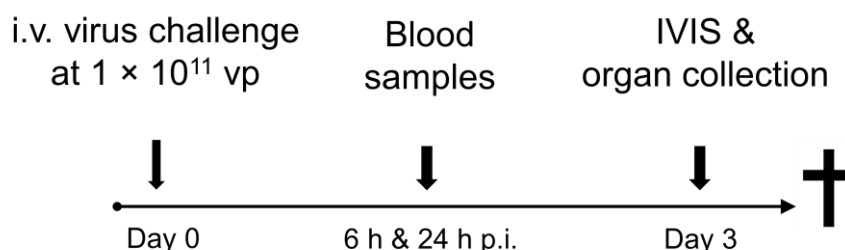


**Figure 2–13. Treatment schedule for *in vivo* biodistribution study.** Mice were challenged with viruses and blood collected for cytokine screening. The animals were sacrificed on day 3 post-infection (p.i.). i.v., intravenous; IVIS, In Vivo Imaging System; vp, viral particle.

The biodistribution of replication-deficient vectors was assessed in wild type B6 albino mice (B6N-$Tyr^{c-Brd}$/BrdCrCrl) that is a spontaneous albino mutant co-isogenic C57BL/6 strain with an MHC haplotype H2$^b$. This immunocompetent strain was chosen due to its white coloured coat, which makes luciferase tracking much more feasible compared to the commonly used black C57BL/6 phenotype. 6-week-old mice (n = 5/group) were ordered from Charles River Laboratories International (USA) and allowed to acclimatise for one week prior to experiments (Figure 2–13). Viruses were diluted in PBS at $1 \times 10^{11}$ vp in a total volume of 100 µL and injected into the lateral tail vein. Animals were monitored daily for distress and vector-induced toxicities. All mice were sacrificed immediately after IVIS imaging at 72 h by inhalation of $CO_2$ and organs harvested to assess vector distribution by *ex vivo* imaging, immunohistochemical staining of paraffin-embedded tissues (IHC-P) and quantification of viral copy number.

**Table 2–8. Treatment groups in the biodistribution study.** All viruses were replication-deficient. A20, peptide NAVPNLRGDLQVLAQKVART (DiCara et al., 2007); KO1, CAR-binding mutation (Smith et al., 2002).

| Group | Replication-deficient vector | Insert | *N* |
|-------|------------------------------|--------|-----|
| A | PBS | – | 5 |
| B | Ad5.Luc | – | 5 |
| C | Ad5.KO1 | – | 5 |
| D | Ad5.A20 | A20 peptide | 5 |
| E | Ad5.KO1.A20 | A20 peptide | 5 |
| F | Ad5.HVR7 | – | 5 |
| G | Ad5.HVR7.A20 | A20 peptide | 5 |
| H | Ad5.3D.A20 | A20 peptide | 5 |
| | **TOTAL** | | **40** |

### 2.5.2 IVIS imaging for temporal and spatial luciferase expression

All viruses express Firefly luciferase, which allowed us to track their temporal and spatial distribution in real time by using the non-invasive, semi-quantitative In Vivo Imaging System (IVIS), Xenogen IVIS-200 Bioluminescent Imager (PerkinElmer, Hopkinton, MA, USA). Live mice were imaged at 72 h time-point to assess vector trafficking to peripheral tissues. The bioluminescence of luciferase is activated by its substrate, D-luciferin. For IVIS imaging, mice were anaesthetised using 2 % isoflurane (1.5 % for maintenance) and 200 µL of D-luciferin at 15 mg/mL (#LUCK; potassium salt, Gold Biotechnology, St. Louis, MO, USA) was injected i.p. and allowed to disseminate for 5 min prior to imaging. Mice were placed in the IVIS imager one group (n = 5) at a time, and bioluminescence recorded with 1 min exposure time. Mice were then sacrificed by inhalation of $CO_2$, organs harvested and each organ placed in a separate well on a 12-well plate with 1 mL of PBS to prevent them from drying out. *Ex vivo* luminometry was performed on tissue blocks immediately after harvesting of the organs to correlate with the observations from IVIS imaging. 1 mL of D-luciferin was added on top of each organ at a final concentration of 300 µg/mL and image taken immediately with 1 min exposure time. Images were further evaluated in Living Image® software version 4.5 (Perkin Elmer, Hopkinton, MA, USA).

### 2.5.3 Viral genome number by quantitative polymerase chain reaction (qPCR)

Viral and total genomic DNA was obtained from non-fixed murine tissues (~ 10 mg of spleen and ~ 25 mg of other organs) using DNeasy Blood & Tissue DNA extraction kit according to the manufacturer's protocol (#69506; Qiagen, Germantown, MD, USA). The concentration of purified DNA was determined using a NanoDrop ND-1000 photospectrometer (NanoDrop Technologies). 40 ng of total DNA was subjected to fluorogenic quantitative PCR using Fast SYBR Green Master Mix system (#4385612; Applied Biosystems, Life Technologies, Paisley, UK). Reactions were performed in triplicate, using primers for the hexon region of the genome, Forward: 5′-CGCGGTGCGGCTGGTG-3′ and Reverse: 5′-TGGCGCATCCCATTCTCC-3′ (Sigma Aldrich, Gillingham, UK). Negative controls were run to ensure that no amplification occurred in the absence of DNA. Cycling conditions were as follows; 50°C for 2 min, 95°C for 10 min, 40 cycles of 95°C for 15 s, followed by 60°C for 1 min. Total adenoviral genomes were calculated using a standard curve of $10^1$–$10^7$ viral genomes; separate standard curve was prepared for each virus.

### 2.5.4 Immunohistochemical staining of paraffin-embedded tissues (IHC-P)

Lungs, liver, spleen, heart, ovaries and tumour tissues were harvested from mice post-mortem. Immediately after *ex vivo* imaging, organs were immersed in 10 mL

volume of 10 % formalin (#032-059; Protocol®, Fisher Scientific, MI, USA). Livers were sent to Histology Core Laboratory, Mayo Clinic Arizona, Scottsdale, AZ, USA for preparation of formalin-fixed paraffin-embedded and haematoxylin/eosin (H&E) stained tissue slides. The presence of Ad particles in liver tissues was visualised by IHC staining. Tissues were first re-hydrated by incubating in three changes of xylene for 5 min. They were then washed twice in 100 % industrial methylated spirit (IMS) for 3 min, once in 90 % IMS for 3 min, distilled $H_2O$ for 5 min and rinsed in PBS. The tissues were circled with ImmEDGE pen (#H-4000; Vector Laboratories, Peterborough, UK), and treated with proteinase K (#4333793; AB, Foster City, CA, USA) at 20 µg/mL in Tris/EDTA (TE) buffer for 10 min at RT. Tissues were then washed in PBS for 5 min and blocked in 2.5 % horse serum (#MP-7401; ImmPRESS™ HRP anti-rabbit IgG-HRP polymer detection kit; Vector Laboratories, Peterborough, UK) for 1 h. After a 5-min wash in PBS, endogenous hydrogen peroxide activity was quenched by treating the tissues with 3 % $H_2O_2$ (#21,676-3; Sigma Aldrich, Gillingham, UK) in PBS for 10 min, after which the tissues were washed in PBS for 5 min. Tissues were then incubated with primary polyclonal rabbit anti-adenovirus type 5 antibody (1 µg/mL; #ab6982, Abcam, Cambridge, UK), anti-*ITGB6* antibody (1:10; #ab197672, Abcam, Cambridge, UK) or anti-CAR antibody (1:100; #ab153740, Abcam, Cambridge, UK) O/N at 4ºC in a humidified container. A rabbit IgG isotype control antibody (1 µg/mL; #GTX35035; GeneTex, Wembley, UK) was included as a negative control to detect any non-specific staining. Tissues were washed in 1 mL of PBS for 5 min and incubated with anti-rabbit secondary (#MP-7401; ImmPRESS™ HRP anti-rabbit IgG-HRP polymer detection kit, made in horse; Vector Laboratories, Peterborough, UK) for 30 min at RT. Tissues were washed in PBS for 5 min and incubated with DAB substrate for 3 min. They were then rinsed in tap water, counterstained in haematoxylin for 15 s and rinsed in running water for 15 min until the water was completely clear. The tissues were then de-hydrated by repeating the re-hydration sequel in reverse, starting from 90 % IMS and proceeding to the xylene washes. Tissues were mounted using DPX Mountant for histology (#06522; Sigma Aldrich, Gillingham, UK), coverslip added on the top, and images acquired at 10 x, 20 x and 40 x magnification using a light microscope (Leica DMC 2900; Leica Microsystems Ltd, CH-9435 Heerbrugg, Switzerland).

### 2.5.5   Cytokine screening

Elicitation of innate immune mediators was assessed in immunocompetent mice as a part of the biodistribution study, as cytokine/chemokine assessment provides important information on vector toxicity and tolerability. Cytokine screening was

performed in its entirety by Dr Angela Bradshaw, BHF Glasgow Cardiovascular Research Centre, UK. Approximately 100 µL of blood was collected from mice at 6 h and 24 h post-injection from the submandibular (cheek) vein into lithium heparin tubes (#365965; BD Microtainer, Becton Dickinson, New Jersey, USA). Whole blood was transferred to 1.5 mL Eppendorf tubes and plasma was separated by centrifugation at 1000 x g for 10 min at 4ºC in a table top centrifuge and stored at –80ºC. Cytokines and chemokines were assessed in a magnetic bead-based Bio-Plex Pro™ Mouse Cytokine 23-plex assay (#M60009RDPD; Bio-Rad Laboratories Ltd, Herts, UK) and Pro reagent kit (#171-304070M; Bio-Rad Laboratories Ltd, Herts, UK) per manufacturer's instructions. The panel assesses the levels of common markers of acute innate immune response activated upon (viral) infections: granulocyte colony-stimulating factor (G-CSF), granulocyte macrophage colony-stimulating factor (GM-CSF), interferon γ (IFN-γ), interleukin (IL) 1α, IL-1β, IL-2, IL-3, IL-4, IL-5, IL-6, IL-9, IL-10, IL-12 (p40/p70), IL-13, IL-17A, tumour necrosis factor α (TNF-α), chemokine ligand 5 (RANTES), keratinocyte-derived cytokine (KC), monocyte chemoattractant protein 1 (MCP-1; MCAF), macrophage inflammatory protein-1 α (MIP-1α), MIP-1β and eotaxin (CC subfamily of eosinophil chemotactic proteins). 30 µL of plasma was mixed with 90 µL Bio-Plex sample diluent (1:4) and incubated with the magnetic beads on ice. Following an O/N vortexing at 4ºC, the coupled beads were incubated with the secondary detection antibody for 30 min on a shaker. Serial washes were performed in wash buffer between each incubation step. The beads were then mixed with assay buffer and analysed in a fluorescence-based Bio-Plex® 200 plate reader with high-throughput fluidics (#171000205; Bio-Rad Laboratories Ltd, Herts, UK). Protein concentration was quantified by BCA assay using 10 µL of the original plasma samples that were diluted 1:10 in PBS and absorbance measured at λ560 nm; values were normalised to total protein in each well (pg/mg). Data were analysed in Bio-Plex® 200 Manager™ software with 5-point log curve fitting and statistical analyses performed in GraphPad Prism.

### 2.5.6   Generation of a SKOV3-β6 ovarian cancer xenograft model
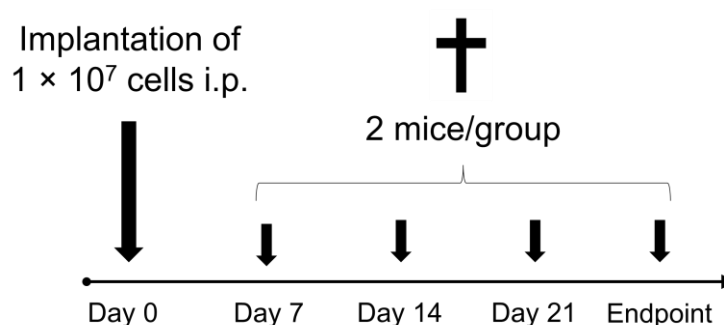


**Figure 2–14. Schedule for the SKOV3-β6 pilot study.** Intraperitoneal (i.p.) SKOV3-β6 tumour xenografts were established in NOD/SCID mice. Two mice were sacrificed on days 7, 14, 21 and at the final endpoint.

A pilot study (Figure 2–14) was set up to establish a timeline for the tumour take rate, and to set up an optimal time point for OAd treatment for a subsequent efficacy study. Prior to implantation to mice, $2 \times 10^7$ SKOV3-β6 cells were sorted into a highly αvβ6-positive cell population by FACS by staining with primary anti-αvβ6 antibody 10D5 (1:100; #MAB2077Z, Millipore, Watford, UK) and secondary anti-mouse-FITC IgG conjugate (1:100; #0855499, MP Biomedicals, USA). Cell sorting was performed on FACSAria cell sorter by trained professionals at Microscopy and Cytometry Core at Mayo Clinic, Rochester, MN, USA. A total number of $3.1 \times 10^6$ positive cells were recovered and sub-cultured for 8 days prior to implantation. Cells in log phase (monolayer ~ 70 % confluent) were rapidly trypsinised and washed twice with PBS immediately prior to implantation. Immunocompromised non-obese diabetic severe combined immune deficiency (NOD/SCID) mice homozygous for the SCID spontaneous mutation (Prkdc$^{scid}$) (Jackson Laboratories, Bar Harbor, Maine, USA) were allowed to acclimatise for a week prior to handling.

On day 0, $1 \times 10^7$ SKOV3-β6 cells were implanted i.p. in eight animals (n = 2/group). Mice were monitored daily for the onset of malignant ascites build-up, and weighed every 7 days. At 7-day intervals two mice were sacrificed, and their peritoneal cavity rinsed with 10 mL of DMEM to collect floating cancer cells. Visible tumours were dissected into a homogenous solution and cells cultured in a T75 tissue culture flask. For flow cytometry, cells were stained with primary anti-CAR RmcB (1:500; #05-644, Millipore, Watford, UK) and anti-αvβ6 10D5 (1:100) antibodies, and a secondary anti-mouse IgG (H+L) Alexa Fluor 647 (#A-21235, Invitrogen). *In vitro* grown SKOV3-β6 cells were used for gating to distinguish the EOC cells from other cell types present in the ascites. A minimum of 10 000 events were recorded for each mouse on FACSCanto at Microscopy and Cytometry Core at Mayo Clinic, Rochester, MN, USA.

## 2.6    Statistical analysis and software used

### 2.6.1    Statistical analyses

All figures were created and statistical analyses performed in GraphPad Prism version 4.03 (GraphPad Software Inc., La Jolla, CA, USA). Unless otherwise stated, data show the mean ± standard deviation (SD) or standard error of the mean (SEM) of $n = 2$–5 (specific $n$ numbers are indicated in each figure legend). P values were as follows: ns, not statistically significant, $p > 0.05$; *, $p < 0.05$; ** $p < 0.01$; ***, $p < 0.001$; ****, $p < 0.0001$.

### 2.6.2    Sequence analyses

All viral BAC sequences were verified by sequencing after mutation by AdZ recombineering. DNA sequences were analysed in CLC Main (Qiagen) or Genome Compiler (Genome Compiler Corporation, CA, USA) software.

### 2.6.3    Protein alignments and structural analyses

All sequences of adenovirus structural proteins were downloaded from National Center for Biotechnology Information (NCBI) website (http://www.ncbi.nlm.nih.gov/protein). Sequences were aligned in BioEdit software (Hall, 1999) using the ClustalW multiple alignment tool. The alignments were then saved as rich text format and further edited in Microsoft Word and PowerPoint.

### 2.6.4    Flow cytometry and fluorescence-activated cell sorting (FACS)

FACS of SKOV3-β6 cells for in vitro studies was performed by Dr. Kristin Ladell, Cardiff University. FACS of SKOV3-β6 cells for *in vivo* xenograft study was performed in Aria cell sorter at Microscopy and Cytometry Core at Mayo Clinic, Rochester, MN, USA. Analyses of flow cytometry data were performed in BD Accuri software (BD Biosciences). FACS data were analysed in FACSDiva 8.0.1 software (BD Biosciences).

# CHAPTER 3.    Results: Characterisation of model cell lines and ovarian ascites

# CHAPTER 3. Characterisation of model cell lines and ovarian ascites

This chapter discusses the characterisation of model cell lines for the assessment of recombinant cancer-targeted Ad vectors. We sought to find suitable cells that would express variable levels of CAR, CD46 and αvβ6 integrin. The second major objective was the establishment of successful *ex vivo* cultures of EOC cells from clinical malignant ascites that had been derived from patients who were receiving chemotherapy for advanced ovarian cancer. The ascitic fluids were also characterised for their presence of anti-Ad antibodies and FX, both of which are likely to play an important role in the efficacy of Ad vector-based therapies that are intended for local i.p. delivery.

## 3.1 Phenotyping of cancer cell lines

### 3.1.1 Receptor expression profile

Epithelial cell lines were assessed for the surface receptor expression profile of αvβ6, CAR, CD44, CD46 and EGFR by flow cytometry (Table 3–1) in order to screen and evaluate suitable candidates for preliminary *in vitro* transduction studies. The native receptor of species C Ads – CAR – was expressed at highly variable levels, while the level of native receptor of species B Ads – CD46 – was consistently high in all cell lines. Levels of a CSC marker CD44 and a common cancer cell marker EGFR were consistently high in all tested human cell lines. BT-20 breast cancer cell line was shown to express natively high levels of αvβ6 integrin.

**Table 3–1. Receptor expression profile of epithelial cell lines.** 100 000 cells were stained in duplicate with primary antibodies (αvβ6, 10D5; CAR, RmcB; CD44, F10442; CD46, MEM258; EGFR, H11) for 1 h on ice, and with secondary AlexaFluor 647 for 30 min on ice. Data were recorded for 10 000–20 000 events in BD Accuri C6 flow cytometer and analysed in BD Accuri software. αvβ6, αvβ6 integrin; CAR, coxsackie and adenovirus receptor; CD46, cluster of differentiation 46 receptor; EGFR, epidermal growth factor receptor; SKOV3-β6, SKOV3 cell line expressing β6 subunit (generated in-house); *, primary cell line; nd, not determined.

| Cell line | Organ | αvβ6 | CAR | CD44 | CD46 | EGFR |
|---|---|---|---|---|---|---|
| A549 | Human lung carcinoma | 7 | 100 | nd | 100 | 100 |
| BT-20 | Human breast cancer | 87 | 40 | 93 | 97 | 96 |
| CHO-K1 | Hamster ovary | 0 | 0 | nd | 0 | 0 |
| CHO-CAR | Hamster ovary | 0 | 100 | nd | 0 | 0 |
| CHO-BC1 | Hamster ovary | 0 | 0 | nd | 100 | nd |
| D007-SFi* | Human skin fibroblast | 0 | 0 | 100 | nd | nd |
| HeLa | Human cervical cancer | 0 | 3 | nd | 40 | 50 |
| HepG2 | Human liver cancer | 0 | 100 | nd | 90 | 100 |
| MDA-MB-231 | Human breast cancer | 0 | 13 | 98 | nd | nd |
| MDA-MB-361 | Human breast cancer | 72 | 87 | 18 | nd | nd |
| OVCAR3 | Human ovarian cancer | 18 | 18 | 0 | 96 | 84 |
| SKOV3 | Human ovarian cancer | 9 | 44 | nd | 98 | nd |
| SKOV3-β6 | Human ovarian cancer | 100 | 90 | nd | 98 | nd |
| T24 | Human bladder cancer | 0 | 9 | nd | 100 | nd |
| T-REx-293 | Human embryonic kidney | 0 | 87 | 77 | nd | nd |

### 3.1.2 Selection of model cell lines for transduction assays

This thesis is focused on the characterisation of vectors targeted to ovarian cancer, which is why we focused on assessing the phenotype of several different ovarian cancer cell lines. Cell lines with high levels of αvβ6 expression were selected as model cell lines for the *in vitro* assessment of αvβ6-targeted vectors. BT-20 is a breast cancer cell line that expresses high levels of αvβ6 and low levels of CAR (Figure 3–1A). In the absence of a suitable CAR$^{low}$/αvβ6$^{high}$ EOC model cell line, BT-20 was used as a αvβ6$^{high}$ control cell line, despite its non-ovarian origin. Chinese hamster ovarian cell lines CHO-K1 (Figure 3–1B), CHO-CAR (Figure 3–1C) and an ovarian ascites-derived cell line SKOV3 (Figure 3–1D), were the main cell lines used for transduction assays in this thesis. CHO-K1 cell line, being devoid of all primary native Ad receptors and the assessed cancer cell markers, was used as a clean negative control cell line for Ad transduction in this thesis. CHO-CAR cell line was chosen as a representative positive control cell line for all *in vitro* studies assessing vector CAR-tropism, due to its high level of CAR-expression. Another ovarian cell line, OVCAR3 (Figure 3–1E), was shown to lack expression of αvβ6 and was therefore not readily suitable for these studies. The CAR$^{high}$ T-REx-293 cell line was shown to lack αvβ6 expression but to express high levels of CAR (Figure 3–1F), and was used routinely for propagation of replication-deficient vectors due to its expression of Ad *E1* and *E3* genes that have been removed from the Ad5 vector backbone.
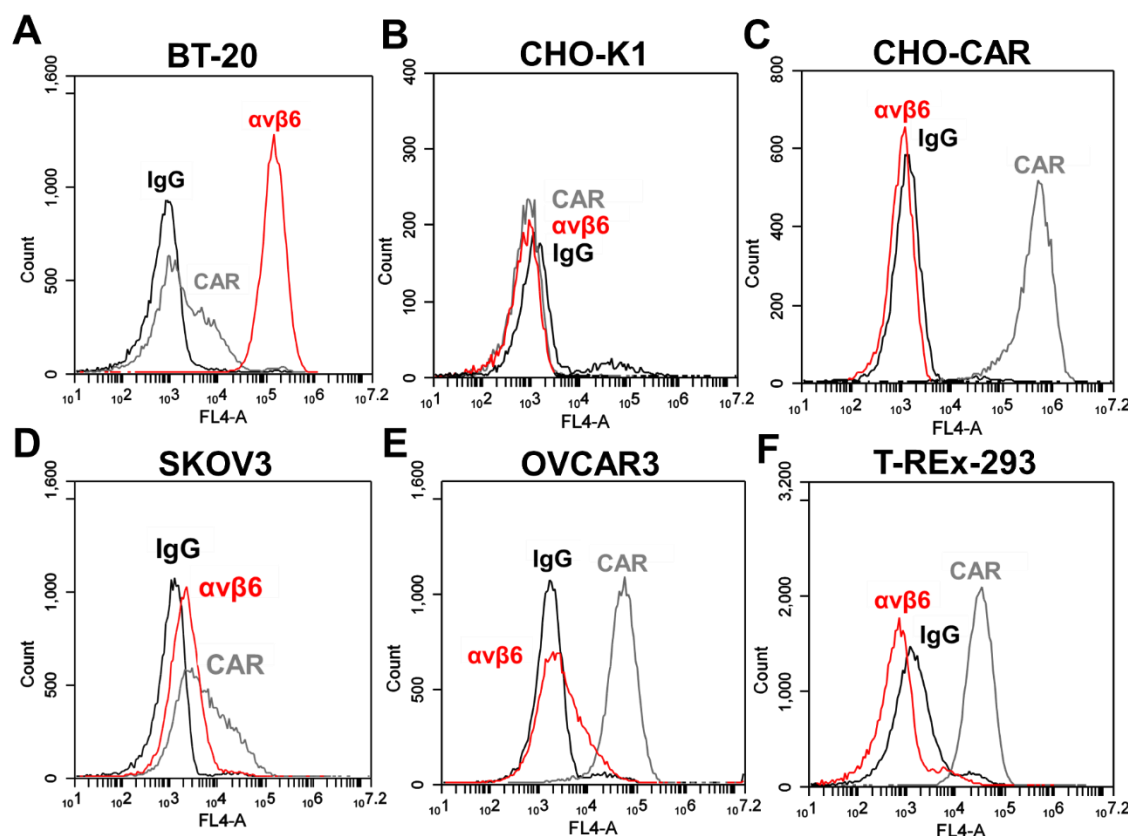
**Figure 3–1. Selected cell lines for transduction studies based on their αvβ6 integrin and CAR expression.** (A) BT-20 breast cancer, (B) CHO-K1 hamster ovarian, (C) CHO-CAR hamster ovarian, (D) SKOV3 ovarian cancer, (E) OVCAR3 ovarian cancer and (F) T-REx-293 kidney cells were stained with primary antibodies (αvβ6, 10D5; CAR, RmcB) for 1 h on ice and with secondary AlexaFluor 647 for 30 min on ice. 10 000–20 000 events were recorded in BD Accuri C6 flow cytometer and data analysed in BD Accuri software. CAR, coxsackie and adenovirus receptor.

The second main part of this thesis is focused on the generation and *in vitro* characterisation of novel pseudotyped vectors based on species D serotypes. We therefore sought to assess the receptor tropism of these vectors on cell lines that would have variable levels of both CAR and CD46 expression, since these receptors are potential entry receptors for viruses from subgroup D. We chose to use CHO-K1 cells as a negative control cell line, since they have no CD46 expression (Figure 3–2A). CHO-BC1 cells (Figure 3–2C) that stably express an isoform BC1 of the CD46 receptor, as previously described by Prof Lieber's research group (Gaggar et al., 2003), were used for all assays evaluating CD46 tropism of Ad serotypes in this thesis. This is a clean model cell line as it does not express CAR or other Ad receptors (data not shown). Model cell lines for αvβ6 targeting, SKOV3 and BT-20, were also shown to express very high levels of CD46 (Figure 3–2D, E).
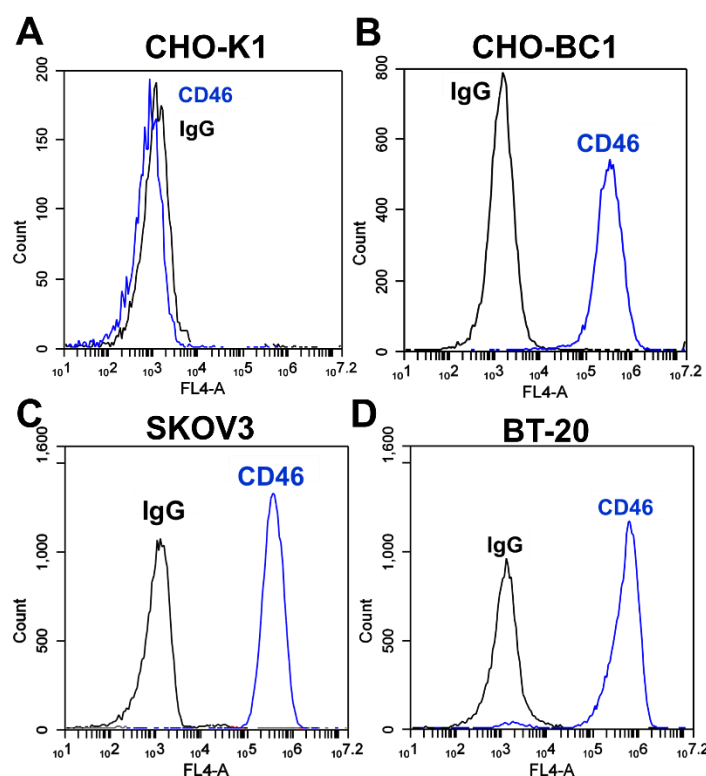
**Figure 3–2. CD46 receptor expression on selected model cell lines.** (A) CHO-K1 Chinese hamster ovarian, (B) CHO-BC1 Chinese hamster ovarian expressing an BC1 isoform of CD46, (C) SKOV3 ovarian cancer and (D) BT-20 breast cancer cell lines were stained with primary CD46 antibody MEM258 for 1 h on ice, and with secondary AlexaFluor 647 for 30 min on ice. 10 000–20 000 events were recorded in BD Accuri C6 flow cytometer and data analysed in BD Accuri software.

### 3.1.3 Generation of an αvβ6-positive model cell line – SKOV3-β6

SKOV3 ovarian cancer cells were used as a cell line counterpart for ascites-derived primary EOC *ex vivo* cultures assessed in this thesis. SKOV3 cells were originally derived from clinical ascites from an ovarian cancer patient donor and further propagated into a permanent cell line (source: ATCC, American Type Culture Collection), which is why they are an optimal cell line for our purposes. These were used as the parent cell line to generate SKOV3-β6 cell line by stable transfection using a pBABE puro β6 retrovirus plasmid expressing the human β6 integrin subunit. Cell line was generated in a week's time, and transduced cells were further propagated for assays for a minimum of several weeks in the presence of puromycin selection marker, until any *in vitro* assays were carried out. The generated SKOV3-β6 cells were propagated through serial passages in the presence of 5 μg/mL of puromycin selection marker in complete DMEM medium. The cells were then sorted into high αvβ6-expressing populations prior to subsequent *in vitro* assays, to ensure that they were highly permissive to viral infection. At the time of the first sort the cells were ~ 88 % positive for αvβ6 (Figure 3–3A). The top 8 % most positive population of

these cells was sorted by FACS, and expanded in subsequent culture in the presence of 5 µg/ml of puromycin until a desired cell number was achieved for second FACS sort. The sorted cells were assessed by flow cytometry and shown to be 100 % positive for αvβ6 (Figure 3–3B). The SKOV3-β6 cells were then further propagated and second round of FACS performed to ensure high proportion of αvβ6-positive cells for transduction assays. At this stage the cells were still 94 % positive for αvβ6 (data not shown). Of this positive population, the top 10 % most αvβ6-positive SKOV3-β6 cells were sorted (Figure 3–3C), further sub-cultured, used for *in vitro* assays, and frozen down for permanent stocks.
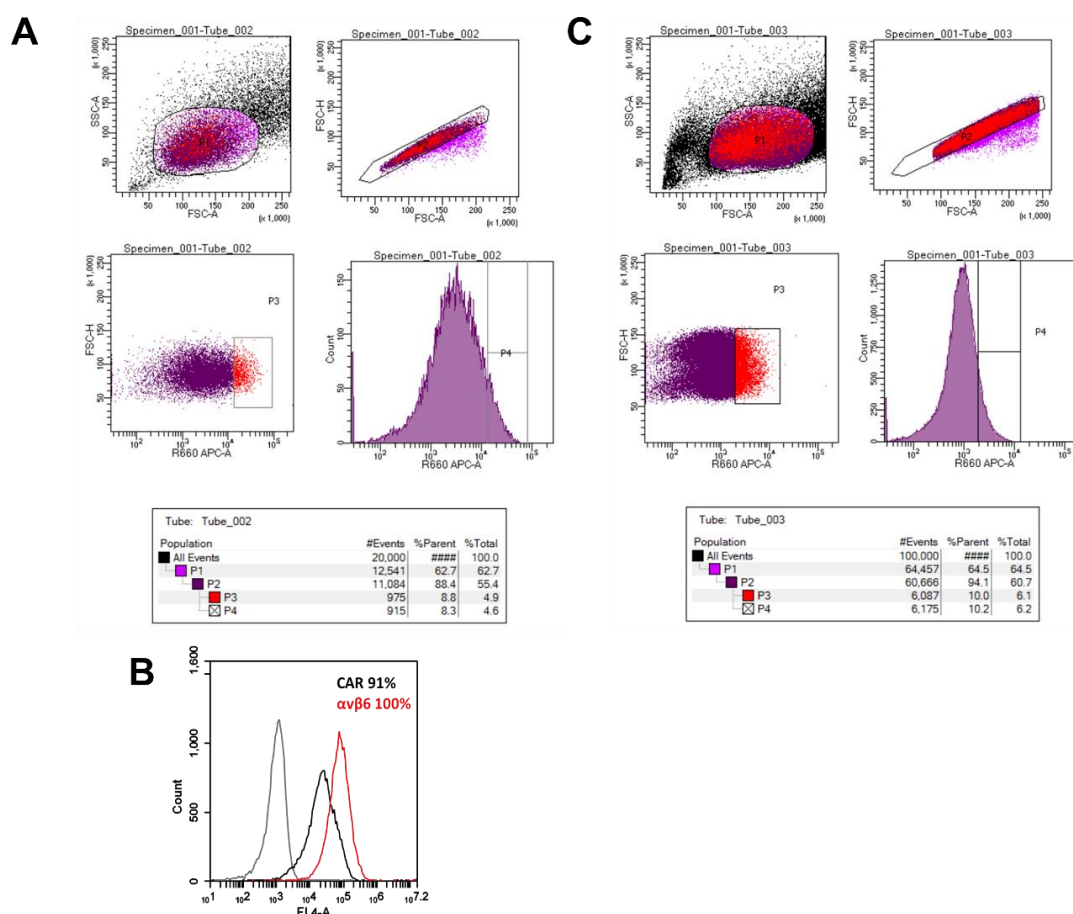


**Figure 3–3. Fluorescence-activated cell sorting (FACS) of SKOV3-β6 cells.** Cells were stained with primary αvβ6 antibody 10D5 for 1 h on ice, and with secondary AlexaFluor 647 for 30 min on ice. (A) In the first round the top 10 % most αvβ6-positive cell population (red) was sorted and further propagated. (B) The level of αvβ6 and CAR expression on SKOV3-β6 cells was assessed by flow cytometry after the first round of FACS, recording 20 000 events. (C) Second round of FACS for SKOV3-β6 cells. Cells were sorted into a 10 % most αvβ6-positive population (red). αvβ6, αvβ6 integrin; CAR, coxsackie and adenovirus receptor.

## 3.2  Characterisation of clinical ovarian ascites

Twenty clinical ovarian ascites samples were received from Velindre Cancer Centre (Cardiff, UK) between December 2014 and August 2016. Ascites samples arrived to our lab in a 500 mL plastic disposable container, generally within ~ 3 h of

isolation from the patient. In few cases samples were stored in the original container O/N in the fridge at 4°C and processed on the following morning. Up to 24 h storage at 4°C did not have a notable effect on the survival of EOC cells, while cell survival was notably decreased in samples that were stored beyond this period. The samples were processed according to established protocols (Thériault et al., 2013, Shepherd et al., 2007, O'Donnell et al., 2014) with a satisfactory success rate. Considerable variation was observed in the colour, thickness and consistency of the clinical ovarian ascites samples. One sample was extremely thick and creamy (Figure 3–4A), which is likely to be a result of lymphatic obstruction by a tumour mass, causing leakage of protein-rich lymphatic fluids into the peritoneal cavity. The parenthesis procedure itself can cause leakage of blood into the peritoneum from the catheter pass, causing bloody appearance in the fluid (Figure 3–4B and C). Most commonly however, the fluid was a shade of dark yellow straw, reminiscent of the colour of serum (Figure 3–4D). Very frequently there were ~ 1–2 cm pieces of connective tissue and/or adipose tissue present in the fluid, which were discarded at the time of sample processing and not included in the EOC *ex vivo* cultures.
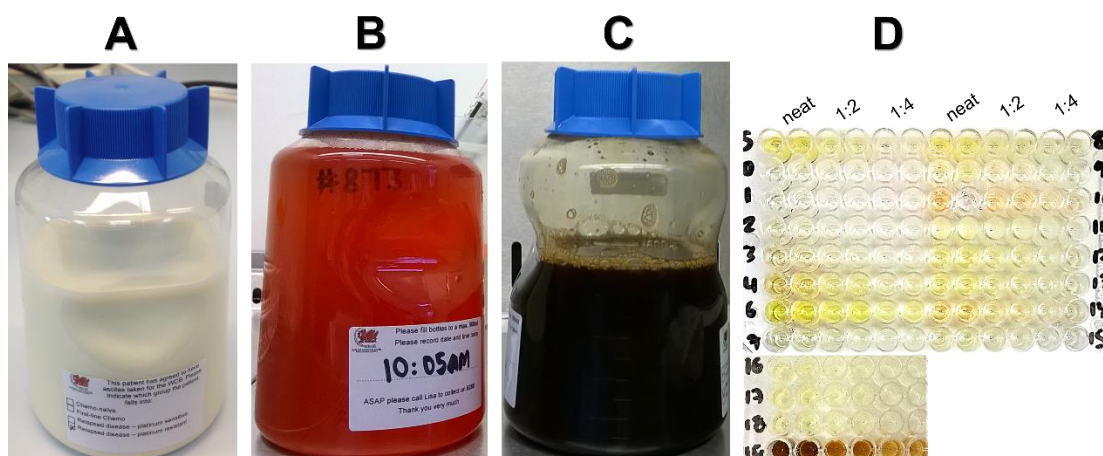


**Figure 3–4. Physical appearance of ovarian ascites samples.** Huge variation was seen in the appearance of ovarian ascites. Some fluids were (A) extremely creamy and thick, (B) contaminated with blood, (C) heavily contaminated with haemolysed blood. (D) Summary of all 20 samples on a 96-well plate showing the range of colour variation; neat ascites, diluted 1:2 and 1:4 in 1 % milk/PBS-T for ELISA; S, serum control (first row).

Cells were isolated from the fluid by centrifugation, and sub-cultured in general T75 cell culture flasks at 37°C for up to several months. The cell-free fluids were stored as 50 mL aliquots at –70°C for permanent long-term stocks, and 1 mL working stocks were stored at –20°C. Two cryovials of cells of each sample were stored at passage 0 in –130°C liquid nitrogen tanks for long term storage and future use. At the time of subsequent use, a vial was rapidly thawed in 37°C water bath and cells sub-cultured in complete EOC growth medium for up to several months until they turned senescent.

Cells were frozen back at passage 1 to establish long-term stocks for future use. Proliferating primary EOC *ex vivo* cultures were successfully established for 13 out 20 ascites samples, corresponding to a 65 % success rate (Table 3–2). Successful culture establishment seemed to be independent on the chemotherapy treatment stage and on the level of blood contamination in the received sample.

**Table 3–2. Clinical ovarian ascites sample summary.** Samples were received from Velindre Cancer Centre (Cardiff, UK) and processed within 24 h. Successful epithelial ovarian cancer (EOC) cell *ex vivo* cultures are shown in black. The level of blood contamination: –, absent/low; +, medium; ++ high/very high. Stage indicates the extent of previous chemotherapies: 1, pre-treatment/chemo naïve; 2, first-line chemo; 3, relapsed disease/platinum-sensitive; 4, relapsed disease/platinum-resistant.

| Sample ID | Date received | Vol. (mL) | Stage | Blood | Remarks |
|---|---|---|---|---|---|
| 000 | 3/12/14 | 500 | 2 | ++ | – |
| 001 | 15/12/14 | 500 | 2 | + | – |
| 002 | 26/2/15 | 500 | 3 | ++ | lots of cells present in the initial sample |
| 003 | 1/4/15 | 650 | 1 | ++ | – |
| 004 | 1/4/15 | 500 | 4 | ++ | – |
| 005 | 27/4/15 | 500 | nd | ++ | heavy bacterial contamination (extremely cloudy); sample not used for any assays |
| 006 | 28/4/15 | 500 | nd | ++ | – |
| 007 | 7/5/15 | 500 | 3 | – | – |
| 008 | 3/6/15 | 600 | 3 | + | – |
| 009 | 25/6/15 | 625 | 1 | – | – |
| 010 | 4/8/15 | 500 | 4 | ++ | – |
| 011 | 3/2/16 | 500 | 4 | – | very creamy and thick - lymphatic obstruction? |
| 012 | 6/7/16 | 400 | nd | ++ | – |
| 013 | 12/7/16 | 500 | 4 | – | yellow colour |
| 014 | 12/7/16 | 500 | 2 | ++ | good cell growth |
| 015 | 15/7/16 | 450 | 4 | – | yellow colour; lots of connective/fat tissue - stored 48 h until processed |
| 016 | 15/7/16 | 500 | 4 | + | brownish yellow colour |
| 017 | 11/8/16 | 550 | 4 | – | – |
| 018 | 17/8/16 | 550 | nd | – | nice yellow colour, some fat/connective tissue; pretty cobblestone cells |
| 019 | 24/8/16 | 450 | 3 | ++ | extremely dark brown colour and thick texture |

### 3.2.1 Epithelial ovarian cancer (EOC) cell morphology and senescence

The EOC primary cells were generally sturdy to culture and tolerated freeze-thaw cycles very well. There was no significant cell loss when cells were revived from frozen. The cells were generally cultured for up to four weeks until a suitable cell confluency was achieved. They were then either sub-cultured or seeded in 96-well tissue culture plates for *ex vivo* assays. In general, primary EOC cells grew very slowly and reached senescence at passage 2–4, after which their morphology changed remarkably, and they stopped dividing. At this stage the cells grew considerably in size and the cells formed outward-reaching elongated structures. Sample 005 was completely unusable due to its thick, creamy appearance and an extremely heavy bacterial contamination. All in all, early senescence and low number of EOC cells

greatly limited the usability of the clinical ascites samples. Ascites contains a variety of cell types, and therefore verification for epithelial origin it was essential. Cultures were monitored approximately three times a week under a general light microscope and images taken at different growth stages to verify that cells were of the typical 'cobblestone' morphology (Figure 3–5). Cultures that appeared to have spider-like elongated cells, were treated as contaminated with fibroblasts. In this case, the cells were briefly trypsinised for 2 min to remove more loosely attached fibroblasts and to enrich the culture with firmly-attached epithelial-type cells. Partial trypsinisation was repeated as many times as required to completely remove fibroblasts from the culture.
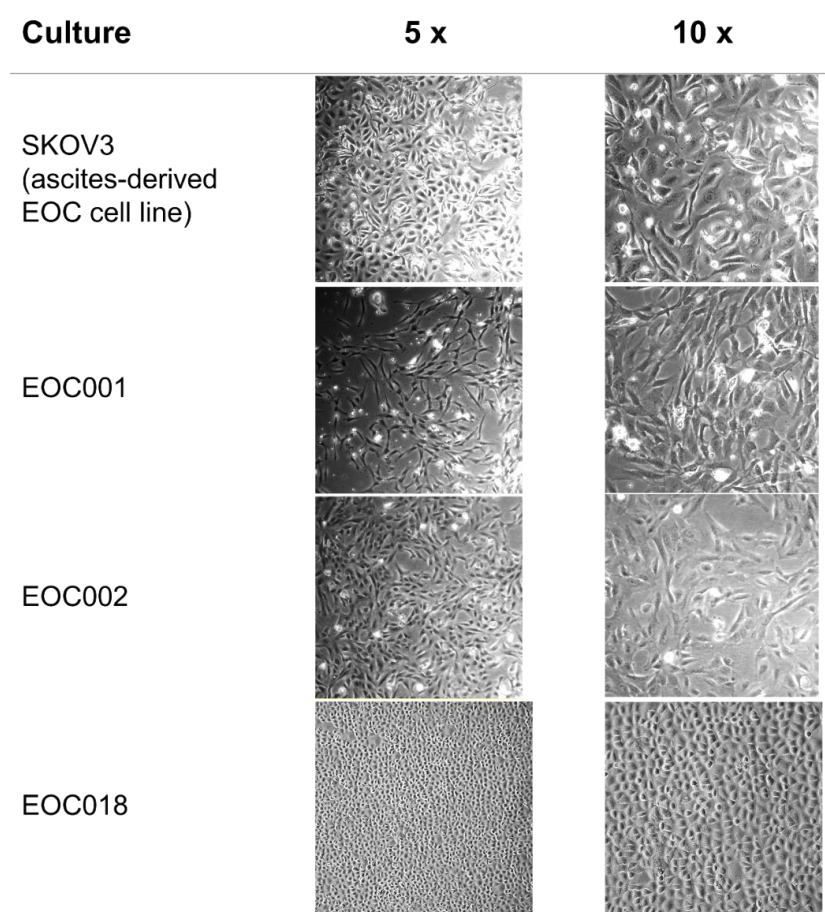


**Figure 3–5. Epithelial ovarian cancer (EOC) cell morphology.** A representative example of the typical 'cobblestone' morphology of EOC cells. Cells were imaged at 5 x and 10 x magnification. SKOV3 cell line is a positive control EOC cell line that was originally derived from ovarian ascites.

### 3.2.2 Phenotyping of epithelial ovarian cancer (EOC) cultures

*Ex vivo* EOC cultures were established from freshly-isolated ovarian ascites, generally within a month of paracentesis. After sufficient propagation, the cells were stained for five different cell surface markers and assessed for their receptor expression profile at passage 1–2 by flow cytometry (Table 3–3).

**Table 3–3. Receptor expression profile of epithelial ovarian cancer (EOC) cells.** Cultures were classified according to their chemotherapy stage: 1, chemo naïve/pre-treatment; 2, first-line chemo; 3, relapsed disease/platinum-sensitive; 4, relapsed disease/platinum-resistant. Only samples for which successful EOC cultures were established, are included in this table. CAR, coxsackie and adenovirus receptor; EGFR, epidermal growth factor receptor. αvβ6-positive cultures highlighted in purple; nd, not determined.

| EOC # | Stage | αvβ6 | CAR | CD44 | CD46 | EGFR |
|-------|-------|------|-----|------|------|------|
| 001 | 2 | 0 | 98 | 98 | 96 | 78 |
| 002 | 3 | 0 | 70 | 99 | 100 | 99 |
| 003 | 4 | 19 | 34 | nd | 100 | nd |
| 004 | 1 | 94 | 30 | 93 | 100 | nd |
| 006 | nd | nd | 89 | 92 | 99 | 98 |
| 008 | 3 | nd | 81 | 87 | 88 | 87 |
| 009 | 1 | nd | 99 | 99 | 99 | 99 |
| 011 | 4 | 0 | 46 | 99 | 99 | 99 |
| 013 | 4 | 0 | 90 | 93 | 100 | 98 |
| 014 | 2 | 0 | 100 | 100 | 100 | 100 |
| 016 | 4 | 40 | 50 | 98 | 100 | 95 |
| 018 | nd | 0 | 38 | 91 | 98 | 98 |
| 019 | 3 | 46 | 65 | 68 | 100 | 96 |

Four out of fourteen EOC cultures (31 %) were shown to be positive for αvβ6 integrin, with expression ranging between 19 and 94 % (Figure 3–6). These cultures were selected to be assessed for transduction efficiency by αvβ6-targeted vectors. Expectedly, the EOC cells were found to express greatly variable levels of CAR (range 0–100 %). However, CAR expression levels did not seem to be dependent on the chemotherapy treatment stage. The level of CD44 expression was very high in all EOC cultures (range 68–100 %). Similarly, all EOC cultures exhibited very high levels of CD46 (range 88–100 %) and EGFR expression (range 78–100 %). Four EOC cultures were positive for both αvβ6 and CD46, while CAR expression in these cells was variable (Figure 3–6) but relatively lower than in the cultures that did not express αvβ6 integrin.
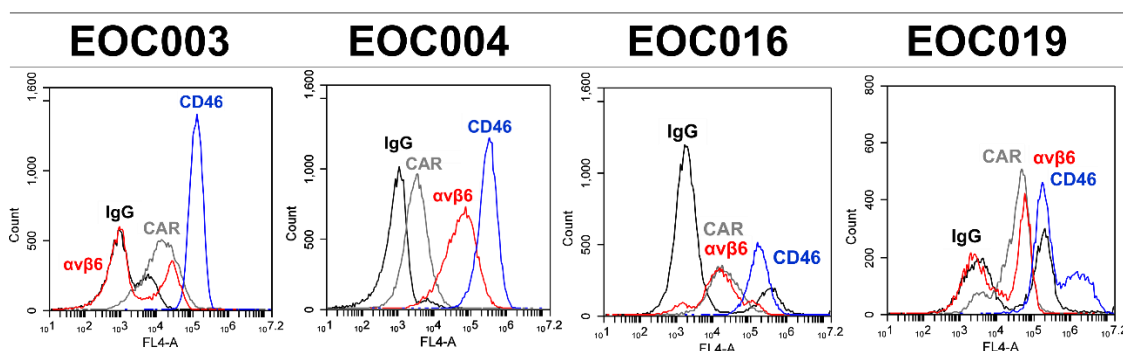


**Figure 3–6. Epithelial ovarian cancer (EOC) cultures positive for αvβ6 integrin.** EOC cultures were stained with primary anti-αvβ6, -CAR and -CD46 antibodies for 1 h on ice, and a secondary AlexaFluor647 antibody for 30 min on ice. 10 000 events were analysed on BD Accuri C6 flow cytometer and data analysed in BD Accuri software.

### 3.2.3 Quantification of coagulation factor 10 (FX) concentration in ascites

The concentration of FX present in cell-free ovarian ascites was evaluated using an in-house developed sandwich ELISA protocol. Sheep anti-FX capture antibodies were bound on a high binding ELISA plate and soluble FX present in ascites was allowed to bind to the capture antibodies. Secondary rabbit anti-human FX antibodies were then bound and complexes detected with a goat anti-rabbit IgG-HRP conjugate antibody. Purified human FX was used for generation of a standard curve, from which the FX concentrations in ascites were extrapolated. Sixty-three per cent of ascites (n = 12) samples had lower, and 37 % of samples (n = 7) higher levels of FX than sera on average (8–10 μg/mL) (

Table 3–**4**). The exact FX concentration could not be determined from nine samples, because eight samples had too low and one had too high FX concentration that gave optical readings outside the detection limits of this assay.

**Table 3–4. Concentration of coagulation factor 10 (FX) in patient-derived ascites.** FX concentration was measured by sandwich ELISA on a 96-well plate from 100 μL of neat, 1:2 and 1:4 dilutions of cell-free ascites samples in duplicate. Polyclonal anti-FX antibody was used as a capture antibody, and bound FX was detected using a rabbit anti-human FX antibody and a secondary anti-rabbit IgG HRP-conjugate. Complexes were detected with TMB substrate and reaction stopped using 0.02 M $H_2SO_4$; absorbance was measured at λ450 nm. Sample values were extrapolated from a standard curve of purified human FX (0–10 μg/mL). +, above detection limit; –, below detection limit.

| OAS sample | FX (μg/mL) | Relative to serum |
|---|---|---|
| 000 | 5.7 | ↓ |
| 001 | – | ↓ |
| 002 | 3.8 | ↓ |
| 003 | 0.4 | ↓ |
| 004 | + | ↑ |
| 006 | 32.4 | ↑ |
| 007 | 142 | ↑ |
| 008 | – | ↓ |
| 009 | – | ↓ |
| 010 | 4.4 | ↓ |
| 011 | – | ↓ |
| 012 | – | ↓ |
| 013 | – | ↓ |
| 014 | – | ↓ |
| 015 | – | ↓ |
| 016 | 36.2 | ↑ |
| 017 | 88.3 | ↑ |
| 018 | 61.9 | ↑ |
| 019 | 76.6 | ↑ |

### 3.2.4 Quantification of anti-Ad antibodies in ascites

The level of anti-Ad5 and anti-Ad10 antibodies was quantified from 19 cell-free ovarian ascites samples and an anonymous control serum from an adult male volunteer by a direct ELISA assay (Figure 3–7). Unfortunately, sample OAS005 was unusable due to heavy bacterial contamination and had to be disposed of. For the quantification of anti-Ad antibodies present in ascites, heat-inactivated replication-

deficient Ad5.Luc or Ad10.Luc virus particles (generated in-house) were bound on highly absorbent 96-well plates, incubated with serial 2-fold dilutions of cell-free OAS and bound anti-Ad antibodies detected with anti-human IgG-HRP conjugate. The levels of anti-Ad5 Abs in OAS that were capable of binding to the heat-inactivated particles, were substantially higher than the levels of anti-Ad10 Abs in the same samples. Half (n = 9) of the OAS samples had higher and half (n = 10) had lower levels of anti-Ad5 antibodies than the control serum, judging from the 1:1600 dilution that gave ~ 50 % binding for the control serum (Figure 3–8A). Similarly, eight ascites samples had higher and 11 samples had lower levels of anti-Ad10 antibodies than the control serum at dilution 1:800 that gave 50 % of the maximum binding for the control serum (Figure 3–8B). Sample OAS008 contained the highest concentration of anti-Ad5 antibodies (Figure 3–8A), while sample OAS019 had the most anti-Ad10 antibodies of all samples (Figure 3–8B). OAS001 had very similar levels of both anti-Ad5 and anti-Ad10 antibodies as the control serum, and was therefore chosen to be used in the subsequent *in vitro* and *ex vivo* vector neutralisation assays.
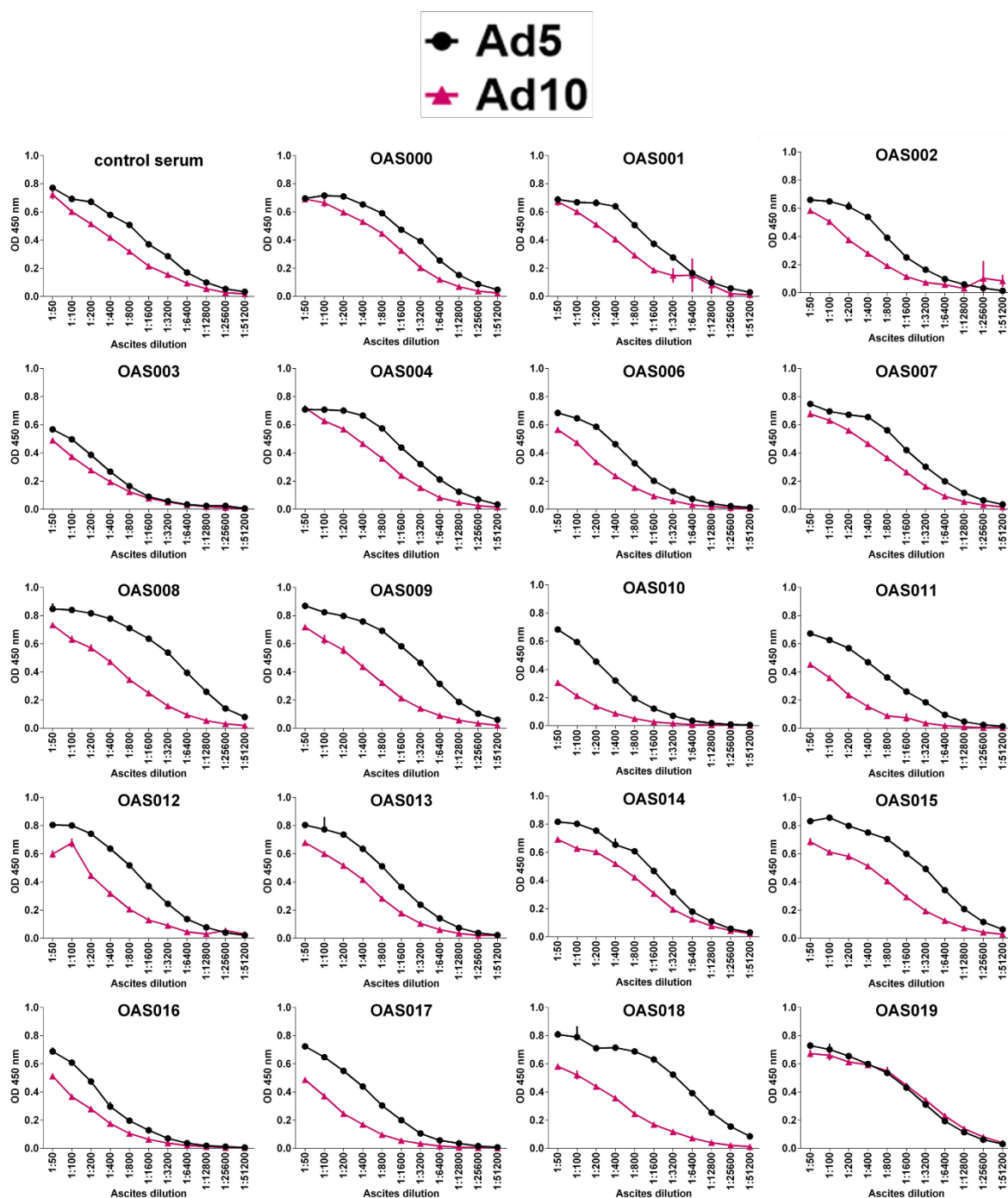
**Figure 3–7. Anti-adenovirus 5 (Ad5) and anti-Ad10 antibodies in ovarian ascites.** Maxisorp 96-well plates were coated with heat-inactivated adenoviruses in carbonate/bicarbonate buffer overnight at 4ºC. Cell-free ascites was added for 2 h and a secondary anti-human IgG-HRP conjugate incubated for 1 h at room temperature. Bound antibodies were detected in a colorimetric reaction using TMB substrate for 20 min. Reaction was stopped using 0.02 M $H_2SO_4$ and absorbance (OD) measured at λ450 nm.
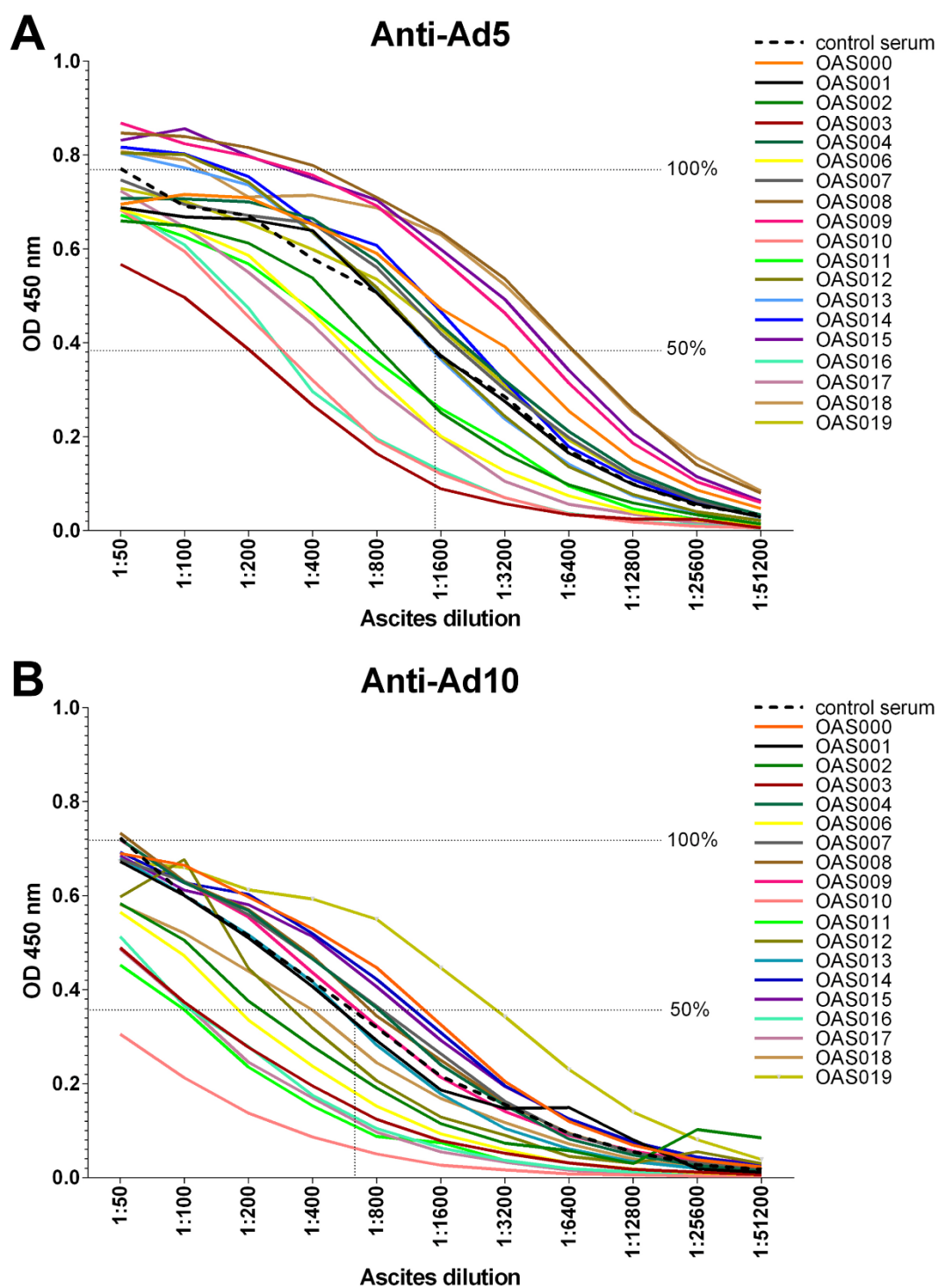
**Figure 3–8. An overview of (A) anti-adenovirus 5 (Ad5) and (B) anti-Ad10 antibodies detected from cell-free ovarian ascites.** 50 % and 100 % of the maximum binding is shown for the control serum as dotted lines. OAS, ovarian ascites; OD, optical density was quantified at λ450 nm.

### 3.2.5  Antigen-specificity of anti-Ad antibodies

The serotype-specificity, cross-reactivity and neutralising potential of pre-existing anti-Ad antibodies present in ovarian ascites was further assessed by luciferase-based neutralisation assays and Western blots. Sample OAS001 was chosen to be used for these assays as it had the highest levels of anti-Ad5 antibodies of all the samples we had collected at the time (Figure 3–8A). OAS001 was shown to neutralise 91 % and 96 % of Ad5 transduction in CHO-CAR cells at a concentration of 2.5 % and 10 %, respectively, determined as reduced virus-induced luciferase expression in these cells (Figure 3–9A). Intriguingly, OAS001 did not show any neutralisation of the Ad10 vector transduction at a concentration of 2.5 %, and exhibited only a modest 27 % neutralisation at a concentration of 10 % (Figure 3–9B). Respectively, the OAS019 fluid was chosen as a representative sample for studying neutralisation of the Ad10 serotype, due to its high level of anti-Ad10 antibodies observed in ELISA (Figure 3–8B). While OAS019 was capable of neutralising 79 % and 93 % of Ad5 transduction at concentrations of 2.5 % and 10 %, respectively (Figure 3–9A), it neutralised only 23 % of Ad10 vector transduction at a concentration of 10 % but had no neutralising effect at the lower 2.5 % ascites concentration in these cells (Figure 3–9B).

We then proceeded to assess the ability of anti-Ad antibodies present in the control serum and OAS001 to recognise the structural components of denatured Ad5 and Ad10 virions by Western blot. Heat-inactivated, whole virions of Ad5 and Ad10 serotypes and the fiber-pseudotyped Ad5/kn10 vector (all generated in-house, see chapter 5) were run in an SDS-PAGE gel and blotted onto a nitrocellulose membrane. The membranes were then incubated with the OAS001 fluid, and bound anti-Ad antibodies detected by using an anti-human IgG-HRP conjugate. The Ad5 vector seemed to capture antibodies with two types of specificities from the control serum, seen as two very strong and distinct bands (Figure 3–9C). The larger of these bands was approximately the size of the fiber protein (~ 60 kDa), while the smaller band was approximately 23 kDa in size (Figure 3–9C). On the contrary, the Ad10 vector seemed to capture only negligible quantities of antibodies by this method, showing the strongest band of ~ 40 kDa for the fiber protein, and two fainter ones at ~ 60 kDa and ~ 23 kDa (Figure 3–9C). However, the pseudotyped Ad5/kn10 was again able to detect fiber-specific antibodies from serum, albeit at lower levels compared to Ad5 (Figure 3–9C). When the experiment was repeated using OAS001 fluid, same banding pattern was observed but the bands were seemingly fainter (Figure 3–9D). Both serum and OAS001 contained antibodies that recognised the most abundant

capsid protein, hexon (Figure 3–9C, D). Surprisingly, the band was considerably weaker than the band for anti-fiber antibodies. Other antibodies present in serum and ascites may be directed against proteins VI and VII or other small capsid proteins.
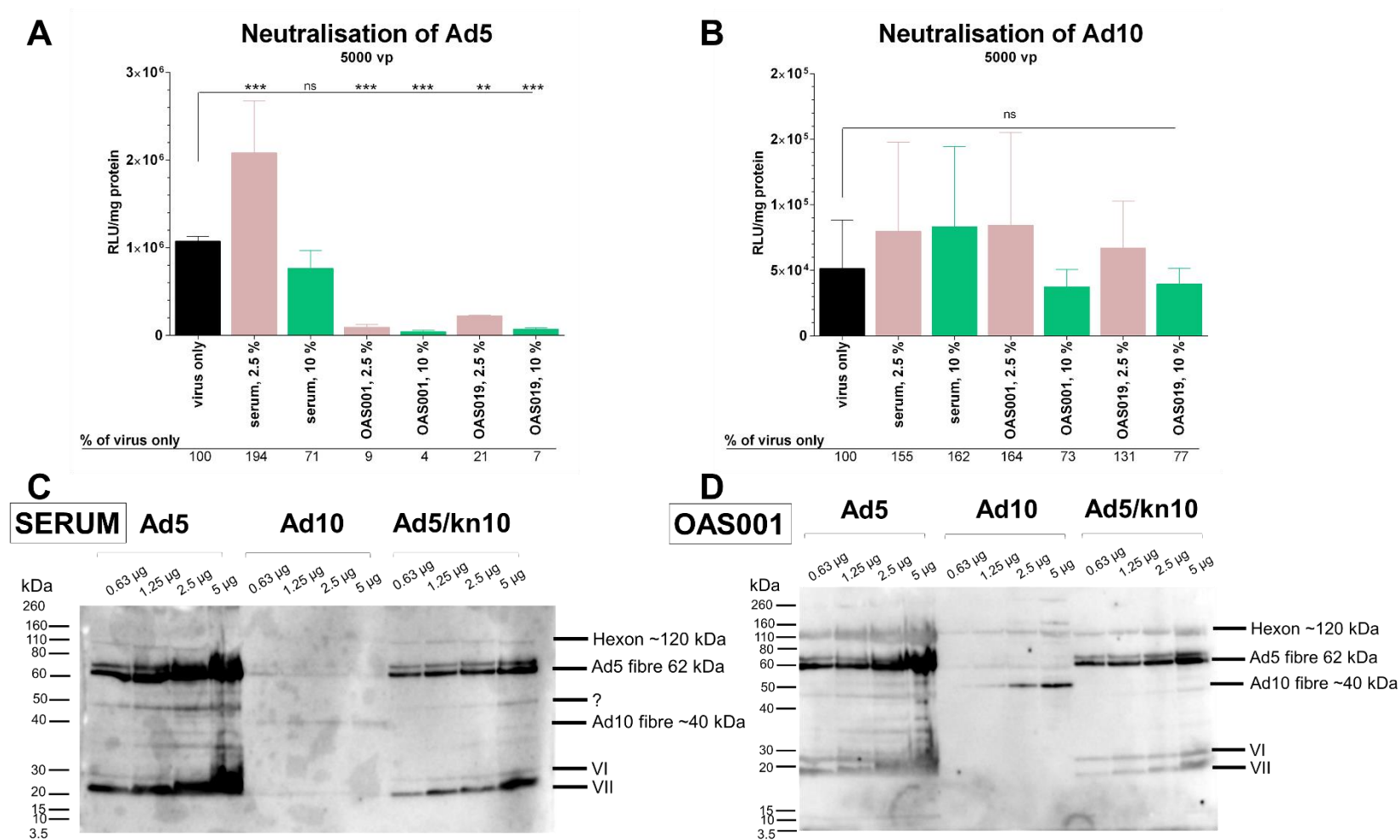
**Figure 3–9. Adenovirus 5 (Ad5)- and Ad10-specific antibodies in serum and ovarian ascites.** (A) Transduction efficiency of Ad5 and (B) Ad10 was measured by infecting CHO-CAR cells with 5000 particles/cell in the presence of control serum or ascites for 3 h and by quantifying luciferase expression 48 h later. For Western blots, viruses were heat-inactivated at 56ºC for 30 min and run at 0.63, 1.25, 2.5 and 5 µg of protein / lane (1 µg of protein corresponding to $4 \times 10^9$ vp) on a 10 % Bis-Tris SDS-PAGE gel at 150 V for 1 h 15 min. Proteins were transferred onto a nitrocellulose membrane in a semi-dry blotter and blocked in 5 % milk in TBS-T overnight at 4ºC. Membranes were incubated in a 1:500 dilution of (B) serum from an adult volunteer or (C) OAS001 ascites for 2 h and in anti-human IgG-HRP conjugate (1:2000) at room temperature for 1 h. Bound antibodies were then detected with SuperSignal West Pico chemiluminescent substrate.

## 3.3 Discussion

In this chapter, several model cancer cell lines were validated in *in vitro* assays for subsequent assessment of the generated recombinant Ad vectors. We identified a breast cancer cell line BT-20 as an excellent positive control cell line for the study of $\alpha v\beta 6$ integrin-mediated vector transduction, due to its very low level of CAR and very high level of $\alpha v\beta 6$ expression. Chinese hamster ovarian cell lines CHO-CAR and CHO-BC1 were selected as model cell lines for studying the CAR- and CD46-tropism of Ad vectors, respectively. These cell lines provide an excellent model for the unambiguous assessment of CAR and CD46 receptor tropisms, since they are devoid of the majority of common cell surface receptors that could contribute to cell transduction. CHO-K1 ($CAR^-/CD46^-$) and CHO-CAR ($CAR^+/CD46^-$) cells were used for the *in vitro* assessment of the receptor tropism of vectors de-targeted from the native tropisms (described in chapter 4), CHO-CAR and CHO-BC1 cells were utilised for the *in vitro* assessment of different Ad serotypes and novel fiber-pseudotyped vector backbones from subgroup D (described in chapter 5).

The ascites-derived and frequently utilised model cancer cell line – SKOV3 – was used as a representative EOC cell line in this project that is mainly focused on ovarian cancer. However, as SKOV3 cells were shown to be naturally devoid of $\alpha v\beta 6$ integrin expression (Figure 3–1), a model cell line SKOV3-$\beta 6$ was generated to represent an $\alpha v\beta 6$-positive EOC for our purposes (Figure 3–3). Parental SKOV3 cells were transfected with a retrovirus vector pBabe puro $\beta 6$ for stable expression of the $\beta 6$ integrin subunit that combines in cells with $\alpha v$ subunit, forming the $\alpha v\beta 6$ integrin receptor on the cell surface. FACS yielded a representative cell population of highly $\alpha v\beta 6$-positive cells that were propagated under strict puromycin selection, and used for *in vitro* assessment of $\alpha v\beta 6$-targeted vectors (described in chapter 6).

The second major part of this chapter describes the establishment of primary EOC *ex vivo* cultures from clinical ovarian ascites samples. Twenty samples were received over a period of two years in 2014–2016 from female volunteers who at the time were undergoing chemotherapy treatment for advanced ovarian cancer at Velindre Cancer Centre in Cardiff. The samples were obtained as a side product of a routine paracentesis of i.p. ovarian ascites – valuable clinical material that would otherwise have gone to waste. Successfully proliferating EOC *ex vivo* cultures were established from 65 % (13/20) of all ascites samples. A third of these cultures were shown to be positive for $\alpha v\beta 6$ integrin expression, while the expression of the CSC marker CD44, Ad receptor CD46 and general cancer cell marker EGFR was ubiquitously high across all cultures. The level of CAR expression was highly variable, which reflects previous

observations of the unpredictable expression profile of this receptor in progressive cancers (Matsumoto et al., 2005, Wunder et al., 2012, Reeh et al., 2013). No connection between the chemotherapy treatment stage and the expression profile of specific receptors was observed in this thesis. EMT frequently occurs in advanced EOC; mesothelin and hyaluronic acid secreted by mesothelial cells enable EOC cell invasion into the peritoneum, facilitated by CD44, β-integrins and CA125 expressed on EOC cell surface [reviewed in (Kipps et al., 2013)].

Malignant ovarian ascites has extremely variable combinations of distinct cell types, such as lymphocytes, mesothelial cells, MΦ, adenocarcinoma cells, epithelial cells, fibroblasts and erythrocytes; high erythrocyte counts are sometimes observed if ascites has developed rapidly (reviewed in (Kipps et al., 2013)). Numerous detailed reports have described EOC cell culture from malignant ovarian ascites (Dunfield et al., 2002, Shepherd et al., 2007, Latifi et al., 2012, Ahmed and Stenvers, 2013, Thériault et al., 2013). O'Donnell and colleagues reported a 91 % success rate for the establishment of EOC cultures from 172 ovarian ascites samples from patients undergoing surgery (O'Donnell et al., 2014). Senescence commonly occurred between passage 2–8, which is also in line with the observations in this thesis. In their study, the epithelial origin of cultured cells was verified by utilising a panel of markers including EpCAM, vimentin, pancytokeratin, CA125, MOC-31 and D2-40. However, the authors state that none of these are represented in all EOC cells, which is why the epithelial cell origin had to be determined from the presence of several different markers. In this present thesis, we did consider enrichment of EOC *ex vivo* cultures by magnetic separation using commercially available magnetic EpCAM (CD326) microbeads. However, this was not attempted as the initial cell numbers were already so low that the risk of remarkable cell loss was considered to be greater than the potential benefit.

Ovarian ascites is known to be rich in various proteins that are also found in serum (Hemminki et al., 2002). We quantified the concentration of FX in ascites by performing FX-specific sandwich ELISA assays that were developed in-house. Concentration of FX was shown to vary greatly across the samples; in the majority the FX concentration being lower than the average concentration in serum (Table 3–4 ). On the contrary, several ascites samples had higher – up to 18-fold higher for OAS007 – concentration of FX relative to serum. Sample OAS004 contained even more FX than that; its exact concentration however could not be measured due to the upper detection limit of the assay. It is well known in Ad vectorology that the presence of FX impacts the biodistribution of Ad5 vectors (Alba et al., 2009), and may

additionally shield the vector from natural IgM and complement attack (Xu et al., 2013). It is therefore important to consider that the presence of FX in ascites has important implications when local i.p. delivery of Ad vectors into the peritoneal cavity is the desired route. A complete ablation of FX-binding mediated by anti-cancer Ad vectors (discussed in section 4.6) is an excellent solution for tackling the large concentration range of FX present in ascites.

Like serum, malignant ovarian ascites contains high levels of anti-Ad antibodies (Hemminki et al., 2002) that can rapidly coat and neutralise the vector, rendering therapies ineffective. Therefore, we assessed the level of anti-Ad IgG antibodies present in ascites by performing direct ELISA assays, in order to establish a good overview of the range of antibody responses in clinical samples. The level of antibodies that recognised the Ad5 virion was generally very high in all samples – similar or even higher than in the control serum obtained from a healthy male adult volunteer (Figure 3–8). The level of anti-Ad10 antibodies was lower than for anti-Ad5 Abs across all ascites samples, with the exception of one sample (OAS019) that had very similar levels of both anti-Ad5 and anti-Ad10 Abs (Figure 3–7). The ascites sample OAS001 that has high levels of anti-Ad5, and intermediate levels of Ad10-reactive antibodies, was selected as the representative example of a highly neutralising fluid for subsequent neutralisation assays for Ad5-based vectors. OAS019 was used as a highly neutralising fluid for assessment of Ad10-pseudotyped vectors.

Additionally, we sought to evaluate the antigen-specificity of the ascites-derived anti-Ad antibodies by Western blot by allowing antibody binding to heat-inactivated and denatured viral particles of Ad5 and Ad10. We found that antibodies both in our serum control and ascites were primarily directed against the Ad5 fiber (Figure 3–9). The control serum showed a very strong anti-Ad5 band that was the size of the fiber trimer (~ 62 kDa), and a fainter band for smaller, possibly capsid, proteins. The pattern was similar but considerably fainter for the OAS001 fluid. Very faint bands for anti-Ad10 antibodies were detected from both the control serum and OAS001; most of these antibodies seemed to be specific for the fiber (~ 40 kDa) and hexon (~ 120 kDa) proteins. We also evaluated the ability of the anti-Ad5 and anti-Ad10 antibodies to recognise the pseudotyped Ad5/kn10 vector. A substantial level of antibodies recognised these virions, although at slightly lower efficiency than the Ad5 virion. It was very surprising to find that the antibody levels against the hexon protein – the structurally most abundant component of the virion capsid – were very low in both samples. Furthermore, there does not seem to be notable cross-reactivity between

the two serotypes from distinct subgroups. The observations from our ELISA and Western blot assays indicates significant limitations of our detection methods. Although ELISA assays indicated high levels of anti-Ad10 antibodies in both serum and OAS001, the Ad10 virions did not recognise these antibodies in the Western blot analyses. This may well be due to the differences in the preparation of the antibody bait, ie. the virion. In ELISA assays the viruses were heat-inactivated and bound to plates as whole virions, while in the Western blots they were additionally denatured by boiling in lithium dodecyl sulphate buffer at 95ºC for 10 min. Disruption of the native conformation is therefore likely to have compromised the recognition of the individual capsid components, at least for the anti-Ad10 antibodies that may have an overall lower affinity to the antigens. It is also important to remember that while the ascites-derived antibodies were able to recognise Ad5 and Ad10 virions in the described *in vitro* assays, it does not implicate their potential to neutralise an infection *in vivo*.

Our observations are in line with the previous findings that native infection mainly elicits anti-fiber antibodies (Parker et al., 2009), while vaccine challenge leads to elicitation of anti-hexon antibodies (Sumida et al., 2005). The ascites donors in this study are not likely to have been treated with Ad-based vaccines, which could explain their low levels of anti-hexon antibodies. Binding of the fiber protein to its native receptor CAR has been suggested to enable viral spread by opening of tight junctions at the cellular interfaces (Walters et al., 2002). Ads are therefore thought to produce and shed excessive amounts of fiber proteins in the initial stages of infection, by means of enhancing epithelial permeability and viral spread, and facilitating basolateral-to-apical trafficking and viral escape from the apical surface. This could well explain the dominance of anti-fiber antibodies over anti-hexon antibodies in natural infections. Although the hexon is the largest and structurally most abundant component of the Ad virion capsid, excessive quantities of the fiber protein may be exposed to the innate immune system in the early stages of an acute Ad infection, steering the antibody production towards the fiber rather than the hexon protein. Interestingly, pseudotyping Ad5 with a knob domain from Ad10 restored recognition of anti-Ad5 antibodies both in serum and ascites. This may therefore indicate that these antibodies are primarily directed towards the fiber shaft rather than the immunodominant knob domain. Further studies are needed to dissect the intriguing nature of antibodies directed against Ad proteins, and their potential to cross-neutralise serotypes from other subgroups.

In this chapter we have established that malignant ovarian ascites has a complex composition that is very likely to influence the efficiency of anti-cancer treatments that

are based on the globally prevalent Ad serotype vector, Ad5. Phenotyping of a panel of suitable ovarian cancer cell lines, malignant ovarian ascites and ascites-derived EOC *ex vivo* cultures is important for the establishment of suitable model systems for subsequent in vitro and *ex vivo* assessment of Ad vectors. These evaluations are described in detail in the following chapters of this thesis.

# CHAPTER 4. Results: *In vitro* assessment of de-targeted vectors and production of recombinant proteins

# CHAPTER 4. In vitro assessment of de-targeted vectors and production of recombinant proteins

This chapter discusses the generation of basal Ad5 vector backbones for subsequent modification for cancer targeting purposes. We have incorporated combinations of point mutations in the three major capsid proteins – fiber, hexon and penton. These sophisticated modifications successfully ablated all three central native tropisms of the Ad5 serotype, namely binding to CAR, FX and $\alpha v\beta 3/5$ integrins. Vectors were rescued from BAC DNA and produced into high viral titres in permissive cell lines that express adenoviral genes and relevant cell surface receptors. *In vitro* assays that are commonly used in Ad vectorology, were utilised for the assessment of the altered tropism of these vectors. Additionally, the transduction efficiency was assessed in the presence of inhibitory factors and purified human FX. Recombinant 6 x His-tagged knob proteins of serotypes Ad5 and Ad48 were produced in *E.coli* and used in competition inhibition assays for the evaluation of vector tropisms.

## 4.1 Generated vectors

A panel of recombinant vectors with a series of versatile de-targeting mutations were generated by AdZ homologous recombineering methods. The method had been previously developed in our laboratory by Dr Richard Stanton as a rapid means to overexpress transgenes (Stanton et al., 2008), and required only minor adjustments to suit our purposes. Selection for successful recombineering products and correct BAC clones was based on IPTG-induced blue/white selection in heat-inducible *E. coli* strain SW102. Colonies generally appeared 48−72 h after incubation at 32ºC. Blue (first step) and white (second step) colonies (Figure 4–1A) were picked from the agar plates and inoculated into LB medium with Kan and LB medium with Strep to verify that each colony was resistance to one and sensitive to the other (Figure 4–1B). The colonies that fulfilled these criteria, were grown into larger cultures and the bacterial DNA was extracted by a miniprep method. The mutated sequence was amplified by PCR and sequenced to verify the correct insertion. Viral BACs were then amplified and purified from maxiprep DNA cultures. T-REx-293 cells were transfected with 1 µg of each of the viral BAC DNAs, and viruses rescued from the cells ~ 10 days later when CPE was observed. CsCl gradient purification of the viruses was generally successful and yielded good viral titres. There were, however, big differences in the quality of the preparations, as well as the appearance and thickness of the mature virion bands. The mature virus particles formed a clearly visible grey band in the lower section of the gradient (Figure 4–1C). This was extracted in a maximum volume of 1 mL using a 19-gauge needle. The virus preparation was dialysed O/N at 4ºC,

aliquoted out, and titered by microBCA assay for the physical viral titre (vp/mL) or by plaque assay for the infectious viral titre (pfu/mL).
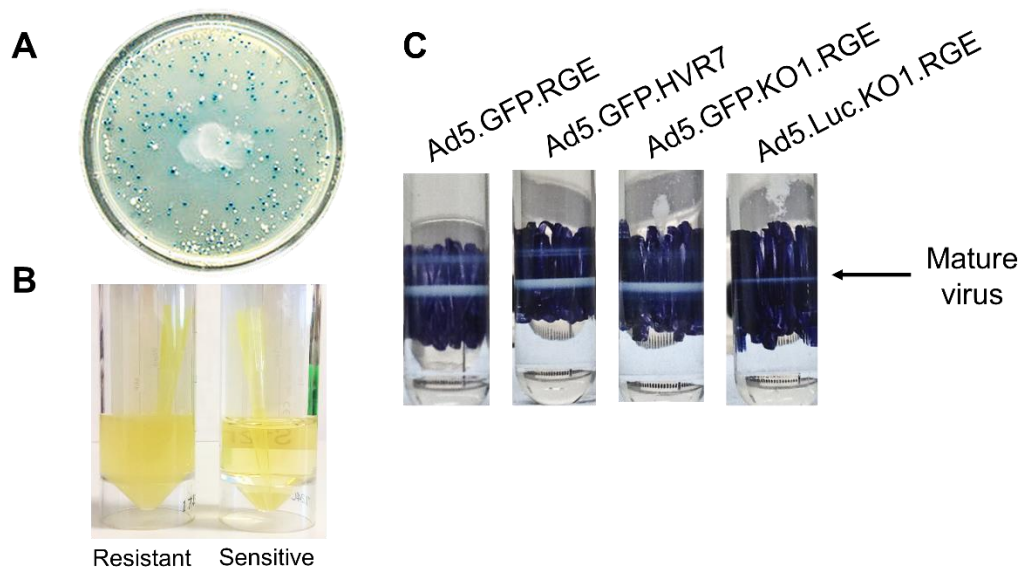


**Figure 4–1. AdZ recombineering and virus purification.** (A) Blue-white screening on agar plates, (B) verification of antibiotic resistance (left) and sensitivity (right), (C) virus banding pattern after the second step of CsCl gradient ultracentrifugation.

The generated de-targeted vectors carry mutations that ablate their native interactions with CAR (KO1 mutation), penton base (RGE mutation) and FX (HVR7 mutation). Fourteen basal replication-deficient vector backbones were generated by AdZ recombineering, 10 of which were rescued as functional virions and grown into high viral titres in T-REx-293 cells (Table 4–1). The viruses with combinations of two (KO1 and HVR7) or three mutations (Ad5.3D) did not form infectious virions, despite numerous transfection attempts. The infectivity of vectors containing the KO1-mutation was facilitated by the addition of FX in the transfection medium; obviously, this was not feasible for the vectors with HVR7 mutation that are not capable of utilising FX for cell entry. This was likely a result of severely compromised fitness due to the lack of available entry receptor for these vectors. The de-targeted vectors were subsequently assessed on a panel of cancer cell lines to evaluate their transduction efficiency via native target receptors and entry pathways. Luciferase-expressing vectors were generated to be used in transduction assays in conjunction with a luciferase reporter gene assay kit, which was the main method of *in vitro* assessment of these vectors in this thesis. GFP-expressing versions of the vectors were generated for potential utilisation for cellular trafficking experiments, flow cytometry or immunofluorescent analysis.

**Table 4–1. Basal and de-targeted replication-deficient Ad5 vectors.** Viral genomes were generated by AdZ homologous recombineering methods, viruses were rescued in T-REx-293 cells, purified by two-step CsCl-purification and tittered by microBCA assay. CAR, coxsackie and adenovirus receptor; FX, coagulation factor 10; GFP, green fluorescent protein; HVR7, FX-binding mutation; KO1, CAR-binding mutation; Luc, luciferase; RGE, integrin-binding mutation; vp, viral particle. *, only genome was generated but no infectious virus was rescued.

| Virus | CAR binding | FX interaction | Physical titre (vp/mL) |
|---|---|---|---|
| Ad5.Luc | + | + | $3.9 \times 10^{12}$ |
| Ad5.GFP | + | + | $1.0 \times 10^{12}$ |
| Ad5.Luc.KO1 | − | + | $1.6 \times 10^{12}$ |
| Ad5.GFP.KO1 | − | + | $7.6 \times 10^{12}$ |
| Ad5.Luc.RGE | + | + | $2.3 \times 10^{12}$ |
| Ad5.GFP.RGE | + | + | $4.6 \times 10^{12}$ |
| Ad5.Luc.HVR7 | + | − | $4.3 \times 10^{12}$ |
| Ad5.GFP.HVR7 | + | − | $4.3 \times 10^{12}$ |
| Ad5.Luc.KO1.RGE | − | + | $2.9 \times 10^{11}$ |
| Ad5.GFP.KO1.RGE | − | + | $3.7 \times 10^{12}$ |
| Ad5.Luc.KO1.HVR7 | − | − | * |
| Ad5.GFP.KO1.HVR7 | − | − | * |
| Ad5.Luc.KO1.RGE.HVR7 ('Ad5.3D') | − | − | * |
| Ad5.GFP.KO1.RGE.HVR7 ('Ad5.3D') | − | − | * |

## 4.2 Transfection efficiency in T-REx-293 cells

The transfection efficiency of the Effectene transfection reagent was assessed in T-REx-293 cells that were used for the production and propagation of all Ad5 vectors in this thesis, except for the αvβ6-targeted vectors that were produced in HEK293-β6 cells. Cells were transfected with 1 µL of pmaxGFP control plasmid according to the Effectene transfection protocol. Cells were then detached from the growth flasks by trypsin treatment 48 h later, washed in 5 % FBS in PBS and fixed in 4 % PFA for 10 min. Of the transfected cells, ~ 45 % were shown to express GFP (Figure 4–2), which translates to transfection efficiency of approximately half of the treated cells.
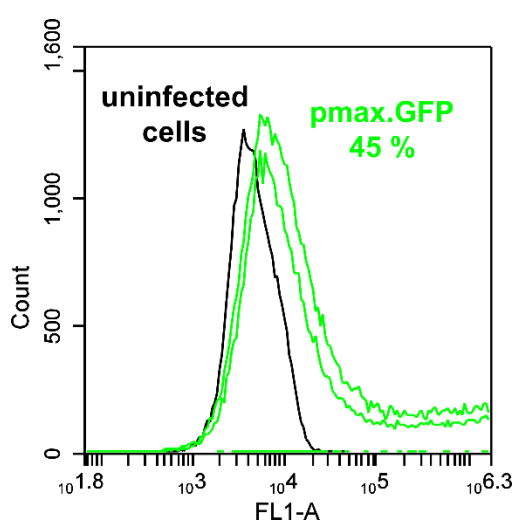


**Figure 4–2. Transfection efficiency of T-Rex-293 cells by Effectene reagent.** T-Rex-293 cells were infected with a green fluorescent protein (GFP)-expressing pmaxGFP control plasmid for 48 h in triplicate. Cells were then washed and fixed in 4 % paraformaldehyde, and 200 000 cells run in BD Accuri flow cytometer. Uninfected T-REx-293 cells (black curve) were used as a negative control for the assay.

## 4.3 Haemagglutination assays

The ability of de-targeted viruses to agglutinate human erythrocytes was evaluated in standard haemagglutination assays. Ad5 binds to CAR on the surface of erythrocytes (Carlisle et al., 2009), which results in the formation of a characteristic red blood cell network on the surface of the well. In the absence of agglutination, the erythrocytes sediment to the bottom of the well, forming a tight erythrocyte cell pellet. In these assays, Ad5.Luc vector successfully agglutinated erythrocytes at all four concentrations tested (Figure 4–3, row 1), while the CAR-binding mutation KO1 completely ablated Ad5 vector binding to erythrocytes at all doses (Figure 4–3, rows 2 and 5). The integrin-binding mutation RGE (Figure 4–3, row 3) and the FX-binding mutation HVR7 (Figure 4–3, row 4) had no visible effect on the haemagglutination properties of these de-targeted Ad5 viruses. The haemagglutination patterns seen in this assay confirm that the CAR-binding mutation KO1 efficiently abolishes the ability of Ad5 to bind to its native receptor CAR. The same effect was seen for all viruses that have the KO1 mutation alone or in combination with other de-targeting mutations.
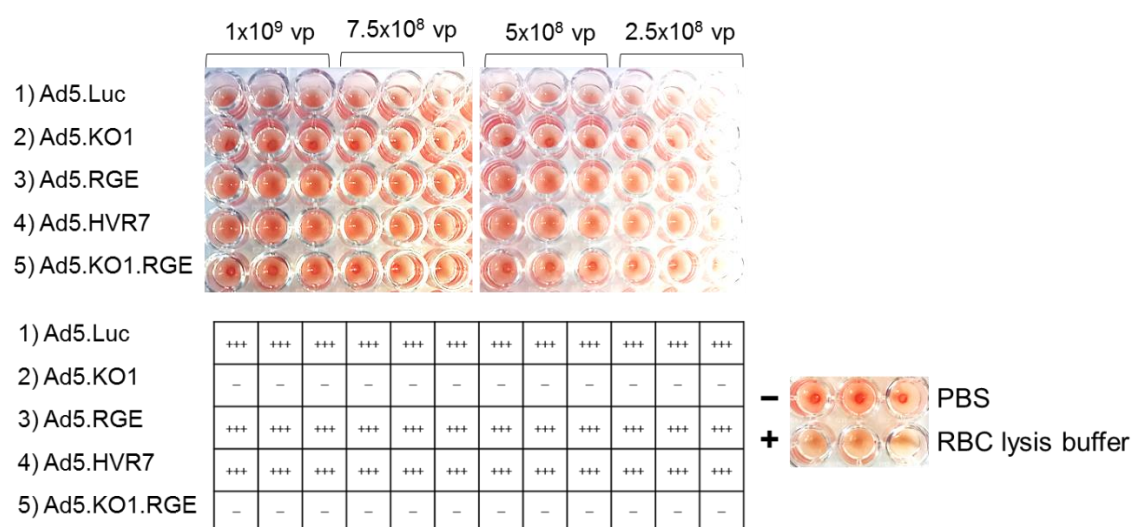


**Figure 4–3. Agglutination of human erythrocytes.** 1 % erythrocyte suspension in PBS was mixed with descending concentrations of viral stocks in PBS and incubated at 37ºC for 2 h. PBS was used as a negative control and red blood cell lysis (RBC) buffer as a positive control for haemagglutination. –, no; +, low; ++, partial; +++, complete agglutination of erythrocytes. HVR7, coagulation factor 10 binding mutation; KO1, coxsackie and adenovirus binding mutation; RGE, αvβ3/5 integrin-binding mutation; vp, viral particle.

## 4.4 Recombinant protein production & purification

The purified and tittered basal, replication-deficient vectors were assessed for their binding and entry via CAR in luciferase transduction assays. Recombinant knob proteins were produced as described below, and used as blocking agents in competition inhibition assays. Protein expression pQE30 plasmids, that already had the knob sequences cloned in, were transformed into SG13009 *E. coli* cells by a heat

shock method. Colonies were picked and pre-cultures grown O/N at 37ºC. Protein production was induced in the SG13009 bacteria by addition of IPTG for 16 h at 250 rpm in a shaking incubator at 20°C. Cell pellets were collected by high-speed centrifugation and lysed in lysozyme-containing buffer. A total volume of 50 mL of the lysate was bound to 0.5 mL of Ni-NTA agarose at 4ºC for 1 h, after which the agarose was loaded into a single-use plastic chromatography column and thoroughly rinsed with abundant wash buffer (5 x of the volume of the column = 100 mL).
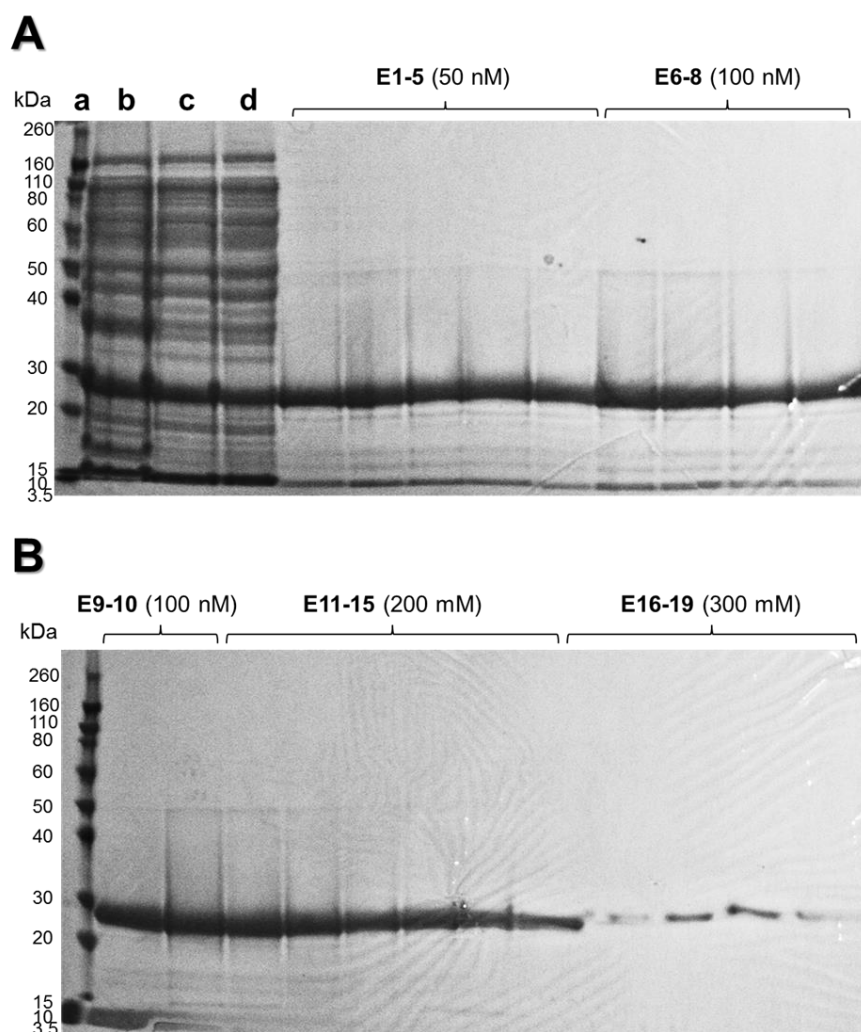
**Figure 4–4. Example of knob protein elution fractions (Ad48 knob protein).** Knob protein was eluted with increasing concentrations of imidazole. 14 µL of each elution fraction was mixed with 1 µL of DTT and 5 µL loading buffer, boiled at 95ºC for 10 min and run on a 10 % SDS-PAGE gel for 1 h 15 min at 150 V. The gel was stained with Coomassie for 30 min and de-stained overnight. (A) Elution fractions E1–8 (a) Novex pre-stained protein marker, (b) lysed cells, (c) cleared lysate, (d) supernatant after Ni-NTA binding.

Recombinant proteins that were bound to the Ni-NTA agarose, were eluted as 1 mL fractions and collected by hand. Individual fractions were analysed on a SDS-PAGE gel to determine which fractions had the highest concentration of the purified protein with minimal impurities. The purest fractions were pooled (~ 10 mL total

volume) and the protein concentration determined by a standard BCA assay. All proteins were produced into high concentration, with the exception of CAR-ablated Ad5 knob that had a ~ 5-fold lower concentration compared to other knob proteins (Figure 4–5A). Both native and denatured (boiled at 95ºC for 10 min) aliquots of each produced protein were analysed on a SDS-PAGE gel to assess their ability to trimerise. All produced knob proteins were shown to form a structurally intact trimer, which was seen as a native trimeric (~ 63–65 kDa) for the un-boiled and as a denatured monomeric form (~ 30–35 kDa) for the boiled protein (Figure 4–5B). The differences in band strength are likely to reflect variation in protein titration by BCA, rather than the abundance of the protein.

**A**

| Protein | Concentration (mg/mL) |
|---------|------------------------|
| kn5.wt | 1.1 |
| kn5.477YT.wt | 0.9 |
| kn5.477YT.A20 | 0.2 |
| kn48.wt | 1.3 |
| kn48.DG.A20 | 1.0 |
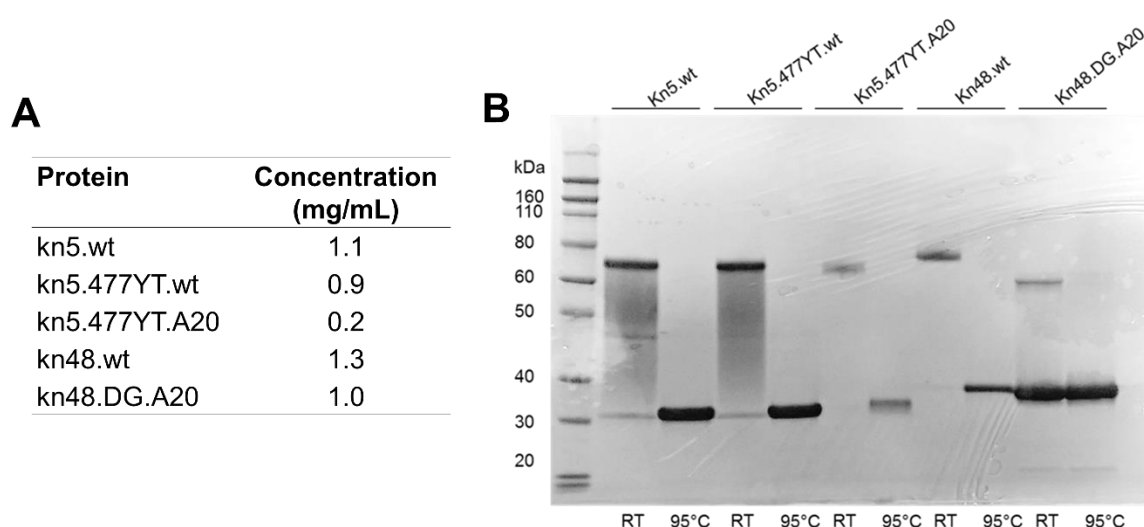


**Figure 4–5. Recombinant 6 x His-tagged knob proteins.** (A) Concentrations of the produced knob proteins. (B) Trimerisation assay. 14 µL of dialysed protein was mixed with 1 µL of DTT and 5 µL of 4 x SDS loading dye and incubated at room temperature (RT) or boiled at 95°C for 10 min. Samples were run on a pre-made Novex gel for 1 h 15 min at 100 V, the gel stained in Coomassie for 30 min and de-stained overnight. A20, αvβ6-targeting peptide; kn, knob; wt, wild type; 477YT, CAR-binding mutation.

## 4.5 Competition inhibition (luciferase) assays

Basal de-targeted vectors were assessed in luciferase transduction assays for their CAR-tropism in CHO-CAR (CAR$^{high}$) cells. The in-house produced recombinant knob proteins (described in section 4.2) were used as blocking agents to inhibit cell entry via CAR. Transduction of the CAR-utilising Ad5.Luc vector was efficiently blocked at all three doses of kn5 protein (10, 20 and 40 µg/$10^5$ cells) but not by the negative control kn5.477YT (kn5.CAR–) protein (Figure 4–6) in CHO-CAR cells. The CAR-binding ablated Ad5.KO1 vector was completely unable to enter these cells due to lack of available entry receptor, and therefore blocking with knob proteins expectedly had no effect on transduction efficiency (Figure 4–6). Successful inhibition of CAR-mediated entry of Ad5.Luc into CHO-CAR cells by the kn5 protein has also been

recently reported in our research publication (Uusi-Kerttula et al., 2016), and is therefore not discussed here in greater detail.
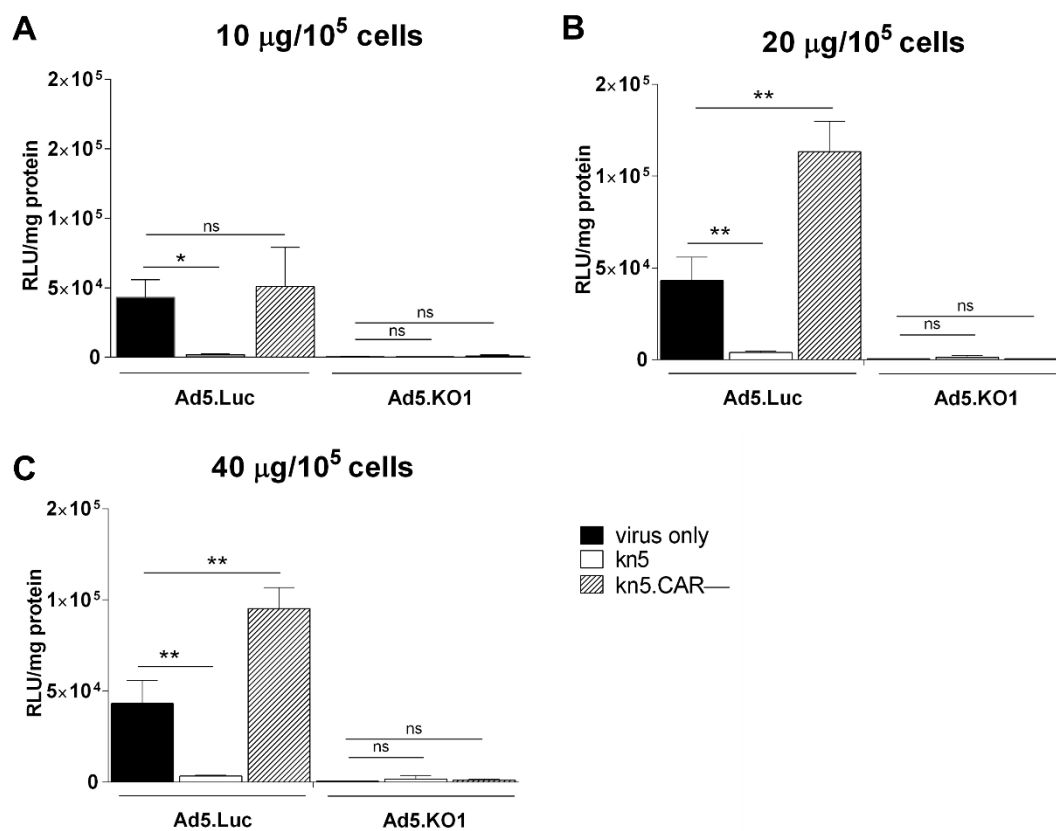


**Figure 4–6. Competition inhibition of Ad5 binding to coxsackie and adenovirus receptor (CAR).** CHO-CAR cells were pre-blocked with recombinant knob proteins Ad5 knob (kn5) or kn5 with CAR-binding ablation mutation (kn5.CAR–) at increasing concentrations of (A) 10, (B) 20 or (C) 40 μg/$10^5$ cells prior to addition of Ad5.Luc or Ad5.KO1 viruses at 5000 viral particles/cell in triplicate for 1 h on ice. Luciferase expression expressed as relative light units (RLU)/mg protein. Data were analysed using one-way ANOVA with Dunnett's multiple comparisons test. ns, $p > 0.05$; *, $p < 0.05$; **, $p < 0.01$.

## 4.6   The effect of FX on vector transduction efficiency

While the CAR-mediated pathway is known to dominate *in vitro* cell entry, FX 'bridging' pathway is the main entry route following systemic delivery of therapeutic Ad vectors. The effect of soluble FX on Ad transduction efficiency can be qualified by performing luciferase transduction assays in the presence of physical concentrations (10 μg/mL) of FX. The transduction-enhancing effect of FX can be neutralised by supplementing the medium with an anticoagulant found in snake venom, X-bp, that binds to FX and therefore prevents it from binding to Ad virions. To achieve as clean impact on the transduction efficiency as possible, assays were performed in CHO-K1 cells that do not express CAR or other known Ad receptors. Addition of FX in the transduction medium increased Ad5.Luc transduction in CHO-K1 cells by 135-fold as compared to FX-free conditions, while the addition of FX together with three-fold molar

excess of X-bp again completely abolished transduction in these cells, back down to the transduction levels that were seen in the absence of FX (Figure 4–7A). In contrast, the well-described hexon mutation HVR7 successfully ablated binding to FX, as transduction efficiency of Ad5.HVR7 remained low despite the supplementation of the transduction media with FX, and independent on the presence of the anticoagulant X-bp (Figure 4–7). The results demonstrate that Ad5 vector binding to FX can be efficiently abolished by introduction of the HVR7 mutations.
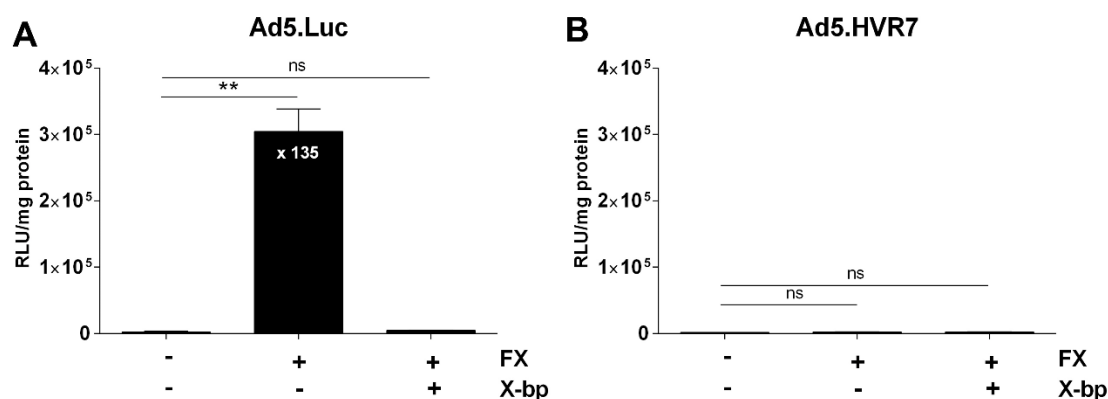


**Figure 4–7. The effect of coagulation factor X (FX) on vector transduction.** (A) Ad5.Luc and (B) Ad5.HVR7 viruses were added at 5000 viral particles/cell for 3 h in serum-free medium alone or in medium supplemented with 10 μg/mL of FX with or without an anticoagulant X-bp in CHO-K1 cells. Luciferase activity was measured at 48 h post-infection and normalised to relative light units (RLU)/mg protein. Data were analysed using one-way ANOVA with Dunnett's multiple comparisons test. ns, $p >$ 0.05; *, $p < 0.05$; **, $p < 0.01$. HVR7, five FX-binding mutations in hexon hypervariable region 7; Luc, luciferase.

## 4.7 Discussion

This chapter describes the design and generation of basal Ad5-based vector backbones for further development for cancer targeting and oncolytic purposes. De-targeted, replication-deficient Ad vectors were generated by AdZ homologous recombineering methods and propagated into high viral titres in permissive T-REx-293 cells that express the Ad *E1* and *E3* genes that are essential for viral replication. The de-targeted vectors were assessed in *in vitro* assays for their structural integrity, receptor usage and entry pathways. The main Ad entry pathways were successfully ablated by introduction of a series of well-described substitution/point mutations into the main capsid proteins fiber, hexon and penton. The luciferase-expressing vectors were comprehensively assessed in luciferase reporter gene assays by quantifying the amount of luciferase reporter gene expression in relative light units in a convenient 96-well plate format. All vectors described in this chapter were generated in replication-deficient background. However, oncolytic and cancer-targeted versions of

some of these vectors have already been generated for further *ex vivo* and *in vivo* assessment (see chapters 6 and 7).

The key interaction to be assessed was the knob-mediated binding of Ad5 to CAR – a receptor that is expressed in tight junctions on most polarised cell types (Coyne and Bergelson, 2005). The well-described 'KO1' mutation in the fiber knob AB loop (Smith et al., 2002) successfully abolished Ad5 binding and entry via the native Ad receptor, CAR. Successful ablation of binding interactions was comprehensively demonstrated in competition inhibition assays by using recombinant knob proteins as inhibitory agents prior to the addition of the viruses on the cells. Haemagglutination assay is an alternative method for studying the CAR interaction of Ad vectors. Human, but not murine, erythrocytes express CAR on the surface (Carlisle et al., 2009), which leads to Ad vector entrapment in the bloodstream and may change vector biodistribution (Seiradake et al., 2009). Although this has been proposed to limit vector bioavailability for its therapeutic target tissue, a recent study showed that Ad binding to erythrocytes is reversible in nature, and does not influence extravasation and organ transduction (Rojas et al., 2016). None of our CAR-binding ablated vectors were capable of agglutinating human erythrocytes, which again confirmed the functionality of the KO1 mutation. As expected, none of the other de-targeting mutations compromised the vector binding to CAR, since haemagglutination was as efficient as for the parental Ad5 vector. Due to the extensively ubiquitous expression of CAR across all nucleated tissues, including erythrocytes and platelets (Carlisle et al., 2009), the ablation of CAR-binding is vital for the prevention of non-specific transduction of non-cancer tissues. The KO1 mutation is therefore an essential de-targeting strategy in Ad vector design.

As observed by Smith and colleagues (Smith et al., 2002), KO1 mutation is insufficient for abolishing *in vivo* liver transduction that is mediated by FX, and occurs between the hexon HVRs and HSPGs. Therefore, the second central modification is the mutation of the HVRs that are responsible for hexon binding to FX. We successfully showed that the extensively characterised 'HVR7' mutation (Alba et al., 2009) – a combination of five point mutations (Figure 1–21) – fully hampered Ad5 entry into cells via FX *in vitro*. We used hamster ovarian CHO-K1 cells as the main representative cell line for studying FX-tropism in this thesis. In these fully CAR-deficient cells, FX provides a whole new cell entry pathway via HSPGs, which is also the main Ad entry pathway *in vivo* (Waddington et al., 2008, Alba et al., 2009). It is therefore an excellent, clean model system for studying the impact of FX on the vector transduction efficiency. The impact of the HVR7 mutation on the Ad5 vector tropism

was evaluated in luciferase transduction assays with physical concentrations of FX (10 μg/mL) supplemented in the assay medium. While the parental Ad5.Luc transduced CAR-negative CHO-K1 cells at ~ 140-fold improved efficiency in the presence of FX, the level of Ad5.HVR7 transduction in these cells was completely unchanged by the addition of FX in the transduction medium. The HVR7 is a combination of five mutations in the hexon, that has been fully validated in previous detailed studies by Alba and colleagues (Alba et al., 2009). The observations in this thesis show successful ablation of this key pathway for the generated recombinant vectors *in vitro*. Additionally, vector de-targeting from liver was evaluated in an *in vivo* biodistribution study following systemic delivery (discussed in chapter 7).

The third receptor tropism of Ad5 is binding to αvβ3/5 integrins, which is the key event for viral internalisation (Wickham et al., 1993). Additionally, αvβ5 integrin has been shown to be essential for efficient Ad-mediated gene transfer in human airway epithelia (Goldman and Wilson, 1995). The penton base protein binds to αvβ3/5 integrins (Wickham et al., 1993) via its highly conserved RGD motif (Neumann et al., 1988, Zubieta et al., 2005). The RGD > RGE mutation in penton base is a well characterised mutation that in the early reports was shown to delay viral reproduction and the onset of viral DNA synthesis (Bai et al., 1993). RGE mutation has also been shown to dampen down innate anti-adenoviral immune responses, relative to the wild type Ad5 that triggers the production of pro-inflammatory cytokines via binding to splenic MΦs through the penton RGD motif, demonstrated using a RGD-deleted virus AdΔRGD (Shayakhmetov et al., 2005a, Di Paolo et al., 2009). The insertion of the penton RGE mutation in the HVR7-mutated Ad5 vector background has also been shown to decrease splenic transduction by 5-fold, and to markedly dampen down antiviral inflammatory responses (Bradshaw et al., 2012). The RGE mutation therefore seems to be a crucial addition in the de-targeting armature of vectors intended for *in vivo* delivery. We attempted to assess the RGE-containing virus binding to αvβ3/5 integrins by surface plasmon resonance (SPR) on several occasions, but unfortunately were not successful. However, we are confident that this modification is fully functional in the context of our viruses, as it is a well-known method in Ad vectorology. In further work we have evaluated the impact of the integrin-binding RGE mutation on the elicitation of innate cytokine responses following systemic vector delivery in wild type mice (section 7.1.5).

In this chapter, a comprehensive panel of de-targeted vectors were generated to establish a reservoir of basal vectors that are readily modifiable for numerous therapeutic applications and cancer targeting. These replication-deficient vector

backbones represent a safe and highly flexible tool for the study of receptor interactions. They serve as a versatile platform for oncolytic modifications, in combination with cancer-targeting moieties for improved cancer-targeting. The modification of these vectors for selective targeting to αvβ6 integrin-expressing EOC is described both in replication-deficient (section 6.2.1) and oncolytic backgrounds (section 6.2.2).

# CHAPTER 5. Results: *In vitro* assessment of novel species D pseudotyped vectors

# CHAPTER 5. In vitro assessment of novel species D vectors

This chapter describes the production and characterisation of novel chimaeric vectors based on the Ad5 backbone with the fiber protein pseudotyped from species D serotypes. Species D Ads have significantly lower seroprevalence in the population than the most commonly used gene therapy vector Ad5 (Abbink et al., 2007). Furthermore, their receptor usage remains largely unknown, which gave us a secondary objective for their characterisation. We have previously generated a novel serotype Ad10, whose vectorisation has not been reported (data not shown). Additionally, a comprehensive panel of chimaeric vectors was generated by pseudotyping the Ad5 genomic backbone with the sequence of either the whole fiber protein or just the fiber knob domain from species D serotypes 10, 15, 24, 29, 48 and 53. We attempted to evaluate the potential three-dimensional conformation of the knob domains of these serotypes. Amino acid sequence alignments with the Ad5 and Ad35 knob sequence was used to predict the likelihood of these vectors using CAR or CD46 as their primary entry receptors, respectively. These vectors were produced into high viral titres and assessed in a series of *in vitro* assays for their receptor tropisms for CAR and CD46 – the central proteins known to be involved in host cell transduction. We were also interested in seeing whether fiber-pseudotyping influenced binding of hexon protein to FX. Furthermore, the ability of these novel pseudotyped vectors to evade pre-existing neutralising humoral immunity was assessed by utilising immune adult serum and malignant ovarian ascites as the source of anti-Ad nAbs.

## 5.1 *In silico* assessment of species D serotype knob domains

Species D Ads are a distinct group of viruses that are known to have variable cell and tissue tropisms from subgroup C, which includes the most commonly utilised gene therapy vector, Ad5. The detailed molecular level interaction of species D virus fiber protein and their primary entry receptors has not been crystallised yet, with the exception of Ad19p (Burmeister et al., 2004) and Ad37 interaction with sialyl-lactose receptors (Burmeister et al., 2004, Johansson et al., 2009). Members of subgroup D are also known to utilise CD46 (Chen et al., 2010, Li et al., 2012) and GD1a glycan (Nilsson et al., 2011) for cell entry. A great deal remains unknown of the receptor and tissue tropisms, infectivity and oncolytic potency of the genetically diverse (Figure 1– 5) and understudied species D serotypes. In this study, a panel of species D Ads were evaluated *in silico* to predict the structure of their fiber knob, based on these two publicly available, previously crystallised knob models from Protein Data Bank (PDB) (Berman et al., 2000). This formed a basis for pseudotyped species D vector

generation in Ad5 background and *in vitro* mapping of their binding to common cell surface receptors, CAR and CD46.

### 5.1.1 *ClustalW alignment of species D Ad knob sequences*

Fiber knob amino acid sequences for all 35 different species D serotypes were downloaded from the NCBI Protein database (NCBI, 2016), and aligned in BioEdit program (Hall, 1999) using the built-in ClustalW Multiple Alignment command. All of the knob amino acid sequences were shown to share two of the main CAR-binding residues S408 and P409 (Smith et al., 2002) with the Ad5 knob, while the third residue Y483 was conserved in all serotypes except Ad9, and the fourth key residue L491 was highly divergent across serotypes (Figure 5–1A; highlighted in red). As for the CD46-tropism, four key CD46-binding residues have been previously determined for the CD46-binding species B Ad35 serotype (Wang et al., 2007). The sequence alignment showed all of the corresponding residues to be completely absent in all species D serotypes (Figure 5–1B; highlighted in blue), which suggested that these serotypes may not use CD46 as their primary target receptor for host cell entry. The findings based on the amino acid sequence therefore indicate that species D Ads do not utilise the CD46 receptor but may bind CAR, albeit likely at a lower affinity compared to Ad5, due to the conservation of two out of four key CAR-binding residues. Both the CAR- and CD46-tropism of the pseudotyped Ad5/species D chimaeras was further assessed in haemagglutination assays, luciferase transduction assays and competition inhibition assays *in vitro* (described in the following sections).
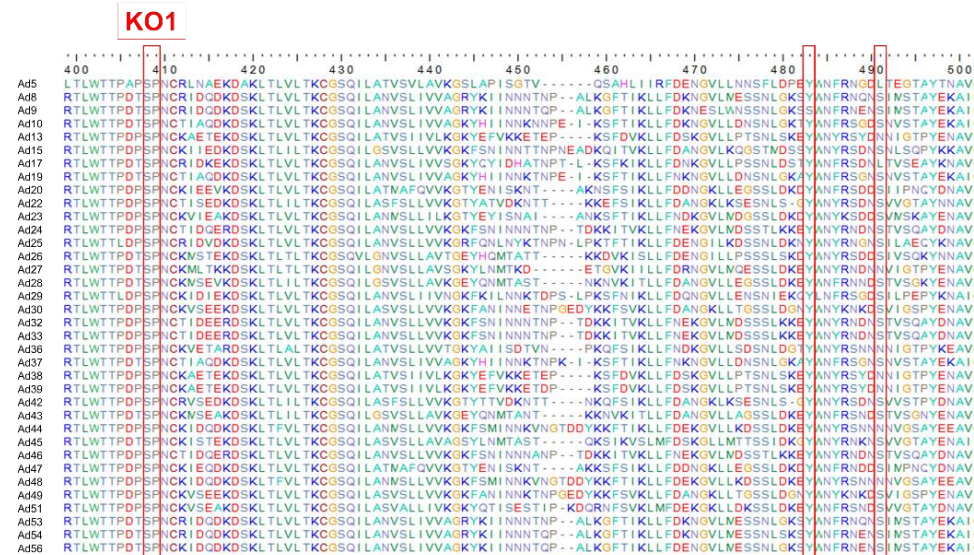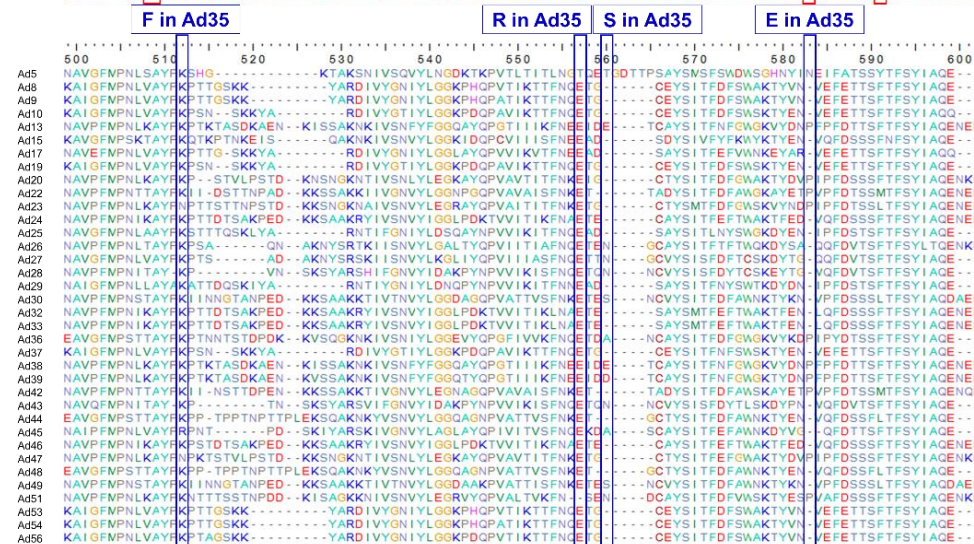
**Figure 5–1. Amino acid sequence alignment of knob domains of all 35 species D adenovirus serotypes.** (A) Key CAR-binding residues (Xia et al., 1994), the KO1 mutation (Smith et al., 2002) and (B) CD46-binding residues as determined for Ad35 (Wang et al. 2007) in the fiber knob domain. Protein sequences were downloaded from National Center for Biotechnology Information (NCBI) website and aligned in BioEdit using ClustalW multiple alignment command using Ad5 knob sequence as a reference sequence. Sequences were further edited in Microsoft PowerPoint.

### 5.1.2   Predictive structural modelling of the knob domain

Species D serotypes Ad10, -15, -24, -29, -48, -53 were chosen for further assessment based on their availability in our laboratory. The conformational structure of their fiber knob domain was visualised in a predictive SWISS-MODEL homology modelling software (Figure 5–2A). The majority of the species D fiber knobs have not yet been crystallised to a molecular detail, which is why the homology modelling was based on either of the published species D virus knob structures, Ad19p knob (PDB ID: 1UXB) or Ad37 (PDB ID: 2WGU). SWISS-MODEL software was run at an automated mode and the template was selected manually based on the highest possible sequence homology suggested by the software. All predicted models of the knob structure had a protruding loop structure whose amino acid sequence is PKPSNSKKY. The size of this loop seemed larger for Ad24 knob than for the other predicted knob structures. Structural modelling did not reveal major differences in the conformation of the fiber knob domain, relative to the Ad5 knob domain (Figure 5–2B). However, in the absence of crystallisation data, the homology modelling only gives a sophisticated estimation of the 3D structure of these domains, and may not accurately reflect their true conformation in the context of the whole virion.
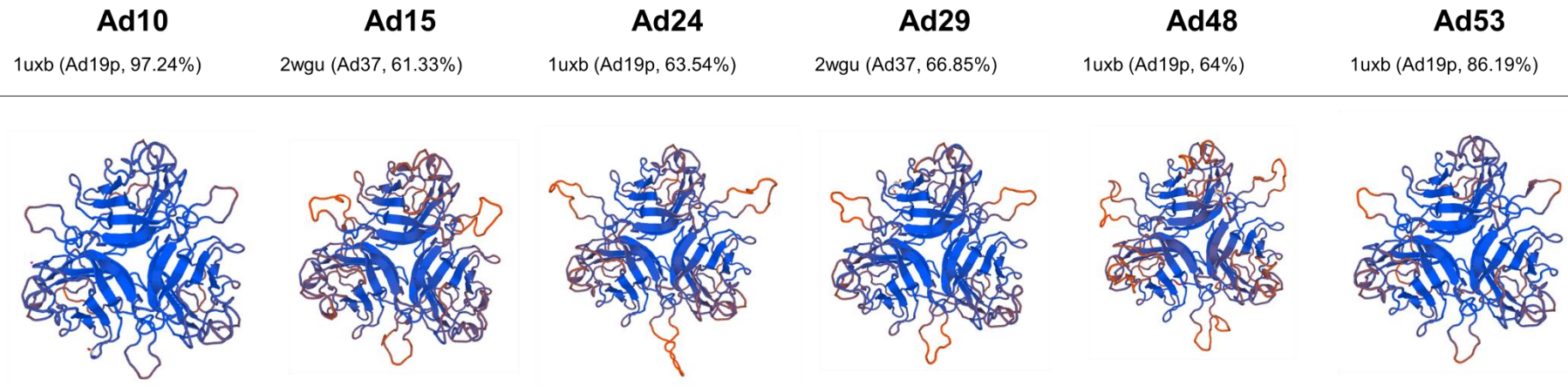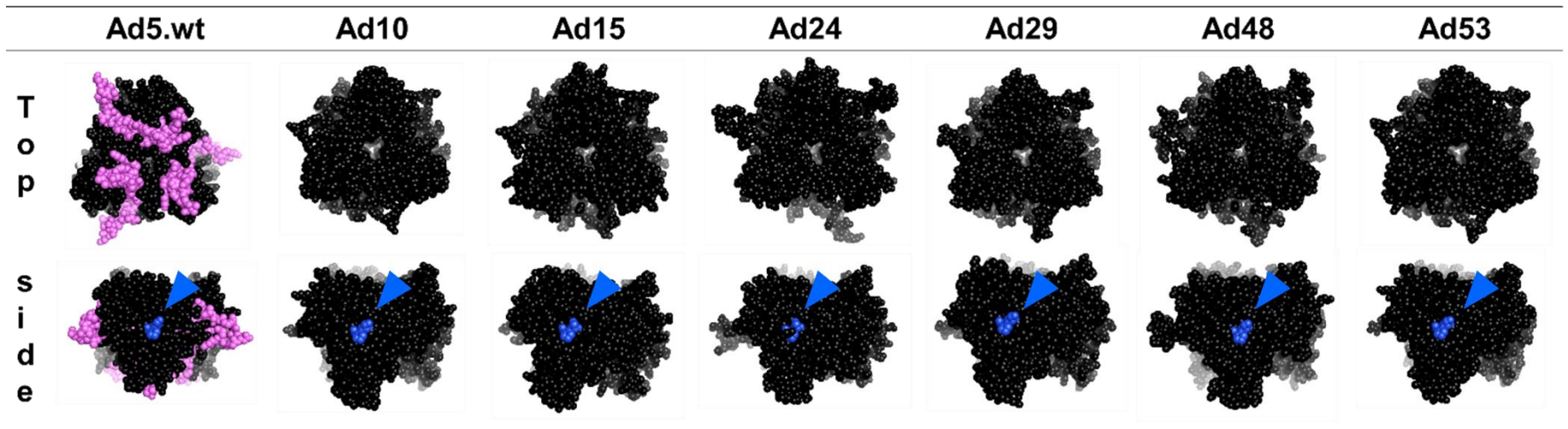
**Figure 5–2. Predicted 3D structures of species D knob domains.** (A) The models were based on either Ad19p or Ad37, depending on the structure with the highest degree of homology (indicated as a percentage). The sequence of the protruding loop structure: PKPSNSKKY. Colour indicates relative hydrophobicity: blue, hydrophobic; red, hydrophilic. (B) Ball view of species D knobs as seen from the top and from the side of the molecule. Immunodominant HI loop (Xia et al., 1994) highlighted in purple for Ad5; CAR-binding site highlighted in blue (Smith et al., 2002).

## 5.2 Generated pseudotyped vectors

A panel of Ad5/species D pseudotyped vectors were generated by AdZ homologous recombineering methods. All vector genomes were based on the parental replication-deficient (*ΔE1/E3*) Ad5.Luc vector described in section 4.1. These vectors were generated by exchanging either the sequence of the whole fiber protein or the knob domain of the fiber protein with the respective sequences from species D serotypes. Nucleotide sequences with overlapping Ad5 homology arms were commercially synthesised and inserted into the Ad5.Luc sequence. Five whole fiber (Table 5–1A) and six fiber knob-pseudotyped Luc-expressing vectors (Table 5–1B) were generated, all of which were rescued as functional virions and produced into very high viral titres. CsCl-gradient ultracentifugation-purified stocks were titered by microBCA assays for their physical viral titre (vp/mL). In addition to the generation of novel pseudotyped vectors, Ad10 serotype with Luc or GFP reporter genes was vectorised by Dr James Davies as a novel vector backbone (Table 5–1C; unpublished data) for future assessment and modification for cancer-therapeutic purposes.

**Table 5–1. Generated a) whole fiber-pseudotyped (F) species D vectors, b) knob-pseudotyped (kn) species D vectors and c) serotype Ad10 vectors.** Vectors were generated by homologous recombineering methods and produced into high viral titres in permissive T-REx-293 cells. The physical viral titre was determined using a microBCA protein kit, 1 μg of protein corresponding to a titre of $4 \times 10^9$ viral particles (vp)/mL (Von Seggern et al., 1998).

### A

| Virus | Physical titre (vp/mL) |
|---|---|
| Ad5/F10.Luc | $4.7 \times 10^{12}$ |
| Ad5/F15.Luc | $1.9 \times 10^{12}$ |
| Ad5/F24.Luc | $3.7 \times 10^{12}$ |
| Ad5/F29.Luc | $6.8 \times 10^{12}$ |
| Ad5/F53.Luc | $3.8 \times 10^{12}$ |

### B

| | |
|---|---|
| Ad5/kn10.Luc | $2.7 \times 10^{12}$ |
| Ad5/kn15.Luc | $1.3 \times 10^{12}$ |
| Ad5/kn24.Luc | $3.6 \times 10^{12}$ |
| Ad5/kn29.Luc | $1.6 \times 10^{12}$ |
| Ad5/kn48.Luc | $2.8 \times 10^{12}$ |
| Ad5/kn53.Luc | $2.3 \times 10^{12}$ |

### C

| | |
|---|---|
| Ad10.GFP | $3.2 \times 10^{12}$ |
| Ad10.Luc | $3.0 \times 10^{12}$ |

### 5.2.1 Verification of fiber integrity

We then went on to assess the fiber integrity of these pseudotyped vectors by methods that are commonly utilised in Ad vector quality control. The pseudotyped vectors were assessed for fiber protein integrity by Western blot, using an Ad2 fiber-

specific 4D2 mAb that recognises both the monomeric and trimeric forms of the fiber protein (Figure 5–3A). Additionally, the presence of all viral proteins was verified by a highly sensitive silver staining method (Figure 5–3B). The size of the Ad5 fiber is around 62 kDa, while species D fibers are ~ 40 kDa in size, as estimated using the ExPASY Bioinformatics Portal molecular weight calculator. This size difference can be seen as two distinct bands on the gel for viruses with the whole fiber (F) or just the knob (kn) domain replaced. Eight out of ten pseudotyped vectors were shown to exhibit a structurally intact fiber, based on the banding pattern on both the immunoblot and the protein silver staining (Figure 5–3). In contrast, both Ad5/F53 and Ad5/kn53 vectors had two separate bands on the fiber Western blot image (Figure 5–3A), which suggest that the structural integrity of these vectors may be compromised, or rather that these stocks are a contaminated with Ad5. However, the genome of both of these vectors was confirmed to be correct by sequencing the BAC DNA following recombineering (data not shown). The Ad10 fiber protein could not be detected by using the anti-Ad2 fiber antibody (Figure 5–3B), which is likely due to the lack of cross-reactivity between the species C and D fibers. However, a distinct, very strong band of the correct size (< 40 kDa) was observed for the Ad10 fiber in the silver staining (Figure 5–3C). The 4D2 antibody recognises the N-terminus (shaft) of the fiber protein that is in contact with the penton base protein. This domain is conserved throughout all pseudotyped vectors, while it is missing in the Ad10 vector. Therefore, the antibody efficiently recognises this sequence in the knob-pseudotyped vectors whose fiber shaft is derived from Ad5 (Figure 5–3A). However, recognition is less efficient for the whole fiber-pseudotyped vectors that only have a short sequence of Ad5 fiber at the N-terminus of their fiber protein, while the rest of the shaft is serotype-specific.
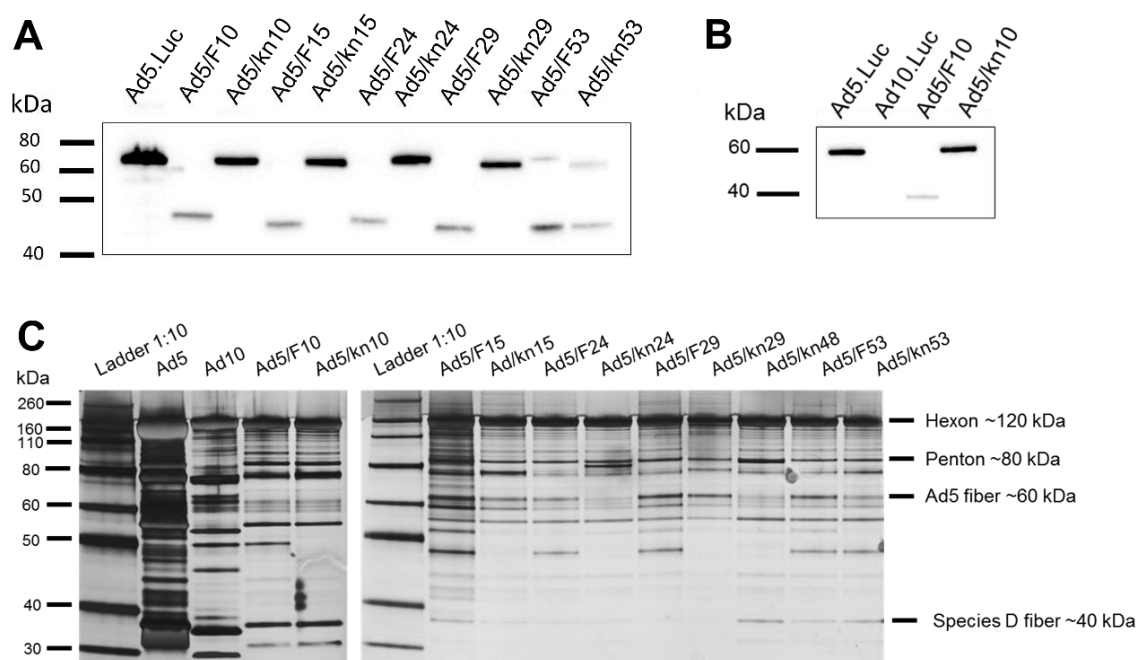
**Figure 5–3. (A) Fiber protein Western blot of the species D pseudotypes and (B) Ad10 vectors.**
1 × 10$^{10}$ viral particles in a total of 14 µL with 5 µL of loading buffer and 1 µL of DTT were loaded into each cell and run for 1 h 20 min at 150 V. The fiber protein was detected using an anti-Ad2 4D2 antibody. The image was developed in SuperSignal West Pico Chemiluminescent substrate for 10 min. (**C) Silver staining of Ad5-based species D pseudotypes.** 1 x 10$^{10}$ viral particles in a total of 14 µL with 5 µL of loading buffer and 1 µL of DTT were loaded into each cell and run for 20 min at 120 V and 1 h at 150 V. The image was developed for 5 min and de-stained according to the Pierce SilverSnap kit instructions.

## 5.3 *In vitro* evaluation of pseudotyped viruses

Following the initial quality control, the generated novel pseudotyped vectors were also assessed in several different *in vitro* assay types. We sought to verify that the fiber pseudotyping had not compromised vector integrity and/or functionality. Additionally, the receptor tropism of these novel vectors and pseudotypes was assessed in a panel of cell lines expressing varying levels of the main Ad receptors.

### 5.3.1 *Haemagglutination assays*

Pseudotyped vectors were assessed for their ability to agglutinate human erythrocytes that express CAR on their surface (Carlisle et al., 2009). Using Ad5.Luc as a positive control virus, Ad10 was shown to be capable of agglutinating erythrocytes, albeit at lower efficiency than Ad5 (Figure 5–4). Two of the lower virus doses were not capable of agglutinating the erythrocytes, which indicates low affinity of Ad10 knob domain to CAR (Figure 5–4; row 3). None of the Ad5-based species D pseudotypes exhibited haemagglutination properties, with the exception of Ad5/kn53 that showed full haemagglutination at all viral doses. Since this vector showed compromised fiber integrity in the Western blot as discussed in section 5.2.1, the

validity of this observation is debatable. The stock may be contaminated with Ad5, which would explain the haemagglutination profile.

**A**

| | 1x10⁹ vp | | | 7.5x10⁸ vp | | | 5x10⁸ vp | | | 2.5x10⁸ vp | | |
|---|---|---|---|---|---|---|---|---|---|---|---|---|
| 1) Ad5.Luc | +++ | +++ | +++ | +++ | +++ | +++ | +++ | +++ | +++ | +++ | +++ | +++ |
| 2) Ad5.KO1 | − | − | − | − | − | − | − | − | − | − | − | − |
| 3) Ad10.Luc | ++ | ++ | ++ | + | + | + | − | − | − | − | − | − |
| 4) Ad5/F10 | − | − | − | − | − | − | − | − | − | − | − | − |
| 5) Ad5/kn10 | − | − | − | − | − | − | − | − | − | − | − | − |
| 6) Ad5/F15 | − | − | − | − | − | − | − | − | − | − | − | − |
| 7) Ad5/kn15 | − | − | − | − | − | − | − | − | − | − | − | − |
| 8) Ad5/F24 | − | − | − | − | − | − | − | − | − | − | − | − |

| | 1x10⁹ vp | | | 7.5x10⁸ vp | | | 5x10⁸ vp | | | 2.5x10⁸ vp | | |
|---|---|---|---|---|---|---|---|---|---|---|---|---|
| 9) Ad5/kn24 | − | − | − | − | − | − | − | − | − | − | − | − |
| 10) Ad5/F29 | − | − | − | − | − | − | − | − | − | − | − | − |
| 11) Ad5/kn29 | − | − | − | − | − | − | − | − | − | − | − | − |
| 12) Ad5/kn48 | − | − | − | − | − | − | − | − | − | − | − | − |
| 13) Ad5/F53 | − | − | − | − | − | − | − | − | − | − | − | − |
| 14) Ad5/kn53 | +++ | +++ | +++ | +++ | +++ | +++ | +++ | +++ | +++ | +++ | +++ | +++ |

**B**

| | | | |
|---|---|---|---|
| PBS | − | − | − |
| lysis buffer | +++ | +++ | +++ |
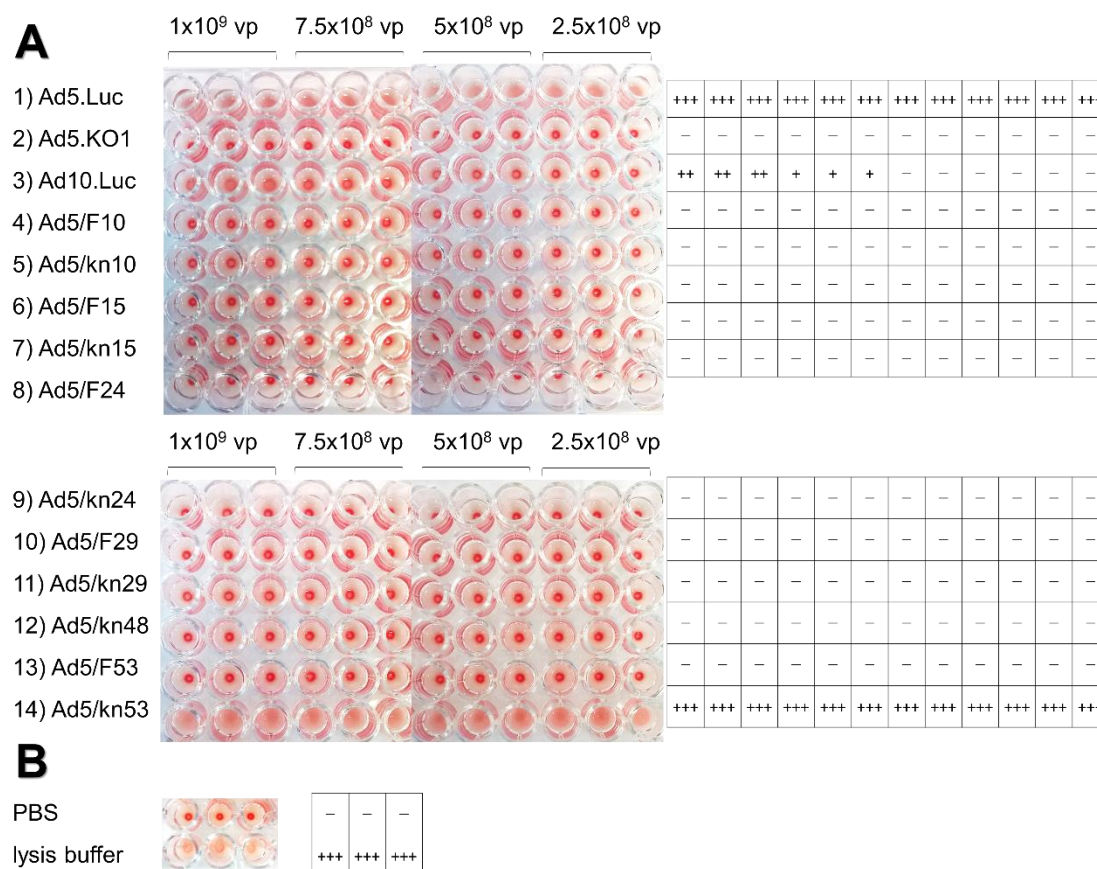
**Figure 5–4. Haemagglutination assay on species D pseudotyped viruses.** (A) Viruses were mixed with 1 % erythrocyte solution in PBS at four different concentrations of viral particles (vp). (B) Negative control in the assay was phosphate buffered saline (PBS), and positive control red blood cell lysis buffer. Haemagglutination grading: +++ complete; ++ midrange; + partial; − no haemagglutination.

### 5.3.2 Transduction assays

The receptor tropism of rare species D Ad serotypes is largely unknown to date. Whole fiber and fiber knob-pseudotyped vectors provide an excellent model system for studying receptor usage, as tropism is known to be determined by interactions between the fiber protein and cell surface receptors. To further elucidate the observations from haemagglutination assays, we sought to assess the receptor usage of the generated vectors in CHO-K1, CHO-CAR and CHO-BC1 model cell lines that have a clean receptor expression profile. We have previously validated luciferase transduction assays as a reliable method for studying CAR-tropism of Ad5.Luc and other vectors that utilise CAR in cellular entry (Uusi-Kerttula et al., 2016). Transduction assays performed in CHO-CAR cells indicated that CAR may not be involved in the cell entry of any of the Ad5-based vectors with whole fiber pseudotyped from species D serotypes (Figure 5–5A), as cell transduction levels were very similar

to the levels in CHO-K1 cells that do not express CAR at all. Statistically significant differences between CHO-K1 and CHO-CAR cells were observed for Ad5/F15 and Ad5/F29, but this may be reduced to variation around nothing, as the fold changes (CHO-K1 vs. CHO-CAR) raw RLU values are low for these viruses. In contrast, all knob-pseudotyped vectors, except Ad5/kn53, had significantly higher transduction efficiency in CHO-CAR as compared to CHO-K1 cells (Figure 5–5B). Interestingly, Ad5/kn10, Ad5/kn15 and Ad5/kn24 transduction in CHO-CAR was 4.7-, 3.2- and 3.3-fold higher than Ad5.Luc transduction on these cells (Figure 5–5B). However, in this particular assay the raw RLU values for Ad5.Luc in CHO-CAR cells were ~ 10-fold lower than commonly observed for this virus in similar assays. This was considered common inter-assay variation since transduction levels returned to normal when the assay was repeated (Figure 5–9C).
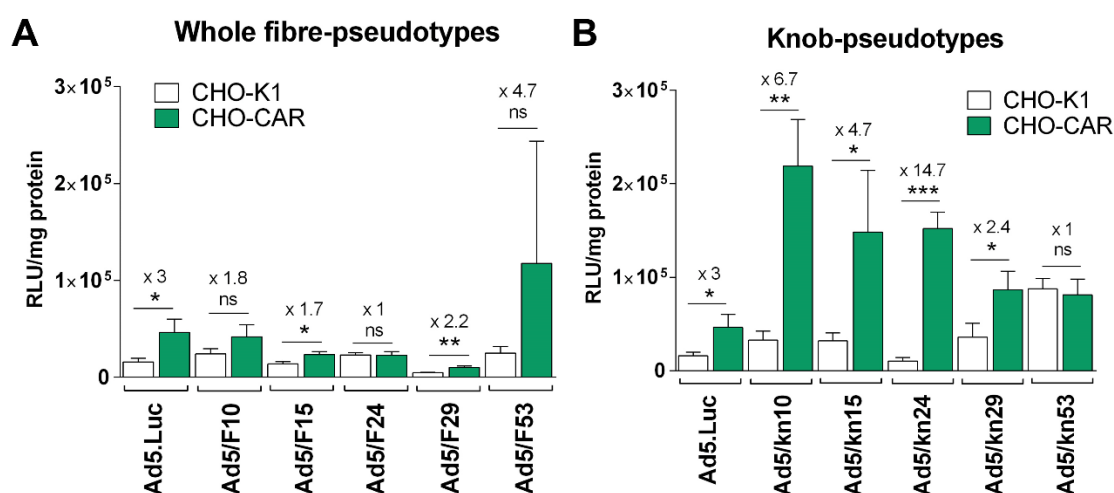


**Figure 5–5. Transduction assays to assess CAR-tropism.** (A) Whole fiber-pseudotyped virus transduction in CHO-K1 and CHO-CAR cells and (B) fiber knob-pseudotyped virus transduction in CHO-K1 and CHO-CAR cells. Cells were infected with 5000 viral particles/cell for 3 h in serum-free medium. Luciferase activity was quantified at 48 h post-infection and normalised to relative light units (RLU)/mg protein in each well. Fold change indicates difference between CHO-K1 and CHO-CAR for the specific virus. Data were analysed in GraphPad Prism using two-tailed unpaired t test. n = 3; ns, p > 0.05; *, p < 0.05; **, p< 0.01; ***, p < 0.001. Error bars represent standard deviation.

We then went on to assess the CD46-tropism of the pseudotyped vectors. CHO-BC1, a CHO-K1 cell line that expresses high levels of the BC1 isoform of the species B Ad receptor, CD46 (Gaggar et al., 2003), was used as a model cell line for these transduction assays. The Ad5/F35 vector (a kind gift from Prof Andrew H. Baker, University of Edinburgh) has the fiber pseudotyped from a CD46-utilising species B virus, and was used as a positive control, as previously reported (Uusi-Kerttula et al., 2016). As expected, the transduction efficiency of Ad5/F35 was significantly higher in CHO-BC1 than in CHO-K1 or CHO-CAR cells (Figure 5–6A). None of the whole fiber-pseudotyped viruses showed significantly increased transduction efficiency in CHO-

BC1 as compared to CHO-K1 cells (Figure 5–6B). Similarly, none of the fiber knob-pseudotyped viruses had an increased transduction efficiency in CHO-BC1 cells as compared to CHO-K1 cells (Figure 5–6C). However, Ad5/kn53 transduced CHO-BC1 cells at 11-fold increased efficiency compared to the non-CD46-utilising Ad5.Luc. Despite the trend suggesting possible CD46 usage for Ad5/kn53, the difference between CHO-K1 and CHO-BC1 was not statistically significant (Figure 5–6C; p = 0.0689). This particular virus also showed inconsistencies in the Western blot and haemagglutination assays discussed in the previous sections, which is why the validity of the observed CD46-binding may also be debatable as this stock may be contaminated with Ad5.Luc. Unfortunately, direct comparison of the transduction levels of Ad5/F35 and species D pseudotypes is not feasible, since the Ad5/F35 vector expresses the β-Gal transgene, while all the other viruses are luciferase-expressing.
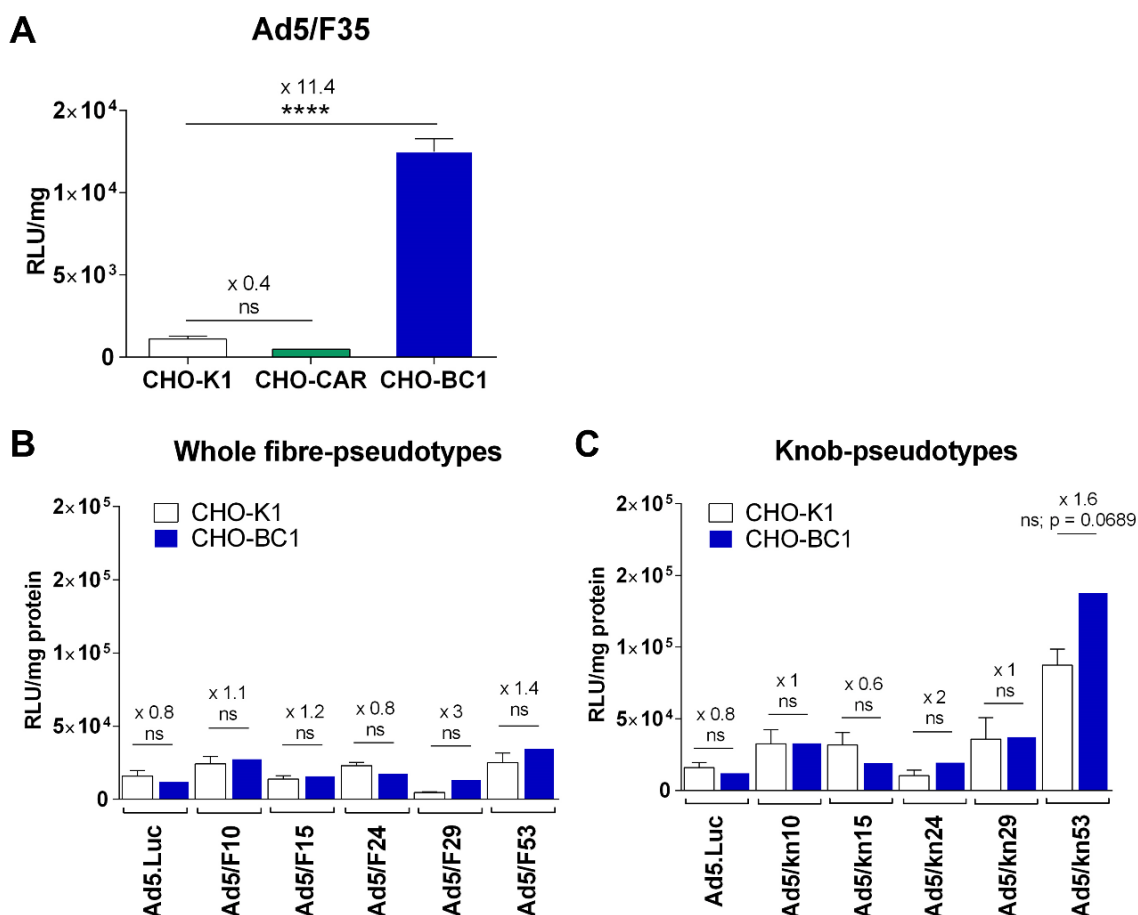


**Figure 5–6. Transduction assays to assess CD46-tropism.** (A) The CD46 receptor-utilising Ad5/F35 virus was used as a positive control, (B) whole fiber pseudotyped viruses and (C) fiber knob-pseudotyped viruses for transduction assays in CHO-K1 and CHO-BC1 cells. Cells were infected with 5000 viral particles/cell for 3 h at 37°C in serum-free medium. Luciferase activity was quantified 48 h post-infection and normalised to relative light units (RLU)/mg protein in each well. Data were analysed in GraphPad Prism using two-tailed unpaired t test. n = 3; ns, not significant; p > 0.05. Error bars represent standard deviation.

### 5.3.3 Competition inhibition assays

In order to further dissect the receptor tropism of the pseudotyped Ad5-based vectors, competition inhibition assays were performed in the described CHO model cell lines. Recombinant knob proteins were produced in house (section 4.2) and utilised as blocking agents along with validated function-blocking antibodies to competitively inhibit receptor binding. Vector receptor tropism was assessed in the CAR$^{neg}$ control cell line CHO-K1 and the CAR$^{high}$ CHO-CAR cell line. Cells were pre-blocked with recombinant knob proteins to inhibit subsequent virus entry. All whole fiber-pseudotyped vectors seemed to be equally incapable of infecting CHO-K1 and CHO-CAR cells (Figure 5–7A, C, E, G, I). Thereby pre-blocking the cells with control kn5.CAR– or kn5 had no measurable effect on transduction efficiency. In contrast, the fiber knob-pseudotyped vectors showed slightly increased transduction in CHO-CAR as compared to CHO-K1 cell line and their whole fiber-pseudotyped counterparts (Figure 5–7B, D, F, H, J), which indicates that they may be able to use CAR for cell entry.

Cell entry via CAR was significantly inhibited for Ad5/kn10 (p = 0.0048) and Ad5/kn15 (p = 0.0063) by pre-blocking the cells with kn5 protein (Figure 5–7B, D). Based on the observations from transduction assays in CHO-CAR cells, Ad5/kn24 and Ad5/kn29 were expected to potentially use CAR for cell entry. However, blocking with kn5 did not result in significant reduction in transduction efficiency for either Ad5/kn24 or Ad5/kn29 by one-way ANOVA (p = 0.1454 and 0.2679, respectively). However, Ad5/kn24 transduction was significantly lower in the presence of the inhibitory kn5 protein than in 'virus only' conditions (p = 0.0172), when analysed by an unpaired t test. CAR-tropism of the pseudotyped Ad5/kn48 vector was assessed in competition inhibition assays in CHO-CAR cells using recombinant knob proteins as inhibitory agents. Ad5.Luc transduction was significantly inhibited by its own knob protein at three of the highest protein concentrations (Figure 5–8A). In contrast, Ad48 knob significantly inhibited Ad5.Luc entry only at the highest protein concentration tested (Figure 5–8A). Conversely, Ad5 knob was capable of inhibiting Ad5/kn48 entry at significant levels at four out of six protein concentrations, while Ad48 knob inhibited Ad5/kn48 entry only at two of the highest protein concentrations (Figure 5–8B). This may indicate lower affinity of Ad48 knob for CAR, relative to Ad5. The tropism of Ad5/kn48 for CAR has been previously evaluated in a recent publication by our group (Uusi-Kerttula et al., 2016), and is therefore not discussed here in further detail.
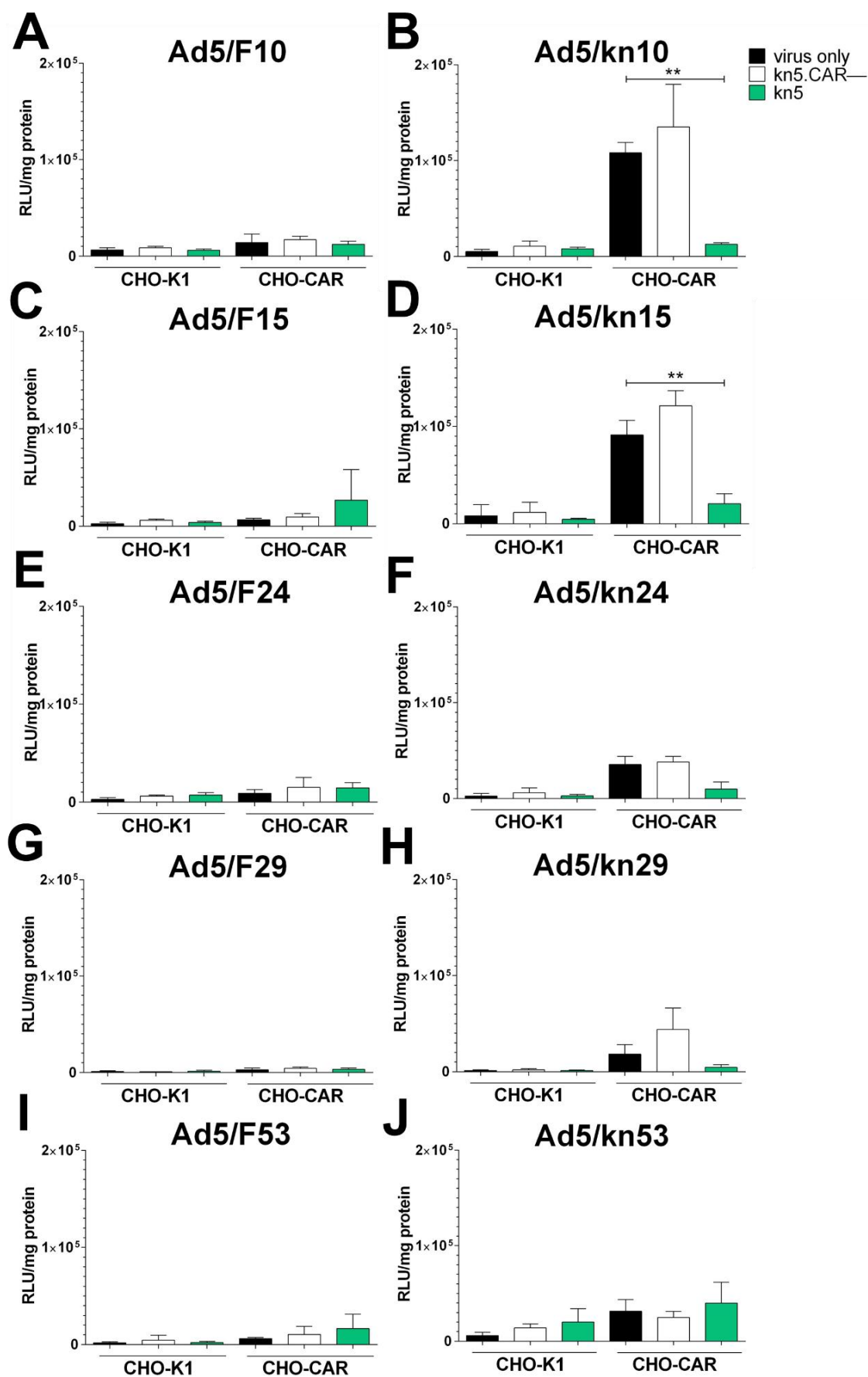
**Figure 5–7. Competition inhibition assays using species D pseudotypes.** Cells were pre-blocked with 10 µg/10^5 cells of the proteins Ad5 knob (kn5) or Ad5 knob with 477YT CAR-binding mutation (kn5.CAR–) for 30 min on ice. Cells were then infected with 5000 viral particles/cell for 1 h on ice and luciferase activity measured at 48 h post-infection. Values were normalised to relative light units (RLU)/mg protein. Data were analysed in GraphPad Prism using one-way ANOVA with Dunnett's multiple comparison. n = 3; ns, p > 0.05; *, p < 0.05; **, p < 0.01; ***, p < 0.001; error bars represent standard deviation. CAR, coxsackie and adenovirus receptor.
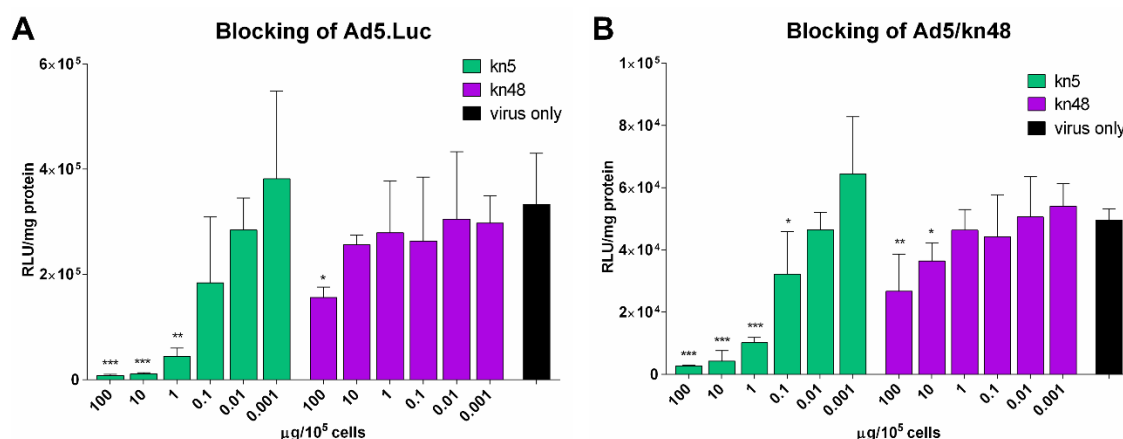


**Figure 5–8. Dose-response inhibition of CAR-mediated cell entry.** CHO-CAR cells were pre-incubated with varying concentrations of knob proteins for 30 min on ice and infected with luciferase-expressing viruses at 5000 vp/cell for 1 h on ice in triplicate. Relative light units were measured at 48 h post-infection and normalised to total protein concentration in each well (RLU/mg). Data were analysed in GraphPad Prism using one-way ANOVA with Dunnett's multiple comparison. n = 3; ns, p > 0.05; *, p < 0.05; **, p < 0.01; ***, p < 0.001. Error bars represent standard deviation.

### 5.3.4  Influence of FX on species D pseudotyped Ad5 vectors

We then went on to assess the tropism of all whole fiber- and knob-pseudotyped Ad5 vectors in CHO-K1 (CAR$^{negative}$), SKOV3 (CAR$^{intermediate}$) and CHO-CAR (CAR$^{high}$) cell lines, both in the absence and in the presence of 10 µg/mL of purified human FX (Figure 5–9). As expected, supplementation of the transduction medium with FX did markedly increase the transduction efficiency for all pseudotyped vectors that carry the Ad5 hexon protein. Since the pseudotyped vectors may bind CAR, the impact of FX on transduction efficiency was the less pronounced, the higher the CAR expression of the particular cell line. This meaning that background transduction levels are higher in cells that express CAR, which is why the relative increase in efficiency upon FX supplementation is less pronounced compared to cells that no not express CAR. Surprisingly, the effect was greatly more pronounced for the knob-pseudotyped vectors than for their whole fiber-substituted counterparts. FX seemed to influence whole fiber-pseudotyped vector transduction less than it did for the parental Ad5, while the knob-pseudotyped vectors had very similar transduction patterns to Ad5. Ad5/kn53 was the only vector whose transduction efficiency was very similar both in the absence and presence of FX in all three cell lines (Figure 5–9). The native tropism of the Ad10 serotype has not been reported previously.

Sequence alignment of all seven hexon HVRs in Ad5 and Ad10 serotypes revealed Ad10 to have homologous amino acids in the HVR7 region with the FX-binding 'HVR7' mutation (Figure 5–10A) that has been described for Ad5 (Alba et al., 2009). In this seminal paper by Alba and colleagues, the subgroup D serotype Ad26 was designated as a non-FX-binder. This prompted the design of the HVR7 mutation based on the exact amino acids in the HVR7 of Ad26, whose corresponding residues are known to be critical for the FX binding of Ad5. We therefore sought to verify *in vitro* that the addition of physiological concentrations of FX in the medium would not impact the transduction efficiency of Ad10 in CHO-K1 cells that do not express either CAR or CD46 receptors, but are amenable to FX-mediated Ad5 uptake via HSPGs. As shown previously (Figure 4–7A), the transduction efficiency of Ad5.Luc vector was significantly enhanced by the addition of FX in the assay medium (Figure 5–10B), while its transduction was neutralised by the addition of neat ovarian ascites OAS019. On the contrary, the transduction efficiency of the novel Ad10 vector remained completely unchanged upon supplementation of the transduction medium with FX (Figure 5–10C). Additionally, transduction of Ad10 was significantly inhibited when cells were transduced in neat OAS019 ascites that was shown to contain anti-Ad10 antibodies (Figure 3–7). We also sought to evaluate whether the depletion of FX from the transduction medium by the addition of the anti-coagulant X-bp would change the effect of OAS019 on vector transduction efficiency. In the case of Ad5, depletion of FX from OAS resulted in slightly more efficient neutralisation of the vector by OAS019 fluid (Figure 5–10A). However, depletion of FX did not further improve neutralisation of Ad10 by OAS019 (Figure 5–10B).
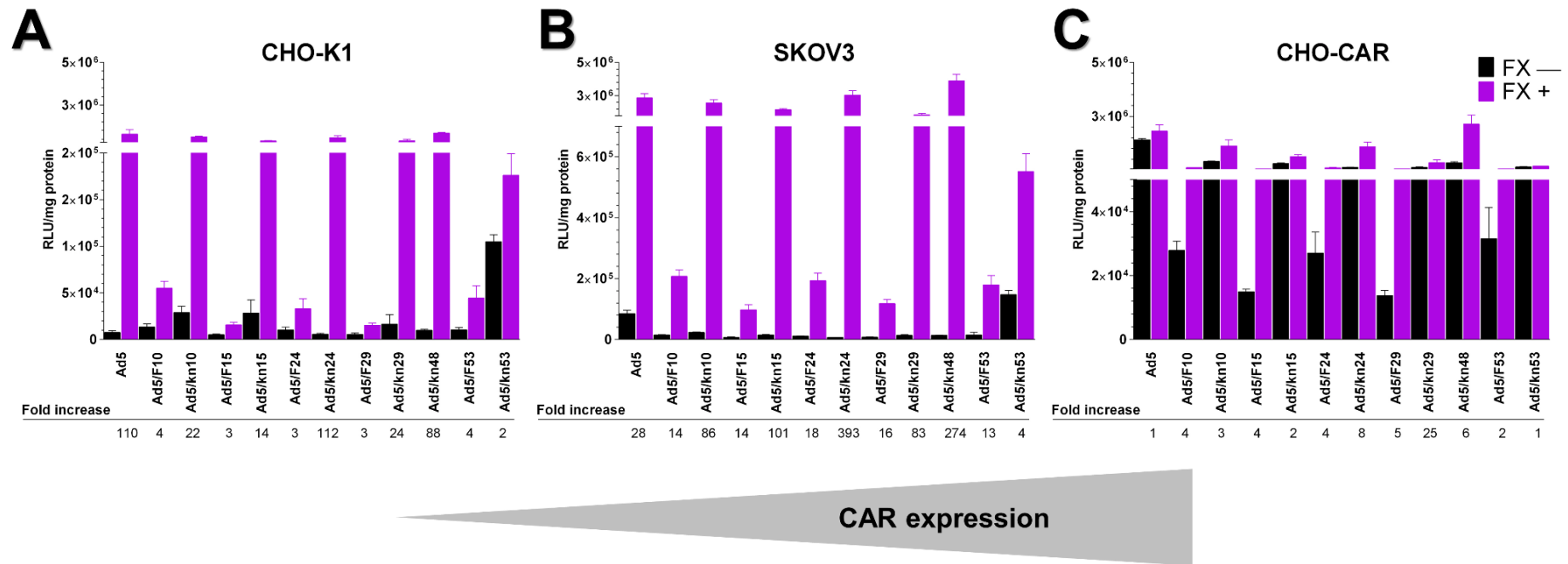
**Figure 5–9. Assessment of pseudotyped vector tropism for coagulation factor 10 (FX).** (A) CHO-K1 hamster ovarian, (B) SKOV3 ovarian cancer and (C) CHO-CAR hamster ovarian cells were infected with 5000 viral particles / cell for 3 h in the absence of presence of 10 µg/mL human coagulation factor 10 (FX). Luciferase expression was quantified 48 h later as relative light units, and normalised to total protein / well (RLU/mg). Fold increase indicates the change relative to FX-free conditions (FX–) for each virus. CAR, coxsackie and adenovirus receptor.
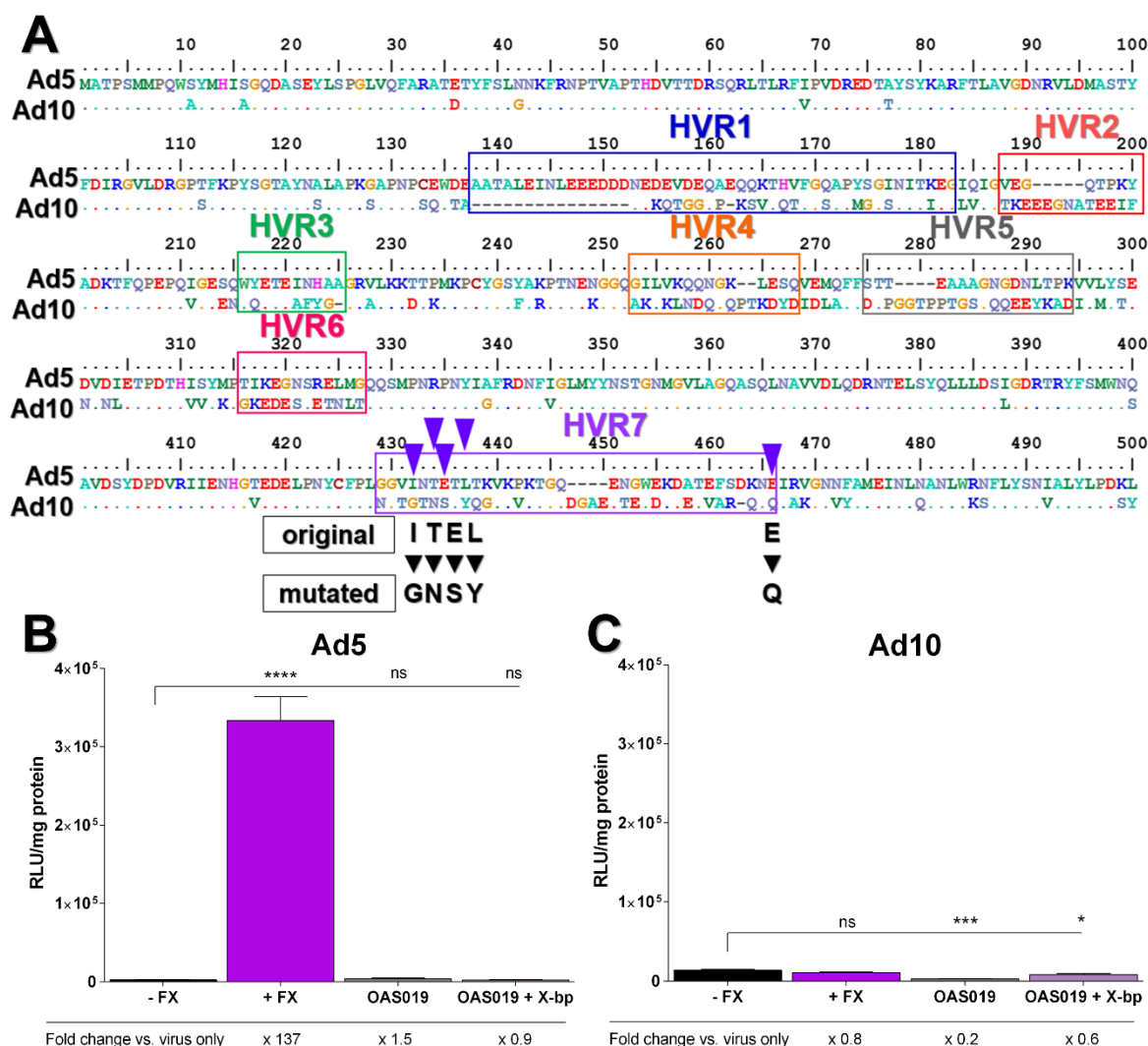
**Figure 5–10. Adenovirus 10 (Ad10) binding to coagulation factor 10 (FX).** (A) Amino acid sequence alignment of hexon hypervariable regions (HVR) in Ad5 and Ad10 serotypes. Sites for 'HVR7' FX-binding mutation in Ad5 shown in purple arrows (Alba et al., 2009); 'original' and 'mutated' amino acids involved in the point mutations are shown in bold black letters. CHO-K1 cells were transduced with (B) Ad5 and (C) Ad10 vectors at 5000 viral particles / cell for 3 h and luciferase activity measured 48 h later. Data shown as mean of triplicate values. Error bars represent standard error of the mean and fold change is relative to 'virus only' conditions for each virus. X-bp is an anticoagulant that was used to deplete FX from ovarian ascites (OAS) at a molar ratio of 3:1 (X-bp:OAS). ns, $p > 0.05$; *, $p < 0.05$; **, $p < 0.01$; ***, $p < 0.001$; ****, $p < 0.0001$.

### 5.3.5 Neutralisation by ovarian ascites

The capsid proteins are thought to be the main immunogenic determinants of Ad virion. The Ad5/species D pseudotyped vectors were generated in order to assess any potential to improve escape from pre-existing humoral immunity. The fiber-pseudotyped vectors were assessed *in vitro* for their ability to resist neutralisation by ovarian ascites and to further refine the role of fiber protein in humoral immune recognition. CHO-CAR (CAR^high) cells were infected with 200 000 vp/cell for 3 h, and luciferase expression measured at 48 h p.i. Both Ad10 and Ad5/kn10 infected the

cells at similar efficiency compared to Ad5.Luc at this very high viral dose, while Ad5/F10 had ~ 1.4-fold lower transduction efficiency in these ascites-free conditions (Figure 5–11A, B; 'virus only'). The lower transduction efficiency for Ad5/F10 compared to Ad5/kn10 is in line with the observations from previous luciferase transduction assays in CHO-CAR cells (Figure 5–5). In the presence of OAS001, that has high levels of anti-Ad5 and moderate levels of anti-Ad10 antibodies (Figure 3–7), Ad5 vector was neutralised more efficiently at all ascites concentrations than any other vector (Figure 5–11A). The overall transduction efficiency of Ad5/F10 was very low, while Ad10 and Ad5/kn10 were capable of transducing the cells much more efficiently than Ad5 at all ascites dilutions (Figure 5–11A). In the presence of OAS019, that has high levels of both anti-Ad5 and anti-Ad10 antibodies (Figure 3–7), Ad10 had a superior transduction efficiency at all ascites concentrations as compared to all other vectors (Figure 5–11B). Additionally, both Ad5/F10 and Ad5/kn10 had greatly improved transduction at all ascites concentrations relative to Ad5 (Figure 5–11B). Overall, the Ad10 vector was capable of resisting neutralisation much better than Ad5 or either of the pseudotyped Ad5/Ad10 vectors.

Importantly, it is noteworthy that the RLU values were already at the maximal threshold for Ad5, Ad10 and Ad5/kn10 in 'virus only' conditions in this assay, since the cells were fully saturated with the very high viral load of 200 000 vp/cell. The transduction efficiency of these vectors may therefore in fact be higher than what could be detected in this assay. This obviously limits the interpretability of the observations. However, as we already used a very low volume of 10 µL of cell lysate for the assay, we did not feel comfortable with further reducing the assay volume. On the other hand, as the tropism of Ad10 for CAR was observed to be much lower than the affinity of Ad5 for CAR, we did not want to reduce the amount of virus in order to be able to observe the full neutralising effect of ovarian ascites. We therefore pushed the assay to its limits to see the differences in protection from neutralisation as clearly as possible.

**A** OAS001

**B** OAS019

| Fold change | 1:10 | 1:5 | 1:2.5 | neat |
|---|---|---|---|---|
| Ad10 | 6 | 55 | 41 | 24 |
| Ad5/F10 | 1 | 7 | 4 | 6 |
| Ad5/kn10 | 6 | 34 | 36 | 94 |

| Fold change | 1:10 | 1:5 | 1:2.5 | neat |
|---|---|---|---|---|
| Ad10 | 4 | 23 | 23 | 27 |
| Ad5/F10 | 4 | 20 | 17 | 16 |
| Ad5/kn10 | 4 | 17 | 15 | 10 |
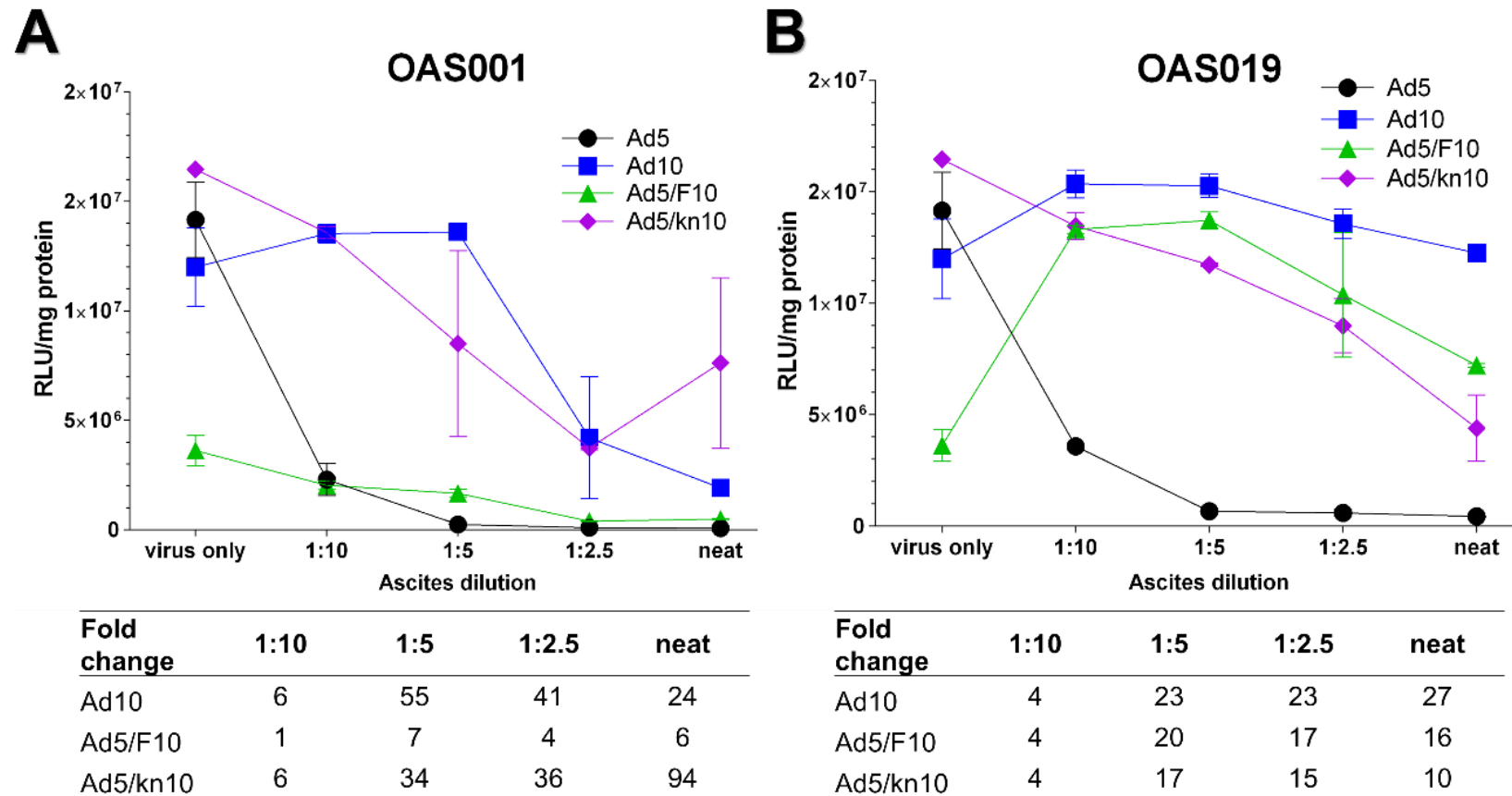
**Figure 5–11. Neutralisation of Ad5/Ad10 pseudotyped vectors by ovarian ascites.** Cells were infected with 200 000 viral particles/cell in the presence of ascending dilutions of ovarian ascites (OAS) from (A) patient 001 and (B) patient 019. Luciferase expression was measured as relative light units 48 h later and normalised to total protein per well (RLU/mg). Tables show fold change in transduction efficiency relative to Ad5 at each ascites dilution. Error bars represent standard error of the mean from duplicate measurements.

166

## 5.4 Discussion

One of the main objectives of this thesis is the assessment of new Ad vector candidates that are based on rare Ad serotypes from subgroup D. Novel Ad10 and Ad5-based vectors with either the full length fiber or the fiber knob domain pseudotyped from species D serotypes were generated by AdZ homologous recombineering, produced to high viral titres in permissive T-REx-293 cells, and assessed for their receptor tropisms and entry pathways *in vitro*. Viral quality control – Western blot for the fiber protein and silver staining for all viral proteins – confirmed all vectors (except Ad5/F53 and Ad5/kn53) to express structurally intact capsid proteins (Figure 5–3). The next step in the vector characterisation was the functional assessment of the generated vector backbones.

Initially, haemagglutination assays were performed on the novel Ad10 vector and the complete panel of pseudotyped Ad5-based vectors using erythrocytes isolated from human blood (Figure 5–4). As described in section 4.2 for the de-targeted vectors, this assay is used routinely for the assessment of CAR-tropism of Ad serotypes, based on their binding to CAR that is expressed on the erythrocyte cell surface (Carlisle et al., 2009). While the CAR-binding vector Ad5 showed strong haemagglutination at all viral doses, Ad10 was capable of agglutinating erythrocytes only at the two of the highest viral doses. Surprisingly, Ad5/kn53 was the only pseudotyped vector that complete agglutinated the cells at all viral doses, while none of the other pseudotyped vectors showed any haemagglutination at any viral dose.

We then proceeded to further assess the receptor tropism of Ad10 and the pseudotyped vectors in *in vitro* infectivity assays (Figure 5–5). Luciferase expression-based transduction assays performed in CHO-CAR (CAR$^{high}$) cells indicated that Ad5/kn10 and Ad5/kn15 vectors may utilise CAR as their entry receptor. However, at low viral doses their transduction levels were low compared to Ad5, which indicates that these vectors may primarily use alternative, yet unidentified receptors for cell entry. However, when CHO-CAR cells were saturated with a very high viral load (200 000 vp/cell) of Ad10 and Ad5/kn10, the transduction efficiency was comparable to Ad5 (Figure 5–11). Surprisingly, none of the Ad5-based vectors with a whole fiber pseudotyped from species D viruses seemed to use CAR (Figure 5–5) or CD46 (Figure 5–6) for cell entry. Luciferase transduction (Figure 5–5) and competition inhibition assays (Figure 5–7) suggested that Ad5/kn10, -kn15 and -kn24, and possibly Ad5/kn29, may utilise CAR for cell entry, albeit less efficiently than Ad5. The Ad5/kn48 vector was confirmed to utilise CAR for cell entry, as the recombinant CAR-binding kn5 protein successfully inhibited CAR-mediated transduction in CHO-CAR

cells (Figure 5–8). However, it was shown that the kn48 protein inhibited Ad5 entry into cells less efficiently than the kn5 protein, which suggests the CAR-affinity of Ad48 to be lower than that of the Ad5 serotype. The CAR-tropism of Ad5/kn48 is further discussed in our recent research publication (Uusi-Kerttula et al., 2016). Although the haemagglutination assay suggested that Ad5/kn53 may use CAR for cell entry, the cell entry of this vector into CHO-CAR cells was not significantly inhibited by the CAR-utilising Ad5 knob protein. Additionally, Ad5/kn53 was more efficient at transducing SKOV3 than the parental Ad5 (Figure 5–9), which suggests that the vector uses an alternative receptor, that is not expressed on CHO-CAR cells but is abundantly expressed on SKOV3 cells. However, this vector showed serious inconsistencies in the different assay types that suggest it may be an impure preparation contaminated with an Ad5 stock.

Transduction levels of all pseudotyped vectors at the lower viral doses were relatively low in CHO-K1, CHO-CAR and CHO-BC1 cells, which may indicate that these vectors utilise a receptor that is absent in these cell types. It is likely that the vectors utilise CAR, and possibly CD46, as their auxiliary rather than primary receptors. Flexibility of the shaft domain is known to be essential for the internalisation step of the viral entry process. Pseudotyping the full amino acid sequence of the long Ad5 fiber with the sequence of a short species D serotype fiber has previously been shown to result in the generation of virions with compromised infectivity due to altered flexibility between the shaft and the knob domains, impairing the interactions between the penton base and αvβ3/5 integrins (Wu et al., 2003). This is in line with our observations of the drastically reduced infectivity for the whole fiber-pseudotyped vectors, and of the less pronounced impairment for the knob-pseudotypes, that may have a favourably flexible fiber protein. Additionally, fiber length has been shown to be crucial for Ad internalisation via CAR- and αv integrin-mediated pathways (Shayakhmetov and Lieber, 2000). The fiber proteins of the species D Ads studied in this thesis are considerably shorter (< 380 aa) than the Ad5 fiber (581 aa) ('Protein' search tool, (NCBI, 2016)), which may influence the infectivity of these serotypes. The pseudotyped vectors may also have altered intracellular processing, which may result in delayed endosomal release or even viral entrapment in the endosomes. An example of this is the species B serotype Ad35 that utilises CD46-mediated macropinocytosis, with delayed release from endocytic vesicles (Kälin et al., 2010). Therefore, the observed reduction in luciferase expression does not necessarily suggest reduced internalisation of the pseudotyped vectors, but may result from inaccessibility of the luciferase gene to the cellular translation machinery. The study

of receptor tropism by luciferase reporter gene assays is therefore not a straightforward indication of the receptor-binding capacity of the vectors. It is also noteworthy that the model cell lines used for the assessment of vector tropism are of hamster origin, and therefore do not simulate an infection in human cells. Further studies on the tropism of these vectors are needed in order to draw meaningful conclusions on their receptor tropism profile, based on transduction efficiency in a wider variety of distinctive cell types. SPR analysis by Biacore or related methods that assess receptor binding kinetics, will be highly valuable tools in the future.

Furthermore, species D Ads are appealing vector candidates due to their low affinity to human FX (Waddington et al., 2008). This has important implications for the desirable avoidance of vector off-target sequestration by hepatocytes, with the view of minimising therapy-related toxicities. We (Figure 4–7) (Parker et al., 2006) and others (Shayakhmetov et al., 2005b, Waddington et al., 2008) have previously shown that the transduction efficiency of Ad5 vectors can be greatly improved by the addition of FX in the transduction medium (Figure 4–7), even in the absence of the primary cellular receptor, CAR. We performed sequence alignments of the Ad5 and Ad10 hexon HVRs and showed that Ad10 and the non-FX-binder serotype Ad26 (Alba et al., 2009) have homologous residues within the five well-described residues that constitute the HVR7 mutation that was developed by Alba and colleagues in order to ablate the FX-binding of Ad5 (Figure 1–21). This finding strongly indicated lack of FX-binding for the novel Ad10 vector, and prompted us to further verify the hypothesis *in vitro*. Supplementation of the transduction medium with physical concentrations of FX had absolutely no impact on the transduction efficiency of the novel vectorised Ad10 serotype in CHO-K1 cells (Figure 5–10C), indicating that this serotype indeed does not bind FX. As discussed in section 4.7, CHO-K1 is a clean model for studying FX-tropism, since the addition of FX enables the transduction of FX-binding Ad serotypes via HSPGs in this otherwise non-permissive cell line.

We then went on to investigate whether pseudotyping with either the full fiber or just the fiber knob with corresponding regions from species D serotypes would have an impact on the FX-tropism of these vectors that carry the Ad5 hexon. Assays performed in CHO-K1, SKOV3 and CHO-CAR cells showed that the higher the CAR-expression level of the cell line, the smaller influence FX supplementation had on vector transduction efficiency as compared to serum-free conditions (Figure 5–9). In the CAR-expressing CHO-CAR cells, the addition of FX had proportionally larger effect on the transduction efficiency of all pseudotyped vectors, than it had on Ad5. As seen in Figure 5–5, Ad5 transduces CHO-CAR cells already more efficiently than

the pseudotyped vectors, which is why FX supplementation does not improve its transduction efficiency as much as it does for the pseudotyped vectors that may be less able to use CAR as their entry receptor, as discussed earlier in this chapter. Taken together, collective observations from all performed *in vitro* assays showed divergent characteristics for both of the Ad5/53 vectors from all other pseudotypes. These vectors will need to be further validated and/or re-generated to exclude the possibility of cross-contamination. All of the pseudotyped Ad5 vectors have Ad5 hexon protein, which is why FX was expected to have a similar impact on their transduction efficiency as it has on Ad5 transduction. The altered pattern seen in our studies may stem from reduced binding to FX, due to physical hindrances in the accessibility of FX to the hexon HVR7, resulting in reduced internalisation. Another explanation could be alternative intracellular processing of the virions and hampered translation of the luciferase gene, as discussed previously in this section.

Species D Ads exhibit lower seroprevalence rates in human populations than the most commonly used gene therapy serotype, Ad5 (Abbink et al., 2007). The lower prevalence of these viruses in the human population may be due to the absence of a suitable cellular receptor in the human epithelia, leading to compromised cell entry and attenuated virulence in humans. Previously it has been proposed that anti-Ad antibodies are primarily directed towards the fiber protein, since pseudotyping Ad5 with Ad45 fiber (Ad5/F45) helped to circumvent vector neutralisation (Parker et al., 2009). It is important to seek alternative vector moieties as the high seroprevalence of Ad5 causes therapeutic vectors to be rapidly eliminated from the blood stream upon systemic delivery, leading to clinically inert vectors [reviewed in (Uusi-Kerttula et al., 2015a)]. In this thesis, we have attempted to evaluate novel Ad candidates from the subgroup D, with the prospect that they could be more suitable vector backbones due to their avoidance of pre-existing humoral anti-Ad5 immunity. To this end, we performed neutralisation assays using the novel vectors Ad10, and two pseudotyped Ad5-based vectors Ad5/F10 and Ad5/kn10, to assess the depth and serotype-specificity of pre-existing humoral immunity in ovarian ascites. Ad10 was better at resisting neutralisation by two different ascitic fluids (OAS001 and OAS019; Figure 3–7), than either of the pseudotyped vectors or the Ad5 vector (Figure 5–11). Based on the presence of anti-Ad10 antibodies in OAS019, this fluid was expected to efficiently neutralise Ad10 and possibly Ad5/F10 and Ad5/kn10 too. As anti-Ad nAbs are thought to be directed against the fiber protein in natural infections (Cheng et al., 2010, Bradley et al., 2012a), it was surprising to find that the vectors with the Ad10 knob-pseudotypes appeared protected from neutralisation, despite the presence of anti-

Ad10 antibodies. However, it is noteworthy that the anti-Ad10 antibodies detected in our anti-Ad ELISA assays may be cross-reactive and/or non-neutralising IgG antibodies rather than nAbs. Regardless, the preliminary data from these *in vitro* assays showed promising potential for using Ad10 or Ad5/Ad10 pseudotyped backbones for improved circumvention of anti-Ad5 vector neutralisation.

We hypothesise that there might be two competing interactions occurring between the Ad vectors and proteins present in ovarian ascites. On the one hand viruses can be efficiently neutralised by nAbs, while on the other hand their efficiency can be enhanced by the high affinity binding to FX that provides an alternative, CAR-independent entry route into the target cells. FX has also been proposed to shield the virion from attack by natural IgM antibodies and the complement, thereby providing a protective shield from innate immune factors (Xu et al., 2013). In this thesis, depletion of FX from ascites further increased the neutralisation of the Ad5 vector but not of the Ad10 vector (Figure 5–10). Since we have shown that Ad10 does not have a measurable tropism for FX (Figure 5–10), and that it is much less readily neutralised by immune ovarian ascites, the observation is in line with the FX:Ad vs. Ad:nAb competition hypothesis. On the contrary for Ad5, in the absence of competition of FX for the virion, nAbs may better access the capsid proteins, coat the virion and prevent it from binding to its cellular entry receptors. It is however, important to consider that not only the affinity but also the relative abundance of FX versus anti-Ad nAbs is likely to contribute to the extent of neutralisation.

Taken together, the novel Ad10 vector generated by our research group seems to have three advantages over the commonly used vector, Ad5: (1) low affinity to CAR that is ubiquitously expressed in healthy tissues but down-regulated in progressive cancers, and (2) lack of FX-binding, both of which may imply favourably decreased off-target delivery *in vivo*, as well as (3) improved resistance of neutralisation by immune ovarian ascites. Ad10 is therefore an appealing candidate for further modifications and functional studies, and can be a useful tool for further modification and utilisation for oncolytic alterations, in combination with cancer-targeting moieties. The work is undergoing in our laboratory to incorporate an αvβ6-targeting peptide in the highly promising Ad10, Ad5/F10 and Ad5/kn10 vector backbones. In this thesis we have also briefly visited the topic of re-targeting the Ad5/kn48 vector to αvβ6-positive EOC *in vitro*, which is further discussed in section 6.2.1.

# CHAPTER 6. Results: *In vitro* assessment of αvβ6 integrin-targeted vectors

# CHAPTER 6. *In vitro* assessment of αvβ6 integrin-targeted vectors

The objective of this chapter was the generation of vectors selectively targeted to αvβ6 integrin receptor, whose expression is exclusively up-regulated in progressive epithelial cancers (Koopman Van Aarsen et al., 2008). This integrin presents an excellent tumour target candidate, since it is completely undetectable in healthy adult epithelia (Ahmed et al., 2002b). This section describes the generation of αvβ6 integrin-targeted replication-deficient and replication-competent oncolytic vectors by AdZ homologous recombineering methods, and their functional assessment in ovarian and other model cancer cell lines *in vitro.* This chapter re-introduces the triple-de-targeted Ad5.3D vector from chapter 4. We were intrigued by the possibility of generating a functional re-targeted Ad5.3D variant by engineering in a new tropism (A20 peptide) and producing this vector in the permissive HEK293-β6 cell line that expresses the αvβ6 receptor. A major part of this chapter is focused on the functional characterisation of the novel, exquisitely tumour-targeted Ad5 vector, Ad5.3D.A20. Generation of an αvβ6 integrin-expressing EOC model cell line for these studies, SKOV3-β6 puro, is described in section 3.1.3. EOC culture phenotyping and selection of αvβ6-positive cultures is further described in section 3.2.2. To better replicate the clinical scenario, vector transduction efficiency was also assessed in primary ovarian cancer ascites-derived EOC cell cultures *ex vivo*, in the presence of neutralising ovarian ascitic fluid.

## 6.1    *In silico* assessment of recombinant knob domains

Chapter 5 describes the generation of novel Ad5 vector backbones with species D serotype fibers. We then went on to evaluate the feasibility of the αvβ6-targeting peptide (A20) insertion in these pseudotyped backgrounds within the four different fiber knob loops – CD, DG, HI and IJ – that have been described for the most commonly used gene therapy vector, species C serotype Ad5. The impact of the targeting peptide insertion on the structural conformation of the knob domain was predicted in an automated homology-modelling software. Furthermore, the location for A20 insertion within the knob sequence was determined based on a sequence alignment of the domain and previously assessed insertion sites for serotypes Ad5 (Coughlan et al., 2009a) and Ad48 (Coughlan et al., 2014).

### 6.1.1   *Sequence alignment of fiber knob loops for A20 peptide insertion*

The FMDV A20 peptide (NAVPNLRGDLQVLAQKVART) has previously been inserted into the Ad5 fiber knob domain within the HI loop in a replication-deficient vector background; the vector was shown to be able to target αvβ6+ cancer cells

(Coughlan et al., 2009a). A20 insertion has also been previously evaluated in the context of a recombinant Ad48 knob protein in knob loops CD, DG loop with a 13-aa deletion (Δ13aaDG.A20), HI and IJ (Coughlan et al., 2014), but has not been incorporated into a whole Ad5/kn48 virion before. In this thesis, the A20 peptide was additionally incorporated in Ad10 fiber knob within regions corresponding to Ad5 knob loops DG and HI. An additional virus was generated with a 5-aa deletion in DG loop (Δ5aaDG.A20) preceding the A20 insertion, whose length and location was selected based on the corresponding 13-aa deletion in the Ad48 knob that had been previously described by our group (Coughlan et al., 2014) (Figure 6–1). The sequence alignment shows the conservation stage of this location in all species D Ad knob domains. This information may be utilised for future re-targeting efforts of alternative species D serotypes.
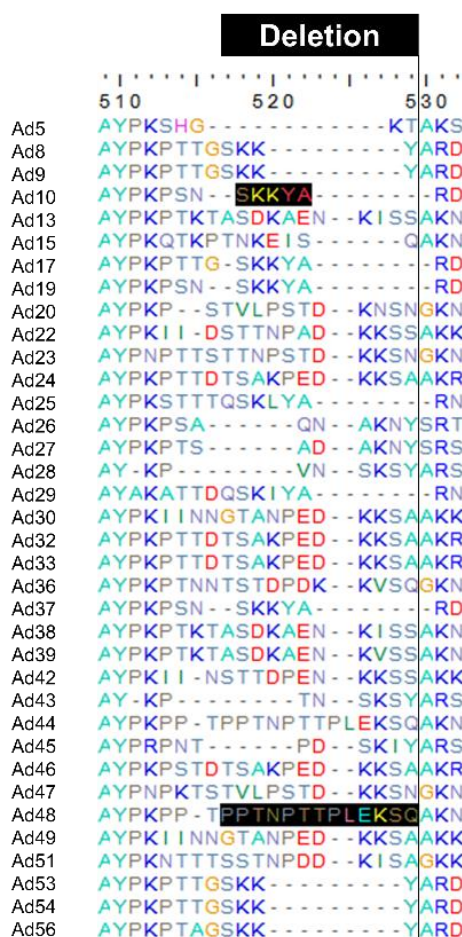


**Figure 6–1. Rationale for the five amino acid deletion in DG loop of the Ad10 fiber knob for the A20 peptide sequence insertion.** Knob sequences were downloaded from National Center for Biotechnology Information website and aligned in BioEdit using ClustalW multiple alignment tool. Sequences were further edited in Microsoft PowerPoint.

The fiber protein of species C Ad5 is 581 aa in length, while the fiber of the species D serotypes Ad10 and Ad48 is considerably shorter, 367 and 373 aa, respectively (NCBI, 2016). Sequence homology between Ad5 and Ad10 fibers is 36 % and 35 % between Ad5 and Ad48 fibers, whilst Ad10 and Ad48 fibers share a larger, 64 % homology. The knob domain itself has a homology of 49 % between Ad5 and Ad10, 48 % between Ad5 and Ad48, and 59 % between Ad10 and Ad48 serotypes. A20 peptide incorporation sites in the fiber knob domain were depicted in a sequence alignment for each of the three serotypes, Ad5, Ad10 and Ad48 (Figure 6–2), based on previously evaluated insertion sites (Coughlan et al., 2009a, Coughlan et al., 2014). DG loop was the only site to accommodate a short deletion in addition to the A20 insertion.
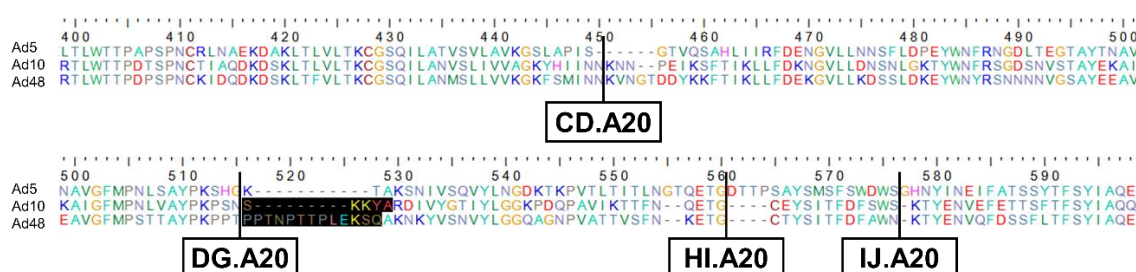


**Figure 6–2. Insertion site for A20 peptide in fiber knob CD, DG, HI and IJ loops.** FMDV A20 peptide was genetically incorporated into locations that had been previously validated for Ad5 knob (Krasnykh et al., 1998, Coughlan et al., 2009a) and Ad48 knob (Coughlan et al., 2014). Amino acid deletion for incorporation into DG loop highlighted in black. A20, NAVPNLRGDLQVLAQKVART.

### 6.1.2   Predictive structural modelling of the knob domain

Trimeric fiber knob protein domains with a genetically inserted A20 peptide sequence were visualised by a predictive SWISS-MODEL structural homology modelling software. A20 insertion sites in each serotype were as follows: loop HI in Ad5; loops DG, Δ5aa.DG (+ 5-aa deletion) and HI in Ad10 knob; loops DG, Δ13aa.DG (+ 13-aa deletion) and HI in Ad48 knob. Predictive modelling indicated favourable spatial conformation the A20 peptide in loops DG and HI, as it was seen as a protruding loop structure projecting away from the core of the domain. In contrast, when A20 was inserted in loops CD and IJ, it seemed to have been buried deep in the domain, indicating that these locations are not likely to be feasible. It is however, crucial to keep in mind that these structures do not represent the whole virion, but merely a hypothetical prediction of the knob domain. Therefore, no conclusions on the viral fitness of the complete virions could be drawn based on these structures. However, these models were useful for matching the predicted structure to the success rate of rescuing the respective virions in a T-REx-293 human production cell line *in vitro* (described in section 6.2).
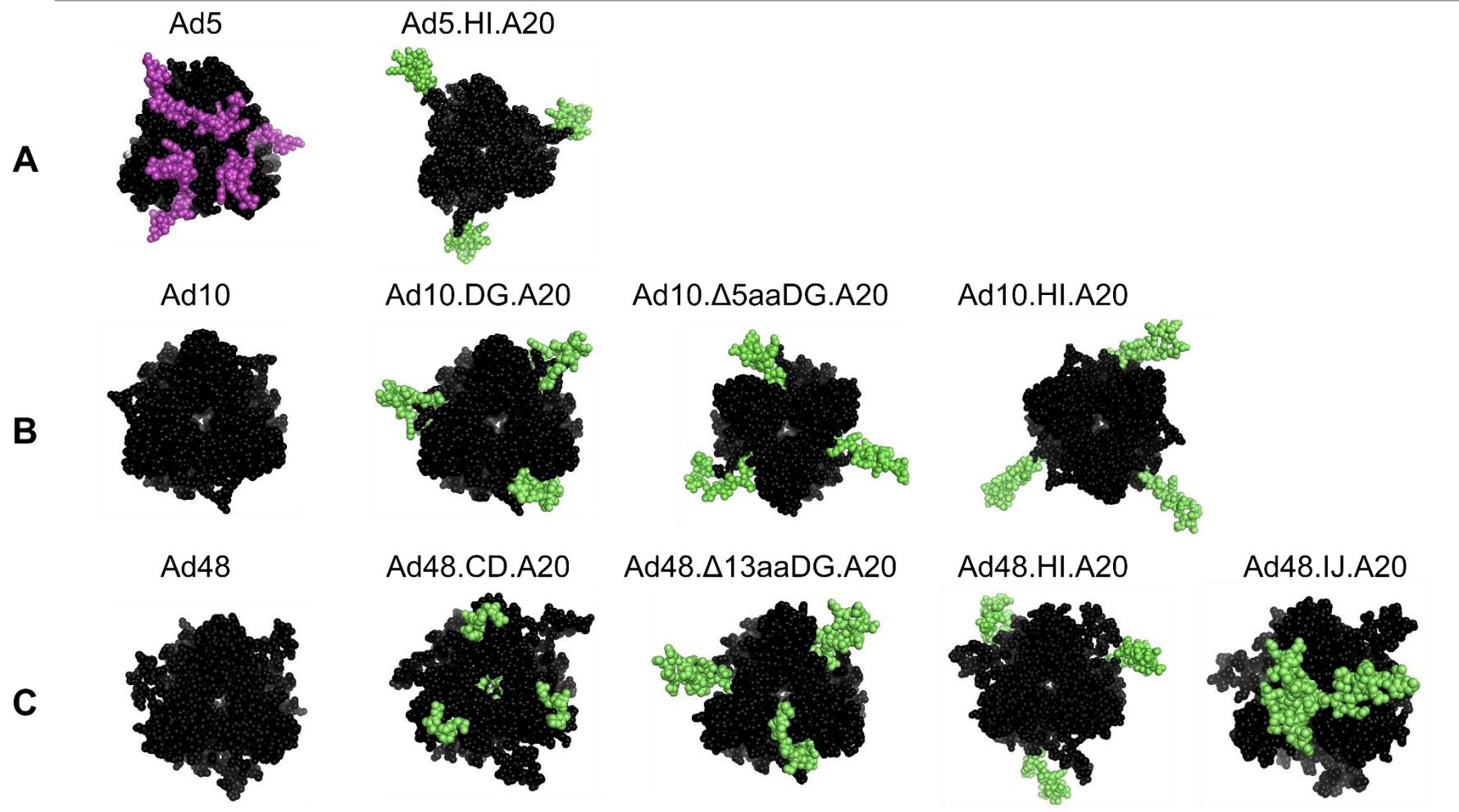
**Figure 6–3. Predictive structural modelling of species D adenovirus knob domains with an A20 targeting peptide insertion.** (A) Ad5, (B) Ad10 and (C) Ad48 fiber knob with A20 peptide insertion in structural knob loops CD, DG, HI and IJ. Structures were based on either the Ad5 knob PDB model (ID: 1KNB) or species D structures Ad19p (PDB ID: 1UXB) or Ad37 (PDB ID: 2WGU), based on highest sequence homology. aa, amino acid; A20 sequence NAVPNLRGDLQVLAQKVART highlighted in green; immunodominant HI loop in Ad5 knob (Xia et al., 1994) highlighted in purple; Δ, amino acid (aa) deletion.

## 6.2   Generated αvβ6 integrin-targeted vectors

Vector genomes were generated as BACs by AdZ homologous recombineering. Infectious viruses were then rescued from the BAC genome and propagated into high viral titres in permissive T-REx-293 or HEK293-β6 puro cells, both of which express the Ad proteins E1 and E3. HEK293-β6 puro cell line stably expresses the target receptor for these vectors – αvβ6 integrin – under puromycin selection, and was utilised to further facilitate virus production (a kind gift from Dr Lynda Coughlan, University of Oxford). After successful transfection and generation of high titre stocks, the vectors were purified by two-step CsCl gradient ultracentrifugation, dialysed and titered by microBCA assay for their physical titre (vp/mL).

### 6.2.1   Replication-deficient vectors

A comprehensive panel of αvβ6 integrin-targeted vector genomes within several different basal backgrounds were generated in close collaboration with Dr James Davies, Cardiff University. The nucleotide sequence corresponding the A20 peptide sequence was inserted into the basal and de-targeted Ad5 vector BAC genomes (Table 6–1) that have also been modified to carry a series of native tropism-ablating mutations in the fiber, hexon and penton proteins (described previously in detail in chapter 4). Both Luc- and GFP-expressing versions of the viral vector backbones were generated as BACs. However, the production of several of the GFP-expressing vectors as infectious viruses was not attempted due to time limitations of this project. Unfortunately, we were unable to rescue viable, infectious virions from several of the vector backbones (Table 6–1; denoted as 'BAC'), despite several transfection attempts in both T-REx-293 and HEK293-β6 puro cells. However, all successfully rescued vectors were produced into very high viral titres (Table 6–1), indicating feasible functioning of the production system. Pleasingly, we were able to generate the remarkably exciting basal Ad5.3D.A20 vector that is fully depleted of all native interactions (αvβ3/5 integrins, CAR, FX) and selectively re-targeted to a cancer marker, αvβ6 integrin.

**Table 6–1. Recombinant αvβ6 integrin-targeted vectors in de-targeted backgrounds.** Vector genomes were generated as bacterial artificial genomes (BAC) and produced in T-REx-293 or HEK293-β6 cells. Viruses were purified by CsCl-gradient ultracentrifugation and titered by microBCA assay. A20, NAVPNLRGDLQVLAQKVART; CAR, coxsackie and adenovirus receptor; FX, human coagulation factor 10; GFP, green fluorescent protein; HVR7, FX-binding mutation; KO1, CAR-binding ablation; Luc, firefly luciferase; RGE, αvβ3/5 integrin-binding mutation; vp, viral particle.

| Virus | Known binding ligands | Physical titre (vp/mL) |
|---|---|---|
| Ad5.Luc.A20 | CAR, αvβ3/5/6, FX | $5.5 \times 10^{12}$ |
| Ad5.GFP.A20 | CAR, αvβ3/5/6, FX | BAC |
| Ad5.Luc.KO1.A20 | αvβ3/5/6, FX | $3.1 \times 10^{12}$ |
| Ad5.GFP.KO1.A20 | αvβ3/5/6, FX | $3.8 \times 10^{11}$ |
| Ad5.Luc.RGE.A20 | CAR, αvβ6, FX | $3.3 \times 10^{12}$ |
| Ad5.GFP.RGE.A20 | CAR, αvβ6, FX | BAC |
| Ad5.Luc.HVR7.A20 | CAR, αvβ3/5/6 | $5.9 \times 10^{12}$ |
| Ad5.GFP.HVR7.A20 | CAR, αvβ3/5/6 | BAC |
| Ad5.Luc.KO1.RGE.A20 | αvβ6, FX | BAC |
| Ad5.GFP.KO1.RGE.A20 | αvβ6, FX | $8.9 \times 10^{10}$ |
| Ad5.Luc.KO1.HVR7.A20 | αvβ3/5/6 | BAC |
| Ad5.GFP.KO1.HVR7.A20 | αvβ3/5/6 | $5.8 \times 10^{10}$ |
| Ad5.Luc.KO1.RGE.HVR7.A20 | αvβ6 | $3.0 \times 10^{12}$ |
| Ad5.GFP.KO1.RGE.HVR7.A20 | αvβ6 | BAC |

The A20 peptide sequence was also incorporated into the species D pseudotyped vector backgrounds (Table 6–2). We attempted to rescue the αvβ6-targeted Ad5/Ad10 pseudotyped vectors in both T-REx-293 and HEK293-β6 cells. Of these vectors only the Ad5/F10 and Ad5/kn10 pseudotyped vectors with A20 in DG loop with or without the 5-aa deletion could be rescued as infectious virions and produced into high viral titres (Table 6–2). These pseudotyped and re-targeted vectors took an average of two weeks to come through, which is about four days longer than for Ad5-based vectors commonly. Unfortunately, despite 4–5 individual transfection attempts in both T-REx-293 and HEK293-β6 cells, A20 insertion in pseudotyped Ad5/F10 or Ad5/kn10 in HI loop did not result in infectious virions. Similarly, rescue of Ad5/kn48 with A20 peptide insertion in CD, HI and IJ loops was not successful despite several individual attempts. This is likely to be due to the compromised fitness of these virions, due to conformational disruptions by A20 insertion in these loops. The BAC genomes of Ad10.A20 vectors with A20 insertions (Table 6–2; 'BAC') have now been generated by homologous recombineering by Ms Jana Váňová, and their rescue as virions is currently undergoing in our laboratory. Unfortunately, the timescale of this project did not allow for the *in vitro* testing of these novel and exciting vector backbones.

**Table 6–2 Generated αvβ6 integrin-targeted vectors in the species D pseudotyped background.** BAC, bacterial artificial genome; CAR, coxsackie and adenovirus receptor; FX, coagulation factor 10; Luc, luciferase; vp, viral particle, –, no infectious virus could be rescued.

| Virus | Predicted binding ligands | Stage or titre (vp/mL) |
|---|---|---|
| Ad10.Luc.DG.A20 | αvβ6, CAR? | BAC |
| Ad10.Luc.Δ5aaDG.A20 | αvβ6, CAR? | BAC |
| Ad10.Luc.HI.A20 | αvβ6, CAR? | BAC |
| Ad5/F10.Luc.DG.A20 | αvβ6, FX, CAR? | $1.0 \times 10^{12}$ vp/mL |
| Ad5/F10.Luc.Δ5aaDG.A20 | αvβ6, FX, CAR? | $1.2 \times 10^{12}$ vp/mL |
| Ad5/F10.Luc.HI.A20 | αvβ6, FX, CAR? | – |
| Ad5/kn10.Luc.DG.A20 | αvβ6, FX, CAR? | $2.1 \times 10^{12}$ vp/mL |
| Ad5/kn10.Luc.Δ5aaDG.A20 | αvβ6, FX, CAR? | $1.6 \times 10^{12}$ vp/mL |
| Ad5/kn10.Luc.HI.A20 | αvβ6, FX, CAR? | – |
| Ad5/kn48.Luc.CD.A20 | αvβ6, FX, CAR? | – |
| Ad5/kn48.Luc.DGΔ13aa.A20 | αvβ6, FX, CAR? | $8.5 \times 10^{11}$ vp/mL |
| Ad5/kn48.Luc.HI.A20 | αvβ6, FX, CAR? | – |
| Ad5/kn48.Luc.IJ.A20 | αvβ6, FX, CAR? | – |

### 6.2.2 Oncolytic vectors

Wild type vectorised Ad5.Luc with intact *E1* and *E3* gene regions was further modified for oncolytic purposes by insertion of two mutations that render the vector cancer-selective and improve its lytic efficiency. Luciferase-expressing, oncolytic vector BAC genomes were all generated by Dr James Davies, Cardiff University, via introduction of de-targeting mutations and genetic A20 peptide sequence insertion within the knob HI loop. An Δ24 mutation, a 24-base pair deletion (*dl*922–947) in the pRB binding domain of *E1A* (Fueyo et al., 2000), was included to restrict viral replication to cancer cells that have a deficient pRB pathway. Additionally, a T1 mutation – a single adenine insertion at position 445 within the ER retention domain of *E3/19K* – was inserted to improve viral particle release from the ER (Gros et al., 2008). These vectors were all rescued and produced into high viral titres in T-REx-293 or HEK293-β6 puro cells (Table 6–3). In this thesis, the oncolytic vectors were assessed *in vitro*. *In vivo* studies for the assessment of the oncolytic activity of these vectors are currently underway at our collaborator Prof Richard Vile's laboratory at Mayo Clinic, Rochester, Minnesota, USA.

**Table 6–3. Generated oncolytic adenovirus vectors.** Δ24, a 24-base pair deletion (*dl922–947*) in the retinoblastoma protein (pRB) binding domain of *E1A*; Luc, luciferase transgene; T1, a single adenine insertion at position 445 within the endoplasmic reticulum (ER) retention domain of *E3/19K*; pfu, plaque forming unit; vp, viral particle. The vectors that were further assessed in this thesis, are abbreviated with an 'O' (oncolytic) to distinguish them from the replication-deficient versions of these vectors.

| | Virus | Abbreviation | Physical titre (vp/mL) | Infectious titre (pfu/mL) | Ratio (vp:pfu) |
|---|---|---|---|---|---|
| **De-targeted** | Ad5.Luc.Δ24 | | $7.02 \times 10^{11}$ | $2.67 \times 10^{10}$ | 26 |
| | Ad5.Luc.Δ24.T1 | OAd5 | $1.12 \times 10^{12}$ | $2.08 \times 10^{10}$ | 54 |
| | Ad5.Luc.Δ24.KO1 | | $1.22 \times 10^{12}$ | $7.20 \times 10^{8}$ | 1695 |
| | Ad5.Luc.Δ24.T1.KO1 | OAd5.KO1 | $1.11 \times 10^{12}$ | $5.32 \times 10^{8}$ | 209 |
| | Ad5.Luc.Δ24.HVR7 | | $1.52 \times 10^{12}$ | $6.06 \times 10^{10}$ | 25 |
| | Ad5.Luc.Δ24.T1.HVR7 | OAd5.HVR7 | $1.06 \times 10^{12}$ | $2.50 \times 10^{10}$ | 42 |
| **Re-targeted** | Ad5.Luc.Δ24.A20 | | $1.74 \times 10^{12}$ | $5.82 \times 10^{10}$ | 30 |
| | Ad5.Luc.Δ24.T1.A20 | OAd5.A20 | $2.17 \times 10^{12}$ | $9.15 \times 10^{10}$ | 24 |
| | Ad5.Luc.Δ24.KO1.A20 | | $3.73 \times 10^{11}$ | $2.44 \times 10^{10}$ | 15 |
| | Ad5.Luc.Δ24.T1.KO1.A20 | OAd5.KO1.A20 | $1.72 \times 10^{12}$ | $4.60 \times 10^{10}$ | 37 |
| | Ad5.Luc.Δ24.HVR7.A20 | | $9.73 \times 10^{11}$ | $4.40 \times 10^{10}$ | 22 |
| | Ad5.Luc.Δ24.T1.HVR7.A20 | OAd5.HVR7.A20 | $1.50 \times 10^{12}$ | $3.62 \times 10^{10}$ | 41 |
| | Ad5.Luc.Δ24.KO1.HVR7.A20 | | $1.12 \times 10^{12}$ | $4.16 \times 10^{10}$ | 27 |
| | Ad5.Luc.Δ24.T1.KO1.HVR7.A20 | OAd5.KO1.HVR7.A20 | $5.78 \times 10^{11}$ | $1.66 \times 10^{10}$ | 35 |
| | Ad5.Luc.Δ24.KO1.HVR7.RGE.A20 | | $1.96 \times 10^{12}$ | $1.07 \times 10^{10}$ | 183 |
| | Ad5.Luc.Δ24.T1.KO1.HVR7.RGE.A20 | OAd5.3D.A20 | $1.51 \times 10^{12}$ | $2.44 \times 10^{9}$ | 619 |

## 6.3    *In vitro* assessment of αβ6 integrin-targeted adenoviruses

The generated replication-deficient vectors were assessed in representative *in vitro* assays for their ability to transduce αβ6 integrin-positive cancer cells, and for their receptor tropism in haemagglutination assays. Furthermore, their selectivity for the αβ6 integrin was assessed in competition inhibition assays using relevant inhibitory proteins and blocking antibodies. Additionally, the oncolytic vectors (OAd) were assessed for their *in vitro* oncolytic potency in cell viability assays over a 10-day time-course. The αβ6 integrin-targeted vectors were also assessed for their ability to evade pre-existing humoral anti-Ad immunity in the presence of highly neutralising clinical ovarian ascites from patients with advanced ovarian cancer.

### 6.3.1    *Haemagglutination assays*

CAR-tropism of the αβ6-targeted vectors was assessed in haemagglutination assays using whole human blood as described in section 4.3. Haemagglutination pattern was determined visually by grading from no agglutination (–) to complete agglutination (+++). Interestingly, the presence of A20 peptide in the context of Ad5.A20, Ad5.RGE.A20 and Ad5.HVR7.A20 vectors was shown to partially compromise CAR-binding, although these viruses do not carry the KO1 mutation that ablates CAR-binding (Figure 6–4; rows 1, 3 and 4). The effect was most pronounced

for the Ad5.RGE.A20 vector that had only partial agglutination at the highest dose, low agglutination at second highest dose, but no agglutination at two of the lowest doses (Figure 6–4; row 3). As expected, the parental Ad5.RGE completely agglutinated erythrocytes due to its native CAR-binding [see previously (Figure 4–3)]. No haemagglutination was observed at any dose for viruses that have both the KO1 mutation and the A20 peptide, including the triple de-targeted virus Ad5.3D.A20. Ad5/kn48.Δ13DG.A20 vector exhibited an altered CAR-tropism due to the A20 peptide insertion, as compared to the pseudotyped Ad5/kn48 vector that did not agglutinate erythrocytes at any viral dose (Figure 5–4 and Figure 6–4; row 9).



**A**

|  | 1x10⁹ vp | | | 7.5x10⁸ vp | | | 5x10⁸ vp | | | 2.5x10⁸ vp | | |
|---|---|---|---|---|---|---|---|---|---|---|---|---|
| 1) Ad5.A20 | +++ | +++ | +++ | ++ | ++ | ++ | + | + | + | − | − | − |
| 2) Ad5.KO1.A20 | − | − | − | − | − | − | − | − | − | − | − | − |
| 3) Ad5.RGE.A20 | ++ | ++ | ++ | + | + | + | − | − | − | − | − | − |
| 4) Ad5.HVR7.A20 | +++ | +++ | +++ | ++ | ++ | ++ | + | + | + | − | − | − |
| 5) Ad5.KO1.RGE.A20 | − | − | − | − | − | − | − | − | − | − | − | − |
| 6) Ad5.KO1.HVR7.A20 | − | − | − | − | − | − | − | − | − | − | − | − |
| 7) Ad5.3D.A20 | − | − | − | − | − | − | − | − | − | − | − | − |
| 8) Ad5/kn48.Δ13DG.A20 | +++ | +++ | +++ | ++ | ++ | ++ | + | + | + | − | − | − |
| 9) Ad5/kn48 | − | − | − | − | − | − | − | − | − | − | − | − |

**B**

− PBS

+ RBC lysis buffer
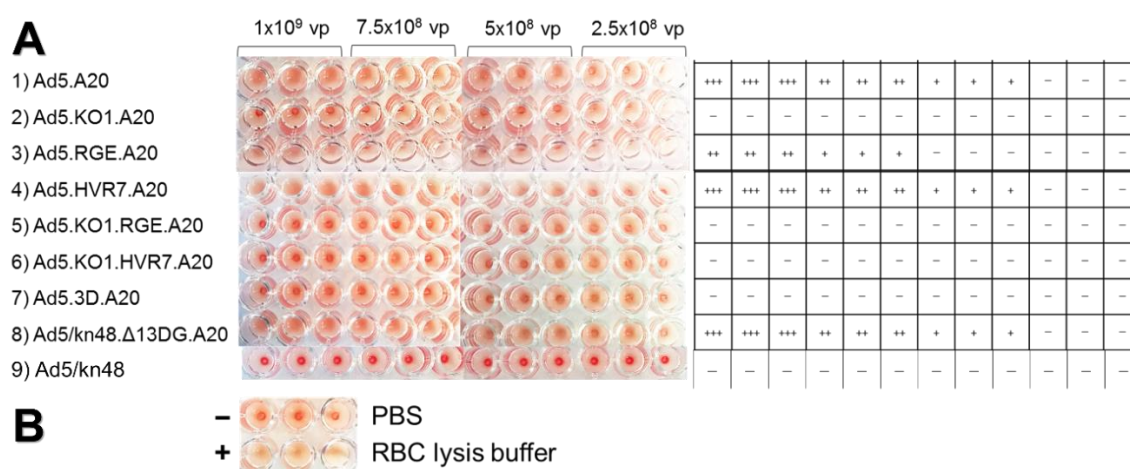
**Figure 6–4. Haemagglutination assay on the αvβ6 integrin-targeted vectors.** (A) Viruses were mixed with 1 % erythrocyte solution in PBS at four different concentrations and incubated for 2 h at 37ºC. (B) Negative control in the assay was PBS, and positive control red blood cell (RBC) lysis buffer. PBS, phosphate buffered saline; vp, viral particle. Haemagglutination grading: +++ complete; ++ midrange; + partial; − no haemagglutination (Nicol et al., 2004).

### 6.3.2  Re-targeting in αvβ6-positive cell lines and primary EOC cultures

The generated αvβ6-targeted viruses were assessed in selected model cell lines that express varying levels of αvβ6 integrin and CAR (Table 3–1). As all of the assessed vectors express the Luc reporter transgene, the relative cell transduction efficiency of each vector could easily be assessed by performing *in vitro* luciferase assays in a 96-well plate format. A model cell line SKOV3-β6 puro (section 3.1.3) was generated as an αvβ6-positive control cell line for the assessment of αvβ6-targeted vectors. Four established primary EOC *ex vivo* cultures that were shown to be positive for αvβ6 (Figure 3–6), were included as a clinically representative counterpart for the vector assessment, to better represent a clinical scenario. We also used the breast cancer cell line BT-20 as a positive control cell line due to its high level of αvβ6 and low level of CAR expression.
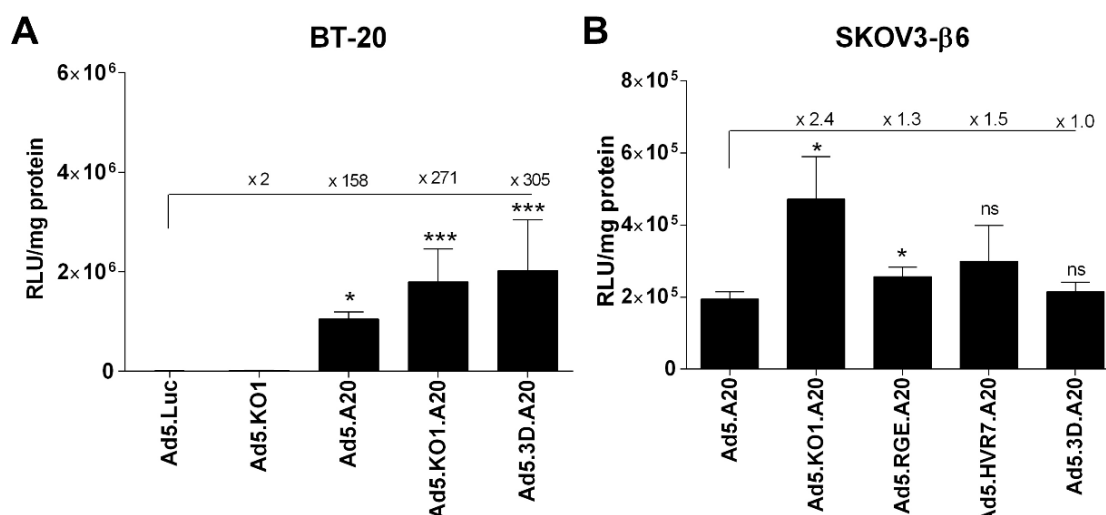
**Figure 6–5. αvβ6 integrin-targeted vector transduction in breast (BT-20) and (B) ovarian cancer cells (SKOV3-β6).** Cells were infected with 5000 viral particles/cell in triplicate for 3 h and luciferase expression quantified 48 h later. Relative light units (RLU) were normalised to total protein in each cell (RLU/mg). Data were analysed in GraphPad Prism using one-way ANOVA with Dunnett's multiple comparisons *post hoc* test. *, $p < 0.05$; **, $p < 0.01$; ***, $p < 0.001$.

We have previously reported that Ad5.KO1.HI.A20, Ad5.HI.A20 and Ad5/kn48.Δ13aaDG.A20 vectors transduced αvβ6$^{high}$/CAR$^{low}$ BT-20 breast cancer cells at 160-, 270- and 180-fold increased efficiency relative to Ad5.Luc (Uusi-Kerttula et al., 2016). Additionally, αvβ6-mediated cell entry of these viruses was significantly inhibited both by a function-blocking anti-αvβ6 antibody 10D5 and a recombinant Ad48.Δ13aaDG.A20 knob protein, but not by control IgG antibody or kn5.CAR–recombinant protein, in these cells. In this thesis we also evaluated the ability of the triple de-targeted and αvβ6-re-targeted Ad5.3D.A20 vector to transduce the BT-20 and SKOV-β6 cells. The Ad5.3D.A20 vector was shown to transduce BT-20 cells at ~ 300-fold increased efficiency relative to Ad5.Luc (Figure 6–5). Similarly, all A20 vectors, regardless of de-targeting mutations, transduced SKOV3-β6 cells at highly efficient levels that were similar to the Ad5.A20 vector (Figure 6–5). Additionally, we assessed the efficiency of these vectors to transduce clinical αvβ6+ EOC cell cultures *ex vivo*. While Ad5.Luc had the highest efficiency of all vectors in the αvβ6$^{low}$/CAR$^{med}$ EOC003 cells, the overall efficiency of all αvβ6-targeted vectors was very low in these cells (Figure 6–6A). On the contrary, all αvβ6-targeted vectors transduced the αvβ6$^{high}$/CAR$^{med}$ EOC004 cells at up to ~ 70-fold improved efficiency relative to Ad5.Luc that cannot utilise αvβ6 for cell entry (Figure 6–6B). The pattern seen in αvβ6$^{low}$/CAR$^{med}$ EOC016 cells was similar to the transduction efficiency observed in EOC003 cells that express only low levels of the αvβ6 integrin (Figure 6–6C).
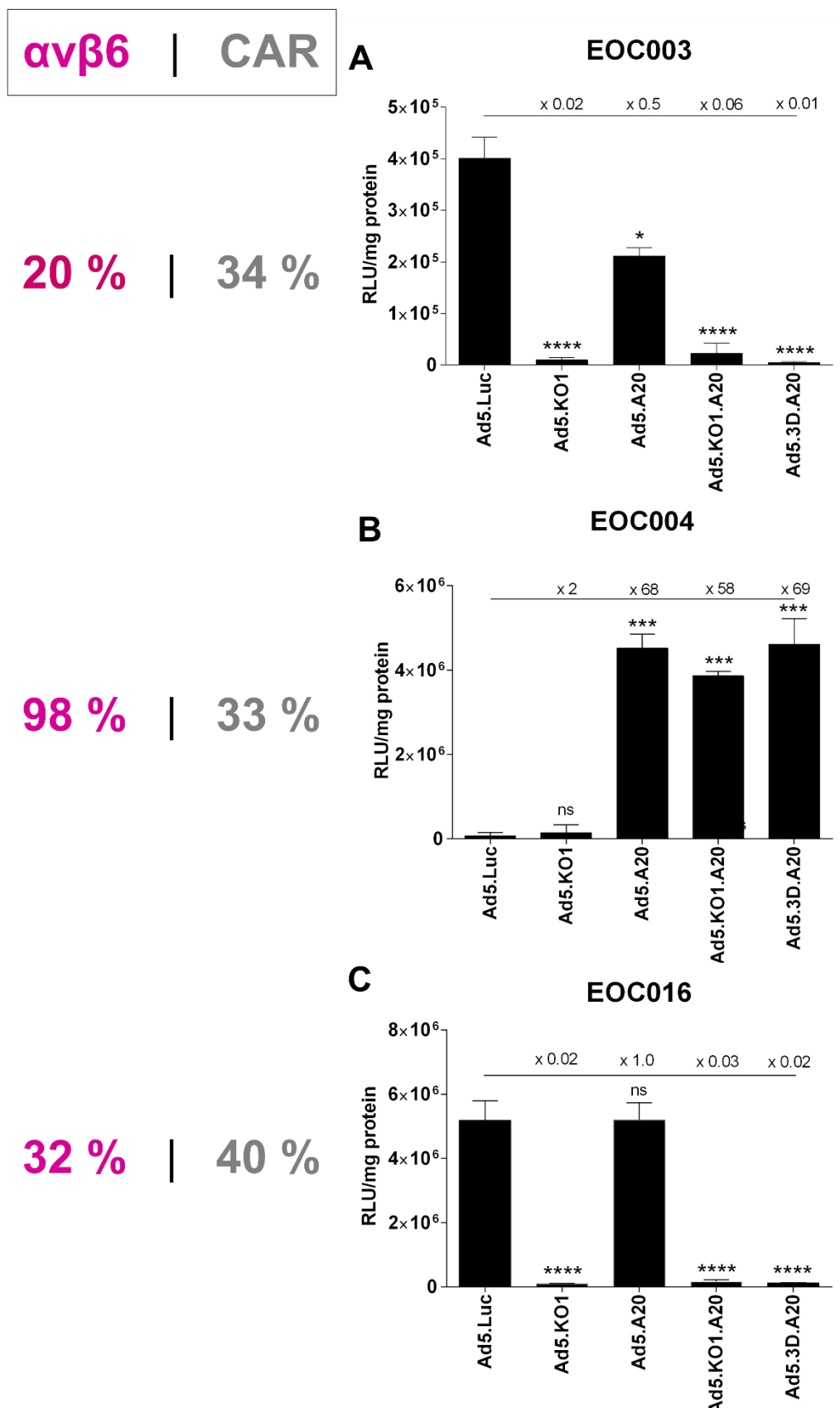
**Figure 6–6. Transduction efficiency in αvβ6-expressing primary *ex vivo* epithelial ovarian cancer (EOC) cultures.** Cells were infected with 5000 viral particles/cell in triplicate for 3 h and luciferase expression quantified 48 h later. Relative light units were normalised to total protein in each cell (RLU/mg). Data were analysed in GraphPad Prism using one-way ANOVA and Dunnett's multiple comparison *post hoc* test. *, $p < 0.05$; **, $p < 0.01$; ***, $p < 0.001$; ****, $p < 0.0001$.

### 6.3.3 Competition inhibition assays for verification of vector tropism for αvβ6

A panel of αvβ6-targeted, Ad5-based viruses were assessed in competition inhibition assays in representative cell lines to verify the central involvement of αvβ6 receptor in cell entry. We have previously shown that transduction of all basal Ad5 vectors carrying the A20 targeting peptide, as well as the pseudotyped Ad5/kn48.Δ13aaDG.A20 vector, was significantly inhibited by both a function-blocking anti-αvβ6 antibody 10D5 and a recombinant kn48.Δ13aaDG.A20 protein in BT-20 (αvβ6$^{high}$/CAR$^{low}$) cells (Uusi-Kerttula et al., 2016). Using the observations from the αvβ6+ BT-20 breast cancer cell line as a positive reference (Figure 6–7A), αvβ6 integrin-blocking assays were additionally performed in SKOV3-β6 ovarian cancer cells, following a second round of cell sorting into highly αvβ6-positive cell populations by FACS (Figure 6–7B). αvβ6-mediated vector transduction was shown to be successfully blocked for both αvβ6-re-targeted A20 viruses, Ad5.A20 (p = 0.0029) and Ad5.3D.A20 (p = 0.001) in SKOV3-β6 cells, as compared to the 'virus only' conditions for each virus (Figure 6–7B).
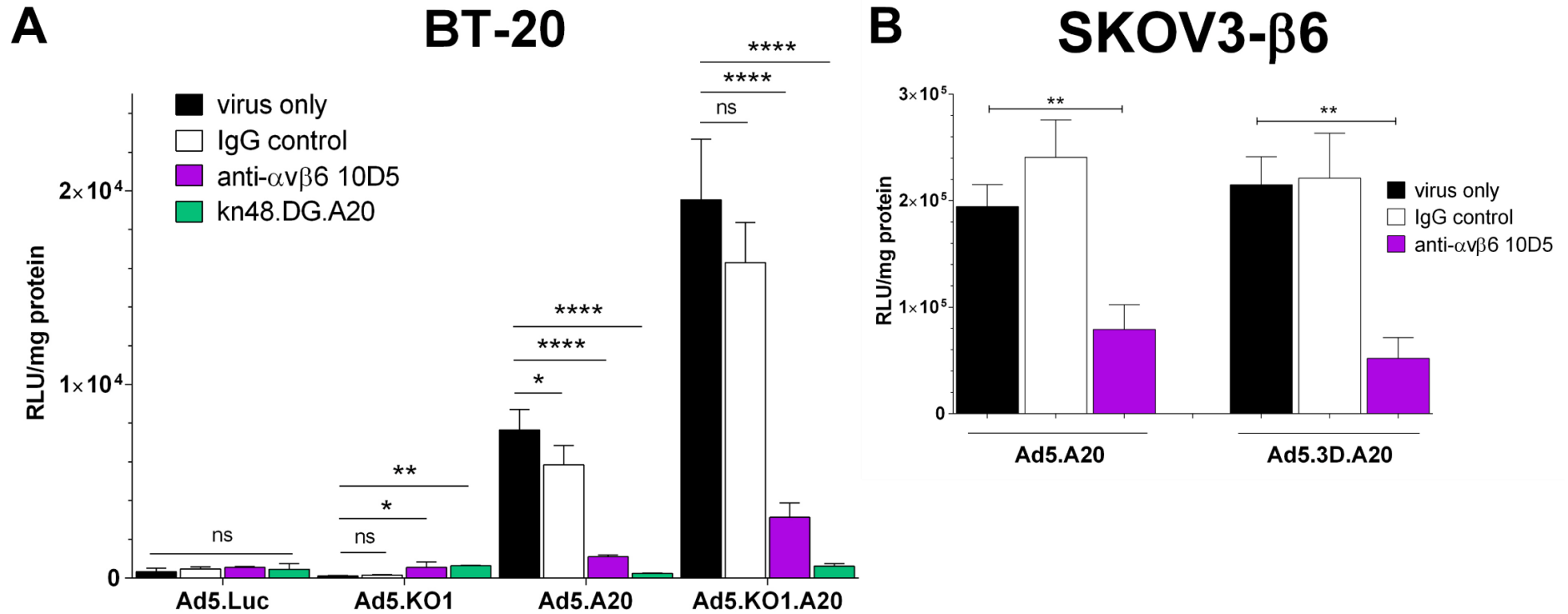
**Figure 6–7. Competition inhibition of αvβ6 integrin-mediated cell entry.** (A) BT-20 breast cancer and (B) SKOV3-β6 ovarian cancer cells were pre-incubated with normal mouse IgG control, recombinant knob proteins or function-blocking antibodies for 30 min on ice, and viruses added at 5000 virus particles/cell for 2 h on ice. Transgene expression was quantified 48 h later. Error bars indicate the difference to the corresponding virus in non-inhibited, serum-free conditions ('virus only'). Statistical analysis was performed using one-way ANOVA and Dunnett's multiple comparisons *post hoc* test; * p < 0.05, ** p < 0.01, *** p < 0.001.

### 6.3.4 Oncolytic vector transduction in vitro

The generated αvβ6 integrin-targeted oncolytic vectors were assessed in luciferase assays for their *in vitro* transduction efficiency to ensure they were capable of transducing αvβ6+ cells at equal efficiency to their replication-deficient counterparts. As predicted, the OAd5 vector transduced both SKOV3 and SKOV3-β6 cells at equal efficiency, due to the equal levels of CAR-expression in these two cell lines (Figure 6–8). On the contrary, all αvβ6-targeted OAds, with the exception of OAd5.HVR7.A20 vector, showed increased transduction in SKOV3-β6 cells as compared to the non-αvβ6-expressing parental cell line SKOV3 (Figure 6–8). Most importantly, the OAd5.3D.A20 vector exhibited the largest increase of all tested viruses in SKOV3-β6 cells relative to SKOV3 cells (> 5-fold increase). We also assessed the transduction efficiency at 72 h post-infection. However, a large proportion of SKOV3-β6 cells had already died – presumably due to oncolytic activity – and therefore luciferase expression could not be reliably quantified at this later time-point (data not shown). Inversely, very low levels of luciferase expression were detected at an earlier time-point, at 24 h post-infection (data not shown).
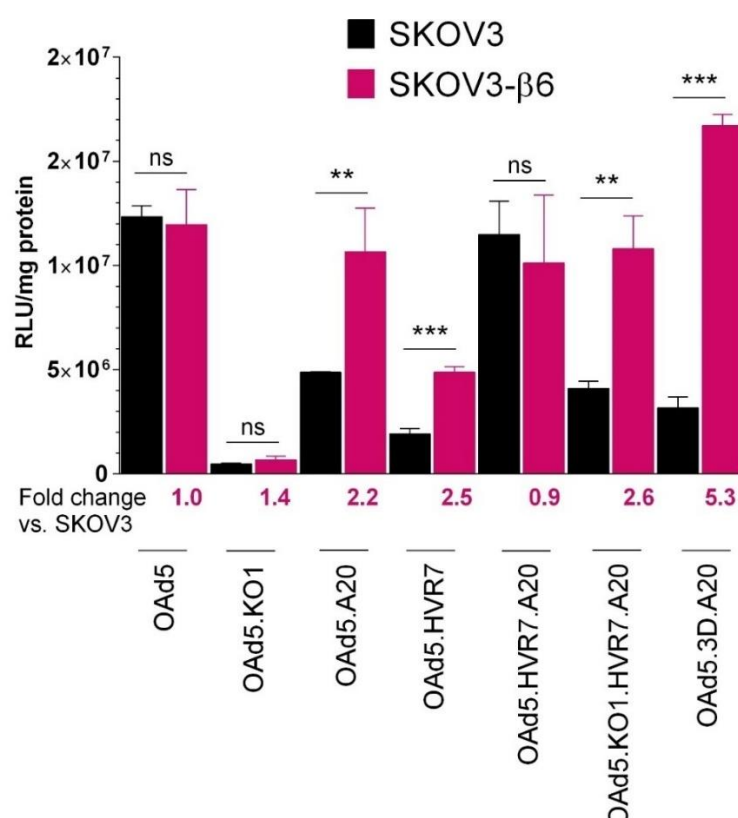


**Figure 6–8. Oncolytic vector transduction efficiency in epithelial ovarian cancer cell lines.** SKOV3 and SKOV3-β6 ovarian cancer cells were infected at 5000 viral particles/cell for 3 h, transgene expression quantified 48 h later, and normalised to relative light units/total protein (RU/mg). Error bars indicate statistical difference between the two cell lines for each virus. Statistical analysis was performed using unpaired, two-tailed T test; ns, $p > 0.05$; * $p < 0.05$; ** $p < 0.01$; *** $p < 0.001$.

### 6.3.5 *Cytotoxicity of oncolytic vectors*

Cell viability assays were utilised to evaluate the cell killing efficiency of the oncolytic vectors by a colorimetric MTS assay. Cells were infected in the same manner as in regular luciferase transduction assays, but plates were incubated in closed humidified containers to prevent the medium from evaporating during the lengthy time-course. At time-points 24, 48, 72, 96, 120, 144, 168, 192, 216 and 240 h (10 days) post-infection, following the addition of assay reagent, the proportion of live SKOV3 cells (Figure 6–9A) and SKOV3-β6 (Figure 6–9B) in each infection well was quantified, and normalised to the absorbance in the 'cells only' control wells (% cell viability). Additionally, BT-20 breast cancer cells were assessed as a representative cell line of $\alpha v\beta 6^{high}/CAR^{low}$ cells (Figure 6–9C). The uninfected control cells remained healthily confluent throughout the duration of the experiment.

At the earliest time-point of 24 h, no cell death was observed for any of the three viruses at any viral dose in either cell line (Figure 6–9). At a dose of 1000 vp/cell, SKOV3 cells were not remarkably affected by any virus at any time-point, and retained close to 100 % viability until day 10 (Figure 6–9A; top panel). At a higher viral dose of 5000 vp/cell, OAd5 vector had killed up to 50 % SKOV3 cells by day 5 (Figure 6–9A; middle panel). However, these cells appeared to have acquired resistance to all of the viruses, as they grew back by day 6, and only slowly started dying off again towards the end of the time-course. Similar, but more pronounced pattern was observed at a viral dose of 25 000 vp/cell, as cells acquired full viability on day 6, despite having had only ~ 20 % viability on day 5 (Figure 6–9A; bottom panel). The triple de-targeted OAd5.3D.A20 vector was not capable of killing SKOV3 cells at doses 1000 and 5000 vp/cell (Figure 6–9A; top and middle panel, respectively). However, the vector unexpectedly killed these cells at equal efficiency to OAd5 and OAd5.A20 when the cells were saturated with a high dose of 25 000 vp/cell (Figure 6–9A; bottom panel). The SKOV3-β6 cells seemed to be overall much more sensitive to the oncolytic treatment by all three vectors than their parental SKOV3 cells (Figure 6–9B). Close to 100 % cell death was observed at all viral doses for all three vectors by the end of the time-course, on day 10. Oncolysis by OAd5 was shown to be the most efficient at viral doses of 1000 and 5000 vp/cell (Figure 6–9B; top and middle panel, respectively), while all three viruses were equally efficient at cell killing at the highest viral dose of 25 000 vp/cell (Figure 6–9B; bottom panel).
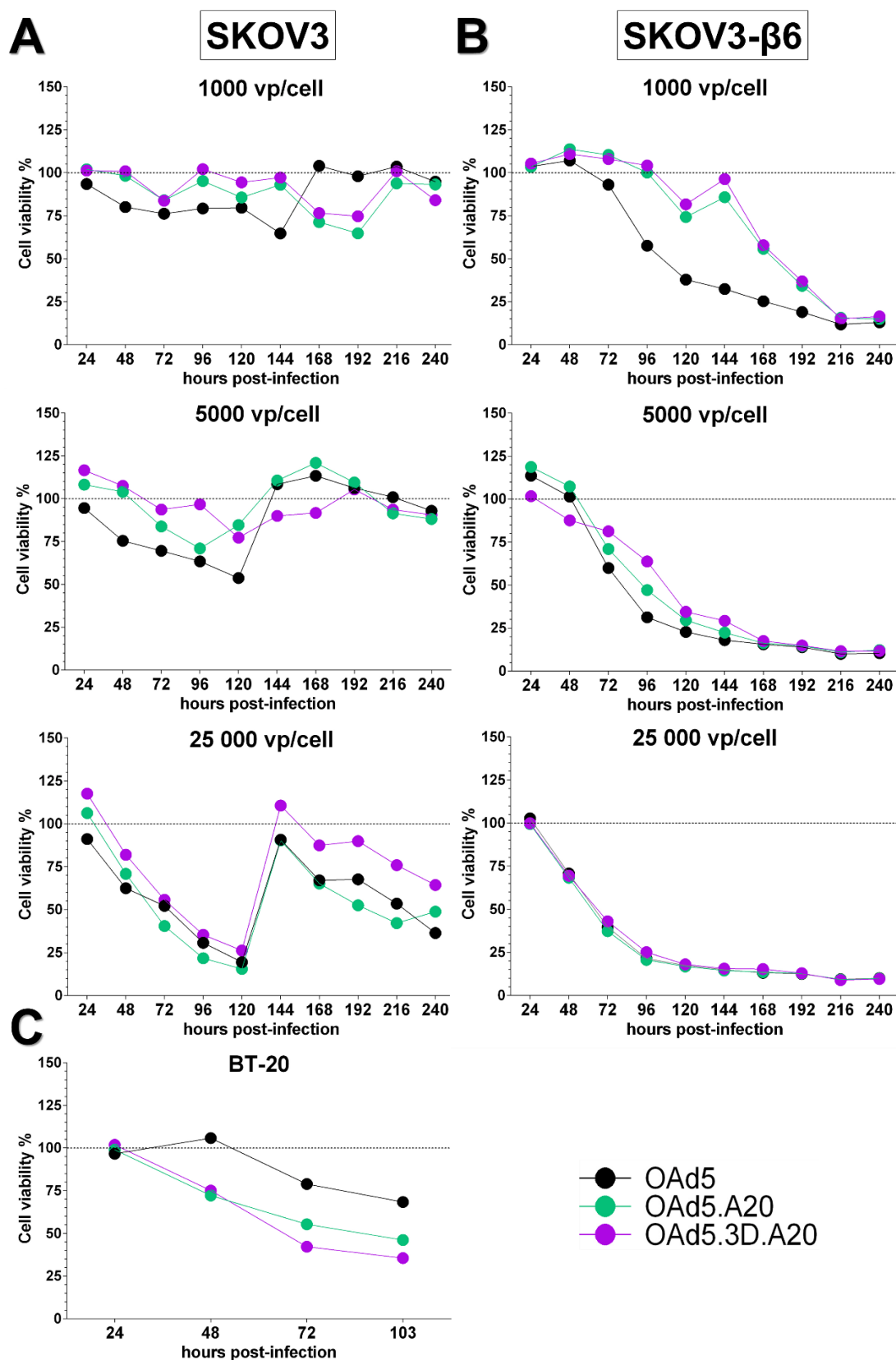
**Figure 6–9. Cytotoxicity of oncolytic vectors.** (A) SKOV3 and (B) SKOV3-β6 epithelial ovarian cancer cells were infected with 1000, 5000 or 25 000 viral particles (vp)/cell and (C) BT-20 breast cancer cells at 25 000 vp/cell for 3 h. 20 μL of assay reagent (5 % total concentration) was added into each well, and absorbance measured at λ490 nm following a 2 h incubation at 37ºC in the dark. Cell viability (%) was quantified by a colorimetric MTS assay, relative to the viability of uninfected cells.

We also assessed oncolytic activity in the positive control cell line BT-20 to demonstrate efficacy in the absence of CAR expression. The Ad5.3D.A20 vector had superior cytotoxicity over the OAd5 and OAd5.A20 vectors at the last two time points, 72 h and 103 h (Figure 6–9C). At the assay endpoint, the viability of cells infected with OAd5, OAd5.A20 and OAd5.3D.A20 was 68.4, 46.2 and 35.6 %, respectively.

### 6.3.6 Neutralisation by ovarian ascites

Transduction efficiency of the αvβ6-targeted replication-deficient vectors was also assessed in the presence of highly neutralising cell-free ascites OAS001 (see Figure 3–9 for antibody titres). Cell line BT-20 and EOC004 primary culture were used as model cultures for this assay due to their high level of αvβ6 and low level of CAR expression. All αvβ6-targeted vectors were shown to transduce BT-20 cells with high efficiency at up to 10 % concentration of ascites, the Ad5.3D.A20 vector having superior protection from neutralisation compared to all other vectors (Figure 6–10A). The other two A20 peptide-carrying vectors had a similar but slightly lower transduction efficiency in these cells (Figure 6–10A; open symbols). Vector transduction in EOC004 cells again showed that Ad5.3D.A20 was able to transduce these cells with high efficiency, resisting neutralisation at up to 5 % concentration of ascites (Figure 6–10B). Similar to BT-20 cells, all non-αvβ6-tropic vectors without the A20 targeting moiety were completely unable to transduce these cells (Figure 6–10B). Despite improved protection, the A20 peptide did not fully help the vectors to evade neutralisation, as each of them, including the Ad5.3D.A20, were completely neutralised in the presence of 40 % and higher concentrations of ascites in both cell cultures (Figure 6–10). Regardless, the A20 targeting moiety enabled efficient vector transduction and remarkably increased vector protection from neutralisation by immune ovarian ascites.

**A — BT-20**

Fold increase vs. Ad5

| | virus | 1:40 | 1:20 | 1:10 | 1:5 | 1:2.5 |
|---|---|---|---|---|---|---|
| Ad5.KO1 | 1 | 2 | 0.2 | 0.1 | 0.1 | 0.6 |
| Ad5.A20 | 9 | 11 | 2 | 2 | 2 | 2 |
| Ad5.KO1.A20 | 9 | 11 | 2 | 3 | 11 | 8 |
| Ad5.3D.A20 | 10 | 11 | 2 | 3 | 6 | 3 |

**B — EOC004**

Fold increase vs. Ad5

| | virus | 1:40 | 1:20 | 1:10 | 1:5 | 1:2.5 |
|---|---|---|---|---|---|---|
| Ad5.KO1 | 46 | 70 | 18 | 3 | 2 | 2 |
| Ad5.A20 | 104 | 876 | 753 | 369 | 60 | 23 |
| Ad5.KO1.A20 | 102 | 860 | 950 | 765 | 99 | 23 |
| Ad5.3D.A20 | 137 | 865 | 902 | 453 | 187 | 18 |
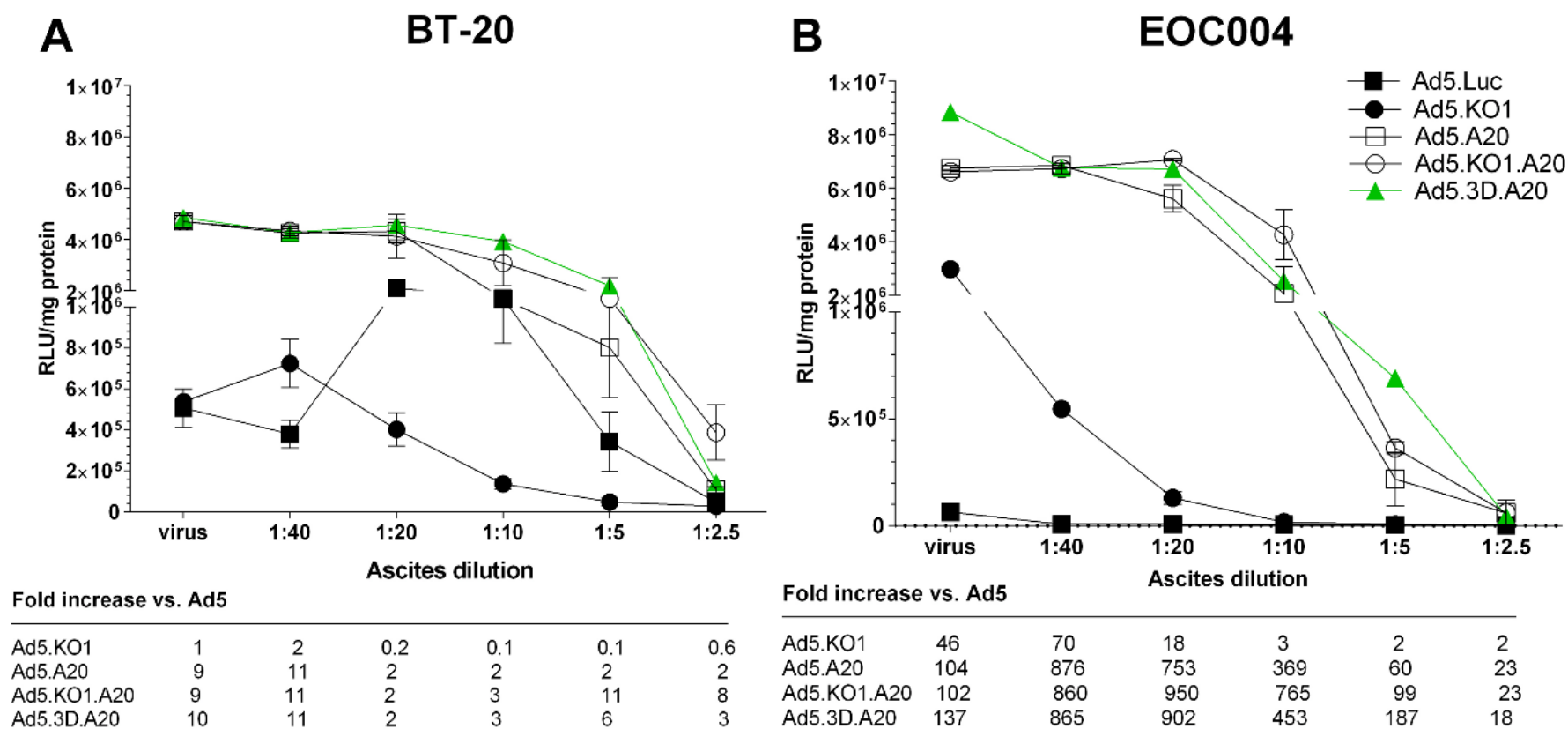
**Figure 6–10. αvβ6-targeted vector transduction efficiency in the presence of neutralising ascites.** (A) BT-20 breast cancer and (B) primary epithelial ovarian cancer cells from patient 4 (EOC004) were transduced with 200 000 viral particles/cell in the presence of descending two-fold dilutions of cell-free ovarian ascites (OAS001). Luciferase activity was measured 48 h post-infection and relative light units normalised to total protein concentration in each well (RLU/mg). 'virus' denotes transduction level in ascites-free conditions.

## 6.4    Discussion

The epithelial-specific integrin αvβ6 is an intriguing cancer marker due to its negligible expression levels in healthy adult epithelium (Ahmed et al., 2002b). It is rapidly up-regulated during epithelial re-modelling events such as foetal development, injury, wound healing and neoplasia (Breuss et al., 1995, Thomas et al., 2006). αvβ6 is known to be involved in cancer progression by functioning as a key up-stream activator of TGF-β1 (Hezel et al., 2012), thereby enhancing cell motility and migration, angiogenesis and EMT, among other mechanisms [reviewed in (Khan and Marshall, 2016)]. It is the main native cellular entry receptor for two positive-strand RNA viruses that belong to the *Picornaviridae* family: FMDV (Miller et al., 2001) that infects pharynx and soft palate of hooved cattle (Monaghan et al., 2005), and of coxsackievirus A9 (CAV-9) that causes respiratory illnesses, infections of the central nervous system and myocarditis (Williams et al., 2004, Heikkilä et al., 2009). Both viruses bind αvβ6 with high affinity via the RGD motif located in the C-terminal extension of their capsid protein VP1. αvβ6 has also been suggested to function as a gH/gL receptor of HSV by promoting viral endocytosis (Gianni et al., 2013). αvβ6 is constitutively expressed in the tongue and interdigital skin epithelium in cattle (Monaghan et al., 2005) but is absent in healthy oral epithelia in humans (Thomas et al., 2006). To date, none of the Ad serotypes have been shown to use αvβ6 integrin as their native receptor for host cell entry.

This chapter describes the generation, production and functional evaluation of Ad5-based vectors targeted to cancer cells that express αvβ6 integrin. The vectors have been rendered αvβ6-specific by a genetic incorporation of an A20 peptide (NAVPNLRGDLQVLAQKVART) from the capsid protein VP1 of FMDV that has a natively high affinity to this receptor (DiCara et al., 2007, Dicara et al., 2008). The αvβ6-targeted vectors were successfully grown into high viral titres and assessed for their transduction efficiency in suitable cell lines *in vitro* and in primary EOC cultures *ex vivo*. We have shown that these vectors are efficiently targeted to cellular αvβ6 integrin in both αvβ6+ cell lines (Figure 6–5) and in αvβ6+ primary EOC *ex vivo* cultures (Figure 6–6). Based on the observations from competition inhibition assays, the A20 peptide indeed does efficiently target the vectors to αvβ6 in cells that express high levels of the receptor, since cell entry could be efficiently inhibited by previously described function-blocking agents, an anti-αvβ6 antibody 10D5 (Weinreb et al., 2004) and recombinant kn48.Δ13aaDG.A20 protein (Uusi-Kerttula et al., 2016) (Figure 6–7). On the contrary, when cellular CAR level is medium or high, and the αvβ6 level low, the αvβ6-mediated cell entry is outcompeted by CAR-mediated entry for

vectors that have natively high affinity to CAR. This observation on the strong affinity of Ad5 to CAR underlines the necessity for the accommodation of the CAR-binding mutation KO1 into therapeutic vectors in order to avoid non-specific sequestration by non-target cells. The combination of KO1 mutation and A20 insertion gave rise to vectors that are capable of selectively entering cells with high αvβ6 integrin expression.

We also performed haemagglutination assays to further elucidate the vector tropism for CAR, based on the observations that erythrocytes express CAR and can therefore trap vectors to the blood stream (Carlisle et al., 2009), possibly impacting off-target delivery. Surprisingly, the A20 peptide remarkably decreased vector binding to CAR, even in the absence of the CAR-binding ablation, KO1 mutation (Figure 6–4). Although the A20 peptide is incorporated in a different knob loop (HI loop) than the KO1 mutation (AB loop), the spatial conformation of the bulky heterologous peptide may physically hinder the access of the CAR-binding residues to the receptor. Predictive 3D models created in SWISS-MODEL software (Figure 6–3) did not reveal major structural disruptions brought on by the A20 insertion. It is however, important to acknowledge that in the absence of high resolution crystallisation data, the models are nothing but a 'best guess' of the knob structure. Furthermore, the 3D predictions did not reliably predict the success of A20 peptide insertion in various different knob loops in the knobs of species D serotype vectors either. Despite the favourable-looking structure of the protruding A20 loop in the HI loop of Ad10 and Ad48 knob domain (Figure 6–3), these viruses could not be rescued as functional virions (Table 6–2). The only exception was Ad48.IJ.A20, whose A20 peptide insertion in Ad48 knob loop IJ did not appear structurally favourable in the predictive 3D model, nor did it produce a functional virion *in vitro*. Although Ad vectors are known to be a very flexible vector backbone that are known to tolerate large insertions and deletions, it is never easy to predict which modifications allow the production of functional virions without compromising viral fitness. In this thesis we have shown that both fiber pseudotyping and heterologous peptide incorporation can result in highly unpredictable tropisms and significantly alter vector functionality.

In this chapter we describe the generation and assessment of a panel of bi-functional vectors that are both de-targeted from native interactions, and simultaneously re-targeted to αvβ6-expressing cancer cells. Our lead candidate vector is Ad5.3D.A20, that has shown simultaneous de-targeting from all native interactions (αvβ3/5 integrins, CAR and FX) and efficient re-targeting to αvβ6 integrin *in vitro* and *ex vivo*. Importantly, cell viability assays showed promising oncolytic

activity in the SKOV3-β6 EOC cell line (αvβ6+/CAR+). However, as the Ad5 vector is able to enter these due to their CAR-expression, it had superior oncolytic efficacy over both of the OAd5.A20 and OAd5.3D.A20 vectors, both in SKOV3 and SKOV3-β6 cells (Figure 6–9). Promisingly, the OAd5.3D.A20 showed superior oncolysis in breast cancer cell line BT-20 to the non-αvβ6-targeted OAd5 that was not capable of entering these cells due to the lack of an entry receptor. This vector presents an exciting candidate for anti-cancer vector targeting to αvβ6-positive ovarian cancer and other cancer types that express high levels of αvβ6, such as cervical or skin cancer that have been shown to have close to 100 % expression of αvβ6 (Koopman Van Aarsen et al., 2008). The replication-deficient version of the Ad5.3D.A20 vector was further assessed *in vivo* in a biodistribution study, whose outcomes are discussed in chapter 7. The oncolytic efficacy of the OAd5.3D.A20 vector will be assessed in an *in vivo* survival study in immunocompromised SKOV3-β6 ovarian cancer xenograft model in NOD/SCID mice in spring 2017.

# CHAPTER 7.  Results: *In vivo* vector biodistribution and generation of an ovarian cancer model

# CHAPTER 7. *In vivo* vector biodistribution and generation of an ovarian cancer model

This chapter describes the *in vivo* characterisation of replication-deficient, αvβ6 integrin-targeted vectors in wild type non-tumour-bearing B6 albino mice. Vectors were administered i.v. and biodistribution in the main off-target organs – liver, spleen, lungs, heart and ovaries – was evaluated at 72 h post-infection by the quantification of luciferase expression and viral genome copy number by qPCR. Additionally, we were interested in assessing the breadth of innate antiviral inflammatory responses elicited by the vectors bearing de-targeted mutations in the capsid proteins (described in chapter 4), since the literature suggests they should have improved toxicological profiles. We have also generated and optimised an i.p. SKOV3-β6 ovarian cancer xenograft model in immunocompromised NOD/SCID mice to represent the clinical scenario of an advanced intraperitoneally metastasised EOC. The model will be utilised for subsequent assessment of oncolytic vector efficacy in a survival study. Due to the time limitations, the results from the efficacy study are not discussed in this thesis.

## 7.1 Biodistribution study in wild type mice

In this study the biodistribution and tissue tropism of replication-deficient, de-targeted and αvβ6-targeted Ad5-based vectors was studied in wild type female B6 albino mice. Mice were allowed to acclimatise for a week, and then challenged with a single i.v. injection of $1 \times 10^{11}$ vp of replication-deficient Ad vectors diluted in a total volume of 100 µL of PBS / mouse on day 0. All animals tolerated the virus challenge very well, and no treatment-related adverse effects or changes in appearance or behaviour were observed. The animals were observed daily, and then sacrificed on day 3 by inhalation of $CO_2$.

### 7.1.1 Temporal and spatial luciferase expression by IVIS imaging

Tropism in peripheral tissues following intravascular delivery of the luciferase-expressing replication-deficient viral vectors was monitored by non-invasive, semi-quantitative IVIS imaging from live animals at 72 h following systemic delivery. Mice were injected i.p. with 200 µL of D-luciferin, rapidly anaesthetised by inhalation of isoflurane, and imaged within 5 min of D-luciferin administration one group (n = 5) at a time. Luminescence signal (total photons/second/cm$^2$/steradian) was normalised on a single representative scale for all images to exclude the negligible levels of background luminescence and to limit saturation of the highly luminescent (red) areas. Luciferase expression from the viral vectors was variable between treatment

groups, and clearly focused within the area of liver and spleen. No luminescence was detected in the control group (PBS) animals, while mice treated with the parental Ad5.Luc vector had the visibly highest level of luminescence of all treatment groups (Figure 7–1).
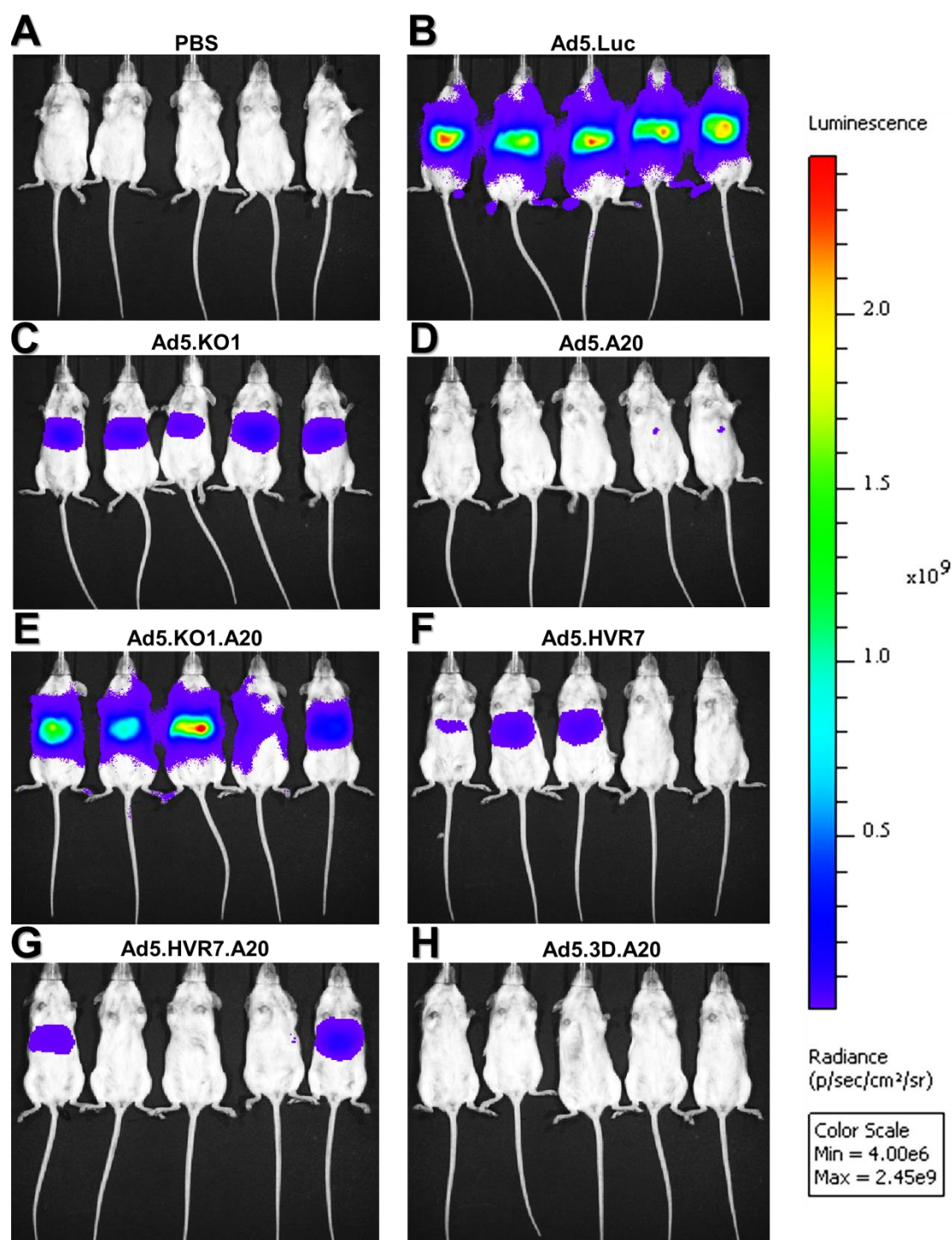


**Figure 7–1. Adenovirus vector biodistribution in live mice at 72 h following systemic delivery.** Mice were anaesthetised by inhalation of isoflurane, and administered intraperitoneally with 200 µL of D-luciferin at 15 mg/mL and imaged after 5 min with 1 min exposure in Xenogen IVIS 200 luminescence imager. Images were adjusted in Living Image software on a normalised scale (photons/second/cm$^2$/steradian). Colours indicate the relative luminescence intensity.

Large differences were observed in the total number of photons emitted by the live animals in each group (Figure 7–2). The mice injected with the Ad5.KO1 or Ad5.A20 (p = 0.0224) vectors had overall ~ 10-fold lower levels of luciferase activity compared to the animals injected with Ad5.Luc, while mice treated with Ad5.KO1.A20 had similar luminescence levels to the Ad5.Luc animals. Both FX-binding -ablated vectors, Ad5.HVR7 and Ad5.HVR7.A20, had ~ 10-fold lower average levels of luciferase activity as compared to Ad5.Luc. In contrast to all other treatment groups, mice infected with the Ad5.3D.A20 vector exhibited extremely low luciferase activity that was close to the background luminescence levels (PBS group) and significantly lower (p = 0.0006) than luminescence in the Ad5.Luc group. The highest level of luminescence in the mice in the Ad5.3D.A20 group was seen in the tail, which was the site of vector administration.
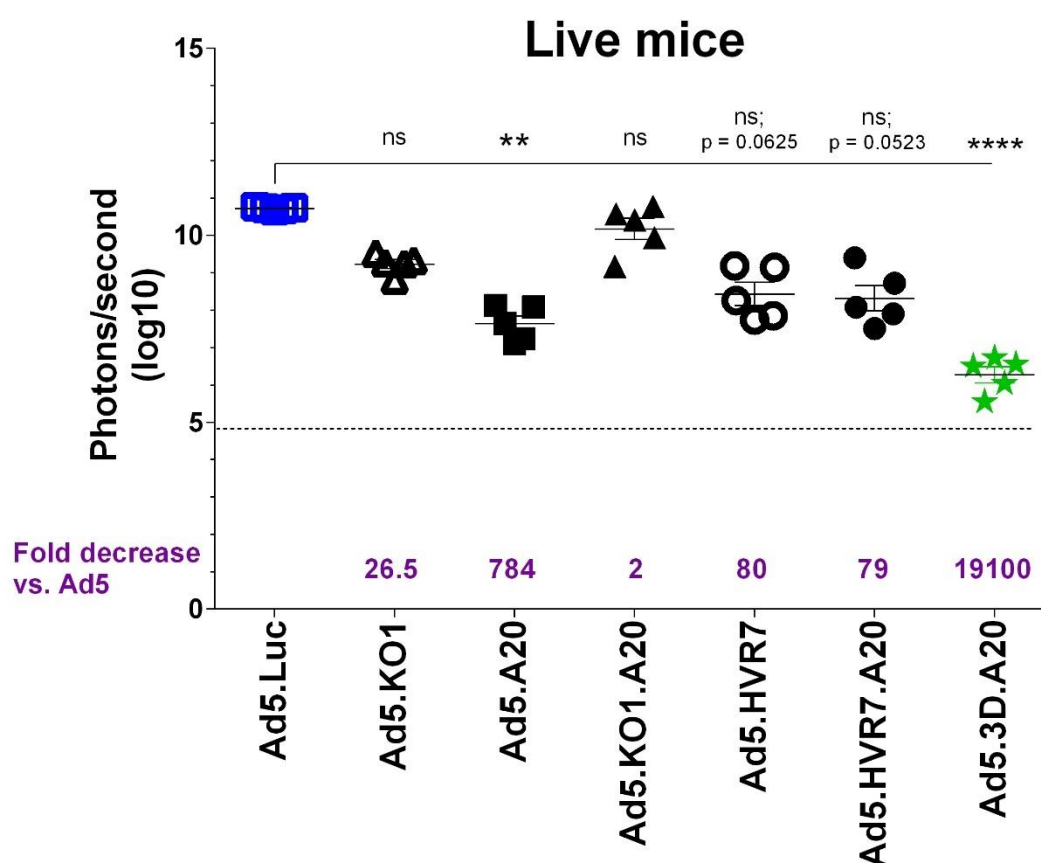


**Figure 7–2. Total luminescence signal in live mice.** The animals were anaesthetised at 72 h post-infection one group at a time, and imaged in Xenogen IVIS 200 imager within 5 min of intraperitoneal D-luciferin injection. Luminescence was recorded for each individual mouse as total photons / second in each treatment group, and presented on a log10 scale with the mean of control (PBS) group subtracted from all values. Data were analysed by Kruskal–Wallis test and multiple comparisons by Dunn's *post hoc* test in GraphPad Prism. Error bars represent standard error of the mean; n = 5/group; *, p < 0.05; **, p < 0.01; ***, p < 0.001; ****, n < 0.0001; ns, no statistical significance relative to Ad5.Luc group. Baseline luminescence for the PBS group is shown as a dotted line.

### 7.1.2  Ex vivo organ luminometry
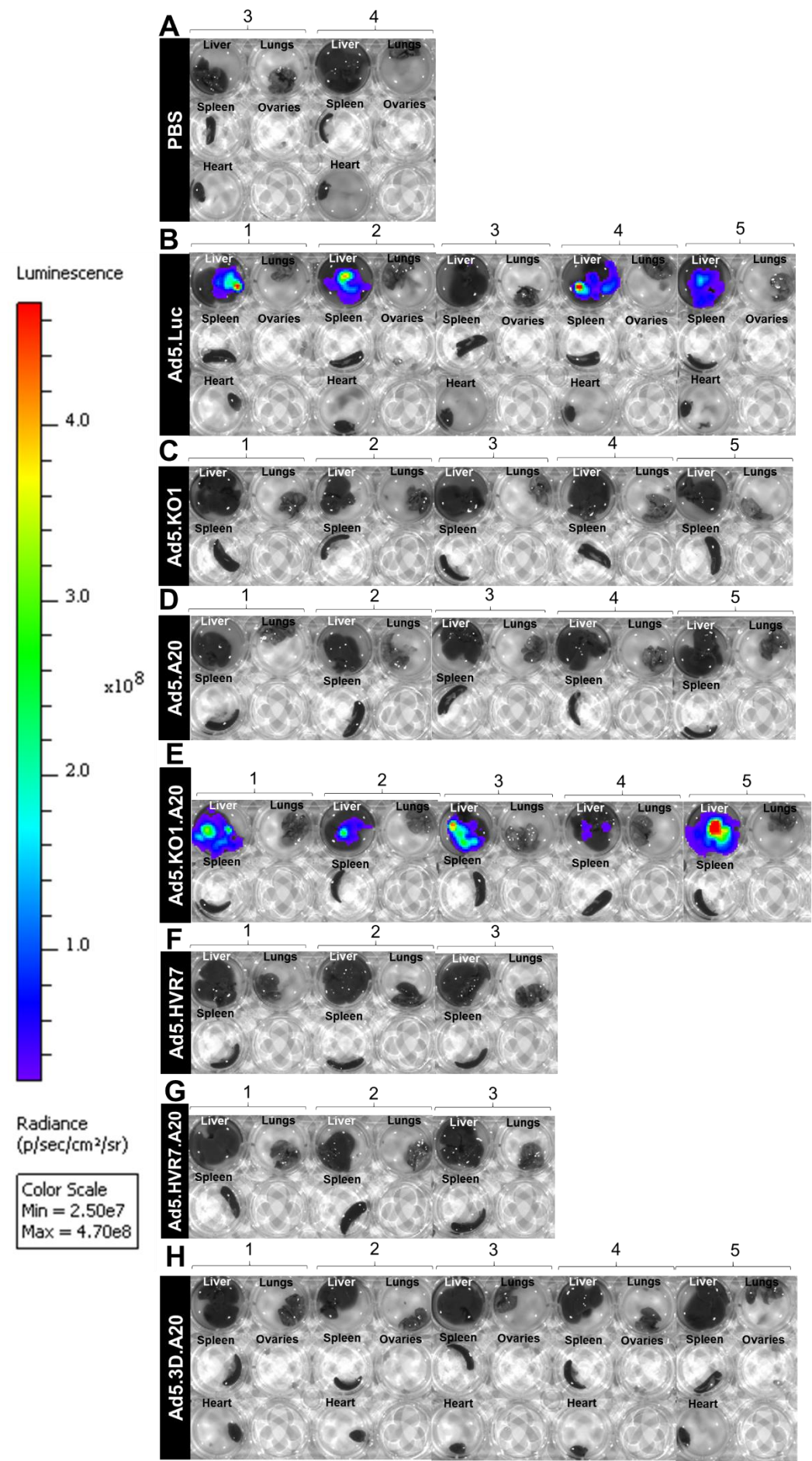
**Figure 7–3. Luciferase expression by adenoviral vectors in individual organs.** Organs were harvested immediately post-mortem and placed in 12-well plates with 2 mL of D-luciferin reagent at 300 µg/mL. Luminescence signal was detected by the Xenogen IVIS 200 imager with 1 min exposure time. The scale was normalised across treatment groups to minimise background luminescence and saturated pixels.

Liver, lungs, spleen, heart and ovaries were harvested from mice in groups A, B and H (n = 5), while only liver, lungs and spleen were harvested from mice in groups C, D, E, F and G (n = 3) post-mortem. Organs were analysed for *ex vivo* luciferase expression to correlate with the pattern seen in *in vivo* imaging. Intact organs were placed on 12-well plates with 1 mL of PBS, 1 mL of D-luciferin added on the top (final concentration: 300 µg/mL), and imaged immediately (Figure 7–3). In general, the majority of luciferase activity was localised in the liver in all treatment groups, and no measurable luminescence was detected in the spleens or other organs by this method. We also observed the organs for any possible abnormalities in size or shape. Mouse #1 in Ad5.KO1 group had an enlarged spleen (image not shown) but no increased luciferase activity was detected in this organ.

As expected, all harvested organs from mice infected with Ad5.Luc had very high levels of luciferase activity (Figure 7–4). The mice infected with the Ad5.3D.A20 vector had significantly decreased luminescence in all harvested organs as determined by multiple comparisons test relative to Ad5.Luc in the same organs (Figure 7–4A–E). Additionally, the transduction mediated by Ad5.KO1, Ad5.A20, Ad5.HVR7 and Ad5.HVR7.A20 was decreased in liver, spleen and lungs, although statistically significant difference was not observed relative to Ad5.Luc, potentially due to high variability of the data (Figure 7–4A, B, C). Mice infected with Ad5.KO1.A20 had a surprisingly high level of luminescence in liver, spleen and lungs – only slightly lower than the luminescence in the Ad5.Luc group (Figure 7–4A, B, C). This was unexpected, since the level of transduction in both Ad5.KO1 and Ad5.A20 groups was lower than in the Ad5.Luc group. Ovaries and heart were harvested only from the PBS, Ad5.Luc and Ad5.3D.A20 groups; the Ad5.3D.A20 vector showed significantly reduced luminescence signal as compared to Ad5.Luc in both of these organs (Figure 7–4D, E).
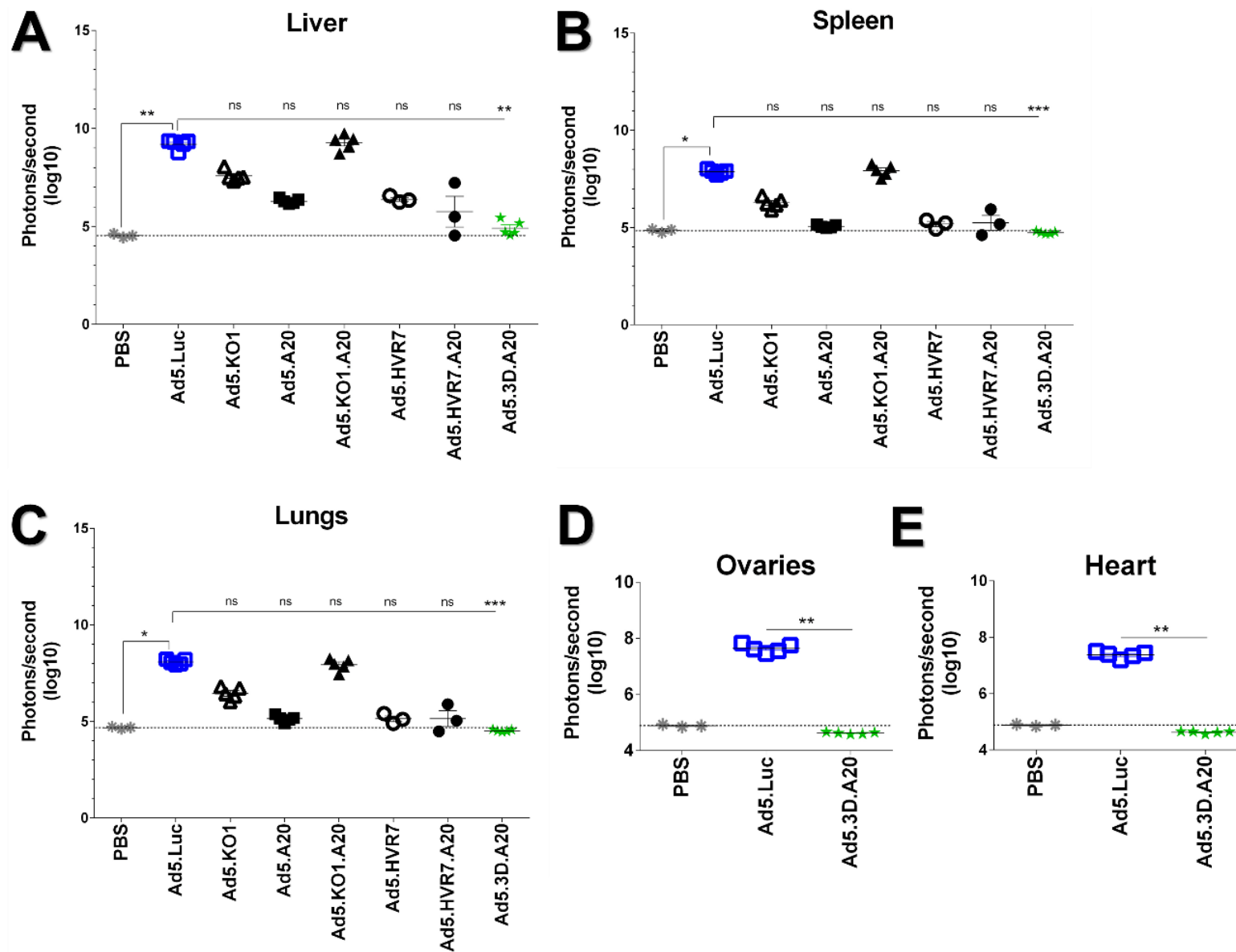
**Figure 7–4. Total luminescence in individual organs *ex vivo*.** (A) Livers, (B) spleens, (C) lungs, (D) ovaries and (E) hearts were harvested immediately post-mortem and placed on 12-well plates with 300 µg/mL final volume of D-luciferin (2 mL in PBS). Organs were imaged in Xenogen IVIS 200 imager with 1 min exposure and adjusted in Living Image software. Data were analysed by Kruskal–Wallis test and multiple comparisons by Dunn's post hoc test in GraphPad Prism. n = 3 or 5/group; *, p < 0.05; **, p < 0.01; ***, p < 0.001; ****, n < 0.0001; the absence of asterisk indicates no statistically significant difference was observed compared to Ad5.Luc group. Baseline luminescence (PBS group) shown as a dotted line.

All groups showed decreased luminescence intensity in all harvested organs, as compared to Ad5.Luc (Table 7–1). Of all challenge groups, Ad5.3D.A20 exhibited the largest differences, most remarkably in liver transduction. On the contrary, the smallest differences relative to Ad5.Luc were observed in the Ad5.KO1 challenge group, consistent with the redundancy of CAR utilisation by systemically administered Ad5.

**Table 7–1. Fold decrease in total luminescence (photons/second) relative to Ad5.Luc.** The mean luminescence intensity of Ad5.Luc was divided by the mean luminescence in each organ in respective groups. –, organ not harvested from this group.

| Fold decrease vs. Ad5.Luc | Organ | | | | |
|---|---|---|---|---|---|
| Group | Liver | Spleen | Lungs | Ovaries | Heart |
| Ad5.KO1 | 45 | 33 | 36 | – | – |
| Ad5.A20 | 650 | 1200 | 841 | – | – |
| Ad5.KO1.A20 | 39 | 2.3 | 1.2 | – | – |
| Ad5.HVR7 | 641 | 694 | 807 | – | – |
| Ad5.HVR7.A20 | 152 | 5500 | 407 | – | – |
| Ad5.3D.A20 | 13300 | 9230 | 3700 | 1100 | 573 |

### 7.1.3 Viral genome quantification by qPCR

Total DNA was extracted from a small section of the harvested organs; 40 ng of DNA was then subjected to qPCR. Purified stocks of each virus were used for preparation of dilutions for generation of control standard curves. Overall, the highest viral copy numbers were observed in the liver, while the viral genome copy number was more than 100-fold lower in the spleen and lungs, and lower in the heart and ovaries (Figure 7–5). The liver-de-targeted FX-binding ablated vectors – Ad5.HVR7 and Ad5.HVR7.A20 – showed a dramatic ~ 7000- and ~ 13 000-fold decrease in viral genome copy number in the liver, as compared to the parental Ad5 (Figure 7–5A), but did not reach statistical significance ($p = 0.4708$ and $p = 0.1836$, respectively). The αvβ6-re-targeted vectors Ad5.A20 and Ad5.3D.A20 exhibited a dramatic decrease in copy number relative to the parental Ad5 – Ad5.3D.A20 showing 7-log ($p = 0.0002$) and 5-log decrease ($p = 0.0023$) in the liver and lungs, respectively (Figure 7–5A, C), while Ad5.A20 had a 6-log ($p = 0.0149$) and 300 000-fold decrease ($p = 0.0009$) in the respective organs (Figure 7–5A, C). Genome copy number of the Ad5.3D.A20 vector was reduced down to baseline levels (PBS group) in the heart and ovaries. Unexpectedly, the Ad5.KO1.A20 vector showed very high copy number levels in liver, spleen and lungs (Figure 7–5A, B, C).
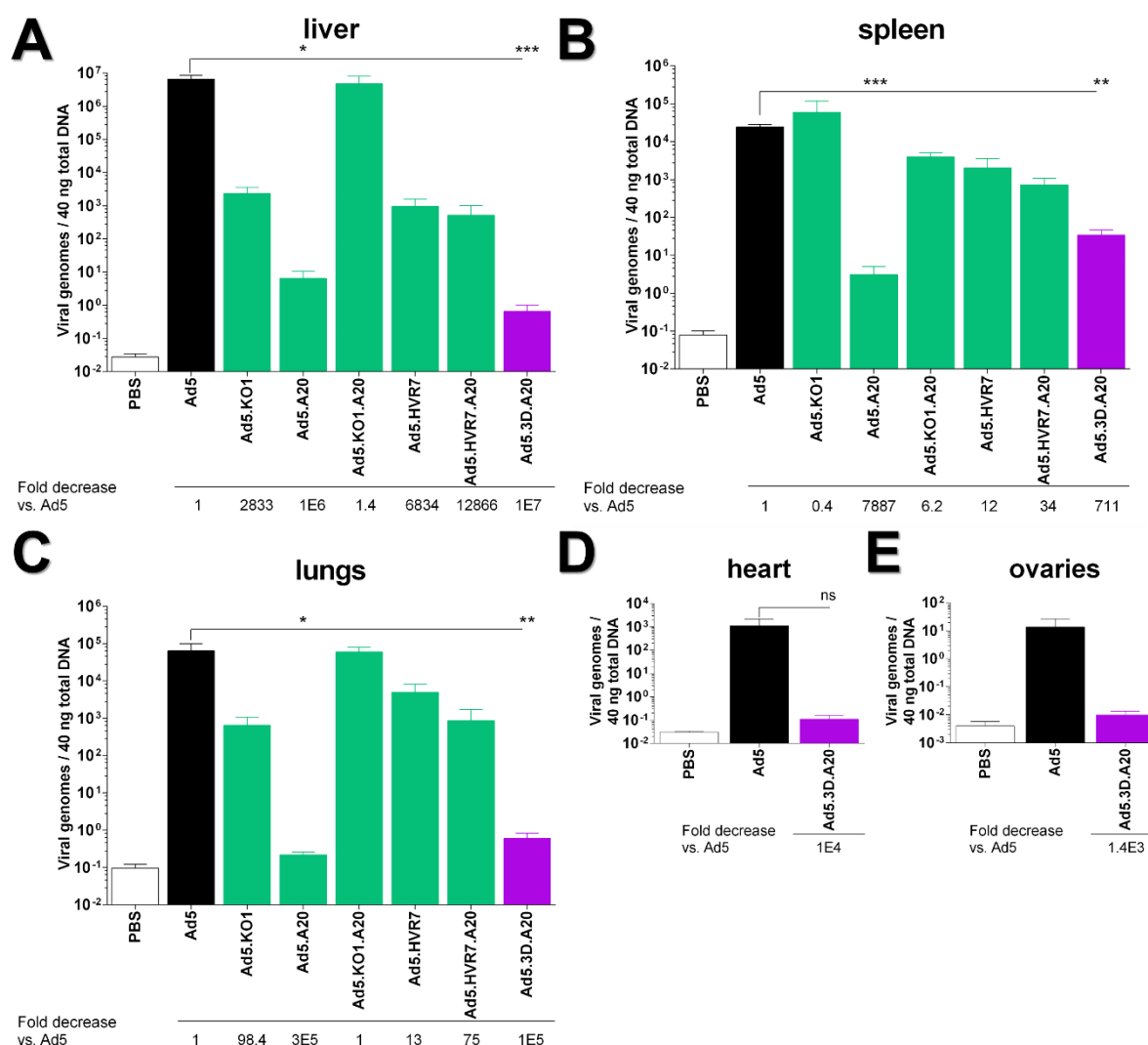
**Figure 7–5. Quantitative PCR (qPCR) for adenovirus genome copy number following systemic vector delivery.** Total DNA was extracted from (A) liver, (B) spleen, (C) lungs, (D) heart and (E) ovaries (~ 10 mg of spleen, ~ 25 mg of other organs) and 40 ng subjected to qPCR using hexon-specific primers. Data in (A–C) were analysed by Kruskal–Wallis test and multiple comparisons by Dunn's *post hoc* test; two-tailed unpaired T test was performed in (D–E) in GraphPad Prism. Error bars represent standard error of the mean; n = 5/group; *, $p < 0.05$; **, $p < 0.01$; ***, $p < 0.001$; ****, $n < 0.0001$; the absence of asterisk indicates no statistically significant difference was observed compared to Ad5.Luc group (black bars).

### 7.1.4  *Immunohistochemistry on paraffin tissue sections*

Formalin-fixed paraffin-embedded liver tissue sections were stained by immunohistochemical methods to visualise the localisation of viral particles within the tissues. After re-hydration in a series of xylene and ethanol washes, antigen retrieval by proteinase K treatment and hydrogen peroxide quenching, the sections were blocked in normal 2.5 % horse serum for 1 h. After washing with PBS, sections were incubated with primary rabbit antibodies O/N at 4ºC and a secondary α-rabbit IgG-HRP conjugate for 30 min. DAB substrate was added for 3 min, and sections counterstained in haematoxylin for a brief 15 s as a standard 60 s wash stained the tissues too dark. After a serial de-hydration in ethanol and xylene washes, the

sections were mounted and images taken under a light microscope at 10 x, 20 x and 40 x magnification.  Using a rabbit IgG as a control antibody, we could optimise the protocol to yield as low background staining as possible. Liver tissues were shown to express very high levels of CAR, as the whole tissue section acquired a brown tone; the strongest staining was observed in the structures lining the cell membranes (Figure 7–6A). As expected, no expression of αvβ6 integrin was observed in the livers (Figure 7–6A). Livers from mice infected with Ad5 and Ad5.3D.A20 vectors showed remarkably variable staining patterns. The representative mouse #5 from the Ad5 treatment group had strongly stained infected cells throughout the section, while no infected cells could be found in the liver of the Ad5.3D.A20-infected animal #5 (Figure 7–6B). Data from other animals in these or other treatment groups is not shown here.
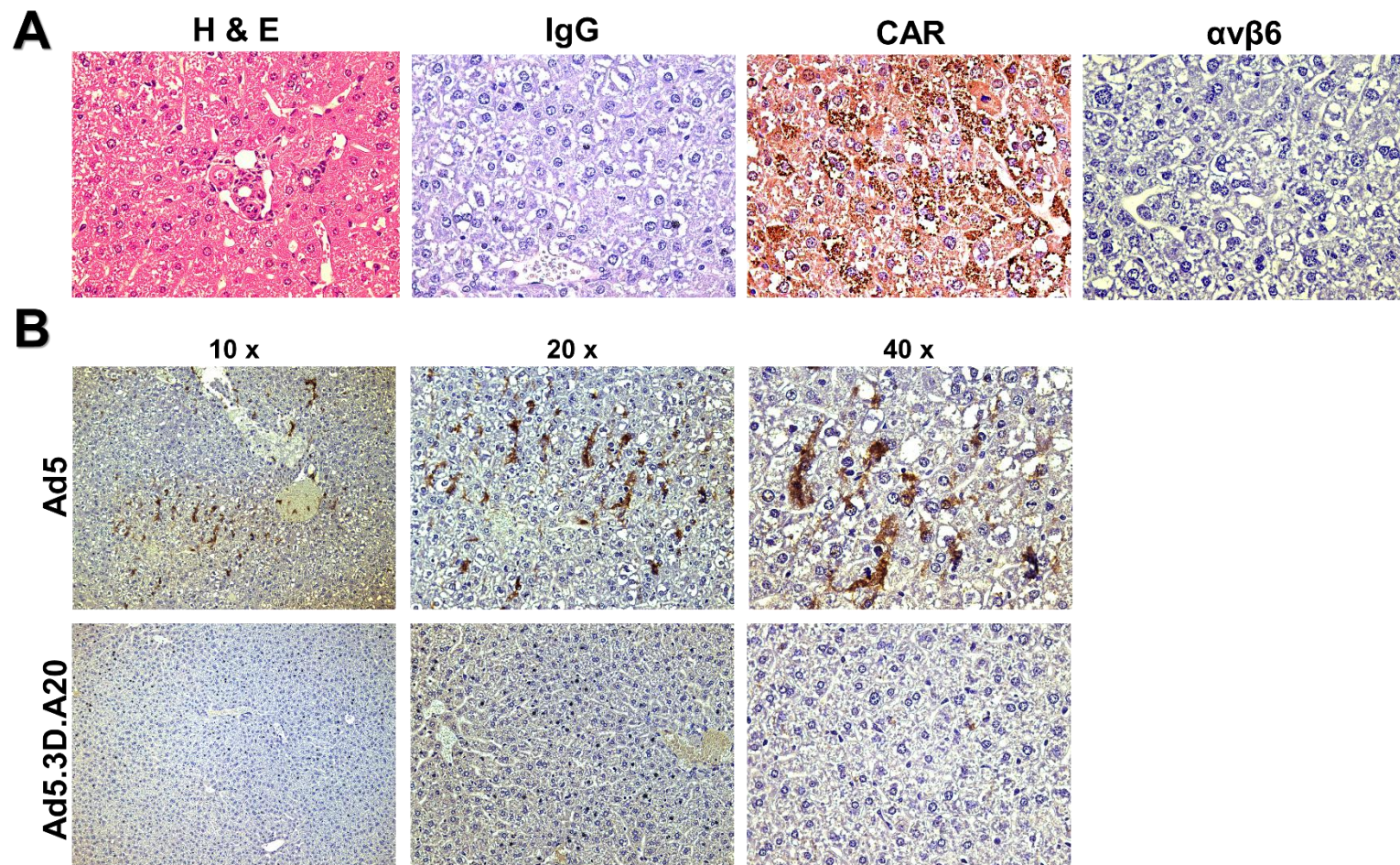
**Figure 7–6. Immunohistochemical staining of paraffin-embedded mouse liver sections.** Formalin-fixed and paraffin-embedded liver sections were stained for (A) haematoxylin/eosin (H & E), rabbit control IgG (1 µg/mL), α-CAR antibody (1:100) or α-αvβ6 antibody (1:10). (B) Liver sections from mouse #5 infected with Ad5 vector and mouse #5 infected with Ad5.3D.A20 vector were stained with anti-Ad5 antibody (1 µg/mL) and imaged at 10 x, 20 x and 40 x magnification. Sections were blocked in normal 2.5 % horse serum for 1 h at room temperature, stained with primary antibodies O/N at 4ºC, incubated with horse anti-rabbit IgG-HRP for 30 min, counterstained with haematoxylin for 15 s, and developed in DAB substrate for 3 min. Images were acquired in Leica DMC 2900 light microscope.

### 7.1.5  Cytokine screening

100 µL of blood was collected from each mouse at 6 h and 24 h post-treatment from the submandibular vein via a cheek puncture. Plasma was separated from whole blood by centrifugation and cytokine screening performed from by Dr Angela Bradshaw at University of Glasgow, UK. Twenty-three different cytokines and chemokines were assessed from 30 µL of plasma in duplicate using an automated bead-based Luminex multiplex array (Figure 7–7). Analyte concentrations are in shown as picograms per µL of sample, and were further normalised to total protein concentration in each sample (pg/mg). Furthermore, the mean of the control (PBS) group was subtracted from each value to directly reflect the Ad vector-driven response. At 6 h post-injection, overall highest concentrations of all cytokines were observed for MCP-1, followed by G-CSF and eotaxin (Figure 7–7; images 1/4 and 2/4). Large intra-group variation was observed in the cytokine concentrations, which is why only very few statistically significant differences were observed between treatment groups at the 6 h time-point. The Ad5.KO1 vector was the only one to elicit significantly lower levels of IL-12p70 as compared to the Ad5 vector ($p = 0.0472$). Conversely, the Ad5.HVR7.A20 vector was the only one to elicit significantly higher levels of MIP-1α relative to Ad5 ($p = 0.0477$) (Figure 7–7; image 2/4); no statistically significant differences were observed for any of the other analytes at the 6 h time-point.

At 24 h post-injection, the overall levels of all chemokines and chemokines were remarkably lower than at the 6 h time-point; for instance, the level of MCP-1, whose concentration was the highest at 6 h, had decreased > 100-fold (Figure 7–7; image 4/4). The Ad5.3D.A20 vector elicited significantly higher levels of IFN-γ and IL-6 (both $p = 0.0436$) (Figure 7–7; image 3/4), while Ad5.HVR7 elicited significantly higher levels of IL-13, relative to Ad5 ($p = 0.0436$) (Figure 7–7; image 4/4). The level of IL-β1 was significantly lower for Ad5.KO1 ($p = 0.0288$) (Figure 7–7; image 3/4), while the level of RANTES was significantly lower for Ad5.3D.A20 ($p = 0.0118$) relative to Ad5 (Figure 7–7; image 4/4). Additionally, vectors Ad5.KO1, Ad5.A20 and Ad5.3D.A20 showed significant reduction of KC ($p = 0.0026$, $p = 0.0394$, $p = 0.0026$, respectively), and MCP-1 ($p = 0.0288$, $p = 0.0260$, $p = 0.0390$, respectively) relative to the Ad5 vector at the 24 h time-point (Figure 7–7; image 4/4).

# 6 h



**Eotaxin**

1.2  2.0  2.5  2.5  2.3  1.5

**G-CSF**

0.2  0.1  1.4  0.9  0.8  0.6

**GM-CSF**

1.2  1.0  1.7  3.2  1.9  1.2

- Ad5
- Ad5.KO1
- Ad5.A20
- Ad5.KO1.A20
- Ad5.HVR7
- Ad5.HVR7.A20
- Ad5.3D.A20

**IFN-γ**

0.5  0.4  2.2  3.8  3.4  0.9

**IL-1α**

1.8  1.0

**IL-1β**

0.4  0.3  1.4  1.5  1.7  0.9

**IL-2**

0.5  0.1  0.9  1.0  2.3  0.7

**IL-3**

0.6  2.0  1.5  1.8  1.0

**IL-4**

**IL-5**

0.4  1.2  1.5  1.5  0.4

**IL-6**

0.6  0.2  2.7  2.6  3.5  1.0

# 6 h

# 24 h

**Eotaxin**

pg/mg

0.9 2.3 0.5 15.3 3.7

**G-CSF**

pg/mg

0.2 0.3 1.9 1.6 3.3 0.3

**GM-CSF**

pg/mg

0.7 1.3 1.3 1.0 2.0 2.5

■ Ad5
□ Ad5.KO1
■ Ad5.A20
□ Ad5.KO1.A20

■ Ad5.HVR7
■ Ad5.HVR7.A20
■ Ad5.3D.A20

**IFN-γ**

pg/mg

*

**IL-1α**

pg/mg

0.1 0.3 1.1 1.6

**IL-1β**

pg/mg

*

0.3 0.3 1.2 0.4 0.6

**IL-2**

pg/mg

**IL-3**

pg/mg

**IL-4**

pg/mg

**IL-5**

pg/mg

6.4 7.3 1.7 1.0 2.1

**IL-6**

pg/mg

*

# 24 h



**Figure 7–7. Cytokine screen at 6 h and 24 h following systemic delivery of replication-deficient vectors.** 40 μL of mouse plasma was subjected to automated magnetic bead-based Luminex array in duplicate. Eosinophil chemoattractant (eotaxin), granulocyte colony-stimulating factor (G-CSF); granulocyte-macrophage colony-stimulating factor (GM-CSF); interferon γ (IFN-γ); interleukin (IL) -1α, -1β, -2, -3, -4, -5, -6, -9, -10, -12p40, -12p70, -13, -17; keratinocyte chemoattractant (KC); monocyte chemotactic protein 1 (MCP-1); macrophage inflammatory protein 1 (MIP-1) α and β; chemokine ligand 5 (RANTES); tumour necrosis factor α (TNF-α). Horizontal line inside the box shows the median; '+' shows the mean, and each dot is an individual animal; n = 5 animals/group. The mean of control (PBS) group was subtracted from all values; the number below each box shows the fold change relative to the mean of Ad5 group (black box). Cytokine concentration (pg) was normalised to total protein in the sample (mg) by BCA assay. Data were analysed using non-parametric Kruskal–Wallis test with Dunn's multiple comparisons post hoc test in GraphPad Prism; *, p < 0.05; **, p < 0.01.

## 7.2 Generation of an ovarian cancer model in immunocompromised mice

A small pilot study was performed in immunocompromised NOD/SCID mice to evaluate tumour growth rate, and to optimise a treatment schedule and final endpoint for a subsequent oncolytic efficacy study. $1 \times 10^7$ SKOV3-β6 cells in PBS were implanted i.p. in eight mice on day 0. Mice were monitored daily and weighed every seven days to record the development of tumour mass and build-up of malignant ascites. Mice were sacrificed at pre-determined time-points and tumours harvested.

### 7.2.1 Tumour growth rate and development of ascites

Two mice were sacrificed at days 7, 14, 21 and the final two mice on days 48 and 49. No weight changes were observed over the course of the study. The last two mice were sacrificed due to high tumour burden and build-up of ascites; this was the pre-determined endpoint of the study. Tumour size increased gradually during the study (Figure 7–8). On days 7 and 14 all mice carried a small tumour at the size of tumour cell implantation, as well as a larger tumour on the side of the pancreas. The mice that were sacrificed on day 14, additionally had a few very small micro tumours between the lobes of the liver. By day 21 both large tumours had grown, and the micro tumour mass within the liver lobes had increased in both volume and number, and had spread to a larger area. The last two mice were very ill on the day of euthanasia. These animals had a visibly extended stomach, tumour growth throughout the peritoneum, purple colour of the skin on the stomach; they were also moving slowly and looking pale. Additionally, in these mice the tumour at the injection site was so large that it was even palpable through the skin. We also monitored the build-up of malignant ascites within the course of tumour growth. The mice that were sacrificed at days 7, 14 and 21 were not found to have any ascites in the peritoneum. On the contrary, the last two severely ill mice had a volume of 2.6 mL of bloody ascites at the time of euthanasia.

| Time-point | Mouse #1 | Mouse #2 | Observations |
|---|---|---|---|
| Day 7 |  |  | Small tumour at the injection site, a larger one by the pancreas (Ø ~ 1 cm)<br><br>No ascites |
| Day 14 |  |  | Tumour at injection site, Ø ~ 1 cm tumour by the pancreas, 4−5 micro tumours between the lobes of the liver<br><br>No ascites |
| Day 21 |  |  | Ø ~ 1 cm tumour at injection site, Ø ~ 1.5 cm tumour by the pancreas, tumour mass between the lobes of the liver<br><br>No ascites |
| Days 48 & 49 |  |  | Ø ~ 1.5 cm tumour at injection site, Ø ~ 2 cm tumour by the pancreas, tumour mass spread all around the lining of abdomen, diaphragm, intestinal lining<br><br>2.6 mL of ascites |

**Figure 7–8. Tumour growth in the intraperitoneal SKOV3-β6 ovarian cancer model.** Eight female NOD/SCID immunocompromised mice were implanted with $1 \times 10^7$ cells in 100 µL PBS by an intraperitoneal injection on day 0. Tumour growth and ascites build-up was monitored by sacrificing two mice at each time-point: days 7, 14, 21 and 48/49 (endpoint) and by harvesting every individual solid tumour from each mouse.

### 7.2.2 Expression of CAR and αvβ6 in the harvested tumours

The expression levels of CAR and αvβ6 integrin receptors were assessed by flow cytometry. It is important to verify that the retrovirus-transfected SKOV3-β6 tumour cells maintain an adequate level of αvβ6 expression even in the non-selective peritoneal environment (ie. no puromycin) of live mice. The harvested tumours were pooled together from each mouse and homogenised though a cell strainer. The recovered cells were washed in 1 % FBS/PBS and stained with primary anti-CAR and anti-αvβ6 antibodies and secondary goat anti-mouse IgG AlexaFluo647 conjugate. Gating was performed with *in vitro* grown SKOV3-β6 cells, and 10 000 events

recorded for cells from each mouse. The expression of αvβ6 decreased by 1.4 %, 6.4 %, 12.0 % and 6.4 % over the time of 7, 14, 21 and 48/49 days, respectively (Figure 7–9). The level of CAR expression, however, remained virtually unchanged throughout the study.
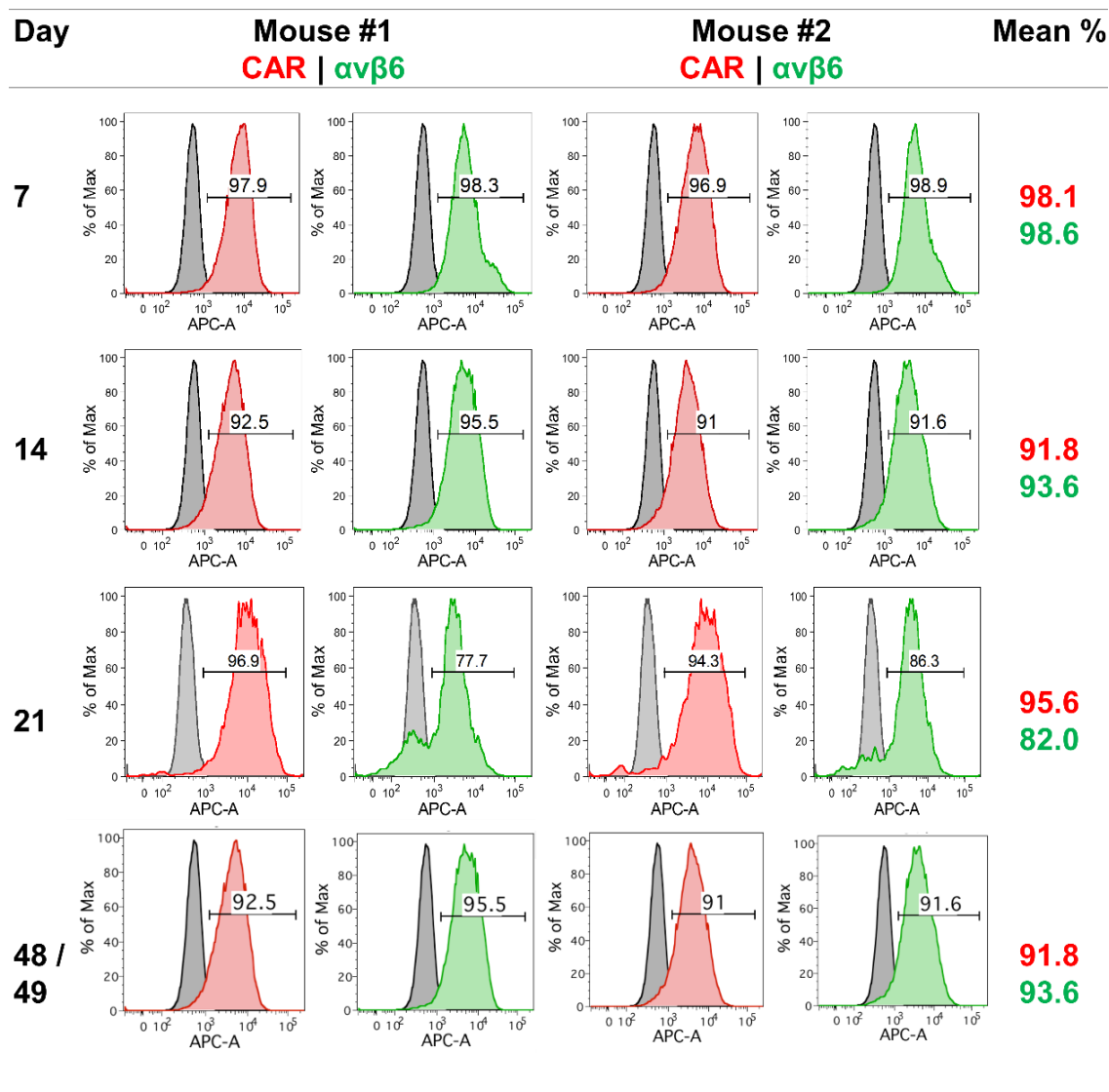


**Figure 7–9. Expression of coxsackie and adenovirus receptor (CAR) and αvβ6 integrin in SKOV3-β6 cancer model over time.** Tumour cells were pooled together from each mouse immediately after euthanasia, and stained for CAR and αvβ6 surface markers. 10 000 cells/animal were analysed in FACSAria flow cytometer and images edited in FACSDiva software. Mean % shows the average expression of CAR (red) and αvβ6 (green) at each time-point.

## 7.3   Discussion

The first objective of this chapter was the assessment of the biodistribution profile of αvβ6-targeted replication-deficient vectors with single, double or triple de-targeting mutations in wild type mice. We used the inbred albino B6 mouse strain due to its white coat colour, which allowed better luciferase signal detection using the IVIS

imager, compared to the widely used laboratory strain C57BL/6 that has a black coat. These two strains are genotypically equal, except for the albino phenotype as a result of a spontaneous mutation in the tyrosinase gene. Live mouse imaging produced noteworthy luminescence data with inter-group variation (Figure 7–1). As expected, and in accordance with previous observations, Ad5.Luc mediated saturating level luminescence signal within the upper abdominal area where liver and spleen are located. All other treatment groups had lower luminescence originating from this area. Groups Ad5.A20 and Ad5.3D.A20 had and 784- and 19 100-fold lower number of total photons (p = 0.0046 and p < 0.0001, respectively). Despite visibly lower luminescence signal observed relative to Ad5.Luc, other groups did not quite reach statistical difference (Ad5.HVR7, p = 0.0625; Ad5.HVR7.A20, p = 0.0523), presumably due to wider intra-group variability (Figure 7–2). The total luminescence of mice in Ad5.KO1.A20 group was unexpectedly high compared to Ad5.KO1 and Ad5.A20 groups that had greatly lower luminescence than Ad5.Luc. The finding suggests that the combination of KO1 mutation and A20 peptide may somehow be capable of rescuing liver and/or spleen uptake via a yet unknown mechanism that we cannot explain – warrants further investigation.

We then examined individual organs for luminescence signal emitted by the viral vectors that had been taken up by the tissues. All harvested tissues seemed to have taken up large amounts of the parental Ad5.Luc virus, which had stronger signals than any other treatment group in all organs (Figure 7–3). In contrast, the triple de-targeted and $\alpha v \beta 6$-re-targeted vector Ad5.3D.A20 exhibited a greatly reduced tropism relative to the parental Ad5.Luc. It was the only vector whose transduction was significantly lower in all harvested tissues as compared to Ad5.Luc (Figure 7–4). While the KO1 mutation and the HVR7 mutation alone reduced luciferase signal in the liver by 45- and 641-fold, respectively, and in the spleen by 33- and 694-fold, respectively, the combination of these two, together with the $\alpha v \beta 3/5$ integrin-binding ablation mutation RGE and the A20 targeting peptide, efficiently de-targeted the vector from these organs (13 300-fold reduction in the liver and 9230-fold reduction in the spleen, relative to Ad5.Luc) (Table 7–1). The luminescence signal in the Ad5.3D.A20 group was significantly lower in both heart (1100-fold decrease) and ovaries (573-fold decrease) than in the Ad5.Luc group (both p < 0.01) – these organs were not harvested from the other treatment groups (Figure 7–4 and Table 7–1).

The presence of viral vectors was also evaluated by qPCR from a piece of each harvested tissue – the liver, spleen, lungs, heart and ovaries (Figure 7–5A). Very high levels of Ad5 were confirmed in all harvested organs. Overall, the highest genome

copy numbers were quantified in the liver, followed by a ~ 100-fold reduction in the spleen and lungs, and considerably less in the heart and ovaries, consistent with previous findings that the majority of Ad5 ends up in the liver within hours of systemic administration (Smith et al., 2002, Green et al., 2004). The liver-de-targeted, FX-ablated vectors Ad5.HVR7 and Ad5.HVR7.A20 showed a significant ~ 7000- and ~ 13 000-fold decrease in liver transduction relative to the parental vector Ad5.Luc, respectively (Figure 7–5). Intriguingly, the triple-de-targeted Ad5.3D.A20 vector showed significantly altered biodistribution compared to all other viruses. The genome copy numbers of this vector were significantly lower than the levels of Ad5.Luc in all harvested organs, with a substantive and significant 7-log decrease in the liver (Figure 7–5A) and 5-log decrease in the lungs (Figure 7–5C). Unexpectedly, the combination of KO1 mutation and A20 peptide insertion seemed to rescue vector transduction, as the genome copy numbers of this vector were higher than for either of the parental vectors, Ad5.KO1 or Ad5.A20 (Figure 7–5A–C). In fact, the Ad5.A20 vector exhibited significantly lower genome copy numbers (6-log, 7887-fold and 300 000-fold decrease in the liver, spleen and lungs, respectively) compared to the Ad5.Luc vector, showing similar transduction pattern to the fully de-targeted vector, Ad5.3D.A20 (Figure 7–5A–C).

We then went on to further verify the presence of Ad5.Luc vector and the absence of the Ad5.3D.A20 vector particles in the liver by performing a series of IHC staining procedures on formalin-fixed paraffin-embedded tissue slides. First, we confirmed the expression of CAR in the liver, as seen as an intense staining throughout the tissue, and particularly focused at the borders lining the cellular junctions (Figure 7–6A). Second, we confirmed the lack of expression of αvβ6 integrin in these tissues (Figure 7–6A), as expected. Liver sections from mouse number #5 in Ad5.Luc group and mouse #5 in Ad5.3D.A20 group were stained using an antibody that recognises all Ad capsid proteins (immunogen: purified Ad5). Clear differences were observed in the staining pattern; sections from Ad5-infected mice demonstrating strong staining throughout the tissue, whilst little or no staining was observed in the sections from the Ad5.3D.A20-infected animals (Figure 7–6), confirming the observations from luminescence imaging and qPCR. Ad5.3D.A20 vector appears to be efficiently de-targeted from all major off-target sites for the native Ad5 virus, as confirmed by all three distinct analyses – luminescence, qPCR and IHC-P. Ad5.3D.A20 represents an exciting candidate for therapeutic applications, and warrants further investigation.

The secondary objective of this study was the evaluation of the breadth of innate anti-viral immune responses. Following systemic delivery, Ads are known to elicit high

levels of cytokines and chemokines, primarily via recognition of viral RNA and DNA sequences by the inflammasome (Muruve et al., 2008) and cytosolic defensins (Smith et al., 2010). Additionally, the RGD motif in the Ad penton protein has been previously shown to be involved in the activation of immune cells – DCs and MΦs (Worgall et al., 2004, Schoggins and Falck-Pedersen, 2006, Di Paolo et al., 2009) – as well as innate cytokines, such as IL-1α, IFN-γ, IP-10, TNF-α and MIP-1 (Schoggins and Falck-Pedersen, 2006, Di Paolo et al., 2009). In this study, we showed that the parental Ad5.Luc had activated 21 out of 23 cytokines quantified in this assay by the 6 h time-point, whilst levels returned to baseline by 24 h post-injection (Figure 7–7). No IL-4 or IL-17 was detected in any treatment group at either time-point. Levels of different analytes were highly variable between treatment groups; no trend was observed for any vector for having elicited consistently lower or higher levels of specific analytes. The inclusion of the RGE mutation in the penton base protein has previously been shown to reduce the production of innate inflammatory markers *in vivo* (Bradshaw et al., 2012). Following i.v. delivery of the AdRGE vector in non-MΦ-depleted animals, in addition to decreased splenic uptake of the vector, significantly decreased levels of IL-12, IL-5, IL-6, IL-1α, IL-1β, IP-10 and MCP-1, relative to Ad5, were observed (Bradshaw et al., 2012). Additionally, in their study the levels of IL-12, IL-6 and IL-1α were significantly reduced in these animals, relative to the AdT* vector with an FX-binding mutation, whilst in MΦ-depleted animals, the levels of IL-12, IP-10, IFN-γ and MCP-1 were significantly reduced for AdT*RGE compared to AdT*. We were therefore interested in assessing the impact of these de-targeting mutations on the breadth of immune response in our biodistribution study following systemic delivery of the triple-de-targeted, replication-deficient Ad5.3D.A20 vector. Disappointingly, however, Ad5.3D.A20 vector did not appear to show any overall decreased activation of innate immunity in this study. At 6 h following vector injection, no significant decrease was observed for any analyte as compared to Ad5. On the contrary, the levels of RANTES, KC and MCP-1 were significantly lower than for Ad5 at the 24 h time-point (Figure 7–7; image 4/4). However, the overall levels of these analytes were very low, which is why the observed variation may be negligible, and drawing any solid conclusions at this time-point is challenging. In their seminal paper, Di Paolo and colleagues suggested the central involvement of IL-1α on anti-Ad immunity (Di Paolo et al., 2009). In our study, the Ad5 and Ad5.HVR7.A20 vectors activated equal levels of IL-1α, while the Ad5.KO1.A20 elicited 1.8-fold increased levels compared to Ad5; the levels of this cytokine were negligible in all other treatment groups (Figure 7–7).

Activation of innate immune mediators may be dependent on the genetic background of the experimental mouse strain [for alloantigens of common strains, see (BioLegend, 2017)]. Bradshaw and colleagues utilised an outbred MF1 strain for their investigations on innate anti-Ad immunity (Bradshaw et al., 2012), while Di Paolo and colleagues used various knockout strains, all of which were based on the inbred C57/BL6 genetic background (Di Paolo et al., 2009) In our study, we used an inbred B6 albino strain that is coisogenic to the C57/BL6 strain. Outbred animals are genetically diverse with polymorphic MHC alleles, in contrast to inbred strains that have homozygous MHC haplotypes (C57/BL6 strain: H-2$^b$). The differences in cytokine production may also depend on inherent differences in the polarised Th1 and Th2 subpopulations of helper T cells in each mouse strain. While the Th1 arm – that produces IFN-γ, TNF-α, IL-2, IL-12 – is involved in fighting off viral infections (among other cell-mediated immune functions) and Th2 – that produces IL-4, IL-5, IL-6, IL-9, IL-10 and IL-13 – drives humoral immunity, the arms can also down-regulate each other [reviewed in (Romagnani, 2000, Kidd, 2003)]. The use of outbred mice may therefore be preferable, since they better represent the clinical scenario where study participants have highly variable genetic backgrounds with an unpredictable influence on the study outcome.

These preliminary *in vivo* studies form an important part of the functional assessment of these replication-deficient vectors that offer a safe and clean system for the assessment of Ad vector tropism and biodistribution. We demonstrate that the biodistribution of de-targeted vectors was altered in comparison to the parental Ad5.Luc that does not carry any de- or re-targeting mutations. When studying biodistribution profile of human viruses in mouse models, it is important to recognise the limitations of the models and how they do not accurately represent the clinical scenario. One of the key differences is that human, but not murine, erythrocytes express CAR on the cell surface (Carlisle et al., 2009). To better reflect this difference in receptor distribution, and the resulting change in biodistribution, we manipulated our vectors to be devoid of CAR-interaction by the introduction of the KO1 mutation. However, as Ad5 is known to preferentially transduce cells via the FX:HSPG bridging interaction rather than the CAR-mediated pathway *in vivo* (Waddington et al., 2008, Alba et al., 2009), we incorporated an HVR7 mutation in the hexon protein, that was shown to significantly abolish the FX-mediated pathway *in vitro* and to drastically decrease liver transduction *in vivo*. Additionally, we set out to explore whether the expression of αvβ6 may be different in mice than in humans, where it is found only at negligible levels in healthy epithelia. Reassuringly, the luciferase expression pattern

observed in the biodistribution did not show any altered tropisms for the αvβ6-targeted vectors to any unexpected off-target sites (Figure 7–1). The observations indicate that αvβ6 is not expressed in healthy mouse tissues, as the A20 peptide did not detectably alter vector biodistribution or direct the vector to any organs that have not previously been unidentified for Ad5-based vectors. Evidently, we only quantified viral genome copy numbers in organs that have previously been known to be involved in Ad5 tropism, and therefore cannot rule out sequestration by other sites. However, as most of the luciferase signal originated from the area of liver and spleen in the IVIS imaging, we could not justify further exploration of other organs.

The third objective of this chapter was the generation of an i.p. ovarian cancer xenograft model in immunocompromised mice. Previous studies have shown that in a SKOV3 ovarian ascites i.p. model using a dose of $1 \times 10^7$ cells/animal, the mice start building up ascites around day 40. From the onset of ascites build-up, the animals will generally have to be sacrificed within a week due to their very poor health (personal communication with Ianko Iankov, Mayo Clinic, MN, USA). We chose this cell dose based on communication with research groups that had been working on the same cell line. We showed that the cell dose was optimal for generation of a severely ill model within 40 days. The study endpoint was reached on day 49, when the last mouse had to be sacrificed due to excess tumour burden and ill health. Previous studies have shown that the cells slowly lose αvβ6 expression *in vivo*, over longer time periods (personal communication with Dr Lynda Coughlan, University of Oxford). We therefore assessed the expression of αvβ6 integrin from tumour cells harvested at each study time-point. No obvious decrease was observed in the levels of αvβ6 or CAR during the duration of the study. This is reassuring since the absence of a suitable cell receptor would severely compromise the efficacy of therapeutic Ad vectors.

Based on the observations from this preliminary pilot study, we have established a protocol for a follow-up study that will assess the oncolytic efficacy of αvβ6-targeted vectors in the SKOV3-β6 ovarian cancer xenograft model. Mice will be treated with three doses ($1 \times 10^{10}$ vp each) of the oncolytic vectors OAd5, OAd5.A20 and OAd5.3D.A20 on days 14, 16 and 18 post-tumour implantation. The primary outcome of this study will be overall survival. The study is scheduled for spring 2017, and will be carried out at Dr Richard Vile's laboratory (Department of Molecular Medicine/Immunology at Mayo Clinic, Rochester, MN, USA).

# CHAPTER 8.     Final discussion

## CHAPTER 8. Final discussion

The cancer field is in a flux with the clinical maturation of immunotherapies and precision medicine approaches manifesting in significant changes to cancer treatment in the coming years. Immunotherapies are revolutionising the field, and their usage is rapidly becoming the mainstream in the treatment of aggressive immunological cancers such as melanoma. Sequencing of the cancer exome has produced a wealth of genomic data that has yet to be dissected into a clinically meaningful information. Growing knowledge on cancer antigens and neoantigens in individual cancer types, and at the population level, will help tailor the therapies towards targeted and personalised therapies. Antigen cross-presentation is likely to be an important aspect in therapeutic design, since tumours are an ever-evolving environment of original malignant cells, TILs, cancer-initiating cells and the supporting TME. The key questions in cancer immunotherapies persist: how to successfully break the anti-cancer immune tolerance and to enable long-lasting cures by re-programming the body for a permanent attack against malignant cells? Oncolytic cancer virotherapies are an appealing approach due to their dual functionality as direct tumour cell killers and systemic immune stimulators.

The primary focus of this thesis lies on the development of Ad vectors for ovarian cancer-targeted virotherapies. Treatment options for ovarian cancer are evidently insufficient at present. The malignancy commonly presents with highly non-specific symptoms, which leads to delayed initial diagnosis, allowing the development of advanced stage disease that rapidly develops resistance to first-line platinum-based chemotherapies. Despite the new PARP inhibitors for *Brca+* ovarian cancer, tumour relapse and progression commonly occur, causing ovarian cancer to be the deadliest of gynaecological cancers. Late disease stages are characterised with intraperitoneal build-up of malignant ascites that provides a highly pro-tumourigenic environment, facilitating tumour spread and metastasis. EOC cells that are shed from the surface of the ovarian epithelium, can reside in ascites as a resistant population with the ability of acquiring invasive properties and initiating new lesions. Any novel treatment strategy therefore needs to be able to radically eradicate these populations and CSCs. Currently, one of the most promising approaches is the combination of conventional treatment moieties – re-bulking surgery, radiotherapy and chemotherapy – with new innovations, such as immunotherapeutic mAbs and oncolytic virotherapies. The key dogma is combating cancer tolerance and ensuring efficient cell killing, by simultaneous elicitation of long-lasting cancer-specific immune memory.

Oncolytic Ad vectors can be developed as bespoke personalised *in situ* cancer vaccines – capable of potent and selective oncolysis and replication within the tumour mass. Viral amplification bursts the infected cells, releasing the virus progeny that can infect surrounding tumour cells, theoretically multiplying the lytic effects, whilst acting as a factory for the production of therapeutic molecules in neighbouring cells. No other anti-cancer therapy can match this selectivity and power for therapeutic amplification. Release and display of viral-associated antigens and TAAs by the bursting cells can prime T-cells, eliciting a long-lasting tumour-specific immunological memory that will potentially protect the body from a subsequent tumour challenge later in life, as well as providing an immunological means for tumour killing at distant metastatic sites. Tumour cells could also be primed using focused ultrasound (Mo et al., 2012, Carlisle et al., 2013) or cytotoxic agents to weaken them for subsequent oncolysis and release of TAAs for immune recognition. Systemically administered oncolytic virotherapies have great potential to be used for tracing and attacking both primary and metastatic tumour cells that radio- or chemotherapies cannot reach, virtually in all sufficiently vascularised tissues of the body. Direct and local therapeutic vector delivery into the tumour location, such as the peritoneal cavity in ovarian cancer, provides an appealing alternative treatment route. By this approach, the therapeutic vector can spread within the peritoneum and reach both the primary tumour and peritoneal metastases, which would also allow at least partial circumvention of the efficacy-limiting blood interactions. However, as systemic delivery remains the 'Holy Grail' of cancer virotherapies, vigorous development of therapeutic vectors, based on better understanding of the interactions that limit efficacious viral delivery and promote dose-limiting toxicities, has substantially improved Ad-based vectors in recent years. To this end, we developed de-targeted vectors devoid of central interactions with viral receptors and blood factors, that may limit uptake in healthy tissues and act as a platform for targeted delivery to disease sites *in vivo*, through the incorporation of suitable elements into the viral capsid.

We have extensively assessed the properties of malignant ovarian ascites and the potential hindrances for efficient vector treatment in this complex tumour environment. Valuable clinical ascites samples provided an excellent opportunity for the assessment of vector targeting in the *ex vivo* setting. Twenty ascites samples from Velindre Cancer Centre in Cardiff were assessed for multiple characteristics *in vitro* and *ex vivo*. We found that the concentration of FX was highly variable among the twenty samples, approximately half of the fluid samples having an FX concentration lower than that of a physical concentration in whole blood (8 μg/mL), and the other

half having up to 10-fold higher FX concentration than whole blood. The highly variable FX concentration may have important implications for Ad vector delivery via the i.p. route, since the high affinity of Ad5 to FX can promote off-target uptake into cells via HSPG receptors, and subsequent toxicity. To this end, we have approached the vector development with two strategies: (1) introduction of genetic FX-binding ablating HVR7 mutations in the viral hexon protein of Ad5 (Alba et al., 2009), and (2) generation of a novel Ad10 serotype vector backbone from species D, whose members have previously been shown to have natively low affinity to FX (Waddington et al., 2008). The HVR7-binding ablation mutation was shown to efficiently block the Ad5:FX -interaction for a panel of basal vectors both *in vitro* and *in vivo* following systemic vector delivery in wild type B6 albino mice. Additionally, a novel vector candidate that has not previously been vectorised – Ad10 – was shown to be devoid of FX binding, confirmed by *in vitro* transduction assays supplemented with physiological concentrations of FX. Additionally, this serotype has lower tropism for CAR relative to Ad5, and does not seem to utilise CD46 for cell entry. However, Ad10 may utilise these receptors as auxiliary rather than primary cell entry receptors, and further studies are needed to elucidate the primary receptor interactions, tropism and oncolytic potential of this exciting new vector candidate. In line with previous observations, ovarian ascites also contains high levels of anti-Ad5, with lower but detectable levels of anti-Ad10 antibodies in the limited samples we tested. We also assessed the antigenicity of these antibodies, and found that most of them appear to be directed towards the viral Ad5 fiber protein, while the level of anti-hexon antibodies was lower. Additionally, the transduction of Ad5 vector was more readily neutralised by ascites than the rare species D serotype Ad10.

While Ad5-based vectors primarily utilise the hexon:FX:HSPG pathway for cell entry following systemic delivery, their *in vitro* tropism is dictated by binding to CAR. This ubiquitously expressed receptor is found within cellular tight junctions co-localised with ZO-1 [reviewed in (Coyne and Bergelson, 2005)], ubiquitous in human tissues. Importantly, it is commonly down-regulated in progressive cancers (Li et al., 1999b, Pearson et al., 1999, Asaoka et al., 2000, You et al., 2001, Kim et al., 2002a, Kim et al., 2002b), which makes it a poor cancer target. Moreover, as CAR is expressed on erythrocytes and platelets (Carlisle et al., 2009), it has been proposed that the high affinity of Ad5 to this receptor may trap the vector in the bloodstream and limits its availability to the therapeutic target sites, although this appears controversial (Rojas et al., 2016). For the ablation of CAR-tropism, we manipulated our vectors to contain a KO1-mutation in the fiber AB loop, which was shown to abolish CAR-

mediated cell entry, in line with previous literature (Smith et al., 2002). As the CAR-interaction, orchestrated by the fiber knob domain, is a highly undesirable feature for a cancer vector, we have generated a panel of chimaeric vector backbones by pseudotyping the whole fiber or the fiber knob domain form six different Ad serotypes from subgroup D – Ad10, -15, -24, -29, -48 and -53 – to evaluate their potentially favourable tropism profiles. The receptor tropisms of these rare seroprevalence serotypes are largely unknown to date. None of the whole fiber-pseudotyped vectors seemed to utilise CAR for cell entry, while the knob-pseudotyped Ad5/kn10, -15, -24, -48 (and possibly Ad5/kn29) seemed to be able to use CAR, albeit at remarkably lower efficiency than the parental Ad5. While FX improved transduction efficiency of the knob-pseudotyped vectors, the poor efficiency of the whole fiber-pseudotypes in the tested cell lines may be explained by altered or delayed endosomal processing due to the rigidity and/or suboptimal length of the fiber.

Successful anti-cancer Ad vector design involves complementation of refined de-targeting approaches with selective re-targeting to markers that are exclusively cancer cell-specific. In this study, a comprehensive panel of Ad vectors re-targeted to αvβ6 integrin – an epithelial cancer-specific marker – were generated by using sophisticated homologous recombineering techniques. An A20 peptide from FMDV, that has natively high affinity to αvβ6 integrin, was genetically engineered into the viral fiber knob domain. A significant outcome of this project is the generation of a triple de-targeted and αvβ6-re-targeted vector Ad5.3D.A20, that has superior transduction in αvβ6+ cancer cell lines. The vector was shown to exclusively utilise αvβ6 receptor for host cell entry, and had completely ablated native interactions with FX, CAR and αvβ3/5 integrins, as a result of the well-documented de-targeting mutations – HVR7, KO1 and RGE, respectively. To our knowledge, we are the first ones to report the successful generation of an infectious vector with fully ablated native tropisms and simultaneous cancer re-targeting. It is noteworthy that we were unable to rescue the control virus, Ad5.3D, whose viral fitness is likely to be severely hampered due to ablation of all central viral tropisms. By incorporation of the targeting peptide A20, we were able to rescue infectious virions in HEK293-β6 puro cells with stable expression of the αvβ6 integrin. Both replication-deficient and oncolytic versions of this vector were shown to be selectively targeted to αvβ6+ ovarian cancer cell lines *in vitro* and αvβ6+ primary ovarian ascites-derived EOC cells *ex vivo.* Furthermore, the Ad5.3D.A20 showed improved protection from neutralisation by immune ovarian ascites, and promising oncolytic activity in αvβ6+ cells.

The pioneering vector – Ad5.3D.A20 – generated in this thesis has proved superior to its parental Ad5 vector in preliminary *in vitro* and *ex vivo* studies. As a logical next step, we sought to rule out the possibility of any unexpected tropisms or uptake by previously undocumented off-target sites following systemic delivery of the Ad5.3D.A20 vector in non-tumour-bearing B6 albino mice that are not known to express αvβ6. Ad5.3D.A20 had an extensively altered tropism profile compared to the parental Ad5 vector in the primary off-target sites – liver, spleen and lungs. Both *in vivo* IVIS imaging and *ex vivo* imaging of individual organs showed remarkably decreased luciferase transgene expression; luminescence intensity was ~ 20 000-fold lower in live mice, ~ 14 000-fold lower in the liver, ~ 10 000-fold lower in the spleen and ~ 4000-fold lower in the lungs of the Ad5.3D.A20-infected mice than of the Ad5-infected mice. The viral genome copy number of Ad5.3D.A20 was seven logs lower than that of Ad5 in the liver, and four logs lower in the spleen. The absence of Ad5.3D.A20 vector in the liver was confirmed by IHC staining. It is not clear where these virions are trafficked upon systemic delivery. We are developing a means of tracing virions using PET imaging and zirconium-89 labelling in collaboration with Dr Stephen Paisey (Wales Research and Diagnostic PET Imaging Centre, Cardiff University). Dual tracing using both PET and IVIS could more accurately establish viral fate in the early stages following systemic delivery. Future investigations could also involve studying biodistribution of the Ad5.3D.A20 vector in MΦ-depleted (clodronate liposome-treated) mice to dissect the possibility of liver MΦ involvement in the early stages of infection.

In this thesis, we used the ovarian-ascites derived SKOV3 as a representative EOC line. SKOV3 has been shown to exhibit high level of *p53* mutations (Yaginuma and Westphal, 1992). For this reason, it is an excellent ovarian cancer model cell line since approaching 100 % of HGS-OCs have been shown to have mutations in *TP53* in high-throughput genomic analyses of the cancer genome (Bell et al., 2011). We have established i.p. tumour xenografts with SKOV3 cells modified to express a cancer specific integrin, αvβ6. This model will be used for the assessment of the oncolytic efficacy of αvβ6-targeted OAds at Prof Richard Vile's laboratory at Mayo Clinic, Rochester, MN, USA in spring 2017. However, studying human cancer in an immunocompromised mouse model hardly represents the disease observed in humans, which is why better models are urgently required to assess the immunological aspect of oncolytic virotherapies. In this project, we were very lucky to receive extremely valuable ascites samples from ovarian cancer patients who were undergoing chemotherapy for an advanced disease at a local cancer hospital in

Cardiff. In this thesis, *ex vivo* culture of clinical ovarian ascites-derived EOC cells in the presence of autologous ascitic fluid was the most closely representative of the clinical scenario, although it is obvious that these model systems are lacking in many aspects of the TME, including blood supply and immune suppression. Better means are needed to address the maturation of the immune response, both against the virus and any virally encoded immunological transgenes. The utilisation of clinical samples gave us an advantage for being one step closer to potential clinical assessment of these therapies. Further vector development in improved model systems, such as 3D spheroids and organoid cultures in collaboration with local experts (CardiffUni, 2016), is likely to provide closer insight into the suitability of these vectors for cancer therapies. Furthermore, we are in the process of establishing collaborations for the utilisation of patient-derived xenograft (PDX) models for oncolytic vector assessment.

This thesis describes a novel and exciting approach for oncolytic anti-cancer Ad vector design for ovarian cancer targeting. We chose the αvβ6 integrin as the cellular cancer-specific target due to the well-characterised nature of the A20 peptide and αvβ6 interaction, and the cancer-specificity of αvβ6. This receptor, however, is not restricted to ovarian cancer, and therefore the Ad5.3D.A20 has great potential for use in a multitude of cancer types. Most remarkably, 92 % of cervical cancers and 84 % of skin cancers have been shown to express αvβ6 (Koopman Van Aarsen et al., 2008), and therefore may represent better targets. Future studies could potentially consist of screening suitable cancer types, and the development of clinically relevant model systems. Ad5.3D.A20 could form a useful platform for a wider range of targeting applications beyond the αvβ6:A20 interaction, where a suitable peptide:receptor interaction is documented.

Vectors intended for cancer virotherapy require *transcriptional* control, in addition to the *transductional* targeting approach described in this thesis. The OAds generated in this study have been modified to selectively replicate in cells with a defective pRB pathway, which comprises most cancers (Sherr, 1996). The inclusion of tumour-specific promoters and/or miRNA binding sites could further prevent expression of therapeutic transgenes in off-target tissues. Additionally, the vector may be armed with therapeutic molecules for stimulation of anti-cancer immunity, such as the checkpoint inhibitor anti-CTLA4 and anti-PD-1 mAbs, whose efficacy has been demonstrated in countless clinical studies for multiple indications in the recent years. These vectors are currently being developed in our laboratory, and warrant further assessment for their immune-oncolytic potential both in ovarian cancer and other cancer types. There is vast potential for arming the OAds with virtually any moieties

that can be converted into therapeutically active agents, once within the TME. Multimodal approach to cancer eradication in combination with radio- and chemotherapy is likely to pave the way in effective cancer eradication. Targeting the exciting cancer marker, αvβ6 integrin, with oncolytic vectors in innovative combinations together with biological agents, therapeutic antibodies and radiotherapy, has unleashed potential whose clinical adaptation and anti-cancer efficacy remains to be seen in the near future.

# References

ABBINK, P., LEMCKERT, A. A. C., EWALD, B. A., LYNCH, D. M., DENHOLTZ, M., SMITS, S., HOLTERMAN, L., DAMEN, I., VOGELS, R., THORNER, A. R., BRIEN, K. L., CARVILLE, A., MANSFIELD, K. G., GOUDSMIT, J., HAVENGA, M. J. E. & BAROUCH, D. H. 2007. Comparative seroprevalence and immunogenicity of six rare serotype recombinant adenovirus vaccine vectors from subgroups B and D. *J Virol,* 81**,** 4654-4663.

ABEDIA. 2016. *Vectors used in gene therapy trials* [Online]. Journal of Gene Medicine. Available: http://www.abedia.com/wiley/vectors.php [Accessed 5 Dec 2016].

ACHARYA, R., FRY, E., STUART, D., FOX, G., ROWLANDS, D. & BROWN, F. 1989. The three-dimensional structure of foot-and-mouth disease virus at 2.9 Å resolution. *Nature,* 337**,** 709-716.

ACS. 2016. *Ovarian Cancer* [Online]. American Cancer Society. Available: http://www.cancer.org/cancer/ovariancancer/detailedguide/index [Accessed 25 Jun 2016].

AHMED, A. A., ETEMADMOGHADAM, D., TEMPLE, J., LYNCH, A. G., RIAD, M., SHARMA, R., STEWART, C., FEREDAY, S., CALDAS, C., DEFAZIO, A., BOWTELL, D. & BRENTON, J. D. 2010. Driver mutations in TP53 are ubiquitous in high grade serous carcinoma of the ovary. *J Pathol,* 221**,** 49-56.

AHMED, N., NIU, J., DORAHY, D. J., GU, X., ANDREWS, S., MELDRUM, C. J., SCOTT, R. J., BAKER, M. S., MACREADIE, I. G. & AGREZ, M. V. 2002a. Direct integrin alphavbeta6-ERK binding: implications for tumour growth. *Oncogene,* 21**,** 1370-80.

AHMED, N., RILEY, C., RICE, G. E., QUINN, M. A. & BAKER, M. S. 2002b. αvβ6 integrin-A marker for the malignant potential of epithelial ovarian cancer. *J Histochem and Cytochem,* 50**,** 1371-1379.

AHMED, N. & STENVERS, K. L. 2013. Getting to Know Ovarian Cancer Ascites: Opportunities for Targeted Therapy-Based Translational Research. *Front Oncol,* 3**,** 256.

ALBA, R., BRADSHAW, A. C., COUGHLAN, L., DENBY, L., MCDONALD, R. A., WADDINGTON, S. N., BUCKLEY, S. M. K., GREIG, J. A., PARKER, A. L., MILLER, A. M., WANG, H. J., LIEBER, A., VAN ROOIJEN, N., MCVEY, J. H., NICKLIN, S. A. & BAKER, A. H. 2010. Biodistribution and retargeting of FX-binding ablated adenovirus serotype 5 vectors. *Blood,* 116**,** 2656-2664.

ALBA, R., BRADSHAW, A. C., PARKER, A. L., BHELLA, D., WADDINGTON, S. N., NICKLIN, S. A., VAN ROOIJEN, N., CUSTERS, J., GOUDSMIT, J., BAROUCH, D. H., MCVEY, J. H. & BAKER, A. H. 2009. Identification of coagulation factor (F)X binding sites on the adenovirus serotype 5 hexon: Effect of mutagenesis on FX interactions and gene transfer. *Blood,* 114**,** 965-971.

ALLEN, M. D., THOMAS, G. J., CLARK, S., DAWOUD, M. M., VALLATH, S., PAYNE, S. J., GOMM, J. J., DREGER, S. A., DICKINSON, S., EDWARDS, D. R., PENNINGTON, C. J., SESTAK, I., CUZICK, J., MARSHALL, J. F., HART, I. R. & JONES, J. L. 2014. Altered microenvironment promotes progression of preinvasive breast cancer: Myoepithelial expression of avb6 integrin in DCIS identifies high-risk patients and predicts recurrence. *Clin Cancer Res,* 20**,** 344-357.

AMAXA. 2017. *Nucleofector Technology* [Online]. Amaxa Biosystems, Lonza. Available: http://bio.lonza.com/fileadmin/groups/FAQs/public/Technology_Flyer.pdf [Accessed 27 Feb 2017].

ANDTBACKA, R. H. I., COLLICHIO, F. A., AMATRUDA, T., SENZER, N., CHESNEY, J., DELMAN, K., SPITLER, L., PUZANOV, I., AGARWALA, S., MILHEM, M., HARRINGTON, K., MIDDLETON, M., LI, A., SHILKRUT, M., COFFIN, R. & KAUFMAN, H. 2014. Final planned overall survival (OS) from OPTiM, a randomized Phase III trial of talimogene laherparepvec (T-VEC) versus GM-CSF for the treatment of unresected stage IIIB/C/IV melanoma (NCT00769704). *J Immunother Cancer,* 2**,** P263-P263.

APPLEDORN, D. M., MCBRIDE, A., SEREGIN, S., SCOTT, J. M., SCHULDT, N., KIANG, A., GODBEHERE, S. & AMALFITANO, A. 2008. Complex interactions with several arms of the complement system dictate innate and humoral immunity to adenoviral vectors. *Gene Ther,* 15**,** 1606-1617.

ARIYAWANSA, J. P. & TOBIN, J. O. 1976. Fluorescent antibody responses to adenoviruses in humans. *J Clin Pathol,* 29**,** 411-416.

ARNAOUT, M. A., GOODMAN, S. L. & XIONG, J. P. 2007. Structure and mechanics of integrin-based cell adhesion. *Curr Opin Cell Biol,* 19**,** 495-507.

ARNBERG, N., KIDD, A. H., EDLUND, K., NILSSON, J., PRING-AKERBLOM, P. & WADELL, G. 2002. Adenovirus type 37 binds to cell surface sialic acid through a charge-dependent interaction. *Virology,* 302**,** 33-43.

ARNOLD, K., BORDOLI, L., KOPP, J. & SCHWEDE, T. 2006. The SWISS-MODEL workspace: A web-based environment for protein structure homology modelling. *Bioinformatics,* 22**,** 195-201.

ASAOKA, K., TADA, M., SAWAMURA, Y., IKEDA, J. & ABE, H. 2000. Dependence of efficient adenoviral gene delivery in malignant glioma cells on the expression levels of the Coxsackievirus and adenovirus receptor. *J Neurosurg,* 92**,** 1002-8.

ATODA, H. 1998. Coagulation factor X-binding protein from Deinagkistrodon acutus venom is a Gla domain-binding protein. *Biochemistry,* 37**,** 17361-17370.

BAI, M., HARFE, B. & FREIMUTH, P. 1993. Mutations that alter an Arg-Gly-Asp (RGD) sequence in the adenovirus type 2 penton base protein abolish its cell-rounding activity and delay virus reproduction in flat cells. *J Virol,* 67**,** 5198-205.

BANDYOPADHYAY, A. & RAGHAVAN, S. 2009. Defining the Role of Integrin αvβ6 in Cancer. *Curr Drug Targets,* 10**,** 645-652.

BARKER, S. D., CASADO, E., GOMEZ-NAVARRO, J., XIANG, J., ARAFAT, W., MAHASRESHTI, P., PUSTILNIK, T. B., HEMMINKI, A., SIEGAL, G. P., ALVAREZ, R. D. & CURIEL, D. T. 2001. An immunomagnetic-based method for the purification of ovarian cancer cells from patient-derived ascites. *Gynecol Oncol,* 82, 57-63.

BARNES, M. N., COOLIDGE, C. J., HEMMINKI, A., ALVAREZ, R. D. & CURIEL, D. T. 2002. Conditionally replicative adenoviruses for ovarian cancer therapy. *Mol Cancer Ther,* 1**,** 435-9.

BAUERSCHMITZ, G. J., BARKER, S. D. & HEMMINKI, A. 2002. Adenoviral gene therapy for cancer: from vectors to targeted and replication competent agents (review). *Int J Oncol,* 21**,** 1161-1174.

BAUERSCHMITZ, G. J., GUSE, K., KANERVA, A., MENZEL, A., HERRMANN, I., DESMOND, R. A., YAMAMOTO, M., NETTELBECK, D. M., HAKKARAINEN, T., DALL, P., CURIEL, D. T. & HEMMINKI, A. 2006. Triple-targeted oncolytic adenoviruses featuring the cox2 promoter, E1A transcomplementation, and serotype chimerism for enhanced selectivity for ovarian cancer cells. *Mol Ther,* 14**,** 164-74.

BAYO-PUXAN, N., CASCALLO, M., GROS, A., HUCH, M., FILLAT, C. & ALEMANY, R. 2006. Role of the putative heparan sulfate glycosaminoglycan-binding site of the adenovirus type 5 fiber shaft on liver detargeting and knob-mediated retargeting. *J Gen Virol,* 87**,** 2487-95.

BCI. 2015. *Promising antibody against cancer cells characterised at BCI to be developed for clinical trials* [Online]. Barts Cancer Institute. Available: http://bci.qmul.ac.uk/news/general-news/item/264rad-antibody-bci-medimmune-cruk-trials [Accessed 23 Nov 2016 2016].

BELL, D., BERCHUCK, A., BIRRER, M., CHIEN, J., CRAMER, D., DAO, F., DHIR, R., DISAIA, P., GABRA, H., GLENN, P., GODWIN, A., GROSS, J., HARTMANN, L., HUANG, M., HUNTSMAN, D., IACOCCA, M., IMIELINSKI, M., KALLOGER, S., KARLAN, B., LEVINE, D., MILLS, G., MORRISON, C., MUTCH, D., OLVERA, N., ORSULIC, S., PARK, K., PETRELLI, N., RABENO, B., RADER, J., SIKIC, B., SMITH-MCCUNE, K., SOOD, A., BOWTELL, D., PENNY, R., TESTA, J., CHANG, K., DINH, H., DRUMMOND, J., FOWLER, G., GUNARATNE, P., HAWES, A., KOVAR, C., LEWIS, L., MORGAN, M., NEWSHAM, I., SANTIBANEZ, J., REID, J., TREVINO, L., WU, Y., WANG, M., MUZNY, D., WHEELER, D., GIBBS, R., GETZ, G., LAWRENCE, M., CIBULSKIS, K., SIVACHENKO, A., SOUGNEZ, C., VOET, D., WILKINSON, J., BLOOM, T., ARDLIE, K., FENNELL, T., BALDWIN, J., GABRIEL, S., LANDER, E., DING, L. L., FULTON, R., KOBOLDT, D., MCLELLAN, M., WYLIE, T., WALKER, J., O'LAUGHLIN, M., DOOLING, D., FULTON, L., ABBOTT, R., DEES, N., ZHANG, Q., KANDOTH, C., WENDL, M., SCHIERDING, W., SHEN, D., HARRIS, C., SCHMIDT, H., KALICKI, J., DELEHAUNTY, K., FRONICK, C., DEMETER, R., COOK, L., WALLIS, J., LIN, L., MAGRINI, V., HODGES, J., ELDRED, J., SMITH, S., POHL, C., VANDIN, F., RAPHAEL, B., WEINSTOCK, G., MARDIS, E., et al. 2011. Integrated genomic analyses of ovarian carcinoma. *Nature,* 474**,** 609-15.

BELOUSOVA, N., KRENDELCHTCHIKOVA, V., CURIEL, D. T. & KRASNYKH, V. 2002. Modulation of adenovirus vector tropism via incorporation of polypeptide ligands into the fiber protein. *J Virol,* 76**,** 8621-31.

BELOUSOVA, N., MIKHEEVA, G., GELOVANI, J. & KRASNYKH, V. 2008. Modification of Adenovirus Capsid with a Designed Protein Ligand Yields a Gene Vector Targeted to a Major Molecular Marker of Cancer. *J Virol,* 82**,** 630-637.

BERGH, J., TORBJJRN, N., SJOGREN, S., LINDGREN, A. & HOLMBERG, L. 1995. Complete sequencing of the p53 gene provides prognostic information in breast cancer patients, particularly in relation to adjuvant systemic therapy and radiotherapy. *Nature Medicine,* 1**,** 1029-1034.

BERMAN, H. M., WESTBROOK, J., FENG, Z., GILLILAND, G., BHAT, T. N., WEISSIG, H., SHINDYALOV, I. N. & BOURNE, P. E. 2000. The Protein Data Bank. *Nucleic Acids Res,* 28**,** 235-242.

BETT, A. J., PREVEC, L. & GRAHAM, F. L. 1993. Packaging capacity and stability of human adenovirus type 5 vectors. *J Virol,* 67**,** 5911-5921.

BEWIG, B. & SCHMIDT, W. E. 2000. Accelerated titering of adenoviruses. *BioTechniques,* 28**,** 870-873.

BIASINI, M., BIENERT, S., WATERHOUSE, A., ARNOLD, K., STUDER, G., SCHMIDT, T., KIEFER, F., CASSARINO, T. G., BERTONI, M., BORDOLI, L. & SCHWEDE, T. 2014. SWISS-MODEL: Modelling protein tertiary and quaternary structure using evolutionary information. *Nucleic Acids Res,* 42**,** W252-W258.

BIOLEGEND. 2017. *Mouse Alloantigens* [Online]. BioLegend Ltd. Available: http://www.biolegend.com/media_assets/support_resource/BioLegend_Mouse_Alloantigens.pdf [Accessed 6 Mar 2017].

BLACKWELL, J. L., HUI, L., GOMEZ-NAVARRO, J., DMITRIEV, I., KRASNYKH, V., RICHTER, C. A., SHAW, D. R., ALVAREZ, R. D., CURIEL, D. T. & STRONG, T. V. 2000. Using a tropism-modified adenoviral vector to circumvent inhibitory factors in ascites fluid. *Hum Gene Ther,* 11**,** 1657-1669.

BORDOLI, L., KIEFER, F., ARNOLD, K., BENKERT, P., BATTEY, J. & SCHWEDE, T. 2009. Protein structure homology modeling using SWISS-MODEL workspace. *Nature Protocols,* 4**,** 1-13.

BORNHORST, J. A. & FALKE, J. J. 2000. [16] Purification of Proteins Using Polyhistidine Affinity Tags. *Methods Enzymol,* 326**,** 245-254.

BRADLEY, R. R., LYNCH, D. M., IAMPIETRO, M. J., BORDUCCHI, E. N. & BAROUCH, D. H. 2012a. Adenovirus Serotype 5 Neutralizing Antibodies Target both Hexon and Fiber following Vaccination and Natural Infection. *J Virol,* 86**,** 625-629.

BRADLEY, R. R., MAXFIELD, L. F., LYNCH, D. M., IAMPIETRO, M. J., BORDUCCHI, E. N. & BAROUCH, D. H. 2012b. Adenovirus serotype 5-specific neutralizing antibodies target multiple hexon hypervariable regions. *J Virol,* 86, 1267-72.

BRADSHAW, A. C., COUGHLAN, L., MILLER, A. M., ALBA, R., VAN ROOIJEN, N., NICKLIN, S. A. & BAKER, A. H. 2012. Biodistribution and inflammatory profiles of novel penton and hexon double-mutant serotype 5 adenoviruses. *J Control Release,* 164, 394-402.

BRANTON, P. E. & ROOPCHAND, D. E. 2001. The role of adenovirus E4orf4 protein in viral replication and cell killing. *Oncogene,* 20**,** 7855-7865.

BREMNER, K. H., SCHERER, J., YI, J., VERSHININ, M., GROSS, S. P. & VALLEE, R. B. 2009. Adenovirus transport via direct interaction of cytoplasmic dynein with the viral capsid hexon subunit. *Cell Host Microbe,* 6**,** 523-35.

BREMNES, R. M., DONNEM, T., AL-SAAD, S., AL-SHIBLI, K., ANDERSEN, S., SIRERA, R., CAMPS, C., MARINEZ, I. & BUSUND, L. T. 2011. The role of tumor stroma in cancer progression and prognosis: emphasis on carcinoma-associated fibroblasts and non-small cell lung cancer. *J Thorac Oncol,* 6**,** 209-17.

BREUSS, J. M., GALLO, J., DELISSER, H. M., KLIMANSKAYA, I. V., FOLKESSON, H. G., PITTET, J. F., NISHIMURA, S. L., ALDAPE, K., LANDERS, D. V., CARPENTER, W. & ET AL. 1995. Expression of the beta 6 integrin subunit in development, neoplasia and tissue repair suggests a role in epithelial remodeling. *J Cell Sci,* 108 ( Pt 6)**,** 2241-51.

BULLER, R. E., RUNNEBAUM, I. B., KARLAN, B. Y., HOROWITZ, J. A., SHAHIN, M., BUEKERS, T., PETRAUSKAS, S., KREIENBERG, R., SLAMON, D. & PEGRAM, M. 2002. A phase I/II trial of rAd/p53 (SCH 58500) gene replacement in recurrent ovarian cancer. *Cancer Gene Ther,* 9**,** 553-66.

BURMEISTER, W. P., GUILLIGAY, D., CUSACK, S., WADELL, G. & ARNBERG, N. 2004. Crystal structure of species D adenovirus fiber knobs and their sialic acid binding sites. *J Virol,* 78**,** 7727-7736.

BUSCARINI, M., QUEK, M. L., GILLIAM-HEGARICH, S., KASAHARA, N. & BOCHNER, B. 2007. Adenoviral receptor expression of normal bladder and transitional cell carcinoma of the bladder. *Urol Int,* 78**,** 160-6.

BUSK, M., PYTELÄ, R. & SHEPPARD, D. 1992. Characterization of the integrin αvβ6 as a fibronectin-binding protein. *J Biol Chem,* 267**,** 5790-5796.

CANTOR, D. I., CHERUKU, H. R., NICE, E. C. & BAKER, M. S. 2015. Integrin αvβ6 sets the stage for colorectal cancer metastasis. *Cancer Metastasis Rev,* 34**,** 715-734.

CAO, C., DONG, X., WU, X., WEN, B., JI, G., CHENG, L. & LIU, H. 2012. Conserved fiber-penton base interaction revealed by nearly atomic resolution cryo-electron microscopy of the structure of adenovirus provides insight into receptor interaction. *J Virol,* 86**,** 12322-12329.

CARDIFFUNI. 2016. *Cancer Research UK funds multi-disciplinary research project* [Online]. Available: http://www.cardiff.ac.uk/news/view/387549-cancer-research-uk-funds-multi-disciplinary-research-project [Accessed 8 March 2017].

CARLISLE, R., CHOI, J., BAZAN-PEREGRINO, M., LAGA, R., SUBR, V., KOSTKA, L., ULBRICH, K., COUSSIOS, C. C. & SEYMOUR, L. W. 2013. Enhanced tumor uptake and penetration of virotherapy using polymer stealthing and focused ultrasound. *J Natl Cancer Inst,* 105**,** 1701-10.

CARLISLE, R. C., DI, Y., CERNY, A. M., SONNEN, A. F. P., SIM, R. B., GREEN, N. K., SUBR, V., ULBRICH, K., GILBERT, R. J. C., FISHER, K. D., FINBERG, R. W. & SEYMOUR, L. W. 2009. Human erythrocytes bind and inactivate type 5 adenovirus by presenting Coxsackie virus-adenovirus receptor and complement receptor 1. *Blood,* 113**,** 1909-1918.

CASCALLO, M., ALONSO, M. M., ROJAS, J. J., PEREZ-GIMENEZ, A., FUEYO, J. & ALEMANY, R. 2007. Systemic toxicity-efficacy profile of ICOVIR-5, a potent and selective oncolytic adenovirus based on the pRB pathway. *Mol Ther,* 15**,** 1607-1615.

CHEN, C. Y., SENAC, J. S., WEAVER, E. A., MAY, S. M., JELINEK, D. F., GREIPP, P., WITZIG, T. & BARRY, M. A. 2011a. Species D adenoviruses as oncolytics against B-cell cancers. *Clin Cancer Res,* 17**,** 6712-22.

CHEN, G.-X., ZHANG, S., HE, X.-H., LIU, S.-Y., MA, C. & ZOU, X.-P. 2014. Clinical utility of recombinant adenoviral human p53 gene therapy: current perspectives. *OncoTargets Ther,* 7**,** 1901-1909.

CHEN, H., XIANG, Z. Q., LI, Y., KURUPATI, R. K., JIA, B., BIAN, A., ZHOU, D. M., HUTNICK, N., YUAN, S., GRAY, C., SERWANGA, J., AUMA, B., KALEEBU, P., ZHOU, X., BETTS, M. R. & ERTL, H. C. 2010. Adenovirus-based vaccines: comparison of vectors from three species of adenoviridae. *J Virol,* 84**,** 10522-32.

CHEN, K. L., PAN, F., JIANG, H., CHEN, J. F., PEI, L., XIE, F. W. & LIANG, H. J. 2011b. Highly enriched CD133 +CD44 + stem-like cells with CD133 +CD44 high metastatic subset in HCT116 colon cancer cells. *Clin Exp Metastasis,* 28**,** 751-763.

CHEN, X., WU, Y., DONG, H., ZHANG, C. Y. & ZHANG, Y. 2013. Platinum-based agents for individualized cancer treatment. *Curr Mol Med,* 13**,** 1603-12.

CHENG, C., GALL, J. G. D., NASON, M., KING, C. R., KOUP, R. A., ROEDERER, M., MCELRATH, M. J., MORGAN, C. A., CHURCHYARD, G., BADEN, L. R., DUERR, A. C., KEEFER, M. C., GRAHAM, B. S. & NABEL, G. J. 2010. Differential specificity and immunogenicity of adenovirus type 5 neutralizing antibodies elicited by natural infection or immunization. *J Virol,* 84**,** 630-638.

CHOI, J. W., LEE, J. S., KIM, S. W. & YUN, C. O. 2012. Evolution of oncolytic adenovirus for cancer treatment. *Adv Drug Deliv Rev*

CHROBOCZEK, J., RUIGROK, R. W. & CUSACK, S. 1995. Adenovirus fiber. *Curr Top Microbiol Immunol,* 199 ( Pt 1)**,** 163-200.

CHU, R. L., POST, D. E., KHURI, F. R. & VAN MEIR, E. G. 2004. Use of replicating oncolytic adenoviruses in combination therapy for cancer. *Clin Cancer Res,* 10**,** 5299-5312.

CICHON, G., BOECKH-HERWIG, S., KUEMIN, D., HOFFMANN, C., SCHMIDT, H. H., WEHNES, E., HAENSCH, W., SCHNEIDER, U., ECKHARDT, U., BURGER, R. & PRING-AKERBLOM, P. 2003. Titer determination of Ad5 in blood: a cautionary note. *Gene Ther,* 10**,** 1012-1017.

CICHON, G., BOECKH-HERWIG, S., SCHMIDT, H. H., WEHNES, E., MÜLLER, T., PRING-AKERBLOM, P. & BURGER, R. 2001. Complement activation by recombinant adenoviruses. *Gene Therapy,* 8**,** 1794-1800.

CLINICALTRIALS.GOV. 2016. *clinicalTrials.gov* [Online]. U.S. National Institutes of Health. Available: www.clinicaltrials.gov [Accessed 24 Oct 2016].

CORJON, S., GONZALEZ, G., HENNING, P., GRICHINE, A., LINDHOLM, L., BOULANGER, P., FENDER, P. & HONG, S. S. 2011. Cell entry and trafficking of human adenovirus bound to blood factor X is determined by the fiber serotype and not hexon:heparan sulfate interaction. *PLoS One,* 6**,** e18205.

COUGHLAN, L., ALBA, R., PARKER, A. L., BRADSHAW, A. C., MCNEISH, I. A., NICKLIN, S. A. & BAKER, A. H. 2010. Tropism-modification strategies for targeted gene delivery using adenoviral vectors. *Viruses*, 2(10):2290-355.

COUGHLAN, L., BRADSHAW, A. C., PARKER, A. L., ROBINSON, H., WHITE, K., CUSTERS, J., GOUDSMIT, J., VAN ROIJEN, N., BAROUCH, D. H., NICKLIN, S. A. & BAKER, A. H. 2012. Ad5:Ad48 Hexon Hypervariable Region Substitutions Lead to Toxicity and Increased Inflammatory Responses Following Intravenous Delivery. *Mol Ther,* 20**,** 2268-2281.

COUGHLAN, L., UUSI-KERTTULA, H., MA, J., DEGG, B. P., PARKER, A. L. & BAKER, A. H. 2014. Retargeting adenovirus serotype 48 fiber knob domain by peptide incorporation. *Hum Gene Ther,* 25**,** 385-394.

COUGHLAN, L., VALLATH, S., SAHA, A., FLAK, M., MCNEISH, I. A., VASSAUX, G., MARSHALL, J. F., HART, I. R. & THOMAS, G. J. 2009a. In Vivo Retargeting of Adenovirus Type 5 to alpha v beta 6 Integrin Results in Reduced Hepatotoxicity and Improved Tumor Uptake following Systemic Delivery. *J Virol,* 83**,** 6416-6428.

COUGHLAN, L., VALLATH, S., SAHA, A., MCNEISH, I. A., VASSAUX, G., MARSHALL, J. F., HART, I. R. & THOMAS, G. J. 2009b. An Ad5 Vector Retargeted to alpha v beta 6 Displays Improved Tumour Transduction Combined with Reduced Liver Uptake Following Systemic Delivery. *Mol Ther,* 17**,** S323-S323.

COYNE, C. B. & BERGELSON, J. M. 2005. CAR: A virus receptor within the tight junction. *Adv Drug Del Rev,* 57**,** 869-882.

CRAWFORD-MIKSZA, L. & SCHNURR, D. P. 1996. Seroepidemiology of new AIDS-associated adenoviruses among the San Francisco Men's Health Study. *J Med Virol,* 50**,** 230-236.

CRUK. 2012. *Ovarian cancer* [Online]. Cancer Research UK. Available: http://www.cancerresearchuk.org/about-cancer/type/ovarian-cancer/ [Accessed 30/9/2015 2015].

DANTHINNE, X. & IMPERIALE, M. J. 2000. Production of first generation adenovirus vectors: A review. *Gene Ther,* 7**,** 1707-1714.

DENBY, L., WORK, L. M., GRAHAM, D., HSU, C., VON SEGGERN, D. J., NICKLIN, S. A. & BAKER, A. H. 2004. Adenoviral serotype 5 vectors pseudotyped with fibers from subgroup D show modified tropism in vitro and in vivo. *Hum Gene Ther,* 15**,** 1054-64.

DI PAOLO, N. C., KALYUZHNIY, O. & SHAYAKHMETOV, D. M. 2007. Fiber shaft-chimeric adenovirus vectors lacking the KKTK motif efficiently infect liver cells in vivo. *J Virol,* 81**,** 12249-59.

DI PAOLO, N. C., MIAO, E. A., IWAKURA, Y., MURALI-KRISHNA, K., ADEREM, A., FLAVELL, R. A., PAPAYANNOPOULOU, T. & SHAYAKHMETOV, D. M. 2009. Virus Binding to a Plasma Membrane Receptor Triggers Interleukin-1α-Mediated Proinflammatory Macrophage Response In Vivo. *Immunity,* 31**,** 110-121.

DI, Y., SEYMOUR, L. & FISHER, K. 2014. Activity of a group B oncolytic adenovirus (ColoAd1) in whole human blood. *Gene Ther,* 21**,** 440-3.

DICARA, D., BURMAN, A., CLARK, S., BERRYMAN, S., HOWARD, M. J., HART, I. R., MARSHALL, J. F. & JACKSON, T. 2008. Foot-and-mouth disease virus forms a highly stable, EDTA-resistant

complex with its principal receptor, integrin alphavbeta6: implications for infectiousness. *J Virol,* 82**,** 1537-46.

DICARA, D., RAPISARDA, C., SUTCLIFFE, J. L., VIOLETTE, S. M., WEINREB, P. H., HART, I. R., HOWARD, M. J. & MARSHALL, J. F. 2007. Structure-function analysis of Arg-Gly-Asp helix motifs in αvβ6 integrin ligands. *J Biol Chem,* 282**,** 9657-9665.

DONG, W., VAN GINKEL, J. W., AU, K. Y., ALEMANY, R., MEULENBERG, J. J. & VAN BEUSECHEM, V. W. 2014a. ORCA-010, a novel potency-enhanced oncolytic adenovirus, exerts strong antitumor activity in preclinical models. *Hum Gene Ther,* 25**,** 897-904.

DONG, X., HUDSON, N. E., LU, C. & SPRINGER, T. A. 2014b. Structural determinants of integrin beta-subunit specificity for latent TGF-beta. *Nat Struct Mol Biol,* 21**,** 1091-6.

DOOLEY, D. C., SIMPSON, J. F. & MERYMAN, H. T. 1982. Isolation of large numbers of fully viable human neutrophils: A preparative technique using Percoll density gradient centrifugation. *Exp Hematol,* 10**,** 591-599.

DORONIN, K., FLATT, J. W., DI PAOLO, N. C., KHARE, R., KALYUZHNIY, O., ACCHIONE, M., SUMIDA, J. P., OHTO, U., SHIMIZU, T., AKASHI-TAKAMURA, S., MIYAKE, K., MACDONALD, J. W., BAMMLER, T. K., BEYER, R. P., FARIN, F. M., STEWART, P. L. & SHAYAKHMETOV, D. M. 2012. Coagulation factor X activates innate immunity to human species C adenovirus. *Science,* 338**,** 795-798.

DUNFIELD, L. D., SHEPHERD, T. G. & NACHTIGAL, M. W. 2002. Primary culture and mRNA analysis of human ovarian cells. *Biol Proced Online,* 4**,** 55-61.

DUTTA, A., LI, J., LU, H., AKECH, J., PRATAP, J., WANG, T., ZERLANKO, B. J., GERALD, T. J. F., JIANG, Z., BIRBE, R., WIXTED, J., VIOLETTE, S. M., STEIN, J. L., STEIN, G. S., LIAN, J. B. & LANGUINO, L. R. 2014. Integrin avb6 Promotes an osteolytic program in cancer cells by upregulating MMP2. *Cancer Research,* 74**,** 1598-1608.

EHRKE-SCHULZ, E., ZHANG, W., SCHIWON, M., BERGMANN, T., SOLANKI, M., LIU, J., BOEHME, P., LEITNER, T. & EHRHARDT, A. 2016. Cloning and Large-Scale Production of High-Capacity Adenoviral Vectors Based on the Human Adenovirus Type 5. *J Vis Exp***,** e52894.

ELIOPOULOS, A. G., KERR, D. J., HEROD, J., HODGKINS, L., KRAJEWSKI, S., REED, J. C. & YOUNG, L. S. 1995. The control of apoptosis and drug resistance in ovarian cancer: influence of p53 and Bcl-2. *Oncogene,* 11**,** 1217-28.

FDA. 2015. *FDA approves first-of-its-kind product for the treatment of melanoma* [Online]. U.S. Food and Drug Administration. Available: http://www.fda.gov/NewsEvents/Newsroom/PressAnnouncements/ucm469571.htm [Accessed 13th Jan 2016].

FUEYO, J., GOMEZ-MANZANO, C., ALEMANY, R., LEE, P. S. Y., MCDONNELL, T. J., MITLIANGA, P., SHI, Y. X., LEVIN, V. A., YUNG, W. K. A. & KYRITSIS, A. P. 2000. A mutant oncolytic adenovirus targeting the Rb pathway produces anti-glioma effect in vivo. *Oncogene,* 19**,** 2-12.

GAGGAR, A., SHAYAKHMETOV, D. M. & LIEBER, A. 2003. CD46 is a cellular receptor for group B adenoviruses. *Nat Med,* 9**,** 1408-12.

GAHÉRY-SÉGARD, H., FARACE, F., GODFRIN, D., GASTON, J., LENGAGNE, R., TURSZ, T., BOULANGER, P. & GUILLET, J. G. 1998. Immune response to recombinant capsid proteins of adenovirus in humans: Antifiber and anti-penton base antibodies have a synergistic effect on neutralizing activity. *J Virol,* 72**,** 2388-2397.

GALL, J., KASS-EISLER, A., LEINWAND, L. & FALCK-PEDERSEN, E. 1996. Adenovirus type 5 and 7 capsid chimera: Fiber replacement alters receptor tropism without affecting primary immune neutralization epitopes. *J Virol,* 70**,** 2116-2123.

GANGULY, K. K., PAL, S., MOULIK, S. & CHATTERJEE, A. 2013. Integrins and metastasis. *Cell Adh Migr,* 7**,** 251-61.

GANLY, I., KIRN, D., ECKHARDT, S. G., RODRIGUEZ, G. I., SOUTAR, D. S., OTTO, R., ROBERTSON, A. G., PARK, O., GULLEY, M. L., HEISE, C., VON HOFF, D. D. & KAYE, S. B. 2000. A Phase I study of Onyx-015, an E1B attenuated adenovirus, administered intratumorally to patients with recurrent head and neck cancer. *Clin Cancer Res,* 6**,** 798-806.

GARSON, K. & VANDERHYDEN, B. C. 2015. Epithelial ovarian cancer stem cells: underlying complexity of a simple paradigm. *Reproduction,* 149**,** R59-70.

GEISBERT, T. W., BAILEY, M., HENSLEY, L., ASIEDU, C., GEISBERT, J., STANLEY, D., HONKO, A., JOHNSON, J., MULANGU, S., PAU, M. G., CUSTERS, J., VELLINGA, J., HENDRIKS, J., JAHRLING, P., ROEDERER, M., GOUDSMIT, J., KOUP, R. & SULLIVAN, N. J. 2011. Recombinant adenovirus serotype 26 (Ad26) and Ad35 vaccine vectors bypass immunity to Ad5 and protect nonhuman primates against ebolavirus challenge. *J Virol,* 85**,** 4222-33.

GIANCOTTI, F. G. & RUOSLAHTI, E. 1999. Integrin signaling. *Science,* 285**,** 1028-1032.

GIANNI, T., SALVIOLI, S., CHESNOKOVA, L. S., HUTT-FLETCHER, L. M. & CAMPADELLI-FIUME, G. 2013. alphavbeta6- and alphavbeta8-integrins serve as interchangeable receptors for HSV gH/gL to promote endocytosis and activation of membrane fusion. *PLoS Path,* 9**,** e1003806.

GOLDMAN, M. J. & WILSON, J. M. 1995. Expression of alpha v beta 5 integrin is necessary for efficient adenovirus-mediated gene transfer in the human airway. *J Virol,* 69**,** 5951-8.

GREEN, N. K., HERBERT, C. W., HALE, S. J., HALE, A. B., MAUTNER, V., HARKINS, R., HERMISTON, T., ULBRICH, K., FISHER, K. D. & SEYMOUR, L. W. 2004. Extended plasma circulation time and decreased toxicity of polymer-coated adenovirus. *Gene Ther,* 11**,** 1256-1263.

GROS, A., MARTÍNEZ-QUINTANILLA, J., PUIG, C., GUEDAN, S., MOLLEVÍ, D. G., ALEMANY, R. & CASCALLO, M. 2008. Bioselection of a gain of function mutation that enhances adenovirus 5 release and improves its antitumoral potency. *Cancer Res,* 68**,** 8928-8937.

GUPALO, E., BURIACHKOVSKAIA, L. & OTHMAN, M. 2011. Human platelets express CAR with localization at the sites of intercellular interaction. *Virol J,* 8**,** 456.

HAAPASALMI, K., ZHANG, K., TONNESEN, M., OLERUD, J., SHEPPARD, D., SALO, T., KRAMER, R., CLARK, R. A. F., UITTO, V. J. & LARJAVA, H. 1996. Keratinocytes in human wounds express αvβ6 integrin. *J Invest Dermatol,* 106**,** 42-48.

HALL, T. A. 1999. BioEdit: a user-friendly biological sequence alignment editor and analysis program for Windows 95/98/NT.: *Nucl Acids Symp Ser,* 41: 95-98.

HARTMAN, Z. C., APPLEDORN, D. M. & AMALFITANO, A. 2008. Adenovirus vector induced innate immune responses: Impact upon efficacy and toxicity in gene therapy and vaccine applications. *Virus Res,* 132**,** 1-14.

HARVEY, B. G., HACKETT, N. R., EL-SAWY, T., ROSENGART, T. K., HIRSCHOWITZ, E. A., LIEBERMAN, M. D., LESSER, M. L. & CRYSTAL, R. G. 1999. Variability of human systemic humoral immune responses to adenovirus gene transfer vectors administered to different organs. *J Virol,* 73**,** 6729-6742.

HAUSNER, S. H., ABBEY, C. K., BOLD, R. J., GAGNON, M. K., MARIK, J., MARSHALL, J. F., STANECKI, C. E. & SUTCLIFFE, J. L. 2009. Targeted in vivo imaging of integrin alphavbeta6 with an improved radiotracer and its relevance in a pancreatic tumor model. *Cancer Res,* 69**,** 5843-50.

HAWKINS, L. K., LEMOINE, N. R. & KIRN, D. 2002. Oncolytic biotherapy: A novel therapeutic platform. *Lancet Oncol,* 3**,** 17-26.

HEIKKILÄ, O., SUSI, P., STANWAY, G. & HYYPIÄ, T. 2009. Integrin alphaVbeta6 is a high-affinity receptor for coxsackievirus A9. *J Gen Virol,* 90**,** 197-204.

HEMMINKI, A., WANG, M., DESMOND, R. A., STRONG, T. V., ALVAREZ, R. D. & CURIEL, D. T. 2002. Serum and ascites neutralizing antibodies in ovarian cancer patients treated with intraperitoneal adenoviral gene therapy. *Hum Gene Ther,* 13**,** 1505-1514.

HENDRICKX, R., STICHLING, N., KOELEN, J., KURYK, L., LIPIEC, A. & GREBER, U. F. 2014. Innate immunity to adenovirus. *Hum Gene Ther,* 25**,** 265-284.

HEZEL, A. F., DESHPANDE, V., ZIMMERMAN, S. M., CONTINO, G., ALAGESAN, B., O'DELL, M. R., RIVERA, L. B., HARPER, J., LONNING, S., BREKKEN, R. A. & BARDEESY, N. 2012. TGF-beta and alphavbeta6 integrin act in a common pathway to suppress pancreatic cancer progression. *Cancer Res,* 72**,** 4840-5.

HOLSCHNEIDER, C. H. & BEREK, J. S. 2000. Ovarian cancer: Epidemiology, biology, and prognostic factors. *Sem Surg Oncol,* 19**,** 3-10.

HONG, S. S., HABIB, N. A., FRANQUEVILLE, L., JENSEN, S. & BOULANGER, P. A. 2003. Identification of adenovirus (Ad) penton base neutralizing epitopes by use of sera from patients who had received conditionally replicative Ad (Addl1520) for treatment of liver tumors. *J Virol,* 77**,** 10366-10375.

HORAN, G. S., WOOD, S., ONA, V., LI, D. J., LUKASHEV, M. E., WEINREB, P. H., SIMON, K. J., HAHM, K., ALLAIRE, N. E., RINALDI, N. J., GOYAL, J., FEGHALI-BOSTWICK, C. A., MATTESON, E. L., O'HARA, C., LAFYATIS, R., DAVIS, G. S., HUANG, X., SHEPPARD, D. & VIOLETTE, S. M. 2008. Partial inhibition of integrin alpha(v)beta6 prevents pulmonary fibrosis without exacerbating inflammation. *Am J Respir Crit Care Med,* 177**,** 56-65.

HOSIE, K., GILBERT, J. A., KERR, D., BROWN, C. B. & PEERS, E. M. 2001. Fluid dynamics in man of an intraperitoneal drug delivery solution: 4% icodextrin. *Drug Deliv,* 8**,** 9-12.

HOSIE, K. B., KERR, D. J., GILBERT, J. A., DOWNES, M., LAKIN, G., PEMBERTON, G., TIMMS, K., YOUNG, A. & STANLEY, A. 2003. A pilot study of adjuvant intraperitoneal 5-fluorouracil using 4% icodextrin as a novel carrier solution. *Eur J Surg Oncol,* 29**,** 254-60.

HUANG, X. Z., WU, J. F., CASS, D., ERIE, D. J., CORRY, D., YOUNG, S. G., FARESE JR, R. V. & SHEPPARD, D. 1996. Inactivation of the integrin β6 subunit gene reveals a role of epithelial integrins in regulating inflammation in the lungs and skin. *J Cell Biol,* 133**,** 921-928.

HYNES, R. O. 2002. Integrins: bidirectional, allosteric signaling machines. *Cell,* 110**,** 673-87.

INGEMARSDOTTER, C. K., TOOKMAN, L. A., BROWNE, A., PIRLO, K., CUTTS, R., CHELELA, C., KHURRUM, K. F., LEUNG, E. Y. L., DOWSON, S., WEBBER, L., KHAN, I., ENNIS, D., SYED, N., CROOK, T. R., BRENTON, J. D., LOCKLEY, M. & MCNEISH, I. A. 2015. Paclitaxel resistance increases oncolytic adenovirus efficacy via upregulated CAR expression and dysfunctional cell cycle control. *Mol Oncol,* 9**,** 791-805.

IRONS, E. E., FLATT, J. W., DORONIN, K., FOX, T. L., ACCHIONE, M., STEWART, P. L. & SHAYAKHMETOV, D. M. 2013. Coagulation Factor Binding Orientation and Dimerization May Influence Infectivity of Adenovirus-Coagulation Factor Complexes. *J Virol,* 87**,** 9610-9619.

JAKEMAN, P. G., HILLS, T. E., TEDCASTLE, A. B., DI, Y., FISHER, K. D. & SEYMOUR, L. W. 2015. Improved in Vitro Human Tumor Models for Cancer Gene Therapy. *Hum Gene Ther,* 26**,** 249-256.

JIANG, G., XIN, Y., ZHENG, J. N. & LIU, Y. Q. 2011. Combining conditionally replicating adenovirus-mediated gene therapy with chemotherapy: A novel antitumor approach. *Int J Cancer,* 129**,** 263-274.

JIANG, H., GOMEZ-MANZANO, C., RIVERA-MOLINA, Y., LANG, F. F., CONRAD, C. A. & FUEYO, J. 2015. Oncolytic adenovirus research evolution: From cell-cycle checkpoints to immune checkpoints. *Curr Opin Virol,* 13**,** 33-39.

JOHANSSON, S., NILSSON, E., QIAN, W., GUILLIGAY, D., CREPIN, T., CUSACK, S., ARNBERG, N. & ELOFSSON, M. 2009. Design, synthesis, and evaluation of N-acyl modified sialic acids as inhibitors of adenoviruses causing epidemic keratoconjunctivitis. *J Med Chem,* 52**,** 3666-78.

JOOSS, K. & CHIRMULE, N. 2003. Immunity to adenovirus and adeno-associated viral vectors: Implications for gene therapy. *Gene Ther,* 10**,** 955-963.

JUILLARD, V., VILLEFROY, P., GODFRIN, D., PAVIRANI, A., VENET, A. & GUILLET, J. G. 1995. Long-term humoral and cellular immunity induced by a single immunization with replication-defective adenovirus recombinant vector. *Europ J Immunol,* 25**,** 3467-3473.

JUNTTILA, M. R. & DE SAUVAGE, F. J. 2013. Influence of tumour micro-environment heterogeneity on therapeutic response. *Nature,* 501**,** 346-354.

KALYUZHNIY, O., DI PAOLO, N. C., SILVESTRY, M., HOFHERR, S. E., BARRY, M. A., STEWART, P. L. & SHAYAKHMETOV, D. M. 2008. Adenovirus serotype 5 hexon is critical for virus infection of hepatocytes in vivo. *PNAS,* 105**,** 5483-5488.

KANERVA, A., BAUERSCHMITZ, G. J., YAMAMOTO, M., LAM, J. T., ALVAREZ, R. D., SIEGAL, G. P., CURIEL, D. T. & HEMMINKI, A. 2004. A cyclooxygenase-2 promoter-based conditionally replicating adenovirus with enhanced infectivity for treatment of ovarian adenocarcinoma. *Gene Ther,* 11**,** 552-9.

KANERVA, A. & HEMMINKI, A. 2005. Adenoviruses for treatment of cancer. *Ann Med,* 37**,** 33-43.

KANERVA, A., NOKISALMI, P., DIACONU, I., KOSKI, A., CERULLO, V., LIIKANEN, I., TÄHTINEN, S., OKSANEN, M., HEISKANEN, R., PESONEN, S., JOENSUU, T., ALANKO, T., PARTANEN, K., LAASONEN, L., KAIREMO, K., KANGASNIEMI, L. & HEMMINKI, A. 2013. Antiviral and antitumor T-cell immunity in patients treated with GM-CSF-coding oncolytic adenovirus. *Clin Cancer Res,* 19**,** 2734-2744.

KAUFMAN, H. L. & BINES, S. D. 2010. OPTIM trial: a Phase III trial of an oncolytic herpes virus encoding GM-CSF for unresectable stage III or IV melanoma. *Future Oncol,* 6**,** 941-949.

KAUFMANN, J. K. & NETTELBECK, D. M. 2012. Virus chimeras for gene therapy, vaccination, and oncolysis: adenoviruses and beyond. *Trends Mol Med*

KHAN, Z. & MARSHALL, J. F. 2016. The role of integrins in TGFbeta activation in the tumour stroma. *Cell Tissue Res,* 365**,** 657-73.

KHARE, R., REDDY, V. S., NEMEROW, G. R. & BARRY, M. A. 2012. Identification of adenovirus serotype 5 hexon regions that interact with scavenger receptors. *J Virol,* 86**,** 2293-2301.

KHURI, F. R., NEMUNAITIS, J., GANLY, I., ARSENEAU, J., TANNOCK, I. F., ROMEL, L., GORE, M., IRONSIDE, J., MACDOUGALL, R. H., HEISE, C., RANDLEV, B., GILLENWATER, A. M., BRUSO, P., KAYE, S. B., HONG, W. K. & KIRN, D. H. 2000. A controlled trial of intratumoral ONYX-015, a selectively-replicating adenovirus, in combination with cisplatin and 5-fluorouracil in patients with recurrent head and neck cancer. *Nat Med,* 6**,** 879-885.

KIDD, P. 2003. Th1/Th2 balance: the hypothesis, its limitations, and implications for health and disease. *Altern Med Rev,* 8**,** 223-46.

KIM, J. S., LEE, S. H., CHO, Y. S., CHOI, J. J., KIM, Y. H. & LEE, J. H. 2002a. Enhancement of the adenoviral sensitivity of human ovarian cancer cells by transient expression of coxsackievirus and adenovirus receptor (CAR). *Gynecol Oncol,* 85**,** 260-5.

KIM, K. H., DMITRIEV, I., O'MALLEY, J. P., WANG, M., SADDEKNI, S., YOU, Z., PREUSS, M. A., HARRIS, R. D., AURIGEMMA, R., SIEGAL, G. P., ZINN, K. R., CURIEL, D. T. & ALVAREZ, R. D. 2012. A Phase I Clinical Trial of Ad5.SSTR/TK.RGD, a Novel Infectivity-Enhanced Bicistronic Adenovirus, in Patients with Recurrent Gynecologic Cancer. *Clin Cancer Res,* 18**,** 3440-3451.

KIM, M., ZINN, K. R., BARNETT, B. G., SUMEREL, L. A., KRASNYKH, V., CURIEL, D. T. & DOUGLAS, J. T. 2002b. The therapeutic efficacy of adenoviral vectors for cancer gene therapy is limited by a low level of primary adenovirus receptors on tumour cells. *Eur J Cancer,* 38**,** 1917-26.

KIMBALL, K. J., PREUSS, M. A., BARNES, M. N., WANG, M., SIEGAL, G. P., WAN, W., KUO, H., SADDEKNI, S., STOCKARD, C. R., GRIZZLE, W. E., HARRIS, R. D., AURIGEMMA, R., CURIEL, D. T. & ALVAREZ, R. D. 2010. A phase I study of a tropism-modified conditionally replicative adenovirus for recurrent malignant gynecologic diseases. *Clin Cancer Res,* 16**,** 5277-5287.

KIPPS, E., TAN, D. S. & KAYE, S. B. 2013. Meeting the challenge of ascites in ovarian cancer: new avenues for therapy and research. *Nat Rev Cancer,* 13**,** 273-82.

KIRBY, I., DAVISON, E., BEAVIL, A. J., SOH, C. P. C., WICKHAM, T. J., ROELVINK, P. W., KOVESDI, I., SUTTON, B. J. & SANTIS, G. 2000. Identification of contact residues and definition of the CAR-binding site of adenovirus type 5 fiber protein. *J Virol,* 74**,** 2804-2813.

KOGELBERG, H., TOLNER, B., THOMAS, G. J., DI CARA, D., MINOGUE, S., RAMESH, B., SODHA, S., MARSH, D., LOWDELL, M. W., MEYER, T., BEGENT, R. H., HART, I., MARSHALL, J. F. & CHESTER, K. 2008. Engineering a single-chain Fv antibody to alpha v beta 6 integrin using the specificity-determining loop of a foot-and-mouth disease virus. *J Mol Biol,* 382**,** 385-401.

KOONINGS, P. P., CAMPBELL, K., MISHELL JR, D. R. & GRIMES, D. A. 1989. Relative frequency of primary ovarian neoplasms: A 10-year review. *Obstet Gynecol,* 74**,** 921-926.

KOOPMAN VAN AARSEN, L. A., LEONE, D. R., HO, S., DOLINSKI, B. M., MCCOON, P. E., LEPAGE, D. J., KELLY, R., HEANEY, G., RAYHORN, P., REID, C., SIMON, K. J., HORAN, G. S., TAO, N., GARDNER, H. A., SKELLY, M. M., GOWN, A. M., THOMAS, G. J., WEINREB, P. H., FAWELL, S. E. & VIOLETTE, S. M. 2008. Antibody-mediated blockade of integrin αvβ 6 inhibits tumor progression in vivo by a transforming growth factor-β-regulated mechanism. *Cancer Res,* 68**,** 561-570.

KOSKI, A., KANGASNIEMI, L., ESCUTENAIRE, S., PESONEN, S., CERULLO, V., DIACONU, I., NOKISALMI, P., RAKI, M., RAJECKI, M., GUSE, K., RANKI, T., OKSANEN, M., HOLM, S. L., HAAVISTO, E., KARIOJA-KALLIO, A., LAASONEN, L., PARTANEN, K., UGOLINI, M., HELMINEN, A., KARLI, E., HANNUKSELA, P., JOENSUU, T., KANERVA, A. & HEMMINKI, A. 2010. Treatment of cancer patients with a serotype 5/3 chimeric oncolytic adenovirus expressing GMCSF. *Mol Ther,* 18**,** 1874-84.

KRASNYKH, V., DMITRIEV, I., MIKHEEVA, G., MILLER, C. R., BELOUSOVA, N. & CURIEL, D. T. 1998. Characterization of an adenovirus vector containing a heterologous peptide epitope in the HI loop of the fiber knob. *J Virol,* 72**,** 1844-1852.

KRASNYKH, V. N., MIKHEEVA, G. V., DOUGLAS, J. T. & CURIEL, D. T. 1996. Generation of recombinant adenovirus vectors with modified fibers for altering viral tropism. *J Virol,* 70**,** 6839-6846.

KRITZ, A. B., NICOL, C. G., DISHART, K. L., NELSON, R., HOLBECK, S., VON SEGGERN, D. J., WORK, L. M., MCVEY, J. H., NICKLIN, S. A. & BAKER, A. H. 2007. Adenovirus 5 fibers mutated at the putative HSPG-binding site show restricted retargeting with targeting peptides in the HI loop. *Mol Ther,* 15**,** 741-9.

KUHN, I., HARDEN, P., BAUZON, M., CHARTIER, C., NYE, J., THORNE, S., REID, T., NI, S., LIEBER, A., FISHER, K., SEYMOUR, L., RUBANYI, G. M., HARKINS, R. N. & HERMISTON, T. W. 2008. Directed evolution generates a novel oncolytic virus for the treatment of colon cancer. *PLoS ONE,* 3**,** e2409.

KURYK, L., HAAVISTO, E., GAROFALO, M., CAPASSO, C., HIRVINEN, M., PESONEN, S., RANKI, T., VASSILEV, L. & CERULLO, V. 2016. Synergistic anti-tumor efficacy of immunogenic adenovirus ONCOS-102 (Ad5/3-D24-GM-CSF) and standard of care chemotherapy in preclinical mesothelioma model. *Int J Cancer,* 139**,** 1883-93.

KÄLIN, S., AMSTUTZ, B., GASTALDELLI, M., WOLFRUM, N., BOUCKE, K., HAVENGA, M., DIGENNARO, F., LISKA, N., HEMMI, S. & GREBER, U. F. 2010. Macropinocytotic Uptake and Infection of Human Epithelial Cells with Species B2 Adenovirus Type 35. *J Virol,* 84**,** 5336-5350.

LATIFI, A., LUWOR, R. B., BILANDZIC, M., NAZARETIAN, S., STENVERS, K., PYMAN, J., ZHU, H., THOMPSON, E. W., QUINN, M. A., FINDLAY, J. K. & AHMED, N. 2012. Isolation and characterization of tumor cells from the ascites of ovarian cancer patients: molecular phenotype of chemoresistant ovarian tumors. *PLoS One,* 7**,** e46858.

LEHRMAN, S. 1999. Virus treatment questioned after gene therapy death. *Nature,* 401**,** 517-518.

LEOPOLD, P. L. & CRYSTAL, R. G. 2007. Intracellular trafficking of adenovirus: Many means to many ends. *Adv Drug Del Rev,* 59**,** 810-821.

LI, D., DUAN, L., FREIMUTH, P. & O'MALLEY, B. W., JR. 1999a. Variability of adenovirus receptor density influences gene transfer efficiency and therapeutic response in head and neck cancer. *Clin Cancer Res,* 5**,** 4175-81.

LI, H., RHEE, E. G., MASEK-HAMMERMAN, K., TEIGLER, J. E., ABBINK, P. & BAROUCH, D. H. 2012. Adenovirus serotype 26 utilizes CD46 as a primary cellular receptor and only transiently activates T lymphocytes following vaccination of rhesus monkeys. *J Virol,* 86**,** 10862-5.

LI, Y., PONG, R. C., BERGELSON, J. M., HALL, M. C., SAGALOWSKY, A. I., TSENG, C. P., WANG, Z. & HSIEH, J. T. 1999b. Loss of adenoviral receptor expression in human bladder cancer cells: A potential impact on the efficacy of gene therapy. *Cancer Res,* 59**,** 325-330.

LICHTY, B. D., BREITBACH, C. J., STOJDL, D. F. & BELL, J. C. 2014. Going viral with cancer immunotherapy. *Nat Rev Cancer,* 14**,** 559-567.

LION, T. 2014. Adenovirus infections in immunocompetent and immunocompromised patients. *Clin Microbiol Rev,* 27**,** 441-462.

LIU, Y., YASUKAWA, M., CHEN, K., HU, L., BROADDUS, R. R., DING, L., MARDIS, E. R., SPELLMAN, P., LEVINE, D. A., MILLS, G. B., SHMULEVICH, I., SOOD, A. K. & ZHANG, W. 2015. Association of somatic mutations of ADAMTS genes with chemotherapy sensitivity and survival in high-grade serous ovarian carcinoma. *JAMA Oncology,* 1**,** 486-494.

LIU, Z., LIU, H., MA, T., SUN, X., SHI, J., JIA, B., SUN, Y., ZHAN, J., ZHANG, H., ZHU, Z. & WANG, F. 2014. Integrin alphavbeta(6)-Targeted SPECT Imaging for Pancreatic Cancer Detection. *J Nucl Med,* 55**,** 989-94.

MA, J., DUFFY, M. R., DENG, L., DAKIN, R. S., UIL, T., CUSTERS, J., KELLY, S. M., MCVEY, J. H., NICKLIN, S. A. & BAKER, A. H. 2015. Manipulating adenovirus hexon hypervariable loops dictates immune neutralisation and coagulation factor X-dependent cell interaction in vitro and in vivo. *PLoS Pathog,* 11**,** e1004673.

MACK, C. A., SONG, W. R., CARPENTER, H., WICKHAM, T. J., KOVESDI, I., HARVEY, B. G., MAGOVERN, C. J., ISOM, O. W., ROSENGART, T., FALCK-PEDERSEN, E., HACKETT, N. R., CRYSTAL, R. G. & MASTRANGELI, A. 1997. Circumvention of anti-adenovirus neutralizing immunity by administration of an adenoviral vector of an alternate serotype. *Hum Gene Ther,* 8**,** 99-109.

MADISCH, I., HARSTE, G., POMMER, H. & HEIM, A. 2005. Phylogenetic analysis of the main neutralization and hemagglutination determinants of all human adenovirus prototypes as a basis for molecular classification and taxonomy. *J Virol,* 79**,** 15265-15276.

MAJHEN, D., CALDERON, H., CHANDRA, N., FAJARDO, C. A., RAJAN, A., ALEMANY, R. & CUSTERS, J. 2014. Adenovirus-based vaccines for fighting infectious diseases and cancer: Progress in the field. *Hum Gene Ther,* 25**,** 301-317.

MARUTA, F., PARKER, A. L., FISHER, K. D., HALLISSEY, M. T., ISMAIL, T., ROWLANDS, D. C., CHANDLER, L. A., KERR, D. J. & SEYMOUR, L. W. 2002. Identification of FGF receptor-binding peptides for cancer gene therapy. *Cancer Gene Ther,* 9**,** 543-552.

MAST, T. C., KIERSTEAD, L., GUPTA, S. B., NIKAS, A. A., KALLAS, E. G., NOVITSKY, V., MBEWE, B., PITISUTTITHUM, P., SCHECHTER, M., VARDAS, E., WOLFE, N. D., ASTE-AMEZAGA, M., CASIMIRO, D. R., COPLAN, P., STRAUS, W. L. & SHIVER, J. W. 2010. International epidemiology of human pre-existing adenovirus (Ad) type-5, type-6, type-26 and type-36 neutralizing antibodies: Correlates of high Ad5 titers and implications for potential HIV vaccine trials. *Vaccine,* 28**,** 950-957.

MASTRANGELI, A., HARVEY, B. G., YAO, J., WOLFF, G., KOVESDI, I., CRYSTAL, R. G. & FALCK-PEDERSEN, E. 1996. &quot;Sero-switch&quot; adenovirus-mediated in vivo gene transfer: circumvention of anti-adenovirus humoral immune defenses against repeat adenovirus vector administration by changing the adenovirus serotype. *Hum Gene Ther,* 7**,** 79-87.

MATSUMOTO, K., SHARIAT, S. F., AYALA, G. E., RAUEN, K. A. & LERNER, S. P. 2005. Loss of coxsackie and adenovirus receptor expression is associated with features of aggressive bladder cancer. *Urology,* 66**,** 441-6.

MCARDLE, C. S., KERR, D. J., O'GORMAN, P., WOTHERSPOON, H. A., WARREN, H., WATSON, D., VINKE, B. J., DOBBIE, J. W. & EL EINI, D. I. 1994. Pharmacokinetic study of 5-fluorouracil in a novel dialysate solution: a long-term intraperitoneal treatment approach for advanced colorectal carcinoma. *Br J Cancer,* 70**,** 762-6.

MCCORMICK, F. 2000. ONYX-015 selectivity and the p14ARF pathway. *Oncogene,* 19**,** 6670-6672.

MELIOPOULOS, V. A., VAN DE VELDE, L. A., VAN DE VELDE, N. C., KARLSSON, E. A., NEALE, G., VOGEL, P., GUY, C., SHARMA, S., DUAN, S., SURMAN, S. L., JONES, B. G., JOHNSON, M. D., BOSIO, C., JOLLY, L., JENKINS, R. G., HURWITZ, J. L., ROSCH, J. W., SHEPPARD, D., THOMAS, P. G., MURRAY, P. J. & SCHULTZ-CHERRY, S. 2016. An Epithelial Integrin Regulates the Amplitude of Protective Lung Interferon Responses against Multiple Respiratory Pathogens. *PLoS Pathog,* 12**,** e1005804.

MILLER, L. C., BLAKEMORE, W., SHEPPARD, D., ATAKILIT, A., KING, A. M. & JACKSON, T. 2001. Role of the cytoplasmic domain of the beta-subunit of integrin alpha(v)beta6 in infection by foot-and-mouth disease virus. *J Virol,* 75**,** 4158-64.

MO, S., COUSSIOS, C. C., SEYMOUR, L. & CARLISLE, R. 2012. Ultrasound-enhanced drug delivery for cancer. *Exp Opin Drug Del,* 9**,** 1525-1538.

MONAGHAN, P., GOLD, S., SIMPSON, J., ZHANG, Z., WEINREB, P. H., VIOLETTE, S. M., ALEXANDERSEN, S. & JACKSON, T. 2005. The alpha(v)beta6 integrin receptor for Foot-and-mouth disease virus is expressed constitutively on the epithelial cells targeted in cattle. *J Gen Virol,* 86**,** 2769-80.

MOORE, K. M., THOMAS, G. J., DUFFY, S. W., WARWICK, J., GABE, R., CHOU, P., ELLIS, I. O., GREEN, A. R., HAIDER, S., BROUILETTE, K., SAHA, A., VALLATH, S., BOWEN, R., CHELALA, C., ECCLES, D., TAPPER, W. J., THOMPSON, A. M., QUINLAN, P., JORDAN, L., GILLETT, C., BRENTNALL, A., VIOLETTE, S., WEINREB, P. H., KENDREW, J., BARRY, S. T., HART, I. R., JONES, J. L. & MARSHALL, J. F. 2014. Therapeutic Targeting of Integrin αvβ6 in Breast Cancer. *JNCI,* 106**,** dju169-dju169.

MURUVE, D. A., PETRILLI, V., ZAISS, A. K., WHITE, L. R., CLARK, S. A., ROSS, P. J., PARKS, R. J. & TSCHOPP, J. 2008. The inflammasome recognizes cytosolic microbial and host DNA and triggers an innate immune response. *Nature,* 452**,** 103-7.

MYHRE, S., HENNING, P., GRANIO, O., TYLO, A. S., NYGREN, P. A., OLOFSSON, S., BOULANGER, P., LINDHOLM, L. & HONG, S. S. 2007. Decreased immune reactivity towards a knobless, affibody-targeted adenovirus type 5 vector. *Gene Ther,* 14**,** 376-81.

NAKANO, M. Y., BOUCKE, K., SUOMALAINEN, M., STIDWILL, R. P. & GREBER, U. F. 2000. The first step of adenovirus type 2 disassembly occurs at the cell surface, independently of endocytosis and escape to the cytosol. *J Virol,* 74**,** 7085-95.

NCBI. 2016. *National Center for Biotechnology Information* [Online]. Available: https://www.ncbi.nlm.nih.gov/ [Accessed May 2016].

NCI. 2012. *SEER Stat Fact Sheets: Ovarian Cancer* [Online]. National Cancer Institute / U.S. National Institutes of Health. Available: http://seer.cancer.gov/statfacts/html/ovary.html [Accessed 25/06/16].

NEMUNAITIS, J., CUNNINGHAM, C., BUCHANAN, A., BLACKBURN, A., EDELMAN, G., MAPLES, P., NETTO, G., TONG, A., RANDLEV, B., OLSON, S. & KIRN, D. 2001a. Intravenous infusion of a replication-selective adenovirus (ONYX-015) in cancer patients: Safety, feasibility and biological activity. *Gene Ther,* 8**,** 746-759.

NEMUNAITIS, J., KHURI, F., GANLY, I., ARSENEAU, J., POSNER, M., VOKES, E., KUHN, J., MCCARTY, T., LANDERS, S., BLACKBURN, A., ROMEL, L., RANDLEV, B., KAYE, S. & KIRN, D. 2001b. Phase II trial of intratumoral administration of ONYX-015, a replication-selective adenovirus, in patients with refractory head and neck cancer. *J Clin Oncol,* 19**,** 289-98.

NEUMANN, R., CHROBOCZEK, J. & JACROT, B. 1988. Determination of the nucleotide sequence for the penton-base gene of human adenovirus type 5. *Gene,* 69**,** 153-7.

NICKLIN, S. A., VON SEGGERN, D. J., WORK, L. M., PEK, D. C., DOMINICZAK, A. F., NEMEROW, G. R. & BAKER, A. H. 2001. Ablating adenovirus type 5 fiber-CAR binding and HI loop insertion of the SIGYPLP peptide generate an endothelial cell-selective adenovirus. *Mol Ther,* 4**,** 534-42.

NICOL, C. G., GRAHAM, D., MILLER, W. H., WHITE, S. J., SMITH, T. A. G., NICKLIN, S. A., STEVENSON, S. C. & BAKER, A. H. 2004. Effect of adenovirus serotype 5 fiber and penton modifications on in vivo tropism in rats. *Mol Ther,* 10**,** 344-354.

NILSSON, E. C., STORM, R. J., BAUER, J., JOHANSSON, S. M., LOOKENE, A., ANGSTROM, J., HEDENSTROM, M., ERIKSSON, T. L., FRANGSMYR, L., RINALDI, S., WILLISON, H. J., PEDROSA DOMELLOF, F., STEHLE, T. & ARNBERG, N. 2011. The GD1a glycan is a cellular receptor for adenoviruses causing epidemic keratoconjunctivitis. *Nat Med,* 17**,** 105-9.

NOKISALMI, P., PESONEN, S., ESCUTENAIRE, S., SÄRKIOJA, M., RAKI, M., CERULLO, V., LAASONEN, L., ALEMANY, R., ROJAS, J., CASCALLO, M., GUSE, K., RAJECKI, M., KANGASNIEMI, L., HAAVISTO, E., KARIOJA-KALLIO, A., HANNUKSELA, P., OKSANEN, M., KANERVA, A., JOENSUU, T., AHTIAINEN, L. & HEMMINKI, A. 2010. Oncolytic adenovirus ICOVIR-7 in patients with advanced and refractory solid tumors. *Clin Cancer Res,* 16**,** 3035-3043.

NOTHELFER, E. M., ZITZMANN-KOLBE, S., GARCIA-BOY, R., KRÄMER, S., HEROLD-MENDE, C., ALTMANN, A., EISENHUT, M., MIER, W. & HABERKORN, U. 2009. Identification and characterization of a peptide with affinity to head and neck cancer. *J Nucl Med,* 50**,** 426-434.

NOUTSIAS, M., FECHNER, H., DE JONGE, H., WANG, X., DEKKERS, D., HOUTSMULLER, A. B., PAUSCHINGER, M., BERGELSON, J., WARRAICH, R., YACOUB, M., HETZER, R., LAMERS, J., SCHULTHEISS, H. P. & POLLER, W. 2001. Human coxsackie-adenovirus receptor is colocalized with integrins alpha(v)beta(3) and alpha(v)beta(5) on the cardiomyocyte sarcolemma and upregulated in dilated cardiomyopathy: implications for cardiotropic viral infections. *Circulation,* 104**,** 275-80.

NWANEGBO, E., VARDAS, E., GAO, W., WHITTLE, H., SUN, H., ROWE, D., ROBBINS, P. D. & GAMBOTTO, A. 2004. Prevalence of Neutralizing Antibodies to Adenoviral Serotypes 5 and 35 in the Adult Populations of The Gambia, South Africa, and the United States. *Clinical and Diagnostic Laboratory Immunology,* 11**,** 351-357.

O'DONNELL, R. L., MCCORMICK, A., MUKHOPADHYAY, A., WOODHOUSE, L. C., MOAT, M., GRUNDY, A., DIXON, M., KAUFMAN, A., SOOHOO, S., ELATTAR, A., CURTIN, N. J. & EDMONDSON, R. J. 2014. The use of ovarian cancer cells from patients undergoing surgery to generate primary cultures capable of undergoing functional analysis. *PLoS ONE,* 9.

OCHSENBEIN, A. F., FEHR, T., LUTZ, C., SUTER, M., BROMBACHER, F., HENGARTNER, H. & ZINKERNAGEL, R. M. 1999. Control of early viral and bacterial distribution and disease by natural antibodies. *Science,* 286**,** 2156-2159.

OLIVE, M., EISENLOHR, L., FLOMENBERG, N., HSU, S. & FLOMENBERG, P. 2002. The adenovirus capsid protein hexon contains a highly conserved human CD4+ T-cell epitope. *Hum Gene Ther,* 13**,** 1167-1178.

ONION, D., CROMPTON, L. J., MILLIGAN, D. W., MOSS, P. A. H., LEE, S. P. & MAUTNER, V. 2007. The CD4+ T-cell response to adenovirus is focused against conserved residues within the hexon protein. *J Gen Virol,* 88**,** 2417-2425.

OPHORST, O. J. A. E., KOSTENSE, S., GOUDSMIT, J., DE SWART, R. L., VERHAAGH, S., ZAKHARTCHOUK, A., VAN MEIJER, M., SPRANGERS, M., VAN AMERONGEN, G., YÜKSEL, S., OSTERHAUS, A. D. M. E. & HAVENGA, M. J. E. 2004. An adenoviral type 5 vector carrying a type 35 fiber as a vaccine vehicle: DC targeting, cross neutralization, and immunogenicity. *Vaccine,* 22**,** 3035-3044.

OTHMAN, M., LABELLE, A., MAZZETTI, I., ELBATARNY, H. S. & LILLICRAP, D. 2007. Adenovirus-induced thrombocytopenia: The role of von Willebrand factor and P-selectin in mediating accelerated platelet clearance. *Blood,* 109**,** 2832-2839.

PAMEIJER, C. R. J., NAVANJO, A., MEECHOOVET, B., WAGNER, J. R., AGUILAR, B., WRIGHT, C. L., CHANG, W. C., BROWN, C. E. & JENSEN, M. C. 2007. Conversion of a tumor-binding

peptide identified by phage display to a functional chimeric T cell antigen receptor. *Cancer Gene Ther,* 14**,** 91-97.

PARKER, A. L., BAKER, A. H., WADDINGTON, S. N., BUCKLEY, S. M. K., CUSTERS, J., HAVENGA, M. J. E., VAN ROOIJEN, N., GOUDSMIT, J., MCVEY, J. H. & NICKLIN, S. A. 2009. Effect of neutralizing sera on factor X-mediated adenovirus serotype 5 gene transfer. *J Virol,* 83**,** 479-483.

PARKER, A. L., BRADSHAW, A. C., ALBA, R., NICKLIN, S. A. & BAKER, A. H. 2014. Capsid modification strategies for detargeting adenoviral vectors. *Methods Mol Biol*, 1089:45-59.

PARKER, A. L., MCVEY, J. H., DOCTOR, J. H., LOPEZ-FRANCO, O., WADDINGTON, S. N., HAVENGA, M. J., NICKLIN, S. A. & BAKER, A. H. 2007. Influence of coagulation factor zymogens on the infectivity of adenoviruses pseudotyped with fibers from subgroup D. *J Virol,* 81**,** 3627-31.

PARKER, A. L., WADDINGTON, S. N., NICOL, C. G., SHAYAKHMETOV, D. M., BUCKLEY, S. M., DENBY, L., KEMBALL-COOK, G., NI, S., LIEBER, A., MCVEY, J. H., NICKLIN, S. A. & BAKER, A. H. 2006. Multiple vitamin K-dependent coagulation zymogens promote adenovirus-mediated gene delivery to hepatocytes. *Blood,* 108**,** 2554-2561.

PARKER, A. L., WHITE, K. M., LAVERY, C. A., CUSTERS, J., WADDINGTON, S. N. & BAKER, A. H. 2013. Pseudotyping the adenovirus serotype 5 capsid with both the fibre and penton of serotype 35 enhances vascular smooth muscle cell transduction. *Gene Ther,* 20**,** 1158-1164.

PATCH, A. M., CHRISTIE, E. L., ETEMADMOGHADAM, D., GARSED, D. W., GEORGE, J., FEREDAY, S., NONES, K., COWIN, P., ALSOP, K., BAILEY, P. J., KASSAHN, K. S., NEWELL, F., QUINN, M. C., KAZAKOFF, S., QUEK, K., WILHELM-BENARTZI, C., CURRY, E., LEONG, H. S., HAMILTON, A., MILESHKIN, L., AU-YEUNG, G., KENNEDY, C., HUNG, J., CHIEW, Y. E., HARNETT, P., FRIEDLANDER, M., QUINN, M., PYMAN, J., CORDNER, S., O'BRIEN, P., LEDITSCHKE, J., YOUNG, G., STRACHAN, K., WARING, P., AZAR, W., MITCHELL, C., TRAFICANTE, N., HENDLEY, J., THORNE, H., SHACKLETON, M., MILLER, D. K., ARNAU, G. M., TOTHILL, R. W., HOLLOWAY, T. P., SEMPLE, T., HARLIWONG, I., NOURSE, C., NOURBAKHSH, E., MANNING, S., IDRISOGLU, S., BRUXNER, T. J., CHRIST, A. N., POUDEL, B., HOLMES, O., ANDERSON, M., LEONARD, C., LONIE, A., HALL, N., WOOD, S., TAYLOR, D. F., XU, Q., FINK, J. L., WADDELL, N., DRAPKIN, R., STRONACH, E., GABRA, H., BROWN, R., JEWELL, A., NAGARAJ, S. H., MARKHAM, E., WILSON, P. J., ELLUL, J., MCNALLY, O., DOYLE, M. A., VEDURURU, R., STEWART, C., LENGYEL, E., PEARSON, J. V., DEFAZIO, A., GRIMMOND, S. M. & BOWTELL, D. D. 2015. Whole-genome characterization of chemoresistant ovarian cancer. *Nature,* 521**,** 489-94.

PEARSON, A. S., KOCH, P. E., ATKINSON, N., XIONG, M., FINBERG, R. W., ROTH, J. A. & FANG, B. 1999. Factors limiting adenovirus-mediated gene transfer into human lung and pancreatic cancer cell lines. *Clin Cancer Res,* 5**,** 4208-13.

PENALOZA-MACMASTER, P., PROVINE, N. M., RA, J., BORDUCCHI, E. N., MCNALLY, A., SIMMONS, N. L., IAMPIETRO, M. J. & BAROUCH, D. H. 2013. Alternative serotype adenovirus vaccine vectors elicit memory T cells with enhanced anamnestic capacity compared to Ad5 vectors. *J Virol,* 87**,** 1373-84.

PENG, Z. W., IKENAGA, N., LIU, S. B., SVERDLOV, D. Y., VAID, K. A., DIXIT, R., WEINREB, P. H., VIOLETTE, S., SHEPPARD, D., SCHUPPAN, D. & POPOV, Y. 2016. Integrin alphavbeta6 critically regulates hepatic progenitor cell function and promotes ductular reaction, fibrosis, and tumorigenesis. *Hepatology,* 63**,** 217-32.

PENSON, R. T., OLIVA, E., SKATES, S. J., GLYPTIS, T., FULLER JR, A. F., GOODMAN, A. & SEIDEN, M. V. 2004. Expression of multidrug resistance-1 protein inversely correlates with paclitaxel response and survival in ovarian cancer patients: A study in serial samples. *Gynecol Oncol,* 93**,** 98-106.

PETTERSEN, E. F., GODDARD, T. D., HUANG, C. C., COUCH, G. S., GREENBLATT, D. M., MENG, E. C. & FERRIN, T. E. 2004. UCSF Chimera--a visualization system for exploratory research and analysis. *J Comput Chem,* 25**,** 1605-12.

PICKLES, R. J., FAHRNER, J. A., PETRELLA, J. M., BOUCHER, R. C. & BERGELSON, J. M. 2000. Retargeting the coxsackievirus and adenovirus receptor to the apical surface of polarized epithelial cells reveals the glycocalyx as a barrier to adenovirus-mediated gene transfer. *J Virol,* 74**,** 6050-7.

POST, D. E. & VAN MEIR, E. G. 2003. A novel hypoxia-inducible factor (HIF) activated oncolytic adenovirus for cancer therapy. *Oncogene,* 22**,** 2065-2072.

POSTOW, M. A., CALLAHAN, M. K. & WOLCHOK, J. D. 2015. Immune checkpoint blockade in cancer therapy. *J Clin Oncol,* 33**,** 1974-1982.

PROMEGA. 2017. *CellTiter 96® AQueous One Solution Cell Proliferation Assay* [Online]. Promega. Available: https://www.promega.co.uk/-/media/files/resources/protocols/technical-bulletins/0/celltiter-96-aqueous-one-solution-cell-proliferation-assay-system-protocol.pdf [Accessed 27 Feb 2017].

PSIOXUS. 2016. *Smart science for serious disease* [Online]. PsiOxus Therapeutics Ltd. Available: http://www.psioxus.com/index.asp [Accessed 22 Oct 2016].

REEH, M., BOCKHORN, M., GÖRGENS, D., VIETH, M., HOFFMANN, T., SIMON, R., IZBICKI, J. R., SAUTER, G., SCHUMACHER, U. & ANDERS, M. 2013. Presence of the Coxsackievirus and Adenovirus Receptor (CAR) in human neoplasms: a multitumour array analysis. *Brit J Cancer,* 109**,** 1848-1858.

REETZ, J., HERCHENRODER, O. & PUTZER, B. M. 2014. Peptide-based technologies to alter adenoviral vector tropism: ways and means for systemic treatment of cancer. *Viruses,* 6**,** 1540-63.

REN, F., SHEN, J., SHI, H., HORNICEK, F. J., KAN, Q. & DUAN, Z. 2016. Novel mechanisms and approaches to overcome multidrug resistance in the treatment of ovarian cancer. *Biochimica et Biophysica Acta - Reviews on Cancer,* 1866**,** 266-275.

RIBAS, A. 2012. Tumor immunotherapy directed at PD-1. *New England J Med,* 366**,** 2517-2519.

RIGHETTI, S. C., DELLA TORRE, G., PILOTTI, S., MENARD, S., OTTONE, F., COLNAGHI, M. I., PIEROTTI, M. A., LAVARINO, C., CORNAROTTI, M., ORIANA, S., BOHM, S., BRESCIANI, G. L., SPATTI, G. & ZUNINO, F. 1996. A comparative study of p53 gene mutations, protein accumulation, and response to cisplatin-based chemotherapy in advanced ovarian carcinoma. *Cancer Res,* 56**,** 689-93.

ROBERTS, D. M., NANDA, A., HAVENGA, M. J. E., ABBINK, P., LYNCH, D. M., EWALD, B. A., LIU, J., THORNER, A. R., SWANSON, P. E., GORGONE, D. A., LIFTON, M. A., LEMCKERT, A. A. C., HOLTERMAN, L., CHEN, B., DILRAJ, A., CARVILLE, A., MANSFIELD, K. G., GOUDSMIT, J. & BAROUCH, D. H. 2006. Hexon-chimaeric adenovirus serotype 5 vectors circumvent pre-existing anti-vector immunity. *Nature,* 441**,** 239-243.

ROBINSON, C. M., SINGH, G., LEE, J. Y., DEHGHAN, S., RAJAIYA, J., LIU, E. B., YOUSUF, M. A., BETENSKY, R. A., JONES, M. S., DYER, D. W., SETO, D. & CHODOSH, J. 2013. Molecular evolution of human adenoviruses. *Scientific Reports,* 3, 1812.

ROCCONI, R. P., ZHU, Z. B., STOFF-KHALILI, M., RIVERA, A. A., LU, B., WANG, M., ALVAREZ, R. D., CURIEL, D. T. & MAKHIJA, S. K. 2007. Treatment of ovarian cancer with a novel dual targeted conditionally replicative adenovirus (CRAd). *Gynecol Oncol,* 105**,** 113-21.

ROELVINK, P. W., LIZONOVA, A., LEE, J. G., LI, Y., BERGELSON, J. M., FINBERG, R. W., BROUGH, D. E., KOVESDI, I. & WICKHAM, T. J. 1998. The coxsackievirus-adenovirus receptor protein can function as a cellular attachment protein for adenovirus serotypes from subgroups A, C, D, E, and F. *J Virol,* 72**,** 7909-15.

ROGEE, S., GRELLIER, E., BERNARD, C., JOUY, N., LOYENS, A., BEAUVILLAIN, J. C., FENDER, P., CORJON, S., HONG, S. S., BOULANGER, P., QUESNEL, B., D'HALLUIN, J. C. & COLIN, M. 2010. Influence of chimeric human-bovine fibers on adenoviral uptake by liver cells and the antiviral immune response. *Gene Ther,* 17**,** 880-91.

ROJAS, L. A., MORENO, R., CALDERON, H. & ALEMANY, R. 2016. Adenovirus coxsackie adenovirus receptor-mediated binding to human erythrocytes does not preclude systemic transduction. *Cancer Gene Ther,* 23**,** 411-414.

ROMAGNANI, S. 2000. T-cell subsets (Th1 versus Th2). *Ann Allergy Asthma Immunol,* 85**,** 9-18; quiz 18, 21.

ROWE, W. P., HUEBNER, R. J., GILMORE, L. K., PARROTT, R. H. & WARD, T. G. 1953. Isolation of a cytopathogenic agent from human adenoids undergoing spontaneous degeneration in tissue culture. *Proc Soc Exp Biol Med,* 84**,** 570-3.

RUF, B. & LAUER, U. M. 2015. Assessment of current virotherapeutic application schemes: "hit hard and early" versus "killing softly"? *Mol Ther Oncol,* 2**,** 15018.

RUNYON, B. A., HOEFS, J. C. & MORGAN, T. R. 1988. Ascitic fluid analysis in malignancy-related ascites. *Hepatology,* 8**,** 1104-1109.

RUOSLAHTI, E. 1996. RGD and other recognition sequences for integrins. *Annu Rev Cell Dev Biol,* 12**,** 697-715.

RUSSELL, S. J., PENG, K. W. & BELL, J. C. 2012. Oncolytic virotherapy. *Nat Biotechnol,* 10;30(7):658-70.

RUSSELL, W. C. 2000. Update on adenovirus and its vectors. *J Gen Virol,* 81**,** 2573-604.

RUSSELL, W. C. 2009. Adenoviruses: Update on structure and function. *J Gen Virol,* 90**,** 1-20.

SACHS, M. D., RAUEN, K. A., RAMAMURTHY, M., DODSON, J. L., DE MARZO, A. M., PUTZI, M. J., SCHOENBERG, M. P. & RODRIGUEZ, R. 2002. Integrin α v and coxsackie adenovirus receptor expression in clinical bladder cancer. *Urology,* 60**,** 531-536.

SALANI, R., BACKES, F. J., FUNG KEE FUNG, M., HOLSCHNEIDER, C. H., PARKER, L. P., BRISTOW, R. E. & GOFF, B. A. 2011. Posttreatment surveillance and diagnosis of recurrence in women with gynecologic malignancies: Society of Gynecologic Oncologists recommendations. *Am J Obst Gynecol,* 204**,** 466-478.

SCHOGGINS, J. W. & FALCK-PEDERSEN, E. 2006. Fiber and penton base capsid modifications yield diminished adenovirus type 5 transduction and proinflammatory gene expression with retention of antigen-specific humoral immunity. *J Virol,* 80**,** 10634-44.

SCHOGGINS, J. W., NOCIARI, M., PHILPOTT, N. & FALCK-PEDERSEN, E. 2005. Influence of fiber detargeting on adenovirus-mediated innate and adaptive immune activation. *J Virol,* 79**,** 11627-37.

SCOTTON, C. J., WILSON, J. L., MILLIKEN, D., STAMP, G. & BALKWILL, F. R. 2001. Epithelial cancer cell migration: a role for chemokine receptors? *Cancer Res,* 61**,** 4961-5.

SEIDMAN, J. D., HORKAYNE-SZAKALY, I., HAIBA, M., BOICE, C. R., KURMAN, R. J. & RONNETT, B. M. 2004. The Histologic Type and Stage Distribution of Ovarian Carcinomas of Surface Epithelial Origin. *Intl J Gynecol Pathol,* 23**,** 41-44.

SEIRADAKE, E., HENAFF, D., WODRICH, H., BILLET, O., PERREAU, M., HIPPERT, C., MENNECHET, F., SCHOEHN, G., LORTAT-JACOB, H., DREJA, H., IBANES, S., KALATZIS, V., WANG, J. P., FINBERG, R. W., CUSACK, S. & KREMER, E. J. 2009. The cell adhesion molecule "CAR" and sialic acid on human erythrocytes influence adenovirus in vivo biodistribution. *PLoS Path,* 5.

SHARMA, A., TANDON, M., AHI, Y. S., BANGARI, D. S., VEMULAPALLI, R. & MITTAL, S. K. 2010. Evaluation of cross-reactive cell-mediated immune responses among human, bovine and porcine adenoviruses. *Gene Ther,* 17**,** 634-642.

SHAYAKHMETOV, D. M., EBERLY, A. M., LI, Z. Y. & LIEBER, A. 2005a. Deletion of penton RGD motifs affects the efficiency of both the internalization and the endosome escape of viral particles containing adenovirus serotype 5 or 35 fiber knobs. *J Virol,* 79**,** 1053-1061.

SHAYAKHMETOV, D. M., GAGGAR, A., NI, S., LI, Z. Y. & LIEBER, A. 2005b. Adenovirus binding to blood factors results in liver cell infection and hepatotoxicity. *J Virol,* 79**,** 7478-91.

SHAYAKHMETOV, D. M. & LIEBER, A. 2000. Dependence of adenovirus infectivity on length of the fiber shaft domain. *J Virol,* 74**,** 10274-86.

SHEPHERD, T. G., THÉRIAULT, B. L., CAMPBELL, E. J. & NACHTIGAL, M. W. 2007. Primary culture of ovarian surface epithelial cells and ascites-derived ovarian cancer cells from patients. *Nat Protocols,* 1**,** 2643-2649.

SHEPPARD, D. 2000. In vivo functions of integrins: Lessons from null mutations in mice. *Matrix Biology,* 19**,** 203-209.

SHEPPARD, D., ROZZO, C., STARR, L., QUARANTA, V., ERLE, D. J. & PYTELÄ, R. 1990. Complete amino acid sequence of a novel integrin beta subunit (beta 6) identified in epithelial cells using the polymerase chain reaction. *J Biol Chem,* 265**,** 11502-7.

SHERR, C. J. 1996. Cancer cell cycles. *Science,* 274**,** 1672-1674.

SLACK, R. J., HAFEJI, M., ROGERS, R., LUDBROOK, S. B., MARSHALL, J. F., FLINT, D. J., PYNE, S. & DENYER, J. C. 2016. Pharmacological Characterization of the alphavbeta6 Integrin Binding and Internalization Kinetics of the Foot-and-Mouth Disease Virus Derived Peptide A20FMDV2. *Pharmacology,* 97**,** 114-25.

SMITH, J. G., SILVESTRY, M., LINDERT, S., LU, W., NEMEROW, G. R. & STEWART, P. L. 2010. Insight into the mechanisms of adenovirus capsid disassembly from studies of defensin neutralization. *PLoS Pathog,* 6**,** e1000959.

SMITH, T., IDAMAKANTI, N., KYLEFJORD, H., ROLLENCE, M., KING, L., KALOSS, M., KALEKO, M. & STEVENSON, S. C. 2002. In vivo hepatic adenoviral gene delivery occurs independently of the coxsackievirus-adenovirus receptor. *Mol Ther,* 5**,** 770-779.

SMITH, T. A., IDAMAKANTI, N., ROLLENCE, M. L., MARSHALL-NEFF, J., KIM, J., MULGREW, K., NEMEROW, G. R., KALEKO, M. & STEVENSON, S. C. 2003. Adenovirus serotype 5 fiber shaft influences in vivo gene transfer in mice. *Hum Gene Ther,* 14**,** 777-87.

SNAPGENE. 2016. *pBABE-Puro plasmid* [Online]. GSL Biotech LLC. Available: http://www.snapgene.com/resources/plasmid_files/viral_expression_and_packaging_vectors/pBABE-Puro/ [Accessed 27/10/2016].

SOWMYA, G., KHAN, J. M., ANAND, S., AHN, S. B., BAKER, M. S. & RANGANATHAN, S. 2014. A site for direct integrin alphavbeta6.uPAR interaction from structural modelling and docking. *J Struct Biol,* 185**,** 327-35.

STALLWOOD, Y., FISHER, K. D., GALLIMORE, P. H. & MAUTNER, V. 2000. Neutralisation of adenovirus infectivity by ascitic fluid from ovarian cancer patients. *Gene Ther,* 7**,** 637-643.

STANTON, R. J., MCSHARRY, B. P., ARMSTRONG, M., TOMASEC, P. & WILKINSON, G. W. G. 2008. Re-engineering adenovirus vector systems to enable high-throughput analyses of gene function. *BioTechniques,* 45**,** 659-668.

STONEBRAKER, J. R., WAGNER, D., LEFENSTY, R. W., BURNS, K., GENDLER, S. J., BERGELSON, J. M., BOUCHER, R. C., O'NEAL, W. K. & PICKLES, R. J. 2004. Glycocalyx restricts adenoviral vector access to apical receptors expressed on respiratory epithelium in vitro and in vivo: role for tethered mucins as barriers to lumenal infection. *J Virol,* 78**,** 13755-68.

SUMIDA, S. M., TRUITT, D. M., KISHKO, M. G., ARTHUR, J. C., JACKSON, S. S., GORGONE, D. A., LIFTON, M. A., KOUDSTAAL, W., PAU, M. G., KOSTENSE, S., HAVENGA, M. J. E., GOUDSMIT, J., LETVIN, N. L. & BAROUCH, D. H. 2004. Neutralizing Antibodies and CD8+ T Lymphocytes both Contribute to Immunity to Adenovirus Serotype 5 Vaccine Vectors. *J Virol,* 78**,** 2666-2673.

SUMIDA, S. M., TRUITT, D. M., LEMCKERT, A. A. C., VOGELS, R., CUSTERS, J. H. H. V., ADDO, M. M., LOCKMAN, S., PETER, T., PEYERL, F. W., KISHKO, M. G., JACKSON, S. S., GORGONE, D. A., LIFTON, M. A., ESSEX, M., WALKER, B. D., GOUDSMIT, J., HAVENGA, M. J. E. & BAROUCH, D. H. 2005. Neutralizing antibodies to adenovirus serotype 5 vaccine vectors are directed primarily against the adenovirus hexon protein. *J Immunol,* 174**,** 7179-7185.

SÄRKIOJA, M., PESONEN, S., RAKI, M., HAKKARAINEN, T., SALO, J., AHONEN, M. T., KANERVA, A. & HEMMINKI, A. 2008. Changing the adenovirus fiber for retaining gene delivery efficacy in the presence of neutralizing antibodies. *Gene Ther,* 15**,** 921-9.

TARGOVAX. 2016. *Targovax is an innovation driven specialist in immuno-oncology* [Online]. Available: http://www.targovax.com/ [Accessed 22 Oct 2016].

TEDCASTLE, A., ILLINGWORTH, S., BROWN, A., SEYMOUR, L. W. & FISHER, K. D. 2015. Actin-resistant DNAse I Expression From Oncolytic Adenovirus Enadenotucirev Enhances Its Intratumoral Spread and Reduces Tumor Growth. *Mol Ther*, 24(4):796-804.

TEIGLER, J. E., IAMPIETRO, M. J. & BAROUCH, D. H. 2012. Vaccination with adenovirus serotypes 35, 26, and 48 elicits higher levels of innate cytokine responses than adenovirus serotype 5 in rhesus monkeys. *J Virol,* 86**,** 9590-8.

TEIGLER, J. E., PENALOZA-MACMASTER, P., OBENG, R., PROVINE, N. M., LAROCCA, R. A., BORDUCCHI, E. N. & BAROUCH, D. H. 2014. Hexon Hypervariable Region-Modified Adenovirus Type 5 (Ad5) Vectors Display Reduced Hepatotoxicity but Induce T Lymphocyte Phenotypes Similar to Ad5 Vectors. *CVI,* 21**,** 1137-1144.

THACI, B., ULASOV, I. V., WAINWRIGHT, D. A. & LESNIAK, M. S. 2011. The Challenge for Gene Therapy: Innate Immune Response to Adenoviruses. *Oncotarget,* 2**,** 113-121.

THOMAS, G. J., NYSTRÖM, M. L. & MARSHALL, J. F. 2006. αvβ6 integrin in wound healing and cancer of the oral cavity. *J Oral Pathol Med,* 35**,** 1-10.

THORNER, A. R., VOGELS, R., KASPERS, J., WEVERLING, G. J., HOLTERMAN, L., LEMCKERT, A. A. C., DILRAJ, A., MCNALLY, L. M., JEENA, P. M., JEPSEN, S., ABBINK, P., NANDA, A., SWANSON, P. E., BATES, A. T., O'BRIEN, K. L., HAVENGA, M. J. E., GOUDSMIT, J. & BAROUCH, D. H. 2006. Age dependence of adenovirus-specific neutralizing antibody titers in individuals from sub-Saharan Africa. *J Clin Microbiol,* 44**,** 3781-3783.

THÉRIAULT, B. L., PORTELANCE, L., MES-MASSON, A. M. & NACHTIGAL, M. W. 2013. Establishment of primary cultures from ovarian tumor tissue and ascites fluid. *Meth Mol Biol,* 1049:323-36.

TOMASEC, P., WANG, E. C. Y., GROH, V., SPIES, T., MCSHARRY, B. P., AICHELER, R. J., STANTON, R. J. & WILKINSON, G. W. G. 2007. Adenovirus vector delivery stimulates natural killer cell recognition. *J Gen Virol,* 88**,** 1103.

TOOKMAN, L. A., BROWNE, A. K., CONNELL, C. M., BRIDGE, G., INGEMARSDOTTER, C. K., DOWSON, S., SHIBATA, A., LOCKLEY, M., MARTIN, S. A. & MCNEISH, I. A. 2016. RAD51 and BRCA2 enhance oncolytic adenovirus type 5 activity in ovarian cancer. *Mol Cancer Res,* 14**,** 44-55.

UCHINO, J., CURIEL, D. T. & UGAI, H. 2014. Species D human adenovirus type 9 exhibits better virus-spread ability for antitumor efficacy among alternative serotypes. *PLoS ONE,* 9.

USPTO. 2004. *Treatment of acute lung injury, fibrosis and metastasis with antagonists of alpha v beta 6* [Online]. USPTO patent full text and image database. Available: http://patft.uspto.gov/netacgi/nph-Parser?Sect2=PTO1&amp;amp;Sect2=HITOFF&amp;amp;p=1&amp;amp;u=/netahtml/PTO/search-bool.html&amp;amp;r=1&amp;amp;f=G&amp;amp;l=50&amp;amp;d=PALL&amp;amp;RefSrch=yes&amp;amp;Query=PN/7150871 [Accessed 26/10/2016 2016].

UUSI-KERTTULA, H., DAVIES, J., COUGHLAN, L., HULIN-CURTIS, S., JONES, R., HANNA, L., CHESTER, J. D. & PARKER, A. L. 2016. Pseudotyped alphavbeta6 integrin-targeted adenovirus vectors for ovarian cancer therapies. *Oncotarget,* 7(19): 27926–27937.

UUSI-KERTTULA, H., HULIN-CURTIS, S., DAVIES, J. & PARKER, A. L. 2015a. Oncolytic Adenovirus: Strategies and Insights for Vector Design and Immuno-Oncolytic Applications. *Viruses,* 7**,** 6009-42.

UUSI-KERTTULA, H., LEGUT, M., DAVIES, J., JONES, R., HUDSON, E., HANNA, L., STANTON, R. J., CHESTER, J. D. & PARKER, A. L. 2015b. Incorporation of Peptides Targeting EGFR and FGFR1 into the Adenoviral Fiber Knob Domain and Their Evaluation as Targeted Cancer Therapies. *Hum Gene Ther,* 26**,** 320-9.

VARGHESE, R., MIKYAS, Y., STEWART, P. L. & RALSTON, R. 2004. Postentry neutralization of adenovirus type 5 by an antihexon antibody. *J Virol,* 78**,** 12320-12332.

VASSILEV, L., RANKI, T., JOENSUU, T., JAGER, E., KARBACH, J., WAHLE, C., PARTANEN, K., KAIREMO, K., ALANKO, T., TURKKI, R., LINDER, N., LUNDIN, J., RISTIMÄKI, A., KANKAINEN, M., HEMMINKI, A., BACKMAN, C., DIENEL, K., VON EULER, M., HAAVISTO, E., HAKONEN, T., JUHILA, J., JADERBERG, M., PRIHA, P., VUOLANTO, A. & PESONEN, S. 2015. Repeated intratumoral administration of ONCOS-102 leads to systemic antitumor CD8 T-cell response and robust cellular and transcriptional immune activation at tumor site in a patient with ovarian cancer. *Oncoimmunology,* 4**,** e1017702.

VIGNE, E., MAHFOUZ, I., DEDIEU, J. F., BRIE, A., PERRICAUDET, M. & YEH, P. 1999. RGD inclusion in the hexon monomer provides adenovirus type 5-based vectors with a fiber knob-independent pathway for infection. *J Virol,* 73**,** 5156-61.

VOGELSTEIN, B., LANE, D. & LEVINE, A. J. 2000. Surfing the p53 network. *Nature,* 408**,** 307-10.

VON SEGGERN, D. J., KEHLER, J., ENDO, R. I. & NEMEROW, G. R. 1998. Complementation of a fibre mutant adenovirus by packaging cell lines stably expressing the adenovirus type 5 fibre protein. *J Gen Virol,* 79**,** 1461-1468.

VÄHÄ-KOSKELA, M. J. V., HEIKKILÄ, J. E. & HINKKANEN, A. E. 2007. Oncolytic viruses in cancer therapy. *Cancer Letters,* 254**,** 178-216.

WADDINGTON, S. N., MCVEY, J. H., BHELLA, D., PARKER, A. L., BARKER, K., ATODA, H., PINK, R., BUCKLEY, S. M. K., GREIG, J. A., DENBY, L., CUSTERS, J., MORITA, T., FRANCISCHETTI, I. M. B., MONTEIRO, R. Q., BAROUCH, D. H., VAN ROOIJEN, N., NAPOLI, C., HAVENGA, M. J. E., NICKLIN, S. A. & BAKER, A. H. 2008. Adenovirus Serotype 5 Hexon Mediates Liver Gene Transfer. *Cell,* 132**,** 397-409.

WADDINGTON, S. N., PARKER, A. L., HAVENGA, M., NICKLIN, S. A., BUCKLEY, S. M. K., MCVEY, J. H. & BAKER, A. H. 2007. Targeting of adenovirus serotype 5 (Ad5) and 5/47 pseudotyped vectors in vivo: Fundamental involvement of coagulation factors and redundancy of CAR binding by Ad5. *J Virol,* 81**,** 9568-9571.

WALTERS, R. W., FREIMUTH, P., MONINGER, T. O., GANSKE, I., ZABNER, J. & WELSH, M. J. 2002. Adenovirus fiber disrupts CAR-mediated intercellular adhesion allowing virus escape. *Cell,* 110**,** 789-99.

WALTON, J., BLAGIH, J., ENNIS, D., LEUNG, E., DOWSON, S., FARQUHARSON, M., TOOKMAN, L. A., ORANGE, C., ATHINEOS, D., MASON, S., STEVENSON, D., BLYTH, K., STRATHDEE, D., BALKWILL, F. R., VOUSDEN, K., LOCKLEY, M. & MCNEISH, I. A. 2016. CRISPR/Cas9-Mediated Trp53 and Brca2 Knockout to Generate Improved Murine Models of Ovarian High-Grade Serous Carcinoma. *Cancer Res,* 76**,** 6118-6129.

WANG, B., LI, S., MENG, X., SHANG, H. & GUAN, Y. 2015. Inhibition of mdr1 by G-quadruplex oligonucleotides and reversal of paclitaxel resistance in human ovarian cancer cells. *Tumor Biol,* 36**,** 6433-6443.

WANG, H., LI, Z. Y., LIU, Y., PERSSON, J., BEYER, I., MOLLER, T., KOYUNCU, D., DRESCHER, M. R., STRAUSS, R., ZHANG, X. B., WAHL, J. K., 3RD, URBAN, N., DRESCHER, C., HEMMINKI, A., FENDER, P. & LIEBER, A. 2011. Desmoglein 2 is a receptor for adenovirus serotypes 3, 7, 11 and 14. *Nat Med,* 17**,** 96-104.

WANG, H., LIAW, Y. C., STONE, D., KALYUZHNIY, O., AMIRASLANOV, I., TUVE, S., VERLINDE, C. L., SHAYAKHMETOV, D., STEHLE, T., ROFFLER, S. & LIEBER, A. 2007. Identification of CD46 binding sites within the adenovirus serotype 35 fiber knob. *J Virol,* 81**,** 12785-92.

WCRF. 2012. *Ovarian cancer statistics* [Online]. World Cancer Research Fund International. Available: http://www.wcrf.org/int/cancer-facts-figures/data-specific-cancers/ovarian-cancer-statistics [Accessed 25/06/16].

WEFERS, C., LAMBERT, L. J., TORENSMA, R. & HATO, S. V. 2015. Cellular immunotherapy in ovarian cancer: Targeting the stem of recurrence. *Gynecol Oncol,* 137**,** 335-42.

WEINACKER, A., CHEN, A., AGREZ, M., CONE, R. I., NISHIMURA, S., WAYNER, E., PYTELÄ, R. & SHEPPARD, D. 1994. Role of the Integrin αvβ6 in Cell Attachment to Fibronectin: Heterologous expression of intact and secreted forms of the receptor. *J Biol Chem,* 269**,** 6940-6948.

WEINREB, P. H., SIMON, K. J., RAYHORN, P., YANG, W. J., LEONE, D. R., DOLINSKI, B. M., PEARSE, B. R., YOKOTA, Y., KAWAKATSU, H., ATAKILIT, A., SHEPPARD, D. & VIOLETTE, S. M. 2004. Function-blocking integrin alphavbeta6 monoclonal antibodies: distinct ligand-mimetic and nonligand-mimetic classes. *J Biol Chem,* 279**,** 17875-87.

WHILDING, L. M., VALLATH, S. & MAHER, J. 2016. The integrin alphavbeta6: a novel target for CAR T-cell immunotherapy? *Biochem Soc Trans,* 44**,** 349-55.

WHITE, K. M., ALBA, R., PARKER, A. L., WRIGHT, A. F., BRADSHAW, A. C., DELLES, C., MCDONALD, R. A. & BAKER, A. H. 2013. Assessment of a novel, capsid-modified adenovirus with an improved vascular gene transfer profile. *J Cardiothorac Surg,* 8**,** 183.

WICKHAM, T. J., CARRION, M. E. & KOVESDI, I. 1995. Targeting of adenovirus penton base to new receptors through replacement of its RGD motif with other receptor-specific peptide motifs. *Gene Ther,* 2**,** 750-6.

WICKHAM, T. J., MATHIAS, P., CHERESH, D. A. & NEMEROW, G. R. 1993. Integrins alpha v beta 3 and alpha v beta 5 promote adenovirus internalization but not virus attachment. *Cell,* 73**,** 309-19.

WILLIAMS, C. H., KAJANDER, T., HYYPIÄ, T., JACKSON, T., SHEPPARD, D. & STANWAY, G. 2004. Integrin alpha v beta 6 is an RGD-dependent receptor for coxsackievirus A9. *J Virol,* 78**,** 6967-73.

WIMAN, K. G. 2007. Restoration of Wild-Type p53 Function in Human Tumors: Strategies for Efficient Cancer Therapy. *Adv Cancer Res,* 97:321-38.

WOHLFART, C. 1988. Neutralization of adenoviruses: Kinetics, stoichiometry, and mechanisms. *J Virol,* 62**,** 2321-2328.

WOHLFART, C. E. G., SVENSSON, U. K. & EVERITT, E. 1985. Interaction between HeLa cells and adenovirus type 2 virions neutralized by different antisera. *J Virol,* 56**,** 896-903.

WOLFF, G., WORGALL, S., VAN ROOIJEN, N., SONG, W. R., HARVEY, B. G. & CRYSTAL, R. G. 1997. Enhancement of in vivo adenovirus-mediated gene transfer and expression by prior depletion of tissue macrophages in the target organ. *J Virol,* 71**,** 624-9.

WOLLER, N., GÜRLEVIK, E., URECHE, C.-I., SCHUMACHER, A. & KÜHNEL, F. 2014. Oncolytic Viruses as Anticancer Vaccines. *Front Oncol,* 4**,** 188.

WORGALL, S., BUSCH, A., RIVARA, M., BONNYAY, D., LEOPOLD, P. L., MERRITT, R., HACKETT, N. R., ROVELINK, P. W., BRUDER, J. T., WICKHAM, T. J., KOVESDI, I. & CRYSTAL, R. G. 2004. Modification to the capsid of the adenovirus vector that enhances dendritic cell infection and transgene-specific cellular immune responses. *J Virol,* 78**,** 2572-80.

WU, E., PACHE, L., VON SEGGERN, D. J., MULLEN, T. M., MIKYAS, Y., STEWART, P. L. & NEMEROW, G. R. 2003. Flexibility of the adenovirus fiber is required for efficient receptor interaction. *J Virol,* 77**,** 7225-35.

WU, X., HUANG, H., WANG, C., LIN, S., HUANG, Y., WANG, Y., LIANG, G., YAN, Q., XIAO, J., WU, J., YANG, Y. & LI, X. 2013. Identification of a novel peptide that blocks basic fibroblast growth factor-mediated cell proliferation. *Oncotarget,* 4**,** 1819-1828.

WUNDER, T., SCHUMACHER, U. & FRIEDRICH, R. E. 2012. Coxsackie adenovirus receptor expression in carcinomas of the head and neck. *Anticancer Res,* 32**,** 1057-1062.

XIA, D., HENRY, L. J., GERARD, R. D. & DEISENHOFER, J. 1994. Crystal structure of the receptor-binding domain of adenovirus type 5 fiber protein at 1.7 Å resolution. *Structure,* 2**,** 1259-1270.

XU, Z., QIU, Q., TIAN, J., SMITH, J. S., CONENELLO, G. M., MORITA, T. & BYRNES, A. P. 2013. Coagulation factor X shields adenovirus type 5 from attack by natural antibodies and complement. *Nat Med,* 19**,** 452-457.

YAGINUMA, Y. & WESTPHAL, H. 1992. Abnormal structure and expression of the p53 gene in human ovarian carcinoma cell lines. *Cancer Res,* 52**,** 4196-9.

YANG, G. Y., XU, K. S., PAN, Z. Q., ZHANG, Z. Y., MI, Y. T., WANG, J. S., CHEN, R. & NIU, J. 2008. Integrin alphavbeta6 mediates the potential for colon cancer cells to colonize in and metastasize to the liver. *Cancer Science,* 99**,** 879-887.

YEUNG, T. L., LEUNG, C. S., YIP, K. P., AU YEUNG, C. L., WONG, S. T. & MOK, S. C. 2015. Cellular and molecular processes in ovarian cancer metastasis. A Review in the Theme: Cell and Molecular Processes in Cancer Metastasis. *Am J Physiol Cell Physiol,* 309**,** C444-56.

YOU, Z., FISCHER, D. C., TONG, X., HASENBURG, A., AGUILAR-CORDOVA, E. & KIEBACK, D. G. 2001. Coxsackievirus-adenovirus receptor expression in ovarian cancer cell lines is associated with increased adenovirus transduction efficiency and transgene expression. *Cancer Gene Ther,* 8**,** 168-75.

YOUNG, A. & MCNEISH, I. A. 2009. Oncolytic adenoviral gene therapy in ovarian cancer: why we are not wasting our time. *Future Oncol,* 5**,** 339-57.

ZAISS, A. K., FOLEY, E. M., LAWRENCE, R., SCHNEIDER, L. S., HOVEIDA, H., SECREST, P., CATAPANG, A. B., YAMAGUCHI, Y., ALEMANY, R., SHAYAKHMETOV, D. M., ESKO, J. D. & HERSCHMAN, H. R. 2015. Hepatocyte Heparan Sulfate is Required for Adeno-Associated Virus 2 but Dispensable for Adenovirus 5 Liver Transduction In Vivo. *J Virol*, 90(1): 412–420.

ZAROUR, H., DELEO, A., FINN, O. & STORKUS, W. 2003. *Categories of Tumor Antigens. In: Holland-Frei Cancer Medicine.*, BC Decker Inc.

ZEIMET, A. G. & MARTH, C. 2003. Why did p53 gene therapy fail in ovarian cancer? *Lancet Oncol,* 4**,** 415-22.

ZENG, M. 2001. AdEasy system made easier by selecting the viral backbone plasmid preceding homologous recombination. *Biotechniques,* 31**,** 260-262.

ZHANG, M., ZHUANG, G., SUN, X., SHEN, Y., ZHAO, A. & DI, W. 2015. Risk prediction model for epithelial ovarian cancer using molecular markers and clinical characteristics. *J Ovarian Res,* 8**,** 67.

ZHANG, Y. & BERGELSON, J. M. 2005. Adenovirus Receptors. *Journal of Virology,* 79**,** 12125-12131.

ZHAO-YANG, Z., KE-SEN, X., QING-SI, H., WEI-BO, N., JIA-YONG, W., YUE-TANG, M., JIN-SHEN, W., GUO-QIANG, W., GUANG-YUN, Y. & JUN, N. 2008. Signaling and regulatory mechanisms of integrin alphavbeta6 on the apoptosis of colon cancer cells. *Cancer Lett,* 266**,** 209-15.

ZOU, W. 2005. Immunosuppressive networks in the tumour environment and their therapeutic relevance. *Nat Rev Cancer,* 5**,** 263-274.

ZUBIETA, C., SCHOEHN, G., CHROBOCZEK, J. & CUSACK, S. 2005. The Structure of the Human Adenovirus 2 Penton. *Mol Cell,* 17**,** 121-135.

# Publications

COUGHLAN L, **UUSI-KERTTULA H**, MA J, DEGG BP, PARKER AL, BAKER AH. 2014. Retargeting adenovirus serotype 48 fiber knob domain by peptide incorporation. *Hum Gene Ther.* 25(4), 385-94. PMID: 24617540

**UUSI-KERTTULA H**, LEGUT M, DAVIES J, JONES R, HUDSON E, HANNA L, STANTON RJ, CHESTER JD, PARKER AL. 2015. Incorporation of peptides targeting EGFR and FGFR1 into the adenoviral fiber knob domain and their evaluation as targeted cancer therapies. *Hum Gene Ther.* 26(5), 320-9. PMID: 25919378

**UUSI-KERTTULA H**, HULIN-CURTIS SL, DAVIES J, PARKER AL. 2015. Oncolytic adenovirus: strategies and insights for vector design and immuno-oncolytic applications. *Viruses*, 7(11), 6009-42. Review. PMID: 26610547

**UUSI-KERTTULA H**, DAVIES J, COUGHLAN L, HULIN-CURTIS SL, JONES R, HANNA L, CHESTER JD, PARKER AL. 2016. Pseudotyped αvβ6 integrin-targeted adenovirus vectors for ovarian cancer therapies. *Oncotarget.*, 7(19), 27926-37. PMID: 27056886

HULIN-CURTIS SL, **UUSI-KERTTULA H**, JONES R, HANNA L, CHESTER JD, PARKER AL. 2016. Evaluation of CD46 re-targeted adenoviral vectors for clinical ovarian cancer intraperitoneal therapy. *Cancer Gene Ther.,* 23(7), 229-34. PMID: 27229159